THE

PHYSICAL REVIEW

Volume [illegible] Series [illegible] Number 1

JULY [illegible], 1949

for the

[illegible] PHYSICAL SOCIETY

[illegible]

[illegible] Columbia

[illegible] New York, N. Y.

THE PHYSICAL REVIEW

A journal of experi[mental and theoretical physics] established by E. L. Nichols in 1[893]

Published by the American Institute of Physics
for the
AMERICAN PHYSICAL SOCIETY

Officers

President

F. W. Loomis
University of Illinois
Urbana, Illinois

Vice-President

I. I. Rabi
Columbia University
New York, New York

Secretary

K. K. Darrow
Bell Telephone Laboratories
Office:
Columbia University
New York 27, New York

Treasurer

G. B. Pegram
Columbia University
New York 27, New York

Local Secretary
for the Pacific Coast

J. Kaplan
University of California at Los Angeles
Los Angeles, California

Managing Editor

John T. Tate
University of Minnesota
Minneapolis, Minnesota

BOARD OF EDITORS

Associate Editors

S. A. Goudsmit — W. E. [illegible]
E. M. Purcell — R. G. [illegible]
V. F. Weisskopf — J. Barn[illegible]

Manuscripts for publication should be submitted to John T. Tate, [illegible], Minnesota, Minneapolis, Minnesota. The authors' institutions are [illegible] pay a publication charge of $4 per page which, if [illegible] to 100 free reprints. Instructions will be sent with galley [illegible]

All correspondence concerning papers in the process of publication [illegible] addressed to the Publication Manager, American Institute of Physics, 175 [illegible] 55 Street, New York 22, New York.

Subscription Price

United States and Canada ..... $[illegible]
Elsewhere ..... $[illegible]

Back Numbers

Back numbers of the *complete year* is available: $[illegible]
[illegible] 42 numbers, prior to July, 1929;
[illegible] July, 1929–December, 1941;
[illegible] January, 1942–December, 1946:
[illegible] each.
[illegible] each.

Orders and claims for back numbers should be addressed to the [illegible], Pennsylvania, or to the American Institute of Physics, 175 [illegible] 55 Street, New York 22, New York.

Claims will be allowed (in the case of members of the American Physical Society) only if received by the Treasurer; in the case of other subscribers, only if received by the Manager, American Institute of Physics.

[illegible] Physics Department, Cornell University, Ithaca, New York.

The Physical Review is published [illegible] Printing Co., Prince and Lemon Streets, Lancaster, Pennsylvania.

Entered as second-class matter March [illegible] Post Office, Lancaster, Pennsylvania, under the Act of March 3, 1879.

Acceptance for mailing at special rate of postage provided for in paragraph (d-2), section 538, P. L. & R., authorized [illegible]

THE
PHYSICAL REVIEW

A journal of experimental and theoretical physics established by E. L. Nichols in 1893

SECOND SERIES, VOL. 76, NO. 2 JULY 15, 1949

Electrostatic Scattering of Neutrons*

S. M. DANCOFF AND S. D. DRELL
Physics Department, University of Illinois, Urbana, Illinois
(Received January 6, 1949)

A weak force of attraction between electrons and thermal neutrons is indicated in recent experiments by Havens, Rabi, and Rainwater, and by Fermi and Marshall. According to meson theory this would be expected, since the neutron is considered as one charge state of a nucleon (the proton is the other state) which is coupled to a meson field. The attraction is then interpreted as an electrostatic scattering of the neutron which exists part of the time as a proton and meson. We perform a third order perturbation calculation in the approximation of weak coupling between mesons and nucleons. Neutrons and protons are here treated as Dirac particles which are coupled to a meson field of spin zero. The results indicate that the observed interaction is suitably described in terms of the meson field.

1. INTRODUCTION

IF the nuclear forces are to be accounted for wholly or partly in terms of the exchange of charged mesons between nuclear particles then it will follow that the neutron will be subject to a deflection when passing through an inhomogeneous electric field. This is brought about by the action of the field on the proton and mesons which exist in virtual states in the neighborhood of the neutron. Attempts to detect such interaction were made by Havens, Rabi, and Rainwater[1] and by Fermi and Marshall,[2] who studied the scattering of neutrons in lead and in xenon, respectively. The scattering arises predominantly from three sources:

(a) Scattering by the specific nuclear forces;
(b) Electric scattering of the type in question due to the nuclear charge;
(c) Electric scattering due to the atomic electrons.

The scattering (a) is strongly predominant. Nevertheless, the interference which exists between (a) and the electric scattering makes it not unreasonable to look for experimental effects of the latter—effects which would surely be far below the present limits of experimental sensitivity were not (a) simultaneously present.

Scattering of slow (thermal) neutrons by nuclear forces will be spherically symmetric and will, in general, have no dependence on wave-length. On the other hand, thermal neutrons have a wave-length comparable with atomic dimensions, so that scattering of the type (c) will show a marked wave-length dependence and will not be spherically symmetric. Thus if one can extract from the observed scattering any part which varies with wave-length and scattering angle in a manner consistent with the atomic form factor, then one has a measure of the effect being studied.

A theoretical estimate of the magnitude of the effect has been given by Fermi and Marshall.[2] Their calculation is not based on any specific meson theory, but makes use of qualitative features of meson theories in general. Their numerical result might be expected to be in order-of-magnitude agreement with that obtained from any particular formulation. Since the experiment in question is such a critical test for the validity of the meson field hypothesis it was felt desirable to have at hand theoretical values as precise as can be derived.

The present calculation is based on the assumption that protons and neutrons (nucleons) obey the Dirac equation and that the mesons have spin zero (scalar). The assumption is frequently made that the massiveness of nucleons makes it possible to treat them as undeviated by the acts of virtual emission and reabsorption of mesons. Our results show that the latter assumption would lead to a serious quantitative error in this problem. We also find that a change in the equations of motion of the nucleon would lead to a small but appreciable change in the result.

* The method and results of this calculation were first presented at the November, 1948 meetings of the American Physical Society in Chicago (Phys. Rev. **75**, 341A (1949).

[1] W. W. Havens, I. I. Rabi, and L. J. Rainwater, Phys. Rev. **72**, 634 (1947).

[2] E. Fermi and L. Marshall, Phys. Rev. **72**, 1139 (1947).

The work is divided into the following sections:

2. Choice of interaction function, and quantization of the theory.
3. Display of transition schemes and of scattering matrix element.
4. Calculation of the change in neutron scattering due to the electron-neutron interaction.
5. Comparison with experiment.
6. Calculation of neutron scattering with spin flip due to the electron-neutron interaction.
7. Discussion.

2. QUANTIZATION

In the presence of external electromagnetic fields the Lagrangian density is taken as

$$\mathfrak{L}=-c^2[(\partial\psi^*/\partial x_\nu+ie\phi_\nu\psi^*)(\partial\psi/\partial x_\nu-ie\phi_\nu\psi)+\mu^2\psi^*\psi]+\hbar ci\Psi_P^+[\gamma^\nu(\partial/\partial x_\nu-ie\phi_\nu)+M]\Psi_P+\hbar ci\Psi_N^+[\gamma^\nu(\partial/\partial x_\nu)+M]\Psi_N+igc(\Psi_P^+\psi\Psi_N+\Psi_N^+\psi^*\Psi_P). \quad (1)$$

Henceforth $\hbar$ and c will be set equal to one. The components of x are (x,y,z,it). ψ is the wave field of a charged scalar meson. Ψ_P and Ψ_N are the spinor wave fields of protons and neutrons. μ and M are the reciprocal Compton wave-lengths of meson and nucleon, respectively. γ^ν are the four Dirac matrices; the first three are $\gamma^k=i\alpha^k\beta$, while $\gamma^4=\beta$. Also $\Psi^+=i\Psi^*\beta$. The constant g determines the strength of interaction, having the dimensions of an electric charge. ϕ_ν is the externally applied 4-vector potential, having components $(\mathbf{A},i\phi)$, where $\mathbf{A}$ and ϕ are vector and scalar potentials, respectively.

Canonically conjugate variables are

$$\pi=\dot\psi^*-ie\phi\psi^*, \quad \Pi_P=i\Psi_P^*,$$
$$\pi^*=\dot\psi+ie\phi\psi, \quad \Pi_N=i\Psi_N^*.$$

The Hamiltonian density is

$$\mathfrak{IC}=(\pi^*\pi+\mathbf{grad}\psi^*\cdot\mathbf{grad}\psi+\mu^2\psi^*\psi)-i\Psi_P^*(\boldsymbol{\alpha}\cdot\mathbf{grad}+iM\beta)\Psi_P-i\Psi_N^*(\boldsymbol{\alpha}\cdot\mathbf{grad}+iM\beta)\Psi_N+g(\Psi_P^*\beta\Psi_N\psi+\Psi_N^*\beta\Psi_P\psi^*)+ie\phi(\pi^*\psi^*-\pi\psi)+ie\mathbf{A}\cdot(\psi^*\mathbf{grad}\psi-\psi\mathbf{grad}\psi^*)+e^2(\psi^*\psi)\mathbf{A}^2+e\Psi_P^*(-\boldsymbol{\alpha}\cdot\mathbf{A}+\phi)\Psi_P. \quad (2)$$

This expression is conveniently split as follows:

$$\mathfrak{IC}={}^0\mathfrak{IC}+{}^g\mathfrak{IC}+{}^e\mathfrak{IC}. \quad (3)$$

${}^0\mathfrak{IC}$ represents the first three terms of (2). ${}^g\mathfrak{IC}$, the fourth term, gives the meson-nucleon coupling. ${}^e\mathfrak{IC}$, the last four terms, gives the coupling of the charges with the electromagnetic field.

We wish to quantize the fields so that the meson field satisfies Bose statistics, the nucleon fields satisfy Fermi statistics. To achieve this it is necessary that the following commutation relations be maintained for fields measured simultaneously at two points $\mathbf{r}$ and $\mathbf{r}'$:

$$[\pi(\mathbf{r}),\psi(\mathbf{r}')]=[\pi^*(\mathbf{r}),\psi^*(\mathbf{r}')]=-i\delta(\mathbf{r}-\mathbf{r}'), \quad (4)$$

whereas all other pairs of the meson functions commute. Likewise

$$[\Pi_{P\sigma}(\mathbf{r}),\Psi_{P\tau}(\mathbf{r}')]_+=[\Pi_{N\sigma}(\mathbf{r}),\Psi_{N\tau}(\mathbf{r}')]_+=i\delta(\mathbf{r}-\mathbf{r}')\delta_{\sigma\tau}. \quad (5)$$

The subscripts σ and τ refer to particular components of the Dirac spinors. The $(+)$ subscript indicates the anti-commutator. All other pairs of proton functions have vanishing anti-commutators, as do all other pairs of neutron wave functions.

So far the requirements are the usual ones. But now we also demand that all meson field quantities *commute* with all proton as well as all neutron field quantities; and finally that all proton field quantities *anticommute* with all those for the neutron field. The appearance of the coupling terms in the canonical equations of motion makes these requirements non-trivial.

The possibility of quantizing the theory in a manner consistent with the above assumed commutation relations depends on the possibility of expressing them in relativistically covariant form. That is, the values of the various commutators and anticommutators corresponding to simultaneous events in one Lorentz frame should imply the same values for simultaneous events in another. This covariance property of the commutator relations may be demonstrated by the method of Heisenberg and Pauli.[3] (We indicate this in the appendix).

Symmetric Theory

In our formulation of the interaction between scalar and spinor fields we have thus far limited our discussion to a charge-bearing meson field. Charge independence of nuclear forces requires a symmetric theory of the meson field[4] with both electrically charged and neutral mesons. The development of this section remains essentially unaltered if the meson field is modified in order to satisfy the charge-independence requirement. We introduce a real wave field, φ, for the neutral mesons, which commutes with all other wave fields of the nucleons and charged mesons and which satisfies commutator relation (4) with its own conjugate momentum, $\eta=\dot\varphi$:

$$[\eta(\mathbf{r}),\varphi(\mathbf{r}')]=-i\delta(\mathbf{r}-\mathbf{r}').$$

For a symmetric theory the meson-nucleon coupling term in the Hamiltonian density (2) is modified to

$${}^{g'}\mathfrak{IC}=g'(\sqrt{2}\Psi_P^*\beta\Psi_N\psi+\sqrt{2}\Psi_N^*\beta\Psi_P\psi^*+\Psi_P^*\beta\Psi_P\varphi-\Psi_N^*\beta\Psi_N\varphi). \quad (6)$$

Neutral mesons are not coupled with the electromagnetic field, so that ${}^e\mathfrak{IC}$ remains unchanged as in (2).

3. TRANSITION SCHEMES

We wish to calculate the cross section for an incident thermal neutron with momentum $\mathbf{K}_0$ to be scattered

[3] W. Heisenberg and W. Pauli, Zeits. f. Physik **56**, 1 (1929).
[4] N. Kemmer, Proc. Camb. Phil. Soc. **34**, 354 (1938).

elastically to a final state of momentum $\mathbf{K}_f$ (with $|\mathbf{K}_f| = |\mathbf{K}_0|$) in the field of a static, scalar potential ϕ. The interaction terms of the Hamiltonian density in Eqs. (2) and (3) reduce to

$$\begin{aligned} {}^{g}\mathcal{H} &= g[\Psi_P^*\beta\Psi_N\psi + \Psi_N^*\beta\Psi_P\psi^*], \\ {}^{e}\mathcal{H} &= ie\phi(\pi^*\psi^* - \pi\psi - i\Psi_P^*\Psi_P), \end{aligned} \tag{7}$$

for a charged meson theory.

The calculations are carried out using a weak coupling approximation, i.e., with the assumption that ${}^{g}\mathcal{H}$ may be treated as a perturbation. The validity of such an assumption depends on the smallness of the parameter $(g^2/4\pi)$. Arguments based on the strength of nuclear forces would set this parameter at 0.3 (although it is questionable whether the scalar coupling assumed here could adequately describe nuclear forces). Such a magnitude for the coupling parameter would give rise to errors of the order of 30 percent if just the leading terms in a perturbation theory calculation are kept.

Electrostatic scattering occurs in three steps. The matrix element describing a transition from an initial state i to a final state f is

$$M.E. = \sum_{m,m' \neq i} \frac{{}^{e}V_{fm'}{}^{g}V_{m'm}{}^{g}V_{mi} + {}^{g}V_{fm'}{}^{e}V_{m'm}{}^{g}V_{mi} + {}^{g}V_{fm'}{}^{g}V_{m'm}{}^{e}V_{mi}}{(E_i - E_m)(E_i - E_{m'})}, \tag{8}$$

where $V_{mi} = \int \mathcal{H}_{mi} d^3x$ is the spatial integral of the interaction term in the Hamiltonian density describing a transition from state i to state m, E_i is the total energy of state i, and the double sum is carried over all intermediate states m and m', exclusive of the initial state i. Two steps in this process involve the interaction between nucleon and meson fields, treated in the weak coupling approximation. The total momentum of the mesons and nucleons is conserved in these steps. Momentum $\boldsymbol{\Delta} = \mathbf{K}_f - \mathbf{K}_0$ is exchanged with the applied field in the third step. Although the momenta of the virtual intermediate states are arbitrarily large, the *momentum exchange* with the static field is quite small, of magnitude $|\boldsymbol{\Delta}| = 2K_0 \sin\theta/2$ for scattering angle θ. In calculating the cross section for electric scattering of thermal neutrons by atomic electrons bound to heavy nuclei we are thus justified in treating the neutron as interacting with a fixed static field. The matrix element will be proportional to the square of the coupling parameter, g, times the fine structure constant, α.

We list below (Table I) transition schemes for this scattering problem in terms of the virtual intermediate states. The schemes divide conveniently into three classes, as indicated in Eq. (8), according as the interaction, ${}^{e}\mathcal{H}$, with the electric field occurs in the first, second, or third step. We label these classes of transitions as type a, b, and c, respectively.[5] We denote a proton by P, a proton hole by P^*, a neutron by N, a meson of positive electric charge by μ^+, and a meson of negative electric charge by μ^-. The values in parentheses for the propagation vectors are dictated by conservation of momentum for the nucleon-meson coupling and by specification of the final state momentum, $\mathbf{K}_f = \mathbf{K}_0 + \boldsymbol{\Delta}$. A proton, neutron, or positively charged meson, represented by a plane wave with propagation vector $\mathbf{K}$, behaves as a particle with momentum $+\mathbf{K}$; a proton hole, neutron hole, or negatively charged meson, as one with momentum $-\mathbf{K}$. Propagation vector $\mathbf{k}$ assumes all values in the sum over the intermediate particle states.

In order to evaluate matrix element (8), we perform a spatial fourier resolution of the canonical field operators of the meson and Dirac fields. We obtain a discrete momentum spectrum for each field function by quantizing in a box of side L with periodic boundary conditions.

The analysis of the proton field takes the form

$$\begin{aligned} \Psi &= L^{-\frac{3}{2}} \sum_{\mathbf{K},S} f_{\mathbf{K},S} e^{i\mathbf{K}\cdot\mathbf{r}} v_{\mathbf{K},S}, \\ \Psi^* &= L^{-\frac{3}{2}} \sum_{\mathbf{K},S} f_{\mathbf{K},S}^* e^{-i\mathbf{K}\cdot\mathbf{r}} v_{\mathbf{K},S}^*, \end{aligned} \tag{9}$$

where the $v_{\mathbf{K},S}$ and $v_{\mathbf{K},S}^*$ are the four component Dirac plane wave spinors and the sums extend over the entire range of positive and negative momentum values, with two spin orientations, S, and two signs of energy for each value of $\mathbf{K}$. The $f_{\mathbf{K},S}^*$ and $f_{\mathbf{K},S}$ are creation and annihilation operators for the proton field. $f_{\mathbf{K},S}^*$ either creates a proton in a positive energy state, or fills a proton hole in the negative energy range, with the four quantum numbers $(\mathbf{K}, S)$.

We write for the meson field

$$\begin{aligned} \psi &= (2L^3)^{-\frac{1}{2}} \sum_{\mathbf{k}} \omega_{\mathbf{k}}^{-\frac{1}{2}} (a_{\mathbf{k}} + b_{\mathbf{k}}^*) e^{i\mathbf{k}\cdot\mathbf{r}}, \\ \psi^* &= (2L^3)^{-\frac{1}{2}} \sum_{\mathbf{k}} \omega_{\mathbf{k}}^{-\frac{1}{2}} (a_{\mathbf{k}}^* + b_{\mathbf{k}}) e^{-i\mathbf{k}\cdot\mathbf{r}}, \\ \pi &= i(2L^3)^{-\frac{1}{2}} \sum_{\mathbf{k}} \omega_{\mathbf{k}}^{+\frac{1}{2}} (a_{\mathbf{k}}^* - b_{\mathbf{k}}) e^{-i\mathbf{k}\cdot\mathbf{r}}, \\ \pi^* &= -i(2L^3)^{-\frac{1}{2}} \sum_{\mathbf{k}} \omega_{\mathbf{k}}^{+\frac{1}{2}} (a_{\mathbf{k}} - b_{\mathbf{k}}^*) e^{i\mathbf{k}\cdot\mathbf{r}}, \end{aligned} \tag{10}$$

where $a_{\mathbf{k}}^*$ and $a_{\mathbf{k}}$ are creation and annihilation operators, respectively, for positively charged mesons, $b_{\mathbf{k}}^*$ and $b_{\mathbf{k}}$ correspondingly for mesons bearing negative charge, and $\omega_{\mathbf{k}} = (k^2 + \mu^2)^{\frac{1}{2}}$. The operators in (9) and (10) obey commutation and anticommutation rules obtained directly from (4) and (5).

Upon introducing (7), (9), and (10) into (8) and summing over all of the intermediate states indicated in Table I, we get the following expression for the matrix element between the specified initial and final

[5] Renormalization terms, which are usually present in a third-order perturbation calculation, will contribute nothing in this one due to the fact that the neutron (core) itself has no interaction with an electrostatic field.

TABLE I. Transition schemes for the electrostatic scattering of neutrons according to a charged meson theory.

Scheme	States i	m	m'	f
I_a	$N(\mathbf{K}_0)$	$N(\mathbf{K}_0)$, $\mu^+(\mathbf{k})$, $\mu^-(\mathbf{k}-\boldsymbol{\Delta})$	$P(\mathbf{K}_0+\mathbf{k})$, $\mu^-(\mathbf{k}-\boldsymbol{\Delta})$	$N(\mathbf{K}_f)$
II_a	$N(\mathbf{K}_0)$	$N(\mathbf{K}_0)$, $P(\mathbf{K}_f+\mathbf{k})$, $P^*(\mathbf{K}_0+\mathbf{k})$	$P(\mathbf{K}_f+\mathbf{k})$, $\mu^-(\mathbf{k})$	$N(\mathbf{K}_f)$
III_a	$N(\mathbf{K}_0)$	$N(\mathbf{K}_0)$, $P(\mathbf{K}_f+\mathbf{k})$, $P^*(\mathbf{K}_0+\mathbf{k})$	$N(\mathbf{K}_0)$, $N(\mathbf{K}_f)$, $P^*(\mathbf{K}_0+\mathbf{k})$, $\mu^+(\mathbf{k})$	$N(\mathbf{K}_f)$
IV_a	$N(\mathbf{K}_0)$	$N(\mathbf{K}_0)$, $\mu^+(\mathbf{k})$, $\mu^-(\mathbf{k}-\boldsymbol{\Delta})$	$N(\mathbf{K}_0)$, $N(\mathbf{K}_f)$, $P^*(\mathbf{K}_0+\mathbf{k})$, $\mu^+(\mathbf{k})$	$N(\mathbf{K}_f)$
I_b	$N(\mathbf{K}_0)$	$P(\mathbf{K}_0+\mathbf{k})$, $\mu^-(\mathbf{k})$	$P(\mathbf{K}_f+\mathbf{k})$, $\mu^-(\mathbf{k})$	$N(\mathbf{K}_f)$
II_b	$N(\mathbf{K}_0)$	$P(\mathbf{K}_0+\mathbf{k})$, $\mu^-(\mathbf{k})$	$P(\mathbf{K}_0+\mathbf{k})$, $\mu^-(\mathbf{k}-\boldsymbol{\Delta})$	$N(\mathbf{K}_f)$
III_b	$N(\mathbf{K}_0)$	$N(\mathbf{K}_0)$, $N(\mathbf{K}_f)$, $P^*(\mathbf{K}_f+\mathbf{k})$, $\mu^+(\mathbf{k})$	$N(\mathbf{K}_0)$, $N(\mathbf{K}_f)$, $P^*(\mathbf{K}_0+\mathbf{k})$, $\mu^+(\mathbf{k})$	$N(\mathbf{K}_f)$
IV_b	$N(\mathbf{K}_0)$	$N(\mathbf{K}_0)$, $N(\mathbf{K}_f)$, $P^*(\mathbf{K}_0+\mathbf{k})$, $\mu^+(\mathbf{k}-\boldsymbol{\Delta})$	$N(\mathbf{K}_0)$, $N(\mathbf{K}_f)$, $P^*(\mathbf{K}_0+\mathbf{k})$, $\mu^+(\mathbf{k})$	$N(\mathbf{K}_f)$
I_c	$N(\mathbf{K}_0)$	$P(\mathbf{K}_0+\mathbf{k})$, $\mu^-(\mathbf{k})$	$N(\mathbf{K}_f)$, $\mu^-(\mathbf{k})$, $\mu^+(\mathbf{k}-\boldsymbol{\Delta})$	$N(\mathbf{K}_f)$
II_c	$N(\mathbf{K}_0)$	$P(\mathbf{K}_0+\mathbf{k})$, $\mu^-(\mathbf{k})$	$N(\mathbf{K}_f)$, $P(\mathbf{K}_0+\mathbf{k})$, $P^*(\mathbf{K}_f+\mathbf{k})$	$N(\mathbf{K}_f)$
III_c	$N(\mathbf{K}_0)$	$N(\mathbf{K}_0)$, $N(\mathbf{K}_f)$, $P^*(\mathbf{K}_f+\mathbf{k})$, $\mu^+(\mathbf{k})$	$N(\mathbf{K}_f)$, $P(\mathbf{K}_0+\mathbf{k})$, $P^*(\mathbf{K}_f+\mathbf{k})$	$N(\mathbf{K}_f)$
IV_c	$N(\mathbf{K}_0)$	$N(\mathbf{K}_0)$, $N(\mathbf{K}_f)$, $P^*(\mathbf{K}_0+\mathbf{k})$, $\mu^+(\mathbf{k}-\boldsymbol{\Delta})$	$N(\mathbf{K}_f)$, $\mu^-(\mathbf{k})$, $\mu^+(\mathbf{k}-\boldsymbol{\Delta})$	$N(\mathbf{K}_f)$

states:

$$M.E._{es}=(g^2e\phi_\Delta/4L^6)\sum_{\mathbf{k}}\Big[\Big(\frac{\omega_{k-\Delta}-\omega_k}{\omega_k\omega_{k-\Delta}(\omega_k+\omega_{k-\Delta})}\Big)$$
$$\times\Big(\frac{\langle\beta\Lambda^+_{k+K_0}\beta\rangle}{E_{k+K_0}+\omega_k-E_{K_0}}-\frac{\langle\beta\Lambda^+_{k+K_0}\beta\rangle}{E_{k+K_0}+\omega_{k-\Delta}-E_{K_0}}$$
$$+\frac{\langle\beta\Lambda^-_{k+K_0}\beta\rangle}{E_{k+K_0}+\omega_k+E_{K_f}}-\frac{\langle\beta\Lambda^-_{k+K_0}\beta\rangle}{E_{k+K_0}+\omega_{k-\Delta}+E_{K_f}}\Big)$$
$$-\Big(\frac{2}{\omega_k(E_{k+K_0}+E_{k+K_f})}\Big)\Big(\frac{\langle\beta\Lambda^-_{k+K_f}\Lambda^+_{k+K_0}\beta\rangle}{E_{k+K_0}+\omega_k-E_{K_0}}$$
$$+\frac{\langle\beta\Lambda^-_{k+K_f}\Lambda^+_{k+K_0}\beta\rangle}{E_{k+K_f}+\omega_k+E_{K_f}}+\frac{\langle\beta\Lambda^+_{k+K_f}\Lambda^-_{k+K_0}\beta\rangle}{E_{k+K_f}+\omega_k-E_{K_0}}$$
$$+\frac{\langle\beta\Lambda^+_{k+K_f}\Lambda^-_{k+K_0}\beta\rangle}{E_{k+K_0}+\omega_k+E_{K_f}}\Big)+\Big(\frac{1}{\omega_k(E_{k+K_0}+\omega_k-E_{K_0})}\Big)$$
$$\times\Big(\frac{2\langle\beta\Lambda^+_{k+K_f}\Lambda^+_{k+K_0}\beta\rangle}{E_{k+K_f}+\omega_k-E_{K_0}}$$
$$-\frac{(\omega_k+\omega_{k-\Delta})\langle\beta\Lambda^+_{k+K_0}\beta\rangle}{\omega_{k-\Delta}(E_{k+K_0}+\omega_{k-\Delta}-E_{K_0})}\Big)$$
$$+\Big(\frac{1}{\omega_k(E_{k+K_0}+\omega_k+E_{K_f})}\Big)\Big(\frac{2\langle\beta\Lambda^-_{k+K_f}\Lambda^-_{k+K_0}\beta\rangle}{E_{k+K_f}+\omega k+E_{K_f}}$$
$$-\frac{(\omega_k+\omega_{k-\Delta})\langle\beta\Lambda^-_{k+K_0}\beta\rangle}{\omega_{k-\Delta}(E_{k+K_0}+\omega_{k-\Delta}+E_{K_f})}\Big)\Big],\quad(11)$$

where $\Lambda_1^\pm$ are the positive and negative energy projection operators,

$$\Lambda_1^\pm=\tfrac{1}{2}(1\pm(\boldsymbol{\alpha}\cdot\mathbf{l}+\beta M)/E_l),$$

$\langle Q\rangle$ denotes the product of a matrix Q with initial and final state spinors,

$$\langle Q\rangle=(v_{\mathbf{K}_f}{}^*|Q|v_{\mathbf{K}_0}),$$

(α,β) are the usual 4×4 Dirac matrices, $\phi_\Delta=\int e^{-i\Delta\cdot r}\phi d^3x$, the integration being carried over the volume L^3 of the box in which the wave fields are quantized, $E_K=(K^2+M^2)^{\frac{1}{2}}$ for nucleons of rest mass M, and $\omega_k=(k^2+\mu^2)^{\frac{1}{2}}$, for mesons of rest mass μ. The first four terms are contributed by transition schemes I_a, I_c, IV_a, IV_c, in which the scalar potential serves as a source for creation or annihilation of a meson pair. The second set of four terms is contributed by schemes II_a, II_c, III_a, III_c, in which the static field serves to create or annihilate a proton pair. The last four terms come from the type b processes in which scattering of charged particles occurs in the electric field.

4. CALCULATION FOR NO SPIN-FLIP

A. Dirac Nucleons

It is between the part of the neutron wave scattered by the atomic electrons without spin flip and the wave isotropically scattered by the specific nuclear forces that interference exists. We compute here the magnitude of this effect.

For neutrons of thermal velocity, (K_0/μ) and (K_0/M) are both extremely small relative to one, so that we expand (11) in a power series of terms (Δ/ω_k) and (Δ/E_k). The contribution from terms proportional to the zeroth and first powers of Δ vanishes upon taking the sum over intermediate momenta $\mathbf{k}$. The lowest nonvanishing contribution is of order Δ^2:

$$M.E.=(g^2e\phi_\Delta\Delta^2/8L^6)\sum_{\mathbf{k}}\Big[\Big\{\Big(\frac{1+M/E_k}{\omega_kD_1{}^2}\Big)$$
$$\times(1/2\omega_k{}^2-1/\omega_kD_1-k^2/3\omega_k{}^4+2k^2/3\omega_k{}^3D_1-2k^2/3\omega_k{}^2D_1{}^2$$
$$+k^2/3E_k\omega_k{}^2D_1-k^2/E_k\omega_kD_1{}^2-k^2/3E_k{}^2D_1{}^2-k^2/6E_k{}^4)$$
$$+(-1/E_k{}^2\omega_kD_1{}^2+1/E_k{}^3\omega_kD_1+k^2/3E_k{}^4\omega_kD_1{}^2$$
$$-k^2/6E_k{}^5\omega_kD_1)+(Mk^2/E_k{}^3\omega_kD_1{}^2)(1/3\omega_kD_1-1/6\omega_k{}^2$$
$$+1/3E_kD_1)\Big\}+\Big\{\begin{matrix}\text{Same term with } M \text{ replaced}\\ \text{by } -M \text{ and } D_1 \text{ by } D_2\end{matrix}\Big\}\Big],\quad(12)$$

where

$$D_1=M-E_{\mathbf{k}}-\omega_{\mathbf{k}};\quad D_2=-M-E_{\mathbf{k}}-\omega_{\mathbf{k}}.$$

The $\mathbf{k}$ sum in (12) can be performed by taking the sum to an integral,

$$\sum_{\mathbf{k}}\rightarrow(L^3/2\pi^2)\int_0^\infty k^2dk.$$

We insert $M=1835m_e$ for the nucleon mass and $\mu=300m_e$ for the meson mass, introduce a new independent variable $x=\tan^{-1}(k/\mu)$, and integrate numerically over the finite range $(0,\pi/2)$ of x. The integrand is reproduced as the solid line in Fig. 1. We see that most of the contribution to the matrix element comes from low momentum values, $k\lesssim\mu$, for the intermediate particles.

The value obtained is

$$M.E._{es}=(1/25.3)(g^2/4\pi)(e\phi_\Delta/\pi L^3)(\Delta^2/\mu^2). \quad (13)$$

This is the matrix element for electrostatic scattering of neutrons which have the same spin orientation before and after scattering. The numerical factor is a slowly varying function of the meson and nucleon masses, here assumed to be 300 and 1835 electron masses, respectively.

B. Schrödinger-Pauli Nucleons

Most of the contribution to the matrix element (12) comes from the non-relativistic energy range, $k<M$, of the intermediate nucleons. We may thus hope to obtain a good approximation to it if we neglect the small components of the nucleon wave functions—that is, if we treat neutrons and protons as Schrödinger-Pauli particles. Since we no longer have the filled negative energy levels of the hole theory, only transition schemes I_a, I_b, II_b, and I_c, will contribute. This means that all spin terms in Eq. (11) that contain negative energy projection operators, Λ^-, vanish, whereas Λ^+ is replaced by unity. The result is plotted as the dashed line in Fig. 1. The matrix element for $S-P$ nucleons is greater than (13) calculated for Dirac particles by 29 percent. Most of the discrepancy arises from the upper end of the momentum spectrum where small components of the intermediate virtual nucleons are significant.

Only a minor contribution is lost from the matrix element by neglecting, say, scheme III_b relative to I_b. This is because the energy denominator of III_b, $(E_{\mathbf{k}+\mathbf{K}_f}+\omega_{\mathbf{k}}+E_{\mathbf{K}_f})(E_{\mathbf{k}+\mathbf{K}_0}+\omega_{\mathbf{k}}+E_{\mathbf{K}_f})$, is considerably larger than that of I_b, $(E_{\mathbf{k}+\mathbf{K}_f}+\omega_{\mathbf{k}}-E_{\mathbf{K}_0})(E_{\mathbf{k}+\mathbf{K}_0}+\omega_{\mathbf{k}}-E_{\mathbf{K}_0})$, in the important $\mathbf{k}$ region. The disagreement will increase as the pair terms become more important. This will happen for a type of coupling between the nucleon-meson fields which stresses larger momentum values, or, in other words, binds the meson cloud more compactly about the nucleons.

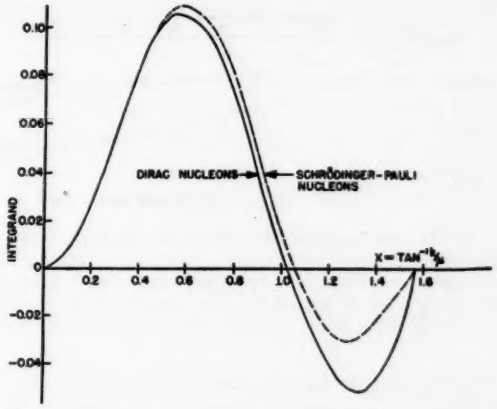

FIG. 1. Graph of the integrand in the matrix element for electrostatic scattering of neutrons without spin flip. The solid line is the result for the case in which nucleons obey Dirac's equation; the dashed line is for the case in which they obey the non-relativistic wave equation.

C. No Recoil

We can evaluate the effect of neglecting recoil of the nucleons by going to the limit $M\rightarrow\infty$ in Eq. (12). Thus $D_1\rightarrow-\omega_{\mathbf{k}}$, $E_{\mathbf{k}}\rightarrow M$, and

$$M.E._{es}=(g^2e\phi_\Delta\Delta^2/8L^6)\sum_{\mathbf{k}}(3-10k^2/3\omega_{\mathbf{k}}^2)/\omega_{\mathbf{k}}^5$$
$$=(\tfrac{1}{12})(g^2/4\pi)(e\phi_\Delta/\pi L^3)(\Delta^2/\mu^2). \quad (14)$$

This approximation is seen to increase the matrix element by a factor two relative to its correct value (12).

D. Symmetric Theory

The presence of the neutral meson wave field in the coupling term (6) of the Hamiltonian density introduces six new transition schemes for the scattering $N(\mathbf{K}_0)\rightarrow N(\mathbf{K}_f)$. Each of these involves a pair creation or annihilation of protons in the potential field. We find that these additional processes do not contribute to the electrostatic neutron scattering cross section. Coupling parameters g and g' in (6) and (7) both have the same value to account for the deuteron binding energy. This equality follows from calculation of the neutron-proton interaction in the approximation of no nucleon recoil. We see then from (6) and (7) that matrix elements (13) and (14) will be multiplied by a factor of two for a calculation based on a symmetric meson theory.

5. COMPARISON WITH EXPERIMENT

The total matrix element for the scattering of thermal neutrons by an atom with zero magnetic moment can be written as the sum of two parts. The dominant part, $M.E._n$, gives the contribution to spherically symmetric scattering as a result of specific nuclear forces and of the charge on the nucleus. The possibility of observing electrostatic scattering of neutrons arises from interference between $M.E._n$ and the matrix element, $M.E._{es}$,

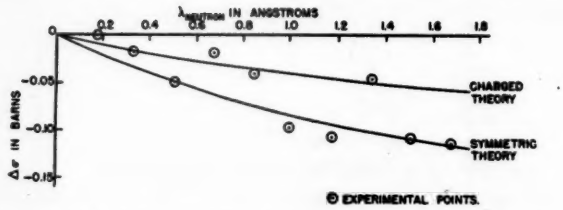

FIG. 2. The curves give the calculated change in the neutron elastic scattering cross section as a function of incident neutron wave-length according to a charged and a symmetric scalar meson theory for $g^2/4\pi=0.30$. The experimental points were obtained by Havens, Rabi, and Rainwater for scattering from lead.

for electric scattering by the atomic electrons, which introduces an asymmetry into the scattering. We can write a cross section by summing over final neutron states and dividing by the incident flux. For a scattering source containing various isotopes, labelled with subscripts i, present in proportions p_i,

$$\sigma d\Omega=\frac{L^6M^2}{4\pi^2}\sum_i p_i|(M.E._n)_i+M.E._{es}|^2d\Omega.$$

Writing $(M.E._n)_i$ in terms of a scattering length[6] $a_i=(ML^3/2\pi)(M.E._n)_i$, and keeping only the linear term, we get for the change in cross section because of electric scattering,

$$\begin{aligned}\Delta\sigma d\Omega&=(\sigma-\sigma_n)d\Omega\\&=(1/25.3)(g^2/4\pi)(e\phi_\Delta\Delta^2/\pi^2)(aM/\mu^2)d\Omega,\\&\qquad\text{(charged meson theory)}\\&=(2/25.3)(g'^2/4\pi)(e\phi_\Delta\Delta^2/\pi^2)(aM/\mu^2)d\Omega,\\&\qquad\text{(symmetric meson theory)}\end{aligned}$$

where a is an average scattering length, $p_1a_1+p_2a_2+\cdots+p_na_n$, for all isotopes. The Δth fourier component of the scattering potential, ϕ_Δ, is conveniently written in terms of the form factor, f, for an atom with Z electrons of charge $-e$, distributed in space with a density $\rho(\mathbf{r}')$.

$$\begin{aligned}\phi_\Delta&=-Ze\int e^{-i\Delta\cdot\mathbf{r}}d\mathbf{r}\int d\mathbf{r}'\rho(\mathbf{r}')/|\mathbf{r}-\mathbf{r}'|\\&=-(4\pi Ze/\Delta^2)f.\end{aligned}$$

We have then for the change in cross section

$$\begin{aligned}\Delta\sigma d\Omega&=-0.632Z\alpha(g^2/4\pi)(aM/\mu^2)(f/4\pi)d\Omega\\&\qquad\text{(charged meson theory)}\\&=-1.26Z\alpha(g'^2/4\pi)(aM/\mu^2)(f/4\pi)d\Omega\\&\qquad\text{(symmetric meson theory).}\end{aligned}\quad(15)$$

The functional dependence exhibited in (15) follows from (14). The numerical coefficient depends weakly on the mass ratio (M/μ). The above value is for $M/\mu=6.12$.

The experiments performed at Columbia and at Chicago provide us with two quantities to compare with theoretical results. Havens, Rabi, and Rainwater give points[7] for the change in the total cross section as a function of the wave-length of the incident neutron for scattering by lead. Fermi and Marshall give the asymmetry in the differential cross section for scattering by xenon atoms as

$$\frac{\sigma(135°)-\sigma(45°)}{\sigma(135°)}=0.0005\pm0.0085.\quad(16)$$

To compare with the Columbia result we introduce a scattering length $a=9.06\times10^{-13}$ cm for lead.[8] An expression for the integrated form factor as a function of incident neutron wave-length is obtained from the graph on page 148 of Compton and Allison.[9] The theoretical curves, for $g^2/4\pi=0.30$, and $g'^2/4\pi=0.30$, appear in Fig. 2 together with the experimental points. The calculated formula is consistent with experiment in indicating an *attraction* between neutrons and electrons and in displaying a wave-length variation characteristic of the atomic form factor.

No estimate of error is supplied in the report of this experiment; the experimental points were obtained only after application of large corrections which were probably valid but which could not be independently checked. In view of this, and of the theoretical uncertainties associated with this calculation, the order of agreement indicated in Fig. 2 must be considered satisfactory.

To compare with the Chicago experiment, we obtain an asymmetry

$$\begin{aligned}\frac{\sigma(135°)-\sigma(45°)}{\sigma(135°)}&=0.00206,\text{ (charged meson theory)}\\&=0.00412,\text{ (symmetric meson theory),}\end{aligned}\quad(17)$$

where we have taken from the paper of Fermi and Marshall[2] $f(45°)=0.776$ and $f(135°)=0.515$ as form factors for Xe, and 4.4 barns as its cross section. These results are larger than the observed asymmetry, but well within the limits of experimental uncertainty.

6. SPIN-FLIP CROSS SECTION

We calculate the value of matrix element (11) for the case in which the scattered neutron has its spin flipped. Again, as in (12), the leading order terms are proportional to the square of the neutron momentum. Contributions from schemes I_a, IV_a, II_b, IV_b, I_c, and IV_c, according to which the static field creates, scatters, or annihilates mesons, are neglected as higher order in (K_0/M). This follows from (6) where the β-matrix,

[6] We use the definition and sign convention of E. Fermi and L. Marshall, Phys. Rev. 71, 666 (1947).

[7] See reference 1, p. 635.

[8] This is the value obtained in the most recent determination by Shull and Wollan (unpublished). It corresponds to a coherent scattering cross section of 10.3b for lead.

[9] A. H. Compton and S. K. Allison, *X-rays in Theory and Experiment* (D. Van Nostrand and Company, Inc., New York, 1938).

through which the neutrons and protons are coupled, does not contribute in leading order to a spin-flip process. The electric scattering cross section with spin flip for a charged meson theory is evaluated numerically for $M/\mu=6.12$:

$$\sigma_{\text{flip}}d\Omega=5.06(g^2/4\pi)^2\phi_\Delta K_0^4|(\mathbf{n}_0\times\mathbf{n}_f)\times\mathbf{n}_{sp}|^2d\Omega \quad 10^{-33}\text{ cm}^2.$$

$\mathbf{n}_0$ and $\mathbf{n}_f$ are unit vectors in the direction of initial and scattered neutron momentum, respectively, and $\mathbf{n}_{sp}$ is a unit vector along the spin axis. We have $\phi_\Delta=4\pi e/\Delta^2$ for scattering by a point charge e. If we put $g^2/4\pi=0.30$, we obtain a total cross section of less than 2×10^{-8} barn for transversely polarized neutrons which are detected by an experimental arrangement in which the neutron counter has an aperture of one minute of arc. (The answer is four times as large according to a symmetric meson theory since transitions schemes involving neutral mesons do not contribute.) This effect is much too small to be detected with present techniques.

The spin flip cross section vanishes for approximate calculations which treat nucleons as Schrödinger-Pauli particles or as infinitely heavy sources (no recoil).

7. DISCUSSION

The interaction of neutrons with electrons has been calculated. The neutron is regarded as one state of a Dirac nucleon which is coupled to a scalar meson field. The mechanism of the interaction is assumed to be the electrostatic coupling between the Coulomb field of the electrons and the virtual protons, pairs, and mesons which, according to field theory, exist in virtual intermediate states of the neutron. Scalar meson fields with charged particles only, and with a symmetric mixture of charged and neutral mesons have been considered. For both cases, qualitative agreement with experiment is established.

The greatest uncertainty in the assignment of a number to our formula for comparison with experiment arises from the choice of 0.30 as the value for the meson-nucleon coupling constant, $g^2/4\pi$. This is the approximate value indicated for a static interaction between two nucleons of the form of the Yukawa potential as derived from the scalar meson theory. We know, however, that the scalar theory used here does not correctly describe the deuteron, particularly as regards the spin dependence of the interaction. In fact there is no satisfactory theory of the deuteron as yet based on any assumed coupling. This is probably because the nucleon recoils have not been taken adequately into account in such calculations and important modifications, even of a qualitative nature, may be expected when account of such recoil is taken.

The static interactions derived from a pseudoscalar meson theory have spin dependences which seem suggestive of the types that may operate in the deuteron. It is therefore worth while to repeat the calculation of this paper for pseudoscalar mesons, although the difficulty of adjusting the coupling constant will be just as serious as for the scalar case.

To transform our calculations to a corresponding one in which pseudoscalar mesons are coupled to the nucleon field with pseudoscalar coupling, we simply replace g by $-iG\gamma_5$, where $\gamma_5=\gamma_1\gamma_2\gamma_3\gamma_4$ is a Dirac matrix appearing between the spinor functions of the neutron and proton fields, in Eqs. 1 and 2. The quantization procedure is unaltered. The result corresponding to (13) is

$$M.E.=(1/287)(G^2/4\pi)(e\phi_\Delta/\pi L^3)(\Delta^2/\mu^2). \quad (18)$$

Following Villars,[10] Dyson,[11] and Luttinger,[12] we take $G^2/4\pi=36$, and obtain a change in cross section, $\Delta\sigma$, 10.6 times as large as those given in Eq. (15) for the scalar theory.

We note from Eqs. (16) and (17) that the above result (18) for pseudoscalar mesons exceeds, by a factor of 2.5, the upper limit for this effect placed by Fermi and Marshall.[2] This would appear to argue against the pseudoscalar theory, but for the reasons noted above definite conclusions cannot be drawn until the situation regarding the two nucleon problem is clarified.

Note added in proof: The value $G^2/4\pi\approx4$ suggested by Bethe at the Spring 1949 meetings in Washington, D. C. (B.A.P.S., vol. 24, no. 4) resolves the discrepancy between (18) and (16) and indicates approximately the same change in cross section on the basis of a pseudoscalar calculation as that given by the scalar theory.

APPENDIX

We indicate briefly the covariance of our formalism for describing the interaction of quantized meson and Dirac nucleon fields. A charge-current conservation equation is exhibited. We consider here a charged scalar meson field.

In the absence of external electromagnetic fields, the Lagrangian density, canonically conjugate variables, and Hamiltonian density are those given in Section 2 of the text (Eqs. (1) and (2)) with $A_\mu=0$. The canonical equations of motion take the form

$$\begin{aligned}
&\dot\psi=\pi^*;\quad \dot\psi^*=\pi;\\
&\dot\pi=(\Delta-\mu^2)\psi^*-g(\Psi_P^*\beta\Psi_N);\\
&\dot\pi^*=(\Delta-\mu^2)\psi-g(\Psi_N^*\beta\Psi_P);\\
&\dot\Psi_P=-(\boldsymbol{\alpha}\cdot\mathbf{grad}+iM\beta)\Psi_P-ig\beta\Psi_N\psi;\\
&\dot\Pi_P=-(\mathbf{grad}\Pi_P\cdot\boldsymbol{\alpha}-iM\Pi_P\beta)-g\Psi_N^*\beta\psi^*;
\end{aligned} \quad (a)$$

with equations analogous to the last two for $\dot\Psi_N$ and $\dot\Pi_N$. Commutation relations (4) and (5) are introduced in order that the meson field satisfy Bose statistics and the nucleon fields satisfy Fermi statistics. We wish to demonstrate that these commutator relations are of covariant form. That is, the values of the various commutators and anticommutators corresponding to simultaneous events in one Lorentz frame should imply the same values for simultaneous events in an other. To study this question, we use the method of Heisenberg and Pauli.[3] We consider, for example, the quantity

$$[\Pi_{N\sigma}(\mathbf{r},t),\Psi_{P\nu}(\mathbf{r}',t')]_+$$

which has been assumed zero for $t=t'$. If we now assume that t and t' are nearly equal, we can calculate the value of this anticommutator bracket to first order in $(t-t')$ by the use of the equations of motion (a) plus the various commutation relations

[10] F. Villars, Helv. Phys. Acta **XX**, 476 (1947).
[11] F. J. Dyson, Phys. Rev. **73**, 929 (1948).
[12] J. M. Luttinger, Helv. Phys. Acta **XXI**, 483, (1948).

assumed above to hold for simultaneous events. We obtain neglecting terms in $(t-t')^2$,

$$[\Pi_{N\sigma}(\mathbf{r},t),\Psi_{P\nu}(\mathbf{r}',t')]_+=g\psi(\mathbf{r})\beta_{\sigma\nu}\{(t-t')\delta(\mathbf{r}-\mathbf{r}')\}. \quad \text{(b)}$$

The quantity in the brace is, to first order, an invariant,† having the value zero for $|t-t'|<|\mathbf{r}-\mathbf{r}'|$. Consider the system in which the events $(\mathbf{r},t)$ and $(\mathbf{r}',t')$ transform into simultaneous events $(\bar{\mathbf{r}},\bar{t})$ and $(\bar{\mathbf{r}}',\bar{t})$. This will represent an infinitesimal Lorentz transformation, since it was assumed that t and t' were nearly equal. The expression on the left of (b) therefore takes on the transformed value

$$[\Pi_{N\sigma}(\bar{\mathbf{r}},\bar{t}),\Psi_{P\nu}(\bar{\mathbf{r}}',\bar{t})]_+=0.$$

The linearity property of the Lorentz transformation then permits us to write in the transformed system

$$[\Pi_{N\sigma}(\bar{\mathbf{r}},\bar{t}),\bar{\Psi}_{P\nu}(\bar{\mathbf{r}}',\bar{t})]_+=0,$$

verifying covariance of this relation for infinitesimal Lorentz transformations. Since a finite transformation can be represented as a sequence of infinitesimal ones, the general covariance follows.

† It is the small argument expansion of the invariant D function of Jordan and Pauli.

The proofs of the covariance of the other relations follow similar patterns and will not be given. We remark only that it does not seem possible to quantize using other commutation rules than those assumed in the text to operate between two field quantities, each belonging to a *different* type of field.

Charge and Current

In the absence of external electromagnetic fields we define charge and current densities as follows:

$$\rho^\mu=-ie(\psi\pi-\psi^*\pi^*);$$
$$\mathbf{s}^\mu=ie(\psi\ \mathbf{grad}\psi^*-\psi^*\ \mathbf{grad}\psi);$$
$$\rho^M=-ie(\Pi_P\Psi_P);$$
$$\mathbf{s}^M=-ie(\Pi_P\boldsymbol{\alpha}\Psi_P).$$

Then, by virtue of the Hamiltonian density and commutation rules that have been assumed, we obtain the differential conservation law:

$$\partial(\rho^\mu+\rho^M)/\partial t+\mathbf{div}(\mathbf{s}^\mu+\mathbf{s}^M)=0.$$

Here, as always,

$$\partial\rho/\partial t=i[\textstyle\int\mathcal{H}d^3x,\rho].$$

PHYSICAL REVIEW VOLUME 76, NUMBER 2 JULY 15, 1949

Correlated Probabilities in Multiple Scattering*

W. T. Scott
Brookhaven National Laboratory, Upton, New York, and Smith College, Northampton, Massachusetts

(Received February 9, 1949)

The correlated probabilities of lateral and angular displacements of cloud-chamber tracks, resulting from multiple small-angle scattering, have been calculated for several cases of interest. The results are applicable to curvatures and other measurements taken in the presence of a magnetic field. The usual Gaussian-type scattering law has been used in the form of the fundamental correlated distribution function derived by Fermi. One direct application of this function is to the effect of scattering on angle measurements in nuclear "stars."

A "three-point formula" is derived, involving a correlated distribution of two successive lateral displacements with the resultant angular displacement. The distribution of scattering-produced curvatures, originally derived by Bethe, is calculated. A "four-point formula" allows a quantitative discussion of the tendency of scattered tracks to appear circular rather than skewed or S-shaped.

Finally, a formula is derived for the distribution of the successive chord angles for a track observed at several points, and used to discuss the best method of averaging the observations to reduce scattering-produced curvature errors. The error produced by scattering is not appreciably diminished by taking the best mean for an observation of the track at a large number of points, instead of a single observation of chord and sagitta (three points).

INTRODUCTION

THE multiple scattering of charged particles is of considerable importance for several types of cloud-chamber experiments, and has been treated by various authors.[1] Several problems of interest involving correlated probabilities of angular and lateral displacements may, in fact, be discussed using a fundamental distribution function due to Fermi.[2] It is the purpose of this paper to derive and discuss some of these results, in particular, those dealing with the measurement of track curvatures in magnetic fields.

I. THE FUNDAMENTAL SOLUTION

We proceed to derive the fundamental distribution function[2,3]

$$W(y,\eta|x)dyd\eta=\frac{\lambda\sqrt{3}}{2\pi x^2}\exp\left\{-\frac{\lambda}{x}\left[\eta^2-\frac{3\eta y}{x}+\frac{3y^2}{x^2}\right]\right\}, \quad (1)$$

which gives the probability that a particle in traversing a distance x in a scattering material suffers a lateral displacement between y and $y+dy$ projected on a plane of observation containing x, and a net change of direction between η and $\eta+d\eta$ projected on the same plane.

The equation satisfied by this function may be derived

* Research carried out at Brookhaven National Laboratory under the auspices of the AEC.

[1] H. A. Bethe, Phys. Rev. **70**, 821 (1946); R. Richard-Foy, J. de phys. et rad. **7**, 370 (1946). Other references are quoted in these papers.

[2] B. Rossi and K. Greisen, Rev. Mod. Phys. **13**, 240 (1941).

[3] We use the vertical bar | to separate given entities on the right from entities whose distribution is under consideration on the left, and shall in this way use the same function symbol W to denote several different distribution functions.

from the general Boltzmann equation,[4] but it is simpler to eliminate consideration of time and velocity and deal only with the deflections resulting from scattering.

We consider the angles involved to be small, i.e., $\sin\theta\cong\theta$ and $\cos\theta\cong 1$. We further ignore any change of energy of the particle during its passage through the material in question. We shall start with a three-dimensional distribution, which is easily reduced to the plane projection in the case of small angles.

Let $W(y, z, \eta, \zeta|x)dydzd\eta d\zeta$ denote the probability that at x, the coordinates of the particle are (y, z) and the projections of the tangent to the track in the yx and zx planes make angles η and ζ, respectively, with the x axis. Since the angles are small, $\eta^2+\zeta^2=\theta^2$, where θ is the angle between tangent and x axis.

$W(y, z, \eta, \zeta|x)$ may be derived from $W(y', z', \eta', \zeta'|x-dx)$ by considering that if no scattering occurs in dx, then $y-y'=dy=\eta dx$, $z-z'=dz=\zeta dx$, $\eta=\eta'$ and $\zeta=\zeta'$; if a scattering occurs from (η', ζ') to (η, ζ), the scattering probability is proportional to dx and transport terms ηdx and ζdx are second order and may be neglected; and the probability of more than one scattering in dx may also be neglected. The resulting equation is

$$\frac{\partial W}{\partial x}+\eta\frac{\partial W}{\partial y}+\zeta\frac{\partial W}{\partial z}=\int_0^{2\pi}d\beta\int_0^{\pi}F(\theta)\sin\theta d\theta \times[W(y, z, \eta-\theta\cos\beta, \zeta-\theta\sin\beta|x)-W(y, z, \eta, \zeta|x)], \quad (2)$$

where we have written $\eta-\eta'=\theta\cos\beta$, and $\zeta-\zeta'=\theta\sin\beta$. $F(\theta)$ is the probability per unit track length and unit solid angle of a single scattering through angle θ.

Making the usual Fokker-Planck approximation of expanding the expression in brackets in a Taylor's series and retaining no terms beyond the second derivatives, we find easily (setting $\sin\theta=\theta$)

$$\frac{\partial W}{\partial x}+\eta\frac{\partial W}{\partial y}+\zeta\frac{\partial W}{\partial z}=\frac{1}{\lambda}\left[\frac{\partial^2 W}{\partial\eta^2}+\frac{\partial^2 W}{\partial\zeta^2}\right], \quad (3)$$

where

$$1/\lambda=\tfrac{1}{4}\int_0^{\pi}\theta^3F(\theta)d\theta=\tfrac{1}{4}\langle\theta^2\rangle_{Av}. \quad (4)$$

λ is a characteristic length describing the amount of scattering, and $\langle\theta^2\rangle_{Av}$ is the mean square angle of scattering per unit path thickness and is given by[5]

$$\frac{4}{\lambda}=\langle\theta^2\rangle_{Av}=\frac{8\pi e^4Z^2Z'^2N}{p^2v^2}\ln\frac{150p}{mcZ^{\frac{1}{3}}}\ \text{cm}^{-1}. \quad (5)$$

Ze is the charge of the scattering nucleus, and N is the number of nuclei per cm^3; $Z'e$ is the charge of the scattered particle, while its mass, momentum, and velocity are denoted, respectively, by m, p, and v.

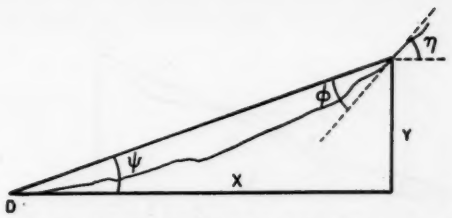

FIG. 1. Illustrating the basic distribution (1) or (10).

Equation (3) is easily separable into two equations for the two projections. Writing

$$W(y, z, \eta, \zeta|x)=W(y, \eta|x)W(z, \zeta|x), \quad (6)$$

we find

$$\left(\frac{\partial}{\partial x}+\eta\frac{\partial}{\partial y}\right)W(y, \eta|x)=\frac{1}{\lambda}\frac{\partial^2W(y, \eta|x)}{\partial\eta^2}. \quad (7)$$

We take as the boundary condition

$$W(y, \eta|0)=\delta(y)\delta(\eta), \quad (8)$$

corresponding to a track passing through the origin tangent to the x axis.

The solution may be found in a straightforward way by applying a Laplace transform in x, and simultaneously Fourier transforms in y and η to Eq. (7). A first-order ordinary differential equation results that is easily soluble, and all inversion integrals can be carried out. The result is Eq. (1). That (1) is the solution of (6) is evident on substitution. That it is normalized is evident on integration over y and η, each from $-\infty$ to $+\infty$. That it satisfies (8) is evident on writing

$$Wdyd\eta=F(Y, \mu)dYd\mu=\left(\frac{\sqrt{3}}{2\pi}\right)dYd\mu\ \exp\{-\mu^2+3\mu Y-3Y^2\}, \quad (8a)$$

where $Y=y\lambda^{\frac{1}{2}}/x^{\frac{3}{2}}$, and $\mu=\eta\lambda^{\frac{1}{2}}/x^{\frac{1}{2}}$ are dimensionless variables. Since F is independent of x, the distribution in Y and μ is constant, i.e., the distribution has a constant *shape* as well as area. The scale factors vary with x so as to yield a very sharply peaked function of y and η as $x\to 0$, approaching $\delta(y)\delta(\eta)$.

In case the original direction of the track makes an angle η_0 with the x direction, we must replace η by $\eta-\eta_0$ and y by $y\cos\eta_0-x\sin\eta_0\cong y-\eta_0x$ in (1). This result is also obtained by writing $\delta(\eta-\eta_0)$ for $\delta(\eta)$ in (8). Hence,

$$W(y, \eta|x; 0, 0, \eta_0)=\left(\frac{\lambda\sqrt{3}}{2\pi x^2}\right)\exp\left\{-\frac{\lambda}{x}\left[(\eta-\eta_0)^2-\frac{3}{x}(\eta-\eta_0)(y-\eta_0x)+\frac{3}{x^2}(y-\eta_0x)^2\right]\right\}. \quad (9)$$

A convenient, symmetric way of writing Eq. (1) is to set $y/x=\psi$, the angle between the chord and the original

[4] Bethe, Rose, and Smith, Proc. Am. Phil. Soc. **78**, 573 (1938).

[5] S. Goudsmit and J. L. Saunderson, Phys. Rev. **57**, 24 (1940), Eq. (9); and Phys. Rev. **58**, 36 (1940), Eqs. (2) and (4), for a Thomas-Fermi atom. For a Wentzel potential the coefficient 150 is to be replaced by 166; to agree with Bethe, (reference 1) and Rossi and Greisen, (reference 2), it is to be replaced by $137\theta_{\max}$. Our λ is the w^2 of reference 2, Eq. (6).

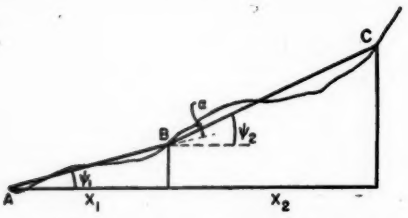

FIG. 2. Illustrating the three-point formula (15).

tangent (see Fig. 1), and $\phi=\eta-\psi$, the angle between the tangent at (x, y) and the chord. The probability of ψ and ϕ is thus,

$$U(\psi, \phi|x)d\psi d\phi=\left(\frac{\lambda\sqrt{3}}{2\pi x}\right)\times\exp\left\{-\frac{\lambda}{x}[\psi^2-\psi\phi+\phi^2]\right\}d\psi d\phi. \quad (10)$$

II. THE EFFECT OF A MAGNETIC FIELD

If a magnetic field H is added perpendicular to the plane of observation, and if ρ denotes the radius of curvature of the given particle in a vacuum, we can readily derive the diffusion equation for the scattered motion in the presence of a gas. In fact, in dx the particle is deflected magnetically by an angle $d\eta=dx\sec\eta/\rho\cong dx/\rho$, which shifts the distribution progressively toward larger values of η. The resulting equation becomes

$$\frac{\partial W_H}{\partial x}+\eta\frac{\partial W_H}{\partial y}+\frac{1}{\rho}\frac{\partial W_H}{\partial\eta}=\frac{1}{\lambda}\frac{\partial^2 W_H}{\partial\eta^2}.$$

Now, if we set $W_H(y, \eta|x)=f(y', \eta'|x)$, where $y'=y-(x^2/2\rho)$ and $\eta'=\eta-(x/\rho)$, we find readily

$$\frac{\partial f}{\partial x}+\eta'\frac{\partial f}{\partial y'}=\frac{1}{\lambda}\frac{\partial^2 f}{\partial\eta'^2}$$

which is just Eq. (7). Further, $W_H(y, \eta|0)=f(y', \eta'|0)=f(y, \eta|0)=\delta(y)\delta(\eta)$, so that $f=W(y, \eta|x)$ given by Eq. (1).

The curve $y_H=x^2/2\rho$, $dy_H/dx=x/\rho$ is a parabola, i.e., a circle within the small angle approximations, of curvature $1/\rho$, tangent to the original direction of the particle. That is, all the results of this paper for $H=0$ may be applied to the case $H\neq 0$, if x is measured along the arc of a circle of radius ρ, and y and η are measured with respect to that circle. Since curvatures in the small angle approximations are linear functions of ordinates y, the magnetic curvature $1/\rho$ is simply to be added to the scattering produced curvatures.

III. CONSEQUENCES OF EQ. (1)

Inasmuch as $\eta^2-3\eta\psi+3\psi^2=(\eta-\frac{3}{2}\psi)^2+\frac{3}{4}\psi^2$, we find on integration over η,

$$W(y|x; 0, 0, 0)=\left(\frac{3\lambda}{4\pi x^3}\right)^{\frac{1}{2}}\exp\left\{-\frac{3\lambda y^2}{4x^3}\right\} \quad (11a)$$

or

$$W(\psi|x; 0, 0, 0)=\left(\frac{3\lambda}{4\pi x}\right)^{\frac{1}{2}}\exp\left\{-\frac{3\lambda}{4x}\psi^2\right\}, \quad (11b)$$

and using the relation derived from elementary probability theory that $W(y, \eta|x)=W(\eta|y, x)W(y|x)$,

$$W(\eta|x, y; 0, 0, 0)=\left(\frac{\lambda}{\pi x}\right)^{\frac{1}{2}}\exp\left[-\frac{\lambda}{x}\left(\eta-\frac{3y}{2x}\right)^2\right]. \quad (12)$$

The mean value of η is $\langle\eta\rangle_{Av}=3y/2x=3\psi/2$, which implies that once a displacement of angle ψ has occurred, the particle is likely to have a direction that will increase this displacement, making evident the correlated nature of the distribution (1).

Similarly, we may integrate over y and find

$$W(\eta|x; 0, 0, 0)=(\lambda/4\pi x)^{\frac{1}{2}}\exp(-\lambda\eta^2/4x). \quad (13)$$

This is essentially the Gaussian scattering formula of Williams.[6] It yields the result that $\langle\eta^2\rangle_{Av}=2x/\lambda$. Of course $\langle\zeta^2\rangle_{Av}$ is identical, so that $\langle\eta^2\rangle_{Av}+\langle\zeta^2\rangle_{Av}=4x/\lambda$ in agreement with (4). It is to be noted that the distribution in displacement $\psi=y/x$ is sharper by a factor $\sqrt{3}$ than the distribution in deflection η.

Equation (10) may be interpreted as the combined probability of a direction ψ at (0, 0) and a direction ϕ at $(x, 0)$, if the particle is known to pass through those two points. Integrated over either ψ or ϕ, it yields the form (11b), which may thus be interpreted as the likelihood of a scattering-produced error in measuring the direction of emergence of a nuclear reaction product observed in a cloud chamber or photographic emulsion.* The mean square error is $2x/3\lambda$; if, in addition, there is an experimental root-mean-square error of ϵ in the location of each end of the track, we have by the usual rule to add $2(\epsilon/x)^2$. The minimum value of $(2x/3\lambda)+2(\epsilon^2/x^2)$ occurs for $x^3=6\lambda\epsilon^2$.

IV. THREE-POINT FORMULAS

For consideration of tracks observed at three points, we calculate the probability that the particle pass through (x_1+x_2, y) in direction η if it is known to pass through (0, 0) and (x_1, y_1), using (9) or (11b):

$$W(y, \eta|x_1+x_2; x_1, y_1; 0, 0)$$
$$=\int_{-\infty}^{\infty}d\eta' W(\eta'|x_1, y_1; 0, 0)W(y, \eta|x_1+x_2; x_1, y_1, \eta')$$
$$=\left\{\frac{3\lambda}{2\pi x_2[x_2(4x_1+3x_2)]^{\frac{1}{2}}}\right\}\exp\left\{-\lambda\left[\frac{3(x_1+x_2)}{x_2(4x_1+3x_2)}\times\left(\eta+\frac{y_1x_2}{2x_1(x_1+x_2)}-\frac{(2x_1+3x_2)(y-y_1)}{2x_2(x_1+x_2)}\right)^2+\frac{3}{4(x_1+x_2)}\left(\frac{y-y_1}{x_2}-\frac{y_1}{x_1}\right)^2\right]\right\}. \quad (14)$$

[6] E. J. Williams, Proc. Roy. Soc. **A168**, 531 (1939).

* I.e., $W(\psi|x; 0, 0, 0)$ may be written as $W(\psi|x, 0; 0\,0,)$. A formula for $W(\psi|x, y; 0, 0)$ is also easily obtainable.

If we set $y_1/x_1=\eta_0$, and then let x_1 and y_1 approach zero, we get in the limit $W(y_2, \eta|x_2; 0, 0, \eta_0)$. If, however, $x_1=x_2=x_3$,

$$W(y, \eta|2x; x, y_1; 0, 0)$$
$$=\left[\frac{3\lambda}{2\pi x^2(7)^{\frac{1}{2}}}\right]\exp\left\{-\frac{\lambda}{x}\left[\frac{6}{7}\left(\eta+\frac{1}{4}\frac{y_1}{x}-\frac{5}{4}\frac{y-y_1}{x}\right)^2+\frac{3}{8}\left(\frac{y-y_1}{x}-\frac{y_1}{x}\right)^2\right]\right\}. \quad (14a)$$

Integrating (14) over η, we obtain

$$W(y|x_1+x_2; x_1, y_1; 0, 0)$$
$$=\left[\frac{3\lambda}{4\pi x_2^2(x_1+x_2)}\right]^{\frac{1}{2}}\times\exp\left\{\frac{-3\lambda}{4(x_1+x_2)}\left(\frac{y-y_1}{x_2}-\frac{y_1}{x_1}\right)^2\right\}. \quad (15)$$

If we write $y_1/x_1=\psi_1$; $(y-y_1)/x_2=\psi_2$, the parenthesis in the exponent is $\psi_2-\psi_1$, or α, the angle between the track chords. (See Fig. 2.) Now, the curvature c of a circle through the three points is $\sin\alpha/\overline{AC}$, which in our approximation of small angles is $c=\alpha/(x_1+x_2)$. Hence, from (15) we may find the probability of observing a curvature c to $c+dc$ by measuring the coordinates of three points on a track:

$$P(c)dc=[3\lambda(x_1+x_2)/16\pi]^{\frac{1}{2}}\times\exp\{-3\lambda(x_1+x_2)c^2/16\}dc, \quad (16)$$

which is the result of Bethe,[1] and is independent of the ratio x_2/x_1 of the two parts of the track.

The mean square curvature is thus $\langle c^2\rangle_{Av}=8/3\lambda(x_1+x_2)$. If, as before, an r.m.s. error ϵ in measurement is made at each point, we may calculate the resulting curvature "error." Using a Gaussian error curve for the measurements and integrating over the "true" ordinates at each point, we get a distribution in c yielding

$$\langle c^2\rangle_{Av}=\frac{8}{3\lambda(x_1+x_2)}+\frac{8\epsilon^2}{(x_1+x_2)^2}\left(\frac{1}{x_1^2}+\frac{1}{x_1x_2}+\frac{1}{x_2^2}\right). \quad (17)$$

Equation (16) may be written as the probability of finding a sagitta u at x_1, when the chord of the track has length x_1+x_2, since $c=2u/x_1x_2$:

$$P(u)du=\left[\frac{3\lambda(x_1+x_2)}{4\pi x_1^2x_2^2}\right]^{\frac{1}{2}}\exp\left\{\frac{-3\lambda(x_1+x_2)u^2}{4x_1^2x_2^2}\right\}du.^7$$

We may now derive, in a similar manner as for Eq. (12), the distribution of track directions at point C when a given y or curvature c is observed. We set $y_1=0$ for simplicity.

$$W(\eta|x_1+x_2, y; x_1, 0; 0, 0)=\left[\frac{3\lambda(x_1+x_2)}{\pi x_2(4x_1+3x_2)}\right]^{\frac{1}{2}}\times\exp\left\{\frac{-3\lambda(x_1+x_2)}{x_2(4x_1+3x_2)}\cdot\left(\eta-\frac{2x_1+3x_2}{2x_2(x_1+x_2)}y\right)^2\right\}. \quad (18)$$

The mean value is

$$\langle\eta\rangle_{Av}=\frac{y}{x_2}\left(\frac{2x_1+3x_2}{2x_1+2x_2}\right)=\psi_2\left[1+\frac{x_2}{2(x_1+x_2)}\right]$$
$$=(\tfrac{3}{4}x_2+\tfrac{1}{2}x_1)c. \quad (19)$$

A circular track through the three points would have a slope $\eta_c=(x_2+\frac{1}{2}x_1)c$ at (x_1+x_2, y). We see then that once a track has been "curved" by scattering, it is likely to maintain this same direction of curvature, but of a lesser amount (Fig. 3). Further discussion is postponed to the next section.

V. FOUR-POINT FORMULAS

In a similar fashion to the derivation of Eq. (14), that expression along with (1) may be combined to find a distribution in y and η at $x=x_1+x_2+x_3$, when the track is known to pass through (0, 0), $(x_1, 0)$, and (x_2, y'). For simplicity, write $y'/x_2=\psi_2$ and $(y-y')/x_3=\psi_3$, and let Δ signify $4(x_1+x_2)(x_2+x_3)-x_2^2$. The result is

$$W(y, \eta|x_1+x_2+x_3; x_1+x_2, y'; x_1, 0; 0, 0)$$
$$=\left[\frac{9\lambda^2(x_1+x_2)}{4\pi^2x_3^3(\Delta-x_1x_3-x_2x_3)}\right]^{\frac{1}{2}}\cdot\exp\left\{\frac{-3\lambda\Delta}{4x_3(\Delta-x_1x_3-x_2x_3)}\times\left[\eta-\frac{\psi_3}{\Delta}(\Delta+2x_1x_3+2x_2x_3)+\frac{\psi_2}{\Delta}(2x_1x_3+3x_2x_3)\right]^2-\frac{3\lambda(x_1+x_2)}{\Delta}\left[\psi_3-\psi_2\frac{2x_1+3x_2}{2(x_1+x_2)}\right]^2\right\}. \quad (20)$$

We then find readily

$$W(y|x_1+x_2+x_3; x_1+x_2, y'; x_1, 0; 0, 0)$$
$$=\left[\frac{3\lambda(x_1+x_2)}{\pi x_3^2\Delta}\right]^{\frac{1}{2}}\exp\left\{\frac{-3\lambda(x_1+x_2)}{\Delta}\times\left[\psi_3-\frac{\psi_2(2x_1+3x_2)}{2(x_1+x_2)}\right]^2\right\}. \quad (21)$$

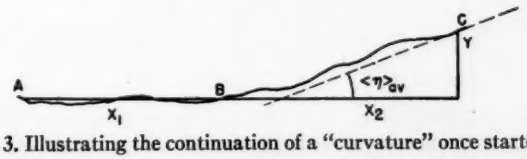

FIG. 3. Illustrating the continuation of a "curvature" once started.

[7] See R. Richard-Foy (reference 1).

This formula yields Eq. (14) when $\psi_3=\eta$ and $x_3\to 0$. One sees immediately that $\langle\psi_3\rangle_{Av}$ is the same as $\langle\eta\rangle_{Av}$ for the three-point formula (Eq. (19)), as it evidently should be. An expression for the distribution in η when the track is observed to pass through four points is given by the ratio of (20) to (21).

Equation (21) is more useful if curvatures are used instead of ψ_3 and ψ_2. Let $c_a=2\psi_2/(x_1+x_2)$ be the curvature for points ABC (Fig. 4) and $c_b=2(\psi_3-\psi_2)/(x_2+x_3)$ be the curvature for points BCD. Then we have the distribution in c_b when c_a is given,

$$P(c_b|c_a;x_1,x_2,x_3)dc_b=(x_2+x_3)\left[\frac{3\lambda(x_1+x_2)}{\pi\Delta}\right]^{\frac{1}{2}}\cdot\exp\left\{\frac{-3\lambda(x_1+x_2)(x_2+x_3)^2}{4\Delta}\times\left[c_b-\frac{x_2c_a}{2(x_2+x_3)}\right]^2\right\}dc_b. \quad (22)$$

We see that $\langle c_b\rangle_{Av}=x_2c_a/2(x_2+x_3)$; if $x_2=x_3$, $\langle c_b\rangle_{Av}=c_a/4$, which bears out the assertion at the end of Section III. If, further, $x_2=x_3=x_1=x$, $\langle[c_b-(c_a/4)]^2\rangle_{Av}=5\lambda x/4$, or just slightly less than the value $4\lambda x/3$ for Eq. (16).

We may calculate the probability that $c_b>0$, and so obtain the probability that the track be of C-type rather than S-type[1] for a given value of c_a. For $x_1=x_2=x_3=x$, we have

$$P_c=\left(\frac{2\lambda x}{5\pi}\right)^{\frac{1}{2}}\int_{-c_a/4}^{\infty}\exp\left(\frac{-2\lambda x c^2}{5}\right)dc=\tfrac{1}{2}+erf\left(\frac{c_a}{(30)^{\frac{1}{2}}c_{\text{r.m.s.}}}\right). \quad (23)$$

The result is most easily expressed as a function of $c_a/c_{\text{r.m.s.}}$ where $c_{\text{r.m.s.}}=4\lambda x/3$ is the root-mean-square curvature for three points, from Eq. (16), and is generally readily available. Figure 5 gives the resulting graph.

Using (22) and (16), we can find the combined probability of c_a and c_b,

$$P(c_a,c_b|x_1,x_2,x_3)=P(c_b|c_a;x_1,x_2,x_3)P(c_a|x_1,x_2)=\left[\frac{3\lambda(x_1+x_2)(x_2+x_3)}{8\pi\Delta^{\frac{1}{2}}}\right]\cdot\exp\left\{\frac{-3\lambda(x_1+x_2)(x_2+x_3)}{4\Delta}\times[(x_1+x_2)c_a^2-x_2c_ac_b+(x_2+x_3)c_b^2]\right\}. \quad (24)$$

The symmetry of this expression shows that large curvatures are equally likely to occur at either end of the track. Let us, however, study the distribution in $r=c_b/c_a$. If $r>0$, the curve is C-type: $r<0$ yields an S-type curve. The curvature increases or decreases accordingly as $r>1$ or $r<1$. Using c_a and r as independent variables, we can integrate over c_a and find

$$p(r)dr=\frac{dr}{\pi}\frac{d}{dr}\tan^{-1}\left[\frac{2(x_2+x_3)}{\Delta^{\frac{1}{2}}}\left(r-\frac{x_2}{2(x_1+x_2)}\right)\right]. \quad (25)$$

$\langle r\rangle_{Av}=x_2/2(x_1+x_2)$ which becomes $\frac{1}{4}$ if $x_2=x_3$. The probability that $r>0$ is

$$p_c=\tfrac{1}{2}+(1/\pi)\tan^{-1}(x_2/\Delta^{\frac{1}{2}}); \quad (26)$$

if $x_1=x_2=x_3$, $p_c=0.58$. The probability that $r>1$ is $\frac{1}{2}-(1/\pi)\tan^{-1}(3/\sqrt{15})=\frac{1}{2}p_c=0.29$. That is, 58 percent of tracks curved by scattering are of C-type, and are equally divided between increasing and decreasing curvatures.

Another symmetric way of writing (24) is to use $c_m=(c_a+c_b)/2$ and $D=c_b-c_a$ as independent variables. The bracket in the exponent becomes

$$(x_1+x_2+x_3)c_m^2+Dc_m(x_3-x_1)+\tfrac{1}{4}(x_1+3x_2+x_3)D^2,$$

and it is evident that if $x_1=x_3$, or the track is divided symmetrically, the distributions in c_m and D are mutually independent. In fact, (24) may be written, setting $x_1=x_3$, as the product of two normalized probabilities:

$$P(c_m,D)dc_m dD=P_1(c_m)dc_m P_2(D)dD,$$

$$P_1(c_m)=\tfrac{1}{2}(x_1+x_2)\left[\frac{3\lambda}{\pi(2x_1+3x_2)}\right]^{\frac{1}{2}}\times\exp\left\{\frac{-3\lambda(x_1+x_2)^2c_m^2}{4(2x_1+3x_2)}\right\}, \quad (27)$$

$$P_2(D)=\tfrac{1}{4}(x_1+x_2)\left[\frac{3\lambda}{\pi(2x_1+x_2)}\right]^{\frac{1}{2}}\times\exp\left\{\frac{-3\lambda(x_1+x_2)^2D^2}{16(2x_1+x_2)}\right\}.$$

An important consequence is that *selection of tracks according to a criterion of symmetry, with other factors being equal*—i.e., with D smaller than some limit determined by the errors of measurements—*results in no narrowing of the distribution of scattering-produced curvatures over that obtained in including unsymmetrical tracks.* This does not preclude the use of a symmetry criterion

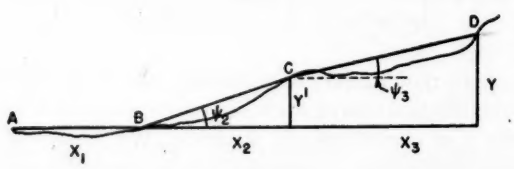

FIG. 4. Illustrating the four-point formula (20).

as a test for freedom from *turbulence* or *convection* errors in a cloud chamber, nor of the use of a mean skewness of a whole set of tracks as a measure of the amount of scattering (see below).

$P_1(c_m)$ in (27) yields the distribution of scattering-produced curvature when the track is observed at four points and the two curvatures are weighted equally. If $x_2=x_1=x$, we find

$$\langle c_m^2\rangle_{Av}=5/6\lambda x=5/2\lambda l, \tag{28}$$

where $l=3x$ is the total track length. The three-point formula (16) yields $\langle c^2\rangle_{Av}=8/3\lambda l$, so that the mean square curvature for four points is smaller by only $\frac{15}{16}$. This result partially justifies the common experimental practice of measuring curvatures by means of a chord and sagitta, rather than by observation of the coordinates of more than three points. At least, that part of the error due to multiple scattering is not materially reduced by more measurements. (See also Section VI below.)

$P_2(D)$ yields a distribution in c_b-c_a, which is independent of any magnetic curvature (Section II). Hence, measurements of D in the presence of a magnetic field for a sufficient number of monoenergetic particles should yield a useful check on the mean scattering (i.e., on the value of λ) and may serve to distinguish scattering-produced skewness from turbulence and convection effects.

$P_1(c_m)$ and $P_2(D)$ may be used jointly to decide the likelihood of error in meson mass-measurements from curvature determinations of apparently perfectly circular tracks of knock-on-electrons.[8]

A modification of the four-point formula is the "internal" probability of observing y' at x_1+x_2 when the particle is known to pass through $(0,0)$, $(x_1,0)$, and $(x_1+x_2+x_3, y)$. The result is best expressed in terms of the curvature c' for points B, C, D (Fig. 4) when c is the (known) curvature for A, B, D.

$$P_{int}(c')dc'=\tfrac{1}{2}(x_2+x_3)\left[\frac{3\lambda(x_1+x_2+x_3)}{\pi\Delta}\right]^{\frac{1}{2}}\cdot\exp\left\{\frac{-3\lambda(x_1+x_2+x_3)}{16\Delta}\times[2(x_2+x_3)c'-(x_2+2x_3)c]^2\right\}. \tag{29}$$

We have $\langle c'\rangle_{Av}=(x_2+2x_3)c/(2x_2+2x_3)=3c/4$ if $x_2=x_3$. This is another indication of the extent to which tracks will appear circular as a result of multiple scattering.

VI. A FORMULA FOR ANY NUMBER OF POINTS

For more than four points on a track, the probability formulas are quite unwieldly. However, if the track is divided into N equal segments x, and only the successive chord angles $\alpha_1, \alpha_2, \cdots\alpha_{N-1}$ are considered (see Fig. 6), an explicit probability distribution may be written down.

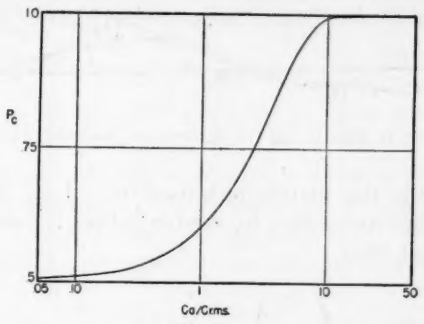

FIG. 5. The probability of C-type tracks as a function of the curvature c_a for the first two-thirds of the track. $c_{r.m.s.}$ is the root-mean-square curvature for the same track length.

We shall start with Eq. (10) for $U(\psi,\phi|x)$, written as a double Fourier transform,

$$U(\psi,\phi|x)=\frac{1}{(2\pi)^2}\int_{-\infty}^{\infty}dt\int_{-\infty}^{\infty}ds\times\exp\left\{-it\psi-is\phi-\frac{x}{3\lambda}(t^2+st+s^2)\right\}. \tag{30}$$

This formula is then applied to each of the N sections. We set

$$\phi_1=\alpha_1-\psi_2;\quad \phi_2=\alpha_2-\psi_3;\quad \cdots\phi_{N-1}=\alpha_{N-1}-\psi_N,$$

and integrate the product of N U's over $\psi_1,\psi_2\cdots\psi_N$, and ϕ_N. All these integrations may be readily carried out by use of the fundamental Fourier integral theorem, yielding

$$W(\alpha_1,\alpha_2,\cdots\alpha_N)=\int_{-\infty}^{\infty}\frac{ds_1}{2\pi}\cdots\int_{-\infty}^{\infty}\frac{ds_{N-1}}{2\pi}\times\exp\left\{-i(s_1\alpha_1+\cdots+s_{N-1}\alpha_{N-1})-\frac{x}{3\lambda}(2s_1^2+s_1s_2+2s_2^2+s_2s_3+2s_3^2+\cdots+s_{N-2}s_{N-1}+2s_{N-1}^2)\right\}.$$

A general and well-known theorem on generalized Gaussian functions[9] states that

$$\int_{-\infty}^{\infty}ds_1\cdots\int_{-\infty}^{\infty}ds_n\exp[-\mu A_{jk}s_js_k-is_j\alpha_j]=\left(\frac{\pi}{\mu}\right)^{n/2}[\det|A_{jk}|]^{-\frac{1}{2}}\exp\left\{\frac{-A_{lm}{}^{-1}\alpha_l\alpha_m}{4\mu}\right\},$$

where $\det|A_{jk}|$ is the determinant of the matrix $\|A_{jk}\|$;

[8] Leprince-Ringuet, Gorodetzky, Nageotte, and Richard-Foy, Phys. Rev. **59**, 460 (1941); L. Leprince-Ringuet and M. Lhéritier, J. de phys. et rad. **7**, 66 (1946).

[9] See, e.g., M. C. Wang and G. E. Uhlenbeck, Rev. Mod. Phys. **17**, 323 (1945), Section 6a and Appendix I.

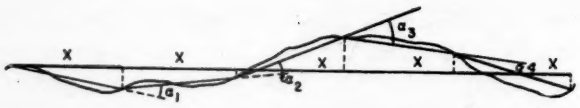

FIG. 6. Illustrating the many-point formula (31).

$\|A_{lm}^{-1}\|$ is the matrix reciprocal to $\|A_{jk}\|$, and the summation convention for double indices is used.

We find, thus,

$$W(\alpha_1 \cdots \alpha_{N-1}) = \left(\frac{3\lambda}{2\pi x}\right)^{(N-1)/2} \Delta_{N-1}^{-\frac{1}{2}} \times \exp\left\{\frac{-3\lambda}{2x} A_{lm}^{-1} \alpha_l \alpha_m\right\}, \quad (31)$$

where $\|A_{jk}\|$ is the $(N-1)$th order matrix:

$$\begin{Vmatrix} 4 & 1 & 0 & 0 & \cdot & \cdot & \cdot & 0 \\ 1 & 4 & 1 & 0 & \cdot & \cdot & \cdot & 0 \\ 0 & 1 & 4 & 1 & \cdot & \cdot & \cdot & 0 \\ 0 & 0 & 1 & 4 & \cdot & \cdot & \cdot & 0 \\ \cdot & \cdot & \cdot & \cdot & \cdot & \cdot & \cdot & \cdot \\ \cdot & \cdot & \cdot & \cdot & \cdot & \cdot & \cdot & \cdot \\ \cdot & \cdot & \cdot & \cdot & \cdot & \cdot & 4 & 1 \\ 0 & 0 & 0 & 0 & 0 & \cdot & 1 & 4 \end{Vmatrix} \quad (32)$$

and Δ_{N-1} is its determinant. To evaluate Δ_N, note first that

$$\Delta_N = 4\Delta_{N-1} - \Delta_{N-2}; \quad (33)$$

second that

$$\sinh Nu = 2\cosh u \sinh(N-1)u - \sinh(N-2)u;$$

and third that if $\cosh u = 2$,

$$\Delta_1 = \sinh 2u/\sinh u \quad \text{and} \quad \Delta_2 = \sinh 3u/\sinh u.$$

Hence, it follows that

$$\Delta_N = \sinh(N+1)u/\sinh u \quad \text{with} \quad u = \cosh^{-1} 2. \quad (34)$$

The recursion relation (33) for Δ_N may be used to show readily that

$$A_{lm}^{-1} = A_{ml}^{-1} = (-1)^{l+m} \Delta_{l-1} \Delta_{N-m-1}/\Delta_{N-1}, \quad l \leq m. \quad (35)$$

A_{lm}^{-1} is, of course, a rational fraction, and may be readily evaluated for any N, using $\Delta_1 = 4$, $\Delta_2 = 15$, and the recursion formula (33).

We shall use Eq. (31) here only to calculate the best method of measuring a curvature when N segments of track are taken, and to find the resulting mean square scattering-produced curvature.[10] Any method of curvature measurement is equivalent to a weighted mean value of the $N-1$ curvatures for adjacent segments.

[10] Eq. (31) is used by the author for the distribution of $\Sigma \alpha_k^2$, in Phys. Rev. **75**, 1763 (1949).

Let us calculate the probability distribution of

$$c_m = \sum_{j=1}^{N-1} b_j c_j = -\frac{1}{x} \sum_{j=1}^{N} b_j \alpha_j, \quad \text{with} \quad \sum_j b_j = 1.$$

We shall use the Fourier representation of the Dirac δ-function $\delta[c_m - \sum b_j \alpha_j/x]$, and integrate $W(\alpha_1 \cdots \alpha_{N-1})$ over all the α's.

$$P_N(c_m) = \frac{1}{2\pi(\Delta_{N-1})^{\frac{1}{2}}} \left(\frac{3\lambda}{2\pi x}\right)^{(N-1)/2} \int_{-\infty}^{\infty} dt \times \exp(itc_m) \int_{-\infty}^{\infty} d\alpha_1 \cdots \int_{-\infty}^{\infty} d\alpha_{N-1} \times \exp\{-(3\lambda A_{kj}^{-1} \alpha_k \alpha_j + 2it b_j \alpha_j)/2x\}$$

$$= \frac{1}{2\pi} \int_{-\infty}^{\infty} dt \exp\left\{itc_m - \frac{t^2}{6\lambda x} A_{jk} b_j b_k\right\} = \left[\frac{3\lambda x}{2\pi A_{jk} b_j b_k}\right]^{\frac{1}{2}} \exp\left\{-\frac{3\lambda x c_m^2}{2A_{jk} b_j b_k}\right\}, \quad (36)$$

so that

$$\langle c_m^2 \rangle_{Av} = \frac{1}{3\lambda x} A_{jk} b_j b_k = \frac{N A_{jk} b_j b_k}{3\lambda l}$$

if l is the total track length. The best choice of the b's is thus that which will minimize $S = A_{jk} b_j b_k$ subject to $\sum_k b_k = 1$.

We shall thus minimize $S' = A_{jk} b_j b_k - \mu \sum_k b_k$, where μ is an undetermined multiplier.

$$\partial S'/\partial b_k = 0 = 2A_{jk} b_j - \mu.$$

Multiplying by b_k and summing, we find that $\mu = 2S$.

TABLE I. The quantities $S = \Sigma_{jk} A_{jk} b_j b_k$ and b_j needed for the "best" way of measuring a mean scattering-produced curvature from N track segments (see Section VI), and the ratio of the resulting mean square curvature $\langle c_m^2 \rangle_{Av}$ for N segments to the value $8/3\lambda l$ for 2 segments.

N	2	3	4	5	6	10
S	4	5/2	7/4	19/14	52/47	724/1137
b_j: $j=1$	1	1/2	3/8	4/14	11/47	153/1137
$j=2$	—	1/2	2/8	3/14	8/47	112/1137
3	—	—	3/8	3/14	9/47	123/1137
4	—	—	—	4/14	8/47	120/1137
5	—	—	—	—	11/47	121/1137
6	—	—	—	—	—	120/1137 etc.
$3\lambda l/8\langle c_m^2 \rangle_{Av} = NS/8$	1.00	0.938	0.875	0.848	0.830	0.796

Hence, $S=A_{jk}b_j$. This system of equations may be solved, yielding

$$b_k=S\sum_m A_{km}^{-1}. \tag{37}$$

Summing over k, we find also

$$1/S=\sum_{k,m} A_{km}^{-1}. \tag{38}$$

The sums in (37) and (38) may be readily carried out with the aid of two formulas derived from (33)

$$\Delta_N=\Delta_j\Delta_{N-j}-\Delta_{j-1}\Delta_{N-j-1};\quad 0\leq j\leq N \tag{39}$$

$$\sum_0^n (-1)^m\Delta_m=\tfrac{1}{6}(-1)^n[5\Delta_n-\Delta_{n-1}+(-1)^n]. \tag{40}$$

Equation (39) reduces to (33) when $j=1$ or $N-1$, and is easily proved for other values of j by induction. Equation (40) results from summing (33).

We find finally from (38) and (37), respectively,

$$S=\frac{3\lambda l}{N}\langle c_m^2\rangle_{Av}=\frac{18\Delta_{N-1}}{[(3N+2)\Delta_{N-1}-\Delta_N+(-1)^N]}, \tag{41}$$

$$b_k=\frac{3[(-1)^{N-1}\Delta_{N-1}-(-1)^{N-k-1}\Delta_{N-k-1}-(-1)^{k-1}\Delta_{k-1}]}{(3N+2)(-1)^{N-1}\Delta_{N-1}+(-1)^N\Delta_N-1}. \tag{42}$$

Table I gives some values of S and b_k for a few values of N. For large N,

$$1/S\simeq N/6-\sqrt{3}/18=N/6-0.0962. \tag{43}$$

We have, therefore,

$$\langle c_m^2\rangle_{Av}\simeq 2/\lambda l[1-(0.577/N)]^{-1}. \tag{44}$$

Comparing with (17), we see that the greatest improvement possible in reduction of scattering-produced curvature errors by taking more measurements on a single track is a reduction of 25 percent in $\langle c_m^2\rangle_{Av}$. For $N=10$, the improvement over (17) is by a factor 0.796. Table I includes some values of $3\lambda l/8\langle c_m^2\rangle_{Av}$.

Another method of reducing $\langle c_m^2\rangle_{Av}$ would be to use $P_1(c_m)$ in (27), with the most favorable ratio of x to x_2. This turns out to be zero, for which case (27) yields $\langle c_m^2\rangle_{Av}=2/\lambda l$, the same as for (44) with $N\to\infty$. We have the surprising result that the same r.m.s. error as for a large number of track divisions would be obtained if the directions of the tangents at the two ends of the track could be accurately measured.

The writer wishes to acknowledge the invaluable assistance of Dr. Hartland S. Snyder of the Brookhaven National Laboratory in connection with these calculations.

Multiple Scattering of Fast Charged Particles*

H. S. SNYDER AND W. T. SCOTT**
Brookhaven National Laboratory, Upton, New York
(Received February 11, 1949)

The theory of multiple scattering of charged particles has been extended in the small-angle approximation valid for thin foils and fast particles. The extension consists of an exact solution of the integral diffusion equation for the correlated probabilities of lateral and angular displacements, and the numerical integration of the resulting expression for the angular distribution. The projection of the scattering on a plane has been used for simplicity. The results are expressed in terms of dimensionless variables η/η_0 and z/λ representing respectively the deflection angle in terms of a small unit determined by the screening, and the foil thickness in terms of the mean free path for scattering. Numerical calculations for values of z/λ from 100 to 84,000, and for an adequate range of η/η_0, have been carried out, and tables have been made available. Curves are presented for a few values of z/λ. The matching is shown between the approximately Gaussian result for small angles and the Rutherford single scattering result valid for large angles. The deviations of the new results from each of these limiting values is quite large over a wide range of angle. An explicit asymptotic formula for large η is given, showing correction terms to the single scattering formula.

1. INTRODUCTION

THE theory of the multiple scattering of charged particles has been treated by several authors.[1] In the present paper the work of these authors has been extended in certain directions at the expense of simplifying assumptions. The major simplifying assumption is that the scattering angle is small; this assumption limits the validity of the results obtained to high energy particles and thin scattering foils, and entails the complete disregard of back scattering and re-entrant particles. The second simplifying assumption is that the scattering cross section is given by the Born approximation for a potential field of the form $V=(ze^2/r)\exp(-r/a)$, the exponential factor representing the screening effect. Energy loss by the particles is neglected. The calculations also have been simplified by taking the projection of the scattering distribution on a fixed plane.

The main objective of this investigation was to determine precisely the manner in which the large angle Rutherford scattering fits on to the small angle highly multiple scattering. We have as a by-product of this investigation obtained accurate angular distributions for the scattered particles for a large number of foil thicknesses. In addition, for large scattering angles an approximate expression was found for the scattering distribution which gives good results when the actual distribution differs from the Rutherford distribution by less than 20 percent.

2. THE DIFFUSION EQUATION

Since Rutherford scattering is predominantly forward, we assume that the incident direction of the particle is the z-direction, that the foil is perpendicular to the z-axis, and that the total angular deviation of the scattered particle is sufficiently small so that we may approximate $\cos\theta$ by 1 and $\sin\theta$ by θ. Let $W(\eta, \epsilon, x, y|z)d\eta d\epsilon dxdy$ represent the probability that a particle initially traveling along the z-axis at $z=0$, pass through the area $dxdy$ at the point (x, y, z), traveling in a direction determined by η to $\eta+d\eta$ and ϵ to $\epsilon+d\epsilon$. η and ϵ are respectively the angles made with the z-axis by the projections of the track in the xz and yz planes. This function satisfies a well-known diffusion equation, written here with the small angle approximation:[2]

$$\left(\frac{\partial}{\partial z}+\eta\frac{\partial}{\partial x}+\epsilon\frac{\partial}{\partial y}\right)W(\eta, \epsilon, x, y|z)$$
$$=N\int_{-\infty}^{\infty}d\eta'\int_{-\infty}^{\infty}d\epsilon'\sigma(((\eta-\eta')^2+(\epsilon-\epsilon')^2)^{\frac{1}{2}})$$
$$\times[W(\eta', \epsilon', x, y|z)-W(\eta, \epsilon, x, y|z)] \quad (1)$$

where $\theta=((\eta-\eta')^2+(\epsilon-\epsilon')^2)^{\frac{1}{2}}$ signifies an angle of single scattering, $\sigma(\theta)$ is the single scattering cross section per unit solid angle and N is the density of scattering centers.

Forming

$$W(\eta, x|z)=\int_{-\infty}^{\infty}\int_{-\infty}^{\infty}d\epsilon d\eta W(\eta, \epsilon, x, y|z) \quad (2)$$

we find that

$$\left(\frac{\partial}{\partial z}+\eta\frac{\partial}{\partial x}\right)W(\eta, x|z)=N\int_{-\infty}^{\infty}\sigma_{\text{proj.}}(\eta-\eta')$$
$$\times\{W(\eta', x|z)-W(\eta, x|z)\}d\eta' \quad (3)$$

where

$$\sigma_{\text{proj.}}(\eta)=\int_{-\infty}^{\infty}\sigma((\eta^2+\epsilon^2)^{\frac{1}{2}})d\epsilon. \quad (4)$$

The function $W(\eta, x|z)$ is the distribution function for the projection of the scattering on the xz plane. Equa-

* Work done at the Brookhaven National Laboratory under contract with AEC.
** Now at Smith College, Northampton, Massachusetts.
[1] E. J. Williams, Proc. Roy. Soc. **169**, 531 (1939); S. Goudsmit and J. L. Saunderson, Phys. Rev. **57**, 24 (1940); **58**, 36 (1940).

[2] W. T. Scott, Phys. Rev. **75**, 212 (1949) and references 2, 3, and 4 of that paper. Note the different notation in this paper.

tion (3) can also be written

$$\left(\frac{\partial}{\partial z}+\frac{\partial}{\partial x}\right)W(\eta, x|z)$$

$$=\frac{1}{\lambda}\int_{-\infty}^{\infty}\{W(\eta', x|z)-W(\eta, x|z)\}p(\eta-\eta')d\eta' \quad (5)$$

where $p(\eta)d\eta$ is the probability that a particle will be scattered in a single scattering into a range between η and $\eta+d\eta$, and λ is the mean free path for scattering with[3]

$$\frac{1}{\lambda}=N\int_{-\infty}^{\infty}\sigma_{\text{proj.}}(\eta)d\eta, \quad \text{and} \quad p(\eta)=N\lambda\sigma_{\text{proj.}}(\eta). \quad (6)$$

The solution of Eq. (5) corresponding to the boundary condition that

$$W(\eta, x|z)=\delta(x)\delta(\eta), \text{ when } z=0$$

is

$$W(\eta, x|z)=\frac{1}{4\pi^2}\int_{-\infty}^{\infty}ds\int_{-\infty}^{\infty}dt$$

$$\times\exp\left\{i(\eta s+xt)-\frac{h(s+tz)-h(s)}{\lambda t}\right\} \quad (7)$$

in which

$$h(s)=\int_0^s[1-q(s)]ds$$

and (8)

$$q(s)=\int_{-\infty}^{\infty}e^{i\eta s}p(\eta)d\eta.$$

This solution was obtained by applying a Laplace transform in z and Fourier transforms in x and η to Eq. (5), solving the resulting first-order ordinary differential equation, and then evaluating the inverse Laplace transform. Equation (7) is easily checked by substitution into (5).

Integrating (8) with respect to x we obtain the angular distribution

$$W(\eta|z)=\int_{-\infty}^{\infty}W(\eta, x|z)dx$$

$$=\frac{1}{2\pi}\int_{-\infty}^{\infty}\exp\left[i\eta s+\frac{z}{\lambda}(q(s)-1)\right]ds$$

$$=\frac{1}{\pi}\int_0^{\infty}\cos\eta s\exp\left[\frac{z}{\lambda}(q(s)-1)\right]ds$$

$$=\text{Real Part}\left\{\frac{1}{\pi}\int_0^{\infty}\exp\left[i\eta s+\frac{z}{\lambda}(q(s)-1)\right]ds\right\}. \quad (9)$$

[3] This use of the symbol λ must not be confused with that in the paper of reference 2.

3. THE CROSS SECTION AND $q(s)$

If we use the potential of the form $V=(ze^2/r)\times\exp(-r/a)$ we find that the differential scattering cross section per unit solid angle becomes

$$\sigma(\theta)=\frac{z^2z'^2e^4}{\mu^2c^4(E-1/E)^2[\sin^2\theta/2+(\eta_0/2)^2]^2}$$

$$\cong\frac{4z^2z'^2e^4}{\mu^2c^4(E-1/E)^2[\theta^2+\eta_0^2]^2} \quad (10)$$

in which

$$\eta_0=\frac{h}{a\mu c(E^2-1)^{\frac{1}{2}}}. \quad (11)$$

In the above equations E is the total energy of the charged particle, measured in units of its rest mass, μ is its rest mass, and $z'e$ is its charge. The constant a, the screening radius, may be given its conventional value

$$a=a_0/z^{\frac{1}{3}}=\hbar^2/me^2z^{\frac{1}{3}} \quad (12)$$

in which a_0 is the Bohr radius of hydrogen.

Using the value of $\sigma(\theta)$ given by (10) we find for λ the value

$$\frac{1}{\lambda}=\frac{4z^2z'^2e^4N\pi}{\mu^2c^4(E-1/E)^2\eta_0^2} \quad (13)$$

and for the projected scattering probability

$$p(\eta)=\frac{\eta_0^2}{2(\eta^2+\eta_0^2)^{\frac{3}{2}}}. \quad (14)$$

Thus

$$q(s)=\tfrac{1}{2}\int_{-\infty}^{\infty}\frac{e^{i\eta s}\eta_0^2d\eta}{(\eta^2+\eta_0^2)^{\frac{3}{2}}}$$

$$=\tfrac{1}{2}\int_{-\infty}^{\infty}\frac{e^{i\eta_0sx}dx}{(1+x^2)^{\frac{3}{2}}}=-s\eta_0K_1(\eta_0s). \quad (15)$$

In Eq. (15) K_1 is the modified Bessel function of the first kind.[4] The power series expansion for $q(s)-1$ is

$$q(s)-1=\frac{(s\eta_0)^2}{2}\left\{\ln\left(\frac{s\eta_0}{2}\right)+0.0772157\cdots\right\}$$

$$+\frac{(s\eta_0)^4}{16}\left\{\ln\left(\frac{s\eta_0}{2}\right)-0.6727843\cdots\right\}$$

$$+\frac{(s\eta_0)^6}{384}\left\{\ln\left(\frac{s\eta_0}{2}\right)-1.089451\cdots\right\}+\cdots. \quad (16)$$

By observing the form of (15) and of (9) one sees that $W(\eta|z)$ is a function of η/η_0 and z/λ so that measuring

[4] Watson, *Bessel Functions* (1945), pp. 80, 172.

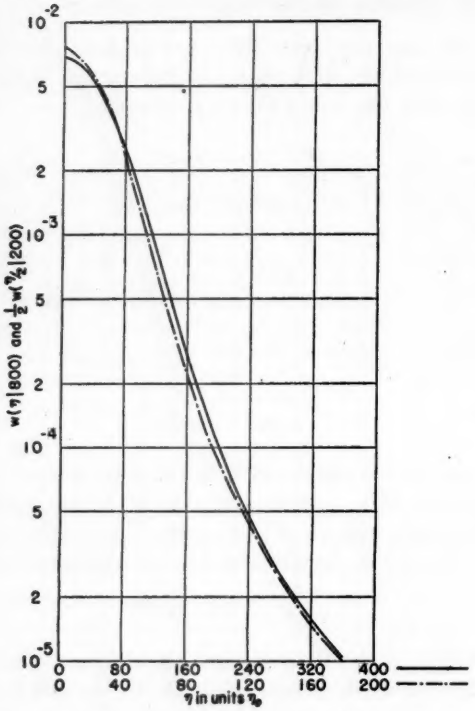

FIG. 1. Plot of $W(\eta|800)$ and $\frac{1}{2}W(\eta/2|200)$ to show the effect of changing the screening radius by a factor two. η represents the angle in units of η_0.

z in units of λ, and η in units of η_0, then the functions $W(\eta|z)$ have a universal form in which z becomes the average number of collisions which the particle undergoes in passing through the foil. This result amounts to setting $\lambda=\eta_0=1$ in the various formulas, which will be done in the rest of this paper. It should be noted that a change in η_0 requires a renormalization of $W(\eta|z)$.

4. AN APPROXIMATION FOR $W(\eta|z)$

It has been pointed out many times that for sufficiently large angles the distribution function in the case of Rutherford scattering should approach the single scattering law multiplied by the average number of times the particle has been scattered. That is,

$$W(\eta|z)\cong z/2\eta^3, \text{ for large } \eta. \tag{17}$$

We now verify this result, and in addition obtain correction terms to (17). Deforming the path of integration in Eq. (9) to the imaginary axis we may write

$$W(\eta|z)=\text{Real Part}\left\{\frac{i}{\pi}\int_0^\infty \exp(-\eta t+z(q(it)-1))dt\right\}$$

$$=\text{Real Part}\left\{\frac{i}{\pi}\int_0^\infty dt\{e^{-\eta t}[1+z\{q(it)-1\}$$

$$+z^2/2\{q(i\theta)-1\}^2+z^3/6\{q(it)-1\}^3+\cdots]\}\right\}. \tag{18}$$

Using the value of $q(s)-1$ given by the first term of (16) we then get

$$W(\eta|z)\cong\text{Real Part}\left\{\frac{i}{\pi}\int_0^\infty dte^{-\eta t}\right.$$

$$\times\left[1-\frac{zt^2}{2}\left(\ln t/2+\frac{\pi i}{2}+0.077215\right)\right.$$

$$+\frac{z^2t^4}{8}\left(\ln t/2+\frac{\pi i}{2}+0.077215\right)^2$$

$$\left.\left.-\frac{z^3t^6}{48}\left(\ln t/2+\frac{\pi i}{2}+0.077215\right)^3+\cdots\right]\right\}. \tag{19}$$

Thus

$$W(\eta|z)=z/4\int_0^\infty t^2e^{-\eta t}dt$$

$$-z^2/8\int_0^\infty t^4e^{-\eta t}\{\ln t/2+0.077215\}$$

$$+z^3/32\int_0^\infty t^6e^{-\eta t}\left\{(\ln t/2+0.077215)^2-\frac{\pi^2}{12}\right\}+\cdots, \tag{20}$$

or

$$W(\eta|z)=z/2\eta^3[1+6z/\eta^2(\ln\eta-0.8840)$$

$$+45z^2/\eta^4\{(\ln\eta+0.616)^2$$

$$-3.852(\ln\eta+0.616)+3.334\}+\cdots]. \tag{21}$$

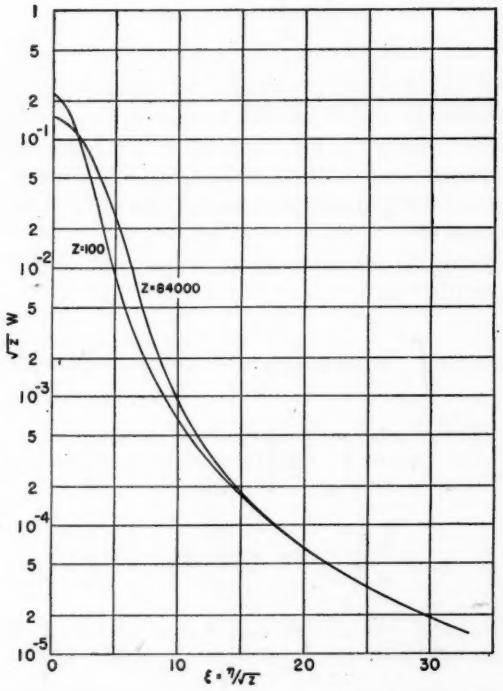

FIG. 2. Semi-logarithmic graphs of $W(\eta|z)$ for $z=100$ and 84000. (z in units of the mean free path for scattering.) $(z)^{\frac{1}{2}}W$ is plotted as a function of $\xi=\eta/(z)^{\frac{1}{2}}$.

TABLE I. $W(\eta|z)$ as a function of η for $z=100$.

η	$W(\eta\|100)\times10^6$	η	$W(\eta\|100)\times10^6$
0	22850	145	18.53
5	21730	150	16.62
10	18740	155	14.96
15	14770	160	13.52
20	10780	165	12.26
25	7422	170	11.15
30	4904	175	10.18
35	3170	180	9.312
40	2041	185	8.542
45	1331	190	7.856
50	888.4	195	7.242
55	608.6	200	6.691
60	430.0	205	6.195
65	314.5	210	5.747
70	236.3	215	5.341
75	180.5	220	4.973
80	140.8	225	4.638
85	113.4	230	4.333
90	93.34	235	4.054
95	76.91	240	3.798
100	63.92	250	3.349
105	53.78	260	2.968
110	45.96	270	2.643
115	39.60	280	2.364
120	34.38	290	2.123
125	30.04	300	1.913
130	26.42	310	1.731
135	23.36	320	1.571
140	20.76	330	1.430

In Eq. (21) we have neglected terms of order $1/z$ as compared to unity as we used only the first term in series (16). Comparison of the results given by (21) with values obtained by the numerical integration of Eq. (9) shows that (21) gives accurate results provided

$$6z/\eta^2(\ln\eta-0.8840)<0.2. \qquad (22)$$

However, when the expression (22) is larger than 0.3 the errors in (21) are quite large.

5. NUMERICAL CALCULATIONS

The values of $W(\eta|z)$ were calculated for small values of η by numerical integration of Eq. (9). The power series for $q(s)-1$ given by Eq. (16) was used for its calculation. For large values of η the approximate formula (21) was used. The numerical integration of (9) to give $W(\eta|z)$ was done for $z=100$, 1500, 3000 and 9000. The major difficulty with the use of (9) for numerical work is that the factor $\cos(\eta s)$ oscillates very rapidly for large values of η with the consequence that very high accuracy is required for the integrand in order that reasonable accuracy is obtained in the final results. In fact $q(s)-1$ had to be computed up to ten significant figures in order that the value of $W(\eta, s)$ would be accurate to three significant figures at the place where the approximate formula (21) overlapped the results of the

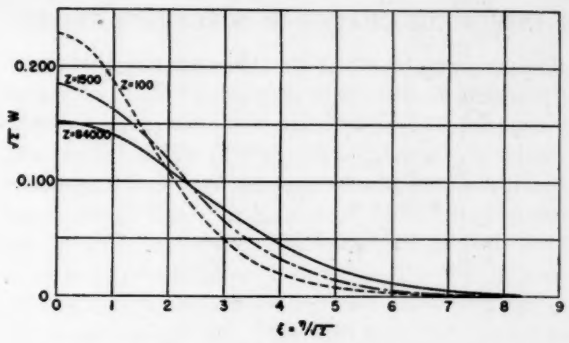

FIG. 3. Linear graphs of $z(W)^{\frac{1}{2}}$ against ξ for $z=100$, 1500, and 84,000.

numerical integrations. The values of $W(\eta|z)$ for other values of z were computed by means of the formula

$$W(\eta|z_1+z_2)=\int_{-\infty}^{\infty}W(\eta|z_1)W(\eta-\eta'|z_2)d\eta'. \qquad (23)$$

Once one has obtained a table of values of $W(\eta|z)$ for a particular $z=z_1$, then $W(\eta|z)$ may be computed for $z=2z_1$, $3z_1$, $4z_1\cdots$ with about one-thirtieth of the labor that is required in the use of Eq. (9). The distribution functions as given in the tables should be accurate to better than 1 percent. The major uncertainty in the values arises from the fact that with repeated application of (23) the errors accumulate. The above estimate of the accuracy is supported by the fact that the areas under the curves, $\int_{-\infty}^{\infty}W(\eta|z)d\eta$, as computed numerically, were in all cases in error by less than 1 percent.

TABLE II. $W(\eta|z)$ as a function of η for $z=1500$.

η	$W(\eta\|1500)\times10^6$
0	4786
50	3931
100	2192
150	912.1
200	327.1
250	121.6
300	53.13
350	27.81
400	16.47
450	10.70
500	7.405
550	5.360
600	3.993
650	3.080
700	2.450
750	1.970
800	1.596
850	1.313
900	1.100
950	0.9300
1000	0.7950

6. EFFECTS OF CHANGE IN SCREENING RADIUS

The precise value which should be used for the screening radius, a, is not known, although it may be estimated by using Eq. (12). The value of the screening radius as given by (12) should be accurate to within ten percent. In addition, the precise manner in which Rutherford cross section should be cut off at small angles is not known. In Fig. 1 we show some results of changing the screening radius by a factor of two, thus changing η_0 by two and λ by four. The dashed curve is $\frac{1}{2}W[(\eta/2)|200]$ and the solid curve is $W(\eta|800)$. The dashed curve thus shows the angular distribution for the same physical angles, the same particle energy and foil thickness but with one quarter the total cross section of the solid curve. For $\eta=0$ the difference between these functions is only seven percent. The maximum difference is about thirty percent. At greater foil thickness the difference between these functions would have been even smaller. Since the total cross section as determined by (12) may be reasonably assumed to be in error by less than 20 percent we felt quite confident that the functions $W(\eta|z)$ as computed by this method are, for $z>100$, in error by less than two percent as a result of uncertainties in the screening effect.

TABLE III. $W(\eta|z)$ as a function of η for $z=84{,}000$.

η	$W(\eta\|84{,}000)\times10^{6}$
0	523.0
200	504.4
400	451.7
600	374.7
800	289.9
1000	210.5
1200	144.1
1400	93.23
1600	58.03
1800	35.33
2000	21.36
2200	13.05
2400	8.228
2600	5.433
2800	3.765
3000	2.725
3200	2.053
3400	1.599
3600	1.278
3800	1.039
4000	0.8611
4200	0.7221
4400	0.6132
4600	0.5245
4800	0.4544
5000	0.3965
5200	0.3482
5400	0.3075
5600	0.2730

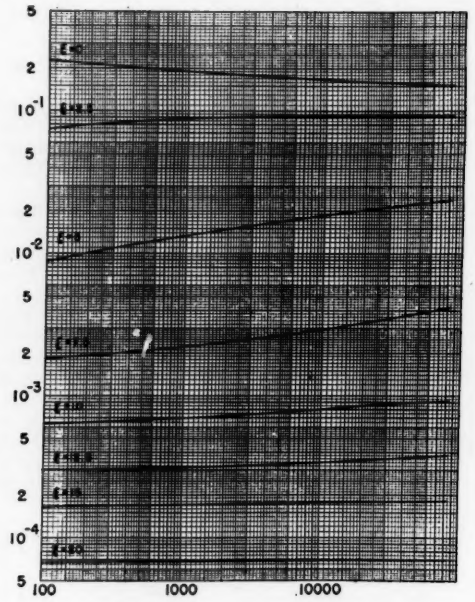

FIG. 4. Logarithmic graphs of $z(W)^{\frac{1}{2}}$ against z for eight values of $\xi=\eta/(z)^{\frac{1}{2}}$.

7. TABLES AND GRAPHS

The tables and graphs make use of the following measures of angle and thickness:

1. The angle η which is the angle of scattering projected on a plane containing the incident direction is measured in units η_0. From Eqs. (11) and (12) we have $\eta_0=(m/\mu)z^{\frac{1}{2}}/137(E^2-1)^{\frac{1}{2}}$ radians. In this formula m is the mass of the electron, μ the mass of the incident particle, z the charge of the scattering nucleus and E the energy of this incident particle, including its rest energy, in units μc^2.

2. The thickness z of the scattering foil is measured in units of the mean free path λ given by Eq. (13):

$$1/\lambda=9.86\times10^{-25}N(m/\mu)^2z^2z'^2/(E-1/E)^2\eta_0^2 \text{ cm}^{-1}.$$

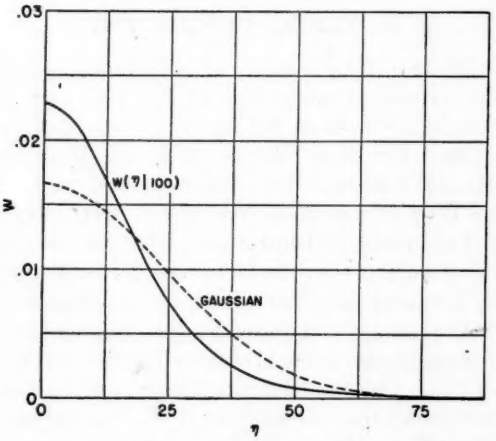

FIG. 5. Linear graphs of $W(\eta|100)$ and the Gaussian curve $W=(1/1151\pi)^{\frac{1}{2}}\exp(-\eta^2/1151)$ as functions of η.

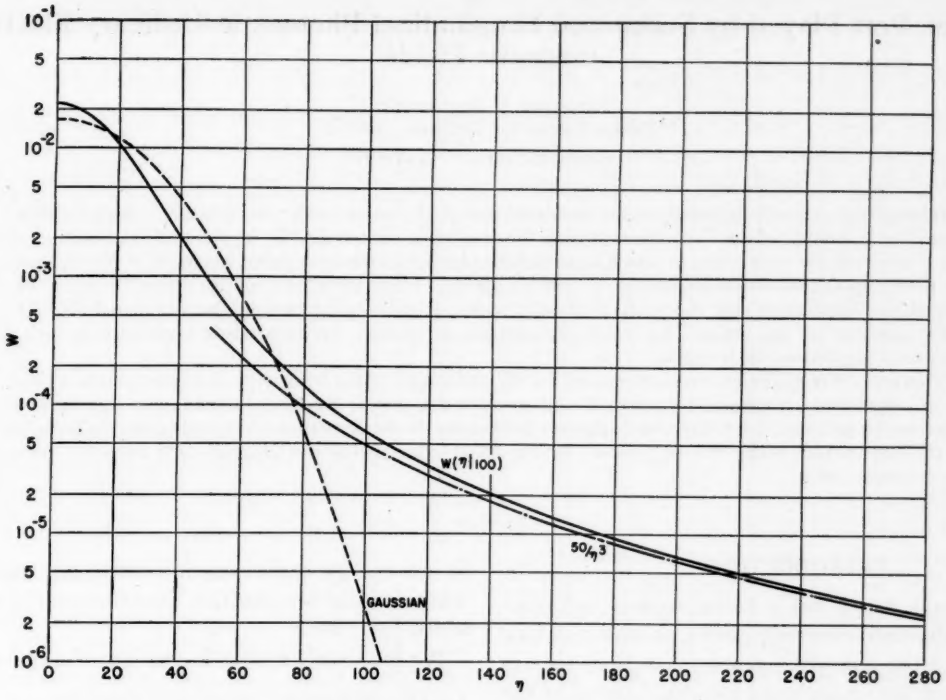

FIG. 6. Semi-logarithmic graphs of $W(\eta|100)$, the Gaussian curve of Fig. 5, and the single scattering approximation $W\simeq 50/\eta^3$, as functions of η.

Here N is the number of atoms per cc in the scattering foil and $z'e$ the charge of the incident particle.

We give in Tables I to III values of $W(\eta|z)$ for three sample values of z: 100, 1500, 84000. Figure 2 gives logarithmic graphs for $z=100$ and $z=84000$; $(z)^{\frac{1}{2}}W$ is here plotted as a function of $\xi=\eta/(z)^{\frac{1}{2}}$ to show the similarity between the two curves with this method of plotting.[5] This similarity is of course already revealed in Fig. 1. Figure 3 shows the upper part of the curves for the three values of z above, on a linear scale, with the same variables plotted. Neither method of plotting is useful for interpolation. We give in Fig. 4 graphs of $(z)^{\frac{1}{2}}W$ against z for eight values of $\xi=\eta/(z)^{\frac{1}{2}}$, which are more practicable for interpolation. These curves also serve to indicate the accuracy of the calculations, since they are smooth to within 2 percent or better. Complete tables for twenty-nine values of z from 100 to 84000 are available elsewhere.[6]

The relation of the new results to the Gaussian approximation is shown in Figs. 5 and 6, for $z=100$. For the Gaussian curve, we have used reference 2, Eqs. (5) and (13). The logarithm involved is evaluated for a 2 Mev electron in aluminum. It is clear that although the Gaussian curve is a reasonable approximation for small angles, the deviation at large angles is of a large order. In our example, $\eta_0\cong 0.0035$ radians $\cong 0.2$ degree. For $\eta=100$ or an angle of $\cong 20°$, the Gaussian result is 0.044 of our value.

The deviations from the single scattering result are also shown in Fig. 6, which includes a graph of $W=50|\eta^3$ (Eq. (17) for $z=100$). It is especially noteworthy to observe how slowly our distributions approach this result; even for small thicknesses z, one has to go to large angles η. For example, for $z=100$ the first correction term in Eq. (21) still amounts to 5 percent for $\eta=230$, where the scattered intensity is only 0.02 percent of the central maximum. For $z=600$ this occurs at $\eta=640$ where the intensity is reduced to 0.015 percent. Choosing as an actual example the scattering of electrons of about 2 Mev kinetic energy by an aluminum foil of about 0.0001 inch thickness, we find $\eta_0\cong 0.0035$ radians, $1/\lambda\cong 3.6\times 10^5$ cm^{-1}, $z\cong 90$. In this case the deviation from single scattering is down to 5 percent for $\eta=210$, corresponding to a scattering angle of over 40 degrees. This is beyond the small angle approximation used in the present treatment but shows nevertheless that single scattering is reached only for very large angles.

The authors wish to express their thanks to Theresa Danielson, Ardith Kenney, and Jean Snover for the numerical calculations.

[5] This method of plotting yields identical curves for different z in the Gaussian approximation.

[6] The tables may be obtained for a charge of ten cents from the Information and Publications Division, Brookhaven National Laboratory, Upton, Long Island, New York.

On the Part Played by Scalar and Longitudinal Photons in Ordinary Electromagnetic Fields

FREDERIK J. BELINFANTE
Purdue University, Lafayette, Indiana
(Received February 21, 1949)

When electromagnetic interactions are calculated directly by second-order perturbation calculus without preceding separation of the Coulomb field from the transverse photon field by a canonical transformation, it is fundamentally not allowed to take a state without photons as zero-order approximation. A more correct zero-order approximation is determined, in which scalar and longitudinal photons are present in pairs. The probability distribution over the numbers of pairs present is given by the Schrödinger functional Eq. (20); these numbers are not limited. No transverse photons are present. The relativistic invariance of such a zero-order approximation is proved.

This zero-order approximation is then used for the calculation of the self-energy of a free electron at rest, of the Møller matrix element for electron-electron scattering and of the Breit interaction energy between electrons in an atom. Apart from mathematical ambiguities in the derivation of the self-energy, this leads to the same results as can also be obtained by the usual separation of the Coulomb field from the transverse photon field.

INTRODUCTION

In recent days, much use is being made of a formulation of quantum electrodynamics, in which all four components of the quantized potential four-vector are treated more or less on an equal footing,[1] instead of the usual elimination of all but the transverse part of its spatial components after a preceding separation of the Coulomb field. Some discussion of the properties of the longitudinal and the time-like (so-called "scalar") part of the quantized potential can be found in old papers by Fock and Podolsky.[2] Also Pais used this field.[3] An advantage of this method lies in the fact that interactions between charges can now be calculated by one single second-order perturbation calculation.

In such calculations, one starts out from a zero-order approximation with "no field present." It is usually assumed that this "no field present" should then be interpreted as "no photons present." A close look at the theory, however, shows immediately that a state with no photons present even in the longitudinal and in the "scalar" field can never exist, as it is not only not relativistically invariant, but even in contradiction to the Lorentz condition.[4] Therefore, such state cannot serve as a zero-order approximation. One might then think that this procedure is completely impossible.

The purpose of this paper is to show how this method still leads to correct results, if one simply uses a different zero-order approximation. This zero-order approximation is determined below. In the following chapters it is shown, by examples, how it can be used. It then leads to results familiar from the ordinary theory, in which the Coulomb field and the transverse photon field are dealt with separately. However, when applied to self-energy questions, its results are not free from mathematical ambiguities. (See the small letters underneath Eq. (40).)

We may start with a Lagrangian function

$$L=(4\pi)^{-1}\{\tfrac{1}{4}F^{\nu\rho}F_{\nu\rho}-F^{\nu\rho}\nabla_\nu A_\rho+\tfrac{1}{2}S^2-S\nabla_\nu A^\nu\}$$
$$+A_\nu j^\nu-\hbar c\psi^\dagger(\kappa\beta-i\alpha^\nu\nabla_\nu)\psi, \quad (1)$$

where the notation is the usual one.[5] In the variational principle

$$\delta\int dt\int dxdydzL=0,$$

the variables $\psi^\dagger$, ψ, A_ν, and the antisymmetric tensor $F_{\nu\rho}(\equiv -F_{\rho\nu})$ are all to be varied independently, while j^ν is an abbreviation for $(-e)\psi^\dagger\alpha^\nu\psi$. This gives the usual field equations of Fermi's quantum electrodynamics. Without difficulty one finds the pairs of canonically conjugate variables (the magnetic field is a *derived variable*[6]); the commutation relations can be written down, and the Hamiltonian is found to be, in the usual three-dimensional vector notation,[5]

$$\mathcal{H}=\mathcal{H}_f+\mathcal{H}_m+\mathcal{W}, \quad (2)$$

$$8\pi\mathcal{H}_f=\int\mathbf{dx}\{\mathbf{E}^2+(\mathrm{curl}\mathbf{A})^2-S^2$$
$$+2S\,\mathrm{div}\mathbf{A}-2\Phi\,\mathrm{div}\mathbf{E}\}, \quad (3)$$

$$\mathcal{W}=\int\mathbf{dx}\{\rho\Phi-\mathbf{j}\cdot\mathbf{A}\}, \quad (4)$$

while the total momentum of the field is

$$\mathbf{P}_f=\int\mathbf{dx}\{(4\pi c)^{-1}(\mathbf{E}\cdot\nabla_f\mathbf{A}+S\nabla_f\Phi)+(\hbar/i)\psi^\dagger\nabla_f\psi\}. \quad (5)$$

We now introduce Jordan-Klein matrices for the electromagnetic field in the usual way. This yields (with

[1] J. Schwinger, Phys. Rev. **74**, 1439 (1948), **75**, 651 (1949); also F. J. Dyson, Phys. Rev. **75**, 486 (1949), (see his Eq. (16)).
[2] V. A. Fock and B. Podolsky, Physik. Zeits. Sowjetunion **1**, 801 (1931); **2**, 275 (1932).
[3] A. Pais, Proc. Roy. Acad. Amsterdam (Verhandelingen, 1e Sectie) **19**, 5 (1947), in particular, pp. 44–45.
[4] F. J. Belinfante, Phys. Rev. **75**, 337 (1949).
[5] F. J. Belinfante, Physica **12**, 1 (1946).
[6] F. J. Belinfante, Physica **7**, 765 (1940).

$\|$ and $\perp$ standing for "longitudinal" and "transverse"):

$$\Phi = i\Omega^{-\frac{1}{2}} \sum_{\mathbf{k}} (hc/k)^{\frac{1}{2}} b_{\mathbf{k}}^* \exp(i\mathbf{k}\cdot\mathbf{x}) + \text{conj.}, \tag{6a}$$

$$\mathbf{A}_{\|} = -i\Omega^{-\frac{1}{2}} \sum_{\mathbf{k}} (hc/k)^{\frac{1}{2}} a_{\mathbf{k}} \mathbf{e}_{\mathbf{k}}^{0} \exp(i\mathbf{k}\cdot\mathbf{x}) + \text{conj.}, \tag{6b}$$

$$\mathbf{A}_{\perp} = -\frac{i}{\Omega^{\frac{1}{2}}} \sum_{\mathbf{k}} \sum_{\mu=1,2} \left(\frac{hc}{k}\right)^{\frac{1}{2}} c_{\mathbf{k},\mu} \mathbf{e}_{\mathbf{k}}^{\mu} \exp(i\mathbf{k}\cdot\mathbf{x}) + \text{conj.}, \tag{6c}$$

$$S = \Omega^{-\frac{1}{2}} \sum_{\mathbf{k}} (hck)^{\frac{1}{2}} (a_{\mathbf{k}} + b_{\mathbf{k}}^*) \exp(i\mathbf{k}\cdot\mathbf{x}) + \text{conj.}, \tag{6d}$$

$$\mathbf{E}_{\|} = \Omega^{-\frac{1}{2}} \sum_{\mathbf{k}} (hck)^{\frac{1}{2}} (a_{\mathbf{k}} + b_{\mathbf{k}}^*) \mathbf{e}_{\mathbf{k}}^{0} \exp(i\mathbf{k}\cdot\mathbf{x}) + \text{conj.}, \tag{6e}$$

$$\mathbf{E}_{\perp} = \Omega^{-\frac{1}{2}} \sum_{\mathbf{k}} \sum_{\mu=1,2} (hck)^{\frac{1}{2}} c_{\mathbf{k},\mu} \mathbf{e}_{\mathbf{k}}^{\mu} \exp(i\mathbf{k}\cdot\mathbf{x}) + \text{conj.} \tag{6f}$$

Here, Ω is the volume of the fundamental cube; $a_{\mathbf{k}}$, $b_{\mathbf{k}}$, $c_{\mathbf{k},1}$ and $c_{\mathbf{k},2}$ are annihilation operators and their conjugates are creation operators satisfying the usual commutation relations such that

$$N_{\mathbf{k}}^{a} = a_{\mathbf{k}}^* a_{\mathbf{k}}, \quad N_{\mathbf{k}}^{b} = b_{\mathbf{k}}^* b_{\mathbf{k}}, \quad \text{and} \quad N_{\mathbf{k},\mu}^{c} = c_{\mathbf{k},\mu}^* c_{\mathbf{k},\mu}. \tag{7}$$

All have eigenvalues 0, 1, 2, 3, $\cdots$ only. Further, $\mathbf{e}_{\mathbf{k}}^{\mu}$ with $\mu=0$, 1, 2 are three mutually perpendicular unit vectors, with $\mathbf{e}_{\mathbf{k}}^{0}=\mathbf{k}/k$, where $k=|\mathbf{k}|$. Substituting the expansions (6) into (3), one finds $\mathcal{H}_f=\mathcal{H}_{\perp}+\mathcal{H}_{\|}$, with

$$\mathcal{H}_{\perp} = \sum_{\mathbf{k}} (N_{\mathbf{k},1}^{c} + N_{\mathbf{k},2}^{c} + 1) hck, \tag{8a}$$

$$\mathcal{H}_{\|} = \sum_{\mathbf{k}} (N_{\mathbf{k}}^{a} - N_{\mathbf{k}}^{b}) hck, \tag{8b}$$

while the part of the total momentum $\mathbf{P}$ depending on the electromagnetic field can be written in a similar way with hck in Eqs. (8) replaced by $\hbar\mathbf{k}$.

It is evident that the energy q-number (8b) is not positive definite. Only states of positive energy are admitted, however, if one imposes the usual auxiliary conditions

$$S(x, y, z)\Psi = 0, \tag{9}$$

$$\{\text{div}\mathbf{E} - 4\pi\rho\}\Phi = 0 \tag{10}$$

on the Schrödinger state functional. It is well known that these conditions cause difficulties with the normalization of the state functional Ψ itself.[7] We shall meet these difficulties as soon as we try to apply the theory to specific problems; but formally we can overcome them there, although they sometimes lead to ambiguity in the mathematics (compare Application 1).

The conditions (9)–(10) are also valid in interaction representation, if Ψ and S, $\mathbf{E}$ and ρ all are taken at one and the same time.

In the applications, we shall consider $\mathcal{W}$ of Eq. (4) as a perturbation, and e as a small coupling constant. The zero-order approximation Ψ_0 shall be an eigenfunction of $\mathcal{H}_f+\mathcal{H}_m$. (Here, $\mathcal{H}_m$ may or may not include some c-number external electrostatic potential.) *The function Ψ_0 shall also satisfy the conditions* (9)–(10) with this difference, that in zero-order approximation we may omit the term $(-4\pi\rho)$ from Eq. (10). In the first term, we use (6e) or

$$\text{div}\mathbf{E} = i\Omega^{-\frac{1}{2}} \sum_{\mathbf{k}} (hck^3)^{\frac{1}{2}} (a_{\mathbf{k}} + b_{\mathbf{k}}^*) \exp(i\mathbf{k}\cdot\mathbf{x}) + \text{conj.} \tag{11}$$

We multiply (9) and (10) by $\exp(-i\mathbf{k}\cdot\mathbf{x})$ and integrate over $\mathbf{x}$, thus picking out one Fourier component. We thus find, from (9) with (6d),

$$(a_{\mathbf{k}} + b_{\mathbf{k}}^* + a_{-\mathbf{k}}^* + b_{-\mathbf{k}})\Psi_0 = 0 \tag{9a}$$

and, from (10) with (11),

$$(a_{\mathbf{k}} + b_{\mathbf{k}}^* - a_{-\mathbf{k}}^* - b_{-\mathbf{k}})\Psi_0 = 0. \tag{10a}$$

Adding and subtracting, we obtain

$$a_{\mathbf{k}}\Psi_0 = -b_{\mathbf{k}}^*\Psi_0, \tag{12}$$

$$b_{\mathbf{k}}\Psi_0 = -a_{\mathbf{k}}^*\Psi_0. \tag{13}$$

If we take the $N_{\mathbf{k}}^{a}$ and $N_{\mathbf{k}}^{b}$ to be on diagonal form, the Eqs. (12)–(13) give the dependence of Ψ_0 on these numbers. Actually, Ψ_0 can be considered as a product of factors, each depending on the values of one pair of numbers $N_{\mathbf{k}}^{a}$ and $N_{\mathbf{k}}^{b}$ belonging to one wave vector $\mathbf{k}$ only. Each such factor in Ψ_0 we shall expand in simultaneous eigenfunctions $\chi_{m,n}$ of $N_{\mathbf{k}}^{a}$ and $N_{\mathbf{k}}^{b}$:

$$\Psi_0 = \cdots \left(\sum_{m=0}^{\infty} \sum_{n=0}^{\infty} c_{m,n} \chi_{m,n} \right) \cdots. \tag{14}$$

Here, m and n stand for the eigenvalues of $N_{\mathbf{k}}^{a}$ and $N_{\mathbf{k}}^{b}$, to which $\chi_{m,n}$ belongs.

We may choose the arbitrary phase factors in the eigenfunctions $\chi_{m,n}$ in such a way that the Jordan-Klein matrices $a_{\mathbf{k}}$ and $b_{\mathbf{k}}$ are represented by

$$a_{\mathbf{k}}\chi_{m,n} = m^{\frac{1}{2}}\chi_{m-1,n}; \qquad b_{\mathbf{k}}\chi_{m,n} = n^{\frac{1}{2}}\chi_{m,n-1}; \tag{15a}$$

$$a_{\mathbf{k}}^*\chi_{m,n} = (m+1)^{\frac{1}{2}}\chi_{m+1,n}; \quad b_{\mathbf{k}}^*\chi_{m,n} = (n+1)^{\frac{1}{2}}\chi_{m,n+1}. \tag{15b}$$

We substitute (14) into (12)–(13), make use of (15), and equate the coefficients of $\chi_{m-1,n}$ on both sides of Eq. (12), and of $\chi_{m,n-1}$ in Eq. (13). This gives the following recursion formulas for $c_{m,n}$,

$$m^{\frac{1}{2}} c_{m,n} = -n^{\frac{1}{2}} c_{m-1,n-1} \quad (\text{for } m \geqslant 1,\ n \geqslant 0), \tag{12a}$$

$$n^{\frac{1}{2}} c_{m,n} = -m^{\frac{1}{2}} c_{m-1,n-1} \quad (\text{for } m \geqslant 0,\ n \geqslant 1). \tag{13a}$$

For $m \geqslant 1$, $n \geqslant 1$, both equations are valid. For $m \neq n$, they have then only the zero solution

$$c_{m,n} = 0, \text{ if } m \neq n, \tag{16}$$

which is also correct, if m **or** n becomes zero. Thus,

$$\Psi_0 = \cdots \left(\sum_{n=0}^{\infty} c_{n,n} \chi_{n,n} \right) \cdots. \tag{17}$$

From (17) we see that Ψ_0 is a superposition of states, in which the numbers $N_{\mathbf{k}}^{a}$ and $N_{\mathbf{k}}^{b}$ have the same value. Considering (8b), we conclude that there are just as many "longitudinal photons" with momentum $\hbar\mathbf{k}$ and

[7] F. J. Belinfante, Physica **12**, 17 (1946).

energy $\hbar ck$ in the field, as there are "scalar photons" with momentum $(-\hbar\mathbf{k})$ and energy $(-\hbar k)$ and energy $(-\hbar ck)$. In other words, in field-free space the longitudinal and "scalar" photons occur in "pairs". Thus, the *value* of $\mathcal{H}_{II}$ is zero, and the *value* of the total electromagnetic energy $\mathcal{H}_f$ becomes positive definite, even if $\mathcal{H}_f$ is not positive definite as a q-number.

For $m=n$, Eqs. (12a)–(13a) give

$$c_{n,n}=-c_{n-1,n-1} \text{ (for } n\geqslant 1), \tag{18}$$

so that

$$c_{n,n}=(-)^n\cdot c_{0,0}, \tag{19}$$

$$\Psi_0=\cdots\left\{c_{0,0}\sum_{n=0}^{\infty}(-)^n\chi_{n,n}\right\}\cdots. \tag{20}$$

The minus signs are due to the choice of the phase factors in $\chi_{m,n}$ made in (15). The particular form (20) of the Schrödinger functional, which in our zero-order approximation ($e=0$) followed directly from the Lorentz condition (9)–(10), shows that *in field-free space pairs of longitudinal and "scalar" photons certainly are present.*[7a]

For the rest, the wave function (20) *cannot properly be normalized*, as the normalization integral reads

$$\mathfrak{N}=(\Psi_0^*,\Psi_0)=\cdots\left\{\sum_{n=0}^{\infty}|c_{n,n}|^2\right\}\cdots$$

$$=\cdots\left\{|c_{0,0}|^2\sum_{n=0}^{\infty}1\right\}\cdots=\text{divergent}. \tag{21}$$

As stated above, this fact is not surprising.[7] In applications of the theory, however, we shall see that, without explicit use of the value of $|c_{0,0}|^2$, we can always take a factor $\mathfrak{N}$ out of the result of our calculations and then *put this factor formally equal to unity*, as if there were no trouble with the normalization at all.

We thus shall assume that in zero-order approximation, in a space "with no field," the numbers of scalar and longitudinal photons present (as well as the relative phases of the probability amplitudes for the different possible values of these numbers) are given by Eq. (20). *The numbers of transverse photons we shall simply take as zero in such a field-free space.*

Before we proceed to the applications, it should be remarked that the above definition of field-free space is *relativistically invariant in our zero-order approximation* ($e=0$). As far as the scalar and longitudinal photons are concerned, this is obvious, as (20) was derived in this approximation from (9)–(10), which are equivalent with the one invariant condition

$$S(x,y,z,t)\Psi_0=0 \text{ (with } S=\nabla_\nu A^\nu) \tag{22a}$$

in Heisenberg representation, or

$$S(x,y,z,t)\Psi_0[\sigma]=4\pi\int_\sigma D(x-x')j^\mu(x')d\sigma_\mu'\cdot\Psi_0[\sigma] \tag{22b}$$

in interaction representation.[1]

[7a] S. T. Ma in a recent Letter to the Editor comes to similar results. See Phys. Rev. **75**, 535 (1949).

As far as the transverse photons are concerned, we have to prove their absence in a moving coordinate system $\{x'y'z't'\}$, if in $\{xyzt\}$ no transverse photons are present, while at the same time the Lorentz condition holds for the longitudinal and the scalar field. It is sufficient to check this for an infinitesimal Lorentz transformation ($\mathbf{x}'=\mathbf{x}-\mathbf{b}x^0$, $x^{0\prime}=x^0-\mathbf{b}\cdot\mathbf{x}$, with $\mathbf{b}=\mathbf{v}/c$).

We can consider the total $\mathbf{A}$, Φ field as a superposition of plane waves $A^\nu(\mathbf{k})\exp(ik_\mu x^\mu)$, with wave four-vectors $\mathbf{k}$, k^0. The wave equation for A^ν then gives[8] $k^0=\pm k$. For such plane waves, the Lorentz condition (22) imposed on Ψ_0 gives in zero-order approximation,[8]

$$\mathbf{k}\cdot\mathbf{A}^{(\pm)}(\mathbf{k})\Psi_0=k^0\Phi^{(\pm)}(\mathbf{k})\Psi_0=\pm k\Phi^{(\pm)}(\mathbf{k})\Psi_0. \tag{23}$$

Here, we denote by $A_\mu^{(+)}(\mathbf{k})$ the part of $A_\mu(\mathbf{k})$ with "positive frequency" $k^0=+k$ (with a time factor $\exp(ik_0x^0)=\exp(-ikct)$). Then, its *spatial* components $\mathbf{A}^{(+)}(\mathbf{k})$ contain only annihilation operators.[1] Our assumption of absence of transverse photons in the unprimed coordinate system can therefore be expressed by[1,4]

$$\mathbf{A}_\perp^{(+)}(\mathbf{k})\Psi_0=0. \tag{24}$$

By $\mathbf{A}^{(+)}=\mathbf{A}_\perp^{(+)}+\mathbf{A}_{II}^{(+)}$ and by (23), this gives

$$\mathbf{A}^{(+)}(\mathbf{k})\Psi_0=\mathbf{A}_{II}^{(+)}(\mathbf{k})\Psi_0=\mathbf{k}k^{-2}\mathbf{k}\cdot\mathbf{A}^{(+)}(\mathbf{k})\Psi_0=\mathbf{k}k^{-1}\Phi^{(+)}(\mathbf{k})\Psi_0. \tag{25}$$

In the primed coordinate system, by the infinitesimal Lorentz transformations

$$\mathbf{A}'=\mathbf{A}-\mathbf{b}\Phi,\quad \mathbf{k}'=\mathbf{k}-\mathbf{b}k^0, \tag{26}$$

we obtain from (25) for the waves with positive frequencies,

$$\mathbf{A}'^{(+)}(\mathbf{k}')\Psi_0=\mathbf{k}k^{-1}\Phi^{(+)}(\mathbf{k})\Psi_0-\mathbf{b}\Phi^{(+)}(\mathbf{k})\Psi_0=\mathbf{k}'k^{-1}\Phi^{(+)}(\mathbf{k})\Psi_0, \tag{25a}$$

where $\mathbf{A}'^{(+)}(\mathbf{k}')$ is the coefficient of $\exp(ik_\nu'x^{\nu\prime})=\exp(ik_\nu x^\nu)$ in the spatial components of the transformed potential four-vector. As the operator in the right-hand member of (25a) is obviously longitudinal in the new coordinate system, it follows from the transverse part of (25a) that now

$$\mathbf{A}_\perp'^{(+)}(\mathbf{k}')\Psi_0=0, \tag{24a}$$

which means that also in the moving (primed) coordinate system no transverse photons are present.

This obviously means that our simple condition (24) in zero-order approximation ($e=0$) is just as relativistically invariant as Schwinger's condition $\mathfrak{A}_\mu^{(+)}\Psi_0=0$. On the other hand, our condition tells a little more: While $\mathfrak{A}_\mu^{(+)}\Psi_0=0$ is only a covariant way of saying that in *one particular* Lorentz system (with time axis along some given time-like unit four-vector n^μ) no transverse photons are present, we express here by (24)–(24a) that in zero-order approximation *in no Lorentz system at all* there are transverse photons in the field.

(Remark that a total absence of *any* kind of photons would have corresponded to conditions $\mathbf{A}^{(+)}\Psi_0=0$ with $\Phi^{(-)}\Psi_0=0$, which obviously would not have been relativistically covariant. Moreover, $\mathbf{A}^{(+)}$ and $\Phi^{(-)}$ do not commute with S, so that such conditions would have been incompatible with (22).)

APPLICATION 1. ELECTRON SELF-ENERGY

As a first application, we shall consider here the calculation of the self-energy of a free electron at rest ($\mathbf{p}=0$) by means of second-order perturbation calculus, using the zero-order approximation of the previous chapter, and using $\mathfrak{W}$ of Eq. (4) as a perturbation. (The self-energy of a moving electron, $\mathbf{p}\neq 0$, could be treated similarly.)

In $\mathfrak{W}$, we expand $\mathbf{A}$ and Φ by Eqs. (6a–c), while ψ and $\psi^\dagger$ in the factors ρ and $\mathbf{j}$ can be expanded similarly,

[8] In Heisenberg representation, the "zero-order" approximation $e=0$ is made in the first step, where we use $\Box A^\nu=0$. In interaction representation, we make the approximation $e=0$ in the next step (23) by neglecting the right-hand member of (22b).

using Jordan-Wigner matrices for them. The matrix elements of $\mathfrak{W}$ for emission or absorption of photons under simultaneous transition of the electron to a state of different momentum then follow directly from (15) and similar equations for the matrices $c_{\mathbf{k},\mu}$ and $c_{\mathbf{k},\mu}^*$ occurring in Eq. (6c). These matrix elements should be used in the numerator of an expression of the type

$$\sum_i \frac{(\Psi_0^*, \mathfrak{W}\Psi_i)(\Psi_i^*, \mathfrak{W}\Psi_0)}{E_0 - E_i}. \tag{27}$$

As by Eq. (20), the number of photon pairs in the initial state Ψ_0 is not definite, substitution of (20) into (27) gives a sum over all possible values of all n's in the factor Ψ_0 in (27) and a sum over all possible values of all n''s in the factor Ψ_0^*. As the numerator of (27) contains only two factors $\mathfrak{W}$, each allowing for a change of only one number $N_{\mathbf{k}}{}^a$, $N_{\mathbf{k}}{}^b$, or $N_{\mathbf{k}}{}^c$, there are only the following nine kinds of terms in (27):

A. First, a transverse photon $(-\hbar\mathbf{k})$ is emitted and the electron takes the recoil $(+\hbar\mathbf{k})$; then this photon is again absorbed and the electron comes to rest.

B. Similarly with longitudinal photons; that is, all numbers N^a but the one $N_{-\mathbf{k}}{}^a$ remain constant, and for that particular $N_{-\mathbf{k}}{}^a$ there are transitions $\chi_{n,n} \to \chi_{n+1,n} \to \chi_{n,n}$.

C. A longitudinal photon with momentum $(+\hbar\mathbf{k})$ is first absorbed, then reappears: $\chi_{n,n} \to \chi_{n-1,n} \to \chi_{n,n}$.

D, E. Similarly with negative energy scalar photons: $\chi_{n,n} \to \chi_{n,n\pm1} \to \chi_{n,n}$. Here, it is $N_{\mathbf{k}}{}^b$ that increases by 1 in case D, and $N_{-\mathbf{k}}{}^b$ that decreases by 1 in case E, if the recoil is always to be $+\hbar\mathbf{k}$.

F. First, a longitudinal photon with momentum $(-\hbar\mathbf{k})$ is emitted then a scalar photon with momentum $(+\hbar\mathbf{k})$ is emitted while the electron comes again to rest: $\chi_{n,n} \to \chi_{n+1,n} \to \chi_{n+1,n+1}$.

G. Similarly with absorptions of, first, a longitudinal photon $+\hbar\mathbf{k}$ and, later, of a scalar photon $(-\hbar\mathbf{k})$: $\chi_{n,n} \to \chi_{n-1,n} \to \chi_{n-1,n-1}$.

H, I. These processes can also take place in the opposite order of sequence, with the opposite momenta of the photons: $\chi_{n,n} \to \chi_{n,n\pm1} \to \chi_{n\pm1,n\pm1}$.

All these effects are to be taken into account. They all have in common that the number of photons $N_{\mathbf{k}}{}^a$ and $N_{\mathbf{k}}{}^b$ for only *one* value of $\mathbf{k}$ are affected; in cases A, B, E, F, I this $\mathbf{k}$ is opposite to the recoil of the electron in units $\hbar$, while in cases C, D, G, H this $\mathbf{k}$ is equal to the momentum of the electron in the intermediate state in units $\hbar$. (These signs are important, as they enter into the matrix elements through the vectors $\mathbf{e}_{\mathbf{k}}{}^0$ in Eq. (6b).) Therefore, we may consider the summation over all numbers n and n' belonging to *other* $\mathbf{k}$ as having been performed tacitly by putting the corresponding normalization integrals $\mathfrak{N}$ equal to 1 (compare Eq. (21)), and only a summation over *one* set of values of n and of n' is left:

$$\sum_i \sum_n \sum_{n'} c_{n',n'}{}^* c_{n,n} \frac{\mathfrak{W}_{n'i}\mathfrak{W}_{in}}{E_0 - E_i}. \tag{28}$$

In the terms A, this summation over n and n' reduces to one single term $(n=n'=0)$, as Ψ_0 is a state without transverse photons. In the other terms, it reduces to a single summation over n, with $n'=n$ in cases B, C, D and E, with $n'=n+1$ in cases F and H, and with $n'=n-1$ in cases G and I.

Not only the electron originally at rest can jump to some intermediate positive energy state, but also a negative energy electron can jump to any positive energy state with exception of the one occupied. (This corresponds to virtual creation of pairs.) According to Weisskopf,[9] we subtract the self-energy of empty space. This overcompensates the jumps from negative energy states, as we now also subtract jumps from negative energy states into the state of an electron at rest. Therefore, we replace (28) by

$$\mathrm{W}_{\mathrm{self}} = \sum_{n'} \sum_{n} \mathrm{c}_{n'}{}^* \mathrm{c}_n \left\{ \sum_i \frac{\mathfrak{W}_{(0n')i}\mathfrak{W}_{i(0n)}}{E_0 - E_i} - \sum_{j,l} \frac{\mathfrak{W}_{(jn')l}\mathfrak{W}_{l(jn)}}{E_j - E_l} \right\}. \tag{29}$$

Here, c_n stands now for $c_{n,n}$. In the first sum, $(0n)$ represents a state with an electron with energy $+mc^2(\mathbf{p}=0)$ and with n photons (or pairs of photons) of the type that are emitted or absorbed in the transitions. By i, we understand an intermediate state with an odd number of photons present and with the electron in some positive energy state. We may sum over both spin orientations of the electron in this intermediate positive energy state by Casimir's method,[10] using the operator Λ^+ given by

$$\Lambda^{\pm} = \tfrac{1}{2}\{1 \pm w^{-1}(\kappa\beta + \boldsymbol{\alpha}\cdot\mathbf{k})\}, \tag{30}$$

with

$$w = +(\kappa^2 + k^2)^{\frac{1}{2}}. \tag{31}$$

This Λ^+ is to be written in the numerator between the two factors $\mathfrak{W}$.

In the second sum in (29), the initial state (jn) is one with an electron originally in some negative energy state j, say with momentum $\mathbf{k}$. Also n photons be present of the type that is of interest. This type now has a momentum opposite to what it was in the previous discussion of cases A to I. The intermediate state l is one with the electron now in the positive energy state $\mathbf{p}=0$, but with an odd number of photons present. Again we use Casimir's method, now for the summation over the spins in the states j. This time, Λ^- should operate from the left on the first factor $\mathfrak{W}$ and from the right on the second factor $\mathfrak{W}$. This is equivalent to interchanging the factors $\mathfrak{W}$ *as far as their Dirac matrices are concerned*, and putting Λ^- in between afterwards.

In the denominators, $E_0 - E_i = \hbar c\{\kappa - w - \eta k\}$ and $E_j - E_l = -\hbar c\{w + \kappa + \eta k\}$, where $\eta = +1$ in case of creation of a vector photon or absorption of a scalar photon in the first transition (cases A, B, E, F, and I), while $\eta = -1$ in the other cases (D, C, G, and H).

With due care for the plus and minus signs, we thus finally obtain, replacing $\Omega^{-1}\sum_{\mathbf{k}}$ by $(2\pi)^{-3}\int \mathbf{dk}$:

$$\mathrm{W}_{\mathrm{self}} = e^2(2\pi)^{-2} \int \mathbf{dk} k^{-1} f(\mathbf{k}), \tag{32}$$

[9] V. F. Weisskopf, Phys. Rev. **56**, 72 (1939), and A. Pais (reference 3), in particular, p. 25.

[10] H. B. G. Casimir, Helv. Phys. Acta **6**, 287 (1933), or W. Heitler, *The Quantum Theory of Radiation* (Clarendon Press, Oxford, 1936) in particular, pp. 84–87 and pp. 149–153.

with the following contributions to $f(\mathbf{k})$ from the various processes A-I:

$$f_A(\mathbf{k})=\sum_{\mu=1,2}\left\{\frac{(\boldsymbol{\alpha}\cdot\mathbf{e}_{-k}{}^{\mu})\Lambda^{+}(\boldsymbol{\alpha}\cdot\mathbf{e}_{-k}{}^{\mu})}{\kappa-w-k}+\frac{(\boldsymbol{\alpha}\cdot\mathbf{e}_{k}{}^{\mu})\Lambda^{-}(\boldsymbol{\alpha}\cdot\mathbf{e}_{k}{}^{\mu})}{\kappa+w+k}\right\}_{Av}, \quad (33A)$$

$$f_B(\mathbf{k})=\sum_{n=0}^{\infty} c_n{}^{*}c_n(n+1)\left\{\frac{(\boldsymbol{\alpha}\cdot\mathbf{e}_{-k}{}^{0})\Lambda^{+}(\boldsymbol{\alpha}\cdot\mathbf{e}_{-k}{}^{0})}{\kappa-w-k}+\frac{(\boldsymbol{\alpha}\cdot\mathbf{e}_{k}{}^{0})\Lambda^{-}(\boldsymbol{\alpha}\cdot\mathbf{e}_{k}{}^{0})}{\kappa+w+k}\right\}_{Av}, \quad (33B)$$

$$f_C(\mathbf{k})=\sum_{n=1}^{\infty} c_n{}^{*}c_n n\left\{\frac{(\boldsymbol{\alpha}\cdot\mathbf{e}_{k}{}^{0})\Lambda^{+}(\boldsymbol{\alpha}\cdot\mathbf{e}_{k}{}^{0})}{\kappa-w+k}+\frac{(\boldsymbol{\alpha}\cdot\mathbf{e}_{-k}{}^{0})\Lambda^{-}(\boldsymbol{\alpha}\cdot\mathbf{e}_{-k}{}^{0})}{\kappa+w-k}\right\}_{Av}, \quad (33C)$$

$$f_D(\mathbf{k})=\sum_{n=0}^{\infty} c_n{}^{*}c_n(n+1)\left\{\frac{\Lambda^{+}}{\kappa-w+k}+\frac{\Lambda^{-}}{\kappa+w-k}\right\}_{Av}, \quad (33D)$$

$$f_E(\mathbf{k})=\sum_{n=1}^{\infty} c_n{}^{*}c_n n\left\{\frac{\Lambda^{+}}{\kappa-w-k}+\frac{\Lambda^{-}}{\kappa+w+k}\right\}_{Av}, \quad (33E)$$

$$f_F(\mathbf{k})=\sum_{n=0}^{\infty} c_{n+1}{}^{*}c_n(n+1)\left\{\frac{\Lambda^{+}(\boldsymbol{\alpha}\cdot\mathbf{e}_{-k}{}^{0})}{\kappa-w-k}+\frac{(\boldsymbol{\alpha}\cdot\mathbf{e}_{k}{}^{0})\Lambda^{-}}{\kappa+w+k}\right\}_{Av}, \quad (33F)$$

$$f_G(\mathbf{k})=\sum_{n=1}^{\infty} c_{n-1}{}^{*}c_n n\left\{\frac{\Lambda^{+}(\boldsymbol{\alpha}\cdot\mathbf{e}_{k}{}^{0})}{\kappa-w+k}+\frac{(\boldsymbol{\alpha}\cdot\mathbf{e}_{-k}{}^{0})\Lambda^{-}}{\kappa+w-k}\right\}_{Av}, \quad (33G)$$

$$f_H(\mathbf{k})=\sum_{n=0}^{\infty} c_{n+1}{}^{*}c_n(n+1)\left\{\frac{(\boldsymbol{\alpha}\cdot\mathbf{e}_{k}{}^{0})\Lambda^{+}}{\kappa-w+k}+\frac{\Lambda^{-}(\boldsymbol{\alpha}\cdot\mathbf{e}_{-k}{}^{0})}{\kappa+w-k}\right\}_{Av}, \quad (33H)$$

$$f_I(\mathbf{k})=\sum_{n=1}^{\infty} c_{n-1}{}^{*}c_n n\left\{\frac{(\boldsymbol{\alpha}\cdot\mathbf{e}_{-k}{}^{0})\Lambda^{+}}{\kappa-w-k}+\frac{\Lambda^{-}(\boldsymbol{\alpha}\cdot\mathbf{e}_{k}{}^{0})}{\kappa+w+k}\right\}_{Av}. \quad (33I)$$

Into these expressions we substitute (30) for $\Lambda^{\pm}$. In the state 0 of the electron at rest, we take the expectation value $\{\ \}_{Av}$ of the products of Dirac matrices thus appearing in the above expressions. We may use here $\{\boldsymbol{\alpha}\}_{Av}=0$, $\{\alpha_i\alpha_j\alpha_k\}_{Av}=0$, $\{\beta\}_{Av}=1$. Thus, by $\mathbf{e}_k{}^{\mu}\cdot\mathbf{e}_k{}^{\mu'}=\delta_{\mu\mu'}$, $[\mathbf{k}\times\mathbf{e}_k{}^{0}]=0$, and omitting terms odd in $[\mathbf{e}_k{}^{\mu}\times\mathbf{e}_k{}^{\mu'}]$, which will vanish anyhow after the later integration over $\mathbf{k}$ in (32), we may replace:

$$\left.\begin{array}{rll}\Lambda^{\pm} & \text{by} & \tfrac{1}{2}\pm\kappa/2w,\\ (\boldsymbol{\alpha}\cdot\mathbf{e})\Lambda^{\pm}(\boldsymbol{\alpha}\cdot\mathbf{e}) & \text{by} & \tfrac{1}{2}\mp\kappa/2w,\\ \Lambda^{\pm}(\boldsymbol{\alpha}\cdot\mathbf{e}_k{}^{0})=-\Lambda^{\pm}(\boldsymbol{\alpha}\cdot\mathbf{e}_{-k}{}^{0}) & \text{by} & \pm k/2w,\\ (\boldsymbol{\alpha}\cdot\mathbf{e}_k{}^{0})\Lambda^{\pm}=-(\boldsymbol{\alpha}\cdot\mathbf{e}_{-k}{}^{0})\Lambda^{\pm} & \text{by} & \pm k/2w.\end{array}\right\} \quad (34)$$

After these substitutions, we put $k=\kappa\sinh z$, $w=\kappa\cosh z$, $w\pm k=\kappa\exp(\pm z)$, and

$$\int \mathbf{dk}/4\pi^2 kw=(\kappa/\pi)\int_0^{\infty}\sinh z\,dz.$$

As the resulting integral over z diverges, we cut it off at some maximum value M for z. By $z=\ln\{(k+w)/\kappa\}$, we may call

$$M=\ln\frac{P+P^0}{mc}, \quad (35)$$

where P is the maximum momentum and cP^0 is the maximum energy of the electron or of the positon in the intermediate state. Thus, one finds easily for the transverse self-energy derived from $f_A(\mathbf{k})$:

$$W_{tr}=\frac{e^2\kappa}{2\pi}(M-\tfrac{1}{2}+\tfrac{1}{2}e^{-2M})\rightarrow\frac{mc^2}{2\pi}\cdot\frac{e^2}{hc}\cdot\left\{\ln\frac{P+P^0}{mc}-\tfrac{1}{2}\right\}, \quad (36)$$

and for the static self-energy derived from the other terms B to I:

$$W_{st}=\frac{e^2\kappa}{4\pi}\left\{\sum_{n=0}^{\infty}|c_n|^2(n+1)(\tfrac{1}{2}e^{2M}+4M-1+\tfrac{1}{2}e^{-2M})+\sum_{n=1}^{\infty}|c_n|^2 n(\tfrac{1}{2}e^{2M}-4M-1+\tfrac{1}{2}e^{-2M})+\left[\sum_{n=0}^{\infty}c_{n+1}{}^{*}c_n(n+1)+\sum_{n=1}^{\infty}c_{n-1}{}^{*}c_n n\right]\times\left[\tfrac{1}{2}e^{2M}-1+\tfrac{1}{2}e^{-2M}\right]\right\}. \quad (37)$$

The two summations from 1 to ∞ can now be changed into summations from 0 to ∞ because of the factor n. Thus, we may write

$$W_{st}=\frac{e^2\kappa}{\pi}\cdot M\cdot\sum_{n=0}^{\infty}|c_n|^2+\frac{e^2\kappa}{2\pi}\cdot\sinh^2 M\cdot\sum_{n=0}^{\infty}\{|c_n|^2(2n+1)+c_{n+1}{}^{*}c_n(n+1)+c_{n-1}{}^{*}c_n n\}. \quad (38)$$

In the last expression, we shall now make use of Eq. (18), by putting

$$c_{n+1}{}^{*}c_n=c_{n-1}{}^{*}c_n=-|c_n|^2. \quad (39)$$

Thus, the last sum in Eq. (38) vanishes, and a quadratic divergence (proportional to P^2) is avoided. Also putting the sum in the first term of (38) formally equal to unity (compare Eq. (21)), we find the well-known result[9]

$$W_{self}=W_{tr}+W_{st}=\frac{mc^2}{2\pi}\cdot\frac{e^2}{hc}\cdot\left\{3\ln\frac{P+P^0}{mc}-\tfrac{1}{2}\right\}. \quad (40)$$

This all seems quite satisfactory, but it should be pointed out that the mathematical method used is ambiguous because of the divergence of the summations over n. Indeed, one might well have preferred to call the summation index n in the processes G and I rather $(n+1)$, with the new n summed at once from 0 to ∞ without need of adding a zero term. This would make f_G and f_I nicely the conjugates of f_H and f_F. It would have changed the $c_{n-1}^*c_n n$ in the last term of (38) into $c_n^*c_{n+1}(n+1)$. Then, after application of (39), we would find that a term

$$-\frac{e^2\kappa}{2\pi}\cdot\sinh^2 M\to\frac{e^2\kappa}{8\pi}\cdot(2-e^{2M})=\frac{mc^2}{8\pi}\cdot\frac{e^2}{hc}\cdot\left\{2-\left(\frac{P+P^0}{mc}\right)^2\right\} \quad (41)$$

would have been added to the self-energy, thus making the latter negative and quadratically divergent.

Similarly, we could have written $(n+1)$ for n in the processes C and E. This would change $|c_n|^2 n$ into $|c_{n+1}|^2(n+1)$ in Eq. (37). For this, we could have written $|c_n|^2(n+1)$ again by Eq. (18), so that we would find that this time a positive and quadratically divergent term

$$\frac{e^2\kappa}{8\pi}\cdot(e^{2M}-8M-2) \quad (42)$$

would have been added to the static self-energy.

If *both* (41) and (42) would be added to (38)–(40), one would find

$$W_{st}'=0; \quad W_{self}'=W_{tr}. \quad (43)$$

All this shows that calculations based on perturbation theory without a preceding separation of Coulomb field and photon field are rather dangerous, if the auxiliary condition is taken seriously as a condition imposed on the state-vector Ψ.

When we compare the above calculation with the usual type of perturbation calculations, then we remark mainly the following differences:

(I) The zero-order approximation is here no longer one with $c_n=\delta_{n0}$.

(II) There are many more intermediate states to be taken into account, and there are processes F, G, H, I, in which a pair of photons is created or annihilated.

(III) The scalar photons in the intermediate states have negative energy, and enter with such energy in the resonance denominators.

If incorrectly Ψ_0 would have been taken to be a state without photons, so that no use would have been made of (I) and (II), then the calculation would lead to an erroneous result, in which the static and the total self-energy would become quadratically divergent.

If at the same time the scalar photons are taken with the wrong energy sign in the resonance denominators, then the static self-energy becomes again logarithmically divergent, but one would wrongly find $(e^2\kappa/2\pi)(-M-\frac{1}{2}+\frac{1}{2}e^{-2M})$ for it. Added to (36), this would give a finite *total* self-energy.

An interesting result is obtained, if *beside* these two mistakes we make a *third* error in the derivation of the self-energy, by taking the contributions from the processes D with the wrong sign. These three *combined* mistakes would change $f(\mathbf{k})$ into

$$F(\mathbf{k})=\left\{\frac{\boldsymbol{\alpha}\cdot\Lambda^+\boldsymbol{\alpha}-\Lambda^+}{\kappa-w-k}+\frac{\boldsymbol{\alpha}\cdot\Lambda^-\boldsymbol{\alpha}-\Lambda^-}{\kappa+w+k}\right\}_{Av}. \quad (44)$$

Thus, the self-energy would become

$$W_{self}=\frac{e^2}{4\pi^2}\int\frac{\mathbf{dk}}{k}\left\{\frac{\alpha^\lambda\Lambda^+\alpha_\lambda}{\kappa-w-k}+\frac{\alpha^\lambda\Lambda^-\alpha_\lambda}{\kappa+w+k}\right\}_{Av}. \quad (45)$$

This expression, which leads again exactly to (40), was guessed in a recent paper by Feynman[11] as a relativistic generalization of the expression for the transverse self-energy. (Compare (44) with (33A).) It was derived by French and Weisskopf[12] directly from a calculation of the self-energy, in which Coulomb field and photon field were treated independently, so that their zero-order approximation (without transverse photons) was correct anyhow. It would be interesting to know, on ground of what symmetry properties of the theory the above three errors here compensate each other completely.

APPLICATION 2. ELECTRON-ELECTRON SCATTERING

As a second application, we shall calculate the matrix element for scattering of free electrons by free electrons. Let $\hbar\mathbf{k}_1$ and $\hbar\mathbf{k}_2$ be the original momenta of two colliding electrons, and $\hbar\mathbf{k}_1'$ and $\hbar\mathbf{k}_2'$ their momenta after scattering. The matrix element for this process is then given by

$$\sum_i\sum_n\sum_{n'}c_{n'}^*c_n\frac{(\mathbf{k}_1'\mathbf{k}_2'n'|\mathcal{W}|\mathbf{k}_1'\mathbf{k}_2 i)(\mathbf{k}_1'\mathbf{k}_2 i|\mathcal{W}|\mathbf{k}_1\mathbf{k}_2 n)}{E_0-E_i}$$
$$+\text{Sym}-\text{Exch}. \quad (46)$$

Here, Sym means the terms obtained by complete interchanging of the two electrons, while Exch stands for the exchange terms,[13] in which the $\mathbf{k}_1$ and $\mathbf{k}_2$ are interchanged, but not the $\mathbf{k}_1'$ and $\mathbf{k}_2'$. Because of the conservation of energy, E_0 is the final as well as the initial energy. Denoting the energies of the single electrons by $hc\epsilon$, we have in the terms written out in (46),

$$E_0-E_i=hc(\epsilon_1-\epsilon_1'-\eta k),$$

where η has the same meaning as in the text between Eqs. (31) and (32), while hk is the magnitude of the momentum of the photon involved.

In the terms written out in (46), we shall put

$$\mathbf{k}=\mathbf{k}_1'-\mathbf{k}_1=\mathbf{k}_2-\mathbf{k}_2'.$$

(In the exchange terms, therefore, $\mathbf{k}=\mathbf{k}_1'-\mathbf{k}_2$.) The contributions of the various processes A–I to (46) give now:

$$\text{(A)}\quad\frac{2\pi e^2}{\Omega k}\sum_{\mu=1,2}\left\{\frac{(\mathbf{e}_{-\mathbf{k}^\mu}\cdot\boldsymbol{\alpha}_2)(\mathbf{e}_{-\mathbf{k}^\mu}\cdot\boldsymbol{\alpha}_1)}{\epsilon_1-\epsilon_1'-k}+\text{Sym}\right\}$$
$$-\text{Exch}. \quad (47)$$

Here, $\boldsymbol{\alpha}_1$ means the matrix element of $\boldsymbol{\alpha}$ between the spin factors of the plane waves corresponding to $\mathbf{k}_1$ and $\mathbf{k}_1'$, respectively. (In the exchange terms this would be between $\mathbf{k}_2$ and $\mathbf{k}_1'$.)

[11] R. P. Feynman, Phys. Rev. **74**, 1430 (1948); Eq. (3).

[12] J. B. French and V. F. Weisskopf, Phys. Rev. **75**, 1240 (1949).

[13] Compare J. R. Oppenheimer, Phys. Rev. **32**, 361 (1928) and N. F. Mott, Proc. Roy. Soc. **A125**, 222 (1929). These exchange terms result from the fact that the two steps of the process may be just as well transitions $\mathbf{k}_2\to\mathbf{k}_1'$ and $\mathbf{k}_1\to\mathbf{k}_2'$. The minus sign comes in through the rules of second quantization (meaning of the Jordan-Wigner matrices as operators).

(B) and (C)

$$\frac{2\pi e^2}{\Omega k}\sum_n c_n^* c_n\left\{\frac{(n+1)(\mathbf{e}_{-\mathbf{k}^0}\cdot\boldsymbol{\alpha}_2)(\mathbf{e}_{-\mathbf{k}^0}\cdot\boldsymbol{\alpha}_1)}{\epsilon_1-\epsilon_1'-k}+\frac{n(\mathbf{e}_{\mathbf{k}^0}\cdot\boldsymbol{\alpha}_2)(\mathbf{e}_{\mathbf{k}^0}\cdot\boldsymbol{\alpha}_1)}{\epsilon_1-\epsilon_1'+k}+\text{Sym}\right\}-\text{Exch.} \quad (48)$$

(D) and (E)

$$\frac{2\pi e^2}{\Omega k}\sum_n c_n^* c_n\left\{\frac{(n+1)I_2I_1}{\epsilon_1-\epsilon_1'+k}+\frac{nI_2I_1}{\epsilon_1-\epsilon_1'-k}+\text{Sym}\right\}-\text{Exch.} \quad (49)$$

Here, I_1 stands for the matrix elements of the unit operator between the spin functions.

The processes F, G, H, I here lead to terms odd in the vector $\mathbf{k}$, and therefore vanish by integration of $\mathbf{k}$ over angles.

The terms "Sym" are different from the ones written down by the sign of the energy difference $\epsilon-\epsilon'$ in the denominators, as by the conservation of energy

$$\epsilon_2-\epsilon_2'=\epsilon_1'-\epsilon_1=\text{say } \epsilon. \quad (50)$$

(In the exchange terms, therefore, $\epsilon=\epsilon_1'-\epsilon_2$.) Taking the "Sym"-terms together with the others, we obtain

$$\frac{4\pi e^2}{\Omega}\cdot\frac{\left[\sum_{\mu=1,2}(\mathbf{e}_{-\mathbf{k}^\mu}\cdot\boldsymbol{\alpha}_2)(\mathbf{e}_{-\mathbf{k}^\mu}\cdot\boldsymbol{\alpha}_1)+\sum_n|c_n|^2\{(\mathbf{e}_{-\mathbf{k}^0}\cdot\boldsymbol{\alpha}_2)(\mathbf{e}_{-\mathbf{k}^0}\cdot\boldsymbol{\alpha}_1)-I_2I_1\}\right]}{\epsilon^2-k^2}-\text{Exch.} \quad (51)$$

For the dependency of the situation function on the numbers of photons, we have used up to here Eq. (17) only. By the normalization prescription $\sum_n|c_n|^2=1$ alone, and without any use of Eqs. (18)–(20), this time we can conclude that the matrix element for scattering is given by

$$\frac{4\pi e^2}{\Omega}\cdot\frac{\boldsymbol{\alpha}_2\cdot\boldsymbol{\alpha}_1-I_2I_1}{\epsilon^2-k^2}-\text{Exch}, \quad (52)$$

which is exactly Møller's expression for this matrix element.[14]

The above considerations are easily generalized to the case of a collision between one free electron and one electron bound in an atom. From this matrix element, Møller[15] and Bethe[16] have calculated cross sections for electron scattering, which were verified experimentally by Champion.[17]

APPLICATION 3. BREIT INTERACTION ENERGY

As a third application, we shall calculate the interaction energy of two electrons in two stationary states a and b in an atom. For this purpose we perform a second-order perturbation calculation with $\mathfrak{W}$ from Eq. (4), and subtract first the second-order perturbation energy for empty space. Indicating by $(i|\alpha|j)$ a contribution to the perturbation energy for a transition, in which an electron jumps from a state j into a state i, we obtain in this way, in symbolic notation (omitting resonance denominators and summation signs and not yet specifying numbers of photons),

$$(a|\alpha|a)(b|\alpha|b)+(b|\alpha|b)(a|\alpha|a)+(a|\alpha|\mathbf{P}_b)(\mathbf{P}_b|\alpha|a)+(b|\alpha|\mathbf{P}_a)(\mathbf{P}_a|\alpha|b)+(\mathbf{N}|\alpha|\mathbf{P}_{ab})(\mathbf{P}_{ab}|\alpha|\mathbf{N})-(\mathbf{N}|\alpha|\mathbf{P})(\mathbf{P}|\alpha|\mathbf{N}). \quad (53)$$

Here, the second factor of each product refers to the first transition; P and N denote arbitrary states of positive and negative energy, respectively, over which we later will have to sum; subscripts a or b mean states to be excluded from such summations.

From (53) we must subtract the self-energies of the two single electrons in states a and b, respectively (compare Eq. (29)):

$$(a|\alpha|\mathbf{P})(\mathbf{P}|\alpha|a)-(\mathbf{N}|\alpha|a)(a|\alpha|\mathbf{N})+(b|\alpha|\mathbf{P})(\mathbf{P}|\alpha|b)-(\mathbf{N}|\alpha|b)(b|\alpha|\mathbf{N}). \quad (54)$$

The difference between (53) and (54) gives the actual *interaction* energy:

$$(a|\alpha|a)(b|\alpha|b)+(b|\alpha|b)(a|\alpha|a)-(a|\alpha|b)(b|\alpha|a)-(b|\alpha|a)(a|\alpha|b), \quad (55)$$

which includes ordinary as well as exchange interaction[18] and can be written as the expectation value in the unperturbed state

$$\Psi_{ab}(1,2)=2^{-\frac{1}{2}}\{\phi_a(1)\phi_b(2)-\phi_b(1)\phi_a(2)\} \quad (56)$$

of an operator of the type

$$\mathrm{W}(1,2)=\alpha(1)\alpha(2)+\alpha(2)\alpha(1) \quad (57)$$

in the symbolic notation used in (53)–(55). In order to calculate here the exact meaning of the symbol $\alpha(1)\alpha(2)$, we have to make use of the proper matrix elements for the various photon processes A to I accompanying the transitions of the electron, and to write the corresponding energy differences in the denominators.

Whatever these photon processes are, we shall first write out here only contributions from electron processes that in the above symbolic notation would have been written as

$$(f|\alpha|a)(g|\alpha|b)+(g|\alpha|b)(f|\alpha|a),$$

[14] C. Møller, Zeits. f. Physik **70**, 786 (1931).
[15] C. Møller, Ann. d. Physik **14**, 531 (1932). See also W. Heisenberg, Ann. d. Physik **13**, 430 (1932) for a correction to Møller's first paper (reference 14).
[16] H. Bethe, Zeits. f. Physik **76**, 293 (1932).
[17] F. C. Champion, Proc. Roy. Soc. **A137**, 688 (1932).
[18] The above derivation of the interaction between two electrons was also suggested by Feynman (reference 11). It is difficult to obtain the exchange interaction by a procedure similar to that used by us in the previous chapter, as intermediate states with both electrons in the same state are naturally excluded.

where f and g stand for a and b or for b and a. By $\boldsymbol{\alpha}_1$ we shall denote here the matrix element

$$(g|\,\boldsymbol{\alpha}e^{i\mathbf{k}\cdot\mathbf{x}}|\,b)=\int \mathbf{dx}\phi_g^{\dagger}e^{i\mathbf{k}\cdot\mathbf{x}}\boldsymbol{\alpha}\phi_b,$$

and by $\boldsymbol{\alpha}_2$ we denote $(f|\,\boldsymbol{\alpha}e^{-i\mathbf{k}\cdot\mathbf{x}}|\,a)$. Similarly, I_1 stands for $(g|e^{i\mathbf{k}\cdot\mathbf{x}}|\,b)$, etc. Further, we write $\epsilon_1'-\epsilon_1$ or ϵ for the energy difference $E_g-E_b=E_a-E_f$ in units $\hbar c$. With this notation, the contributions from the various photon processes with one given $\mathbf{k}$ are given exactly by (47)–(49), where Sym interchanges the subscripts 1 and 2 (with $\epsilon_2-\epsilon_2'=\epsilon$ according to Eq. (50)), and where "−Exch" reminds of the fact that the terms with $f=b$, $g=a$ are to be subtracted from the terms with $f=a$, $g=b$. (The processes F, G, H, I again give contributions odd in $\mathbf{k}$ and therefore may be omitted.) Hence, we may proceed at once to Eqs. (51)–(52) with the new meaning of the sepmlos. We still have to sum this over $\mathbf{k}$.

From here we follow the usual procedure.[19] The Dirac equations for ϕ_b and ϕ_g give $-i\,\mathrm{div}(\phi_g^{\dagger}\boldsymbol{\alpha}\phi_b)=\epsilon\phi_g^{\dagger}\phi_b$; similarly for ϕ_a and ϕ_f. Thence,

$$-\mathbf{k}\cdot\boldsymbol{\alpha}_1=\epsilon I_1;\quad -\mathbf{k}\cdot\boldsymbol{\alpha}_2=\epsilon I_2. \tag{58}$$

Substituting $\mathbf{e}_{-\mathbf{k}}{}^0=-\mathbf{k}/k$ and (58) into (51), equating the "normalization integral" (21) to unity, and summing over $\mathbf{k}$, we get for the interaction energy

$$W=\frac{e^2}{2\pi^2}\int \mathbf{dk}\left\{\frac{\sum_{\mu=1,2}(\mathbf{e}_{\mathbf{k}}{}^{\mu}\cdot\boldsymbol{\alpha}_2)(\mathbf{e}_{\mathbf{k}}{}^{\mu}\cdot\boldsymbol{\alpha}_1)}{\epsilon^2-k^2}+\frac{I_2I_1}{k^2}\right\}$$

$$-\text{Exch.} \tag{59}$$

This corresponds to the expression (55), and therefore is equal to the expectation value in the state (56) of the operator

$$W(1,2)=\frac{e^2}{2\pi^2}\int\frac{\mathbf{dk}}{k^2}e^{i\mathbf{k}\cdot\{\mathbf{x}(1)-\mathbf{x}(2)\}}\times\{1-\sum_{\mu=1,2}(\mathbf{e}_{\mathbf{k}}{}^{\mu}\cdot\boldsymbol{\alpha}(2))(\mathbf{e}_{\mathbf{k}}{}^{\mu}\cdot\boldsymbol{\alpha}(1))\} \tag{60}$$

corresponding to (57). Here, we made use of the definitions of $\boldsymbol{\alpha}_1$, $\boldsymbol{\alpha}_2$, I_1, I_2. We also have replaced here ϵ^2-k^2 in the first denominator of (59) by the slightly different $(-k^2)$, thus neglecting the retardation in the transverse interaction. (In the other terms, it was properly taken into account.) We shall further write $\mathbf{x}_1$ for $\mathbf{x}(1)$, $\boldsymbol{\alpha}_2$ for $\boldsymbol{\alpha}(2)$, etc. Also, we put $\mathbf{x}_1-\mathbf{x}_2=\mathbf{r}$. By

$$\int \mathbf{dk}k^{-2}\exp(i\mathbf{k}\cdot\mathbf{r})=2\pi^2/r \tag{61}$$

and

$$\int \mathbf{dk}k^{-4}\exp(i\mathbf{k}\cdot\mathbf{r})(\boldsymbol{\alpha}_1\cdot\mathbf{k})(\boldsymbol{\alpha}_2\cdot\mathbf{k})=-(\boldsymbol{\alpha}_1\cdot\boldsymbol{\nabla})(\boldsymbol{\alpha}_2\cdot\boldsymbol{\nabla})(-\pi^2r), \tag{62}$$

we can write (60) then in the form

$$W(1,2)=\{(e^2/r)(1-\boldsymbol{\alpha}_1\cdot\boldsymbol{\alpha}_2)+(e^2/2)(\boldsymbol{\alpha}_1\cdot\boldsymbol{\nabla})(\boldsymbol{\alpha}_2\cdot\boldsymbol{\nabla})r\}$$
$$=(e^2/r)\{1-\tfrac{1}{2}\boldsymbol{\alpha}_1\cdot\boldsymbol{\alpha}_2-\tfrac{1}{2}r^{-2}(\boldsymbol{\alpha}_1\cdot\mathbf{r})(\boldsymbol{\alpha}_2\cdot\mathbf{r})\}, \tag{63}$$

which is familiar as Breit's expression for the electron interaction energy.[20]

DISCUSSION

We notice that in Applications 2 and 3, where the terms corresponding to creation or annihilation of photon pairs dropped out for reasons of symmetry, we finally made use of only the properties (16)–(17) of Ψ_0. This explains how one can get the correct Møller and Breit interactions even when wrongly assuming that in zero-order approximation no longitudinal or scalar photons would be present.

In the first application, however, we found that a wrong zero-order approximation definitely leads to an incorrect result, unless one makes two more "mistakes" in order to compensate this first one. On the other hand, with use of the "correct" zero-order approximation consistent with this kind of quantum electrodynamics, the "correct" infinite result for the electromagnetic self-energy of an electron is obtained only as one possible result among many other possibilities, since the procedure of imposing an auxiliary condition on the situation functional leads, through the method of "normalization" of such situation functional, to mathematical ambiguities.

[19] H. Bethe and E. Fermi, Zeits. f. Physik **77**, 296 (1932).

[20] G. Breit, Phys. Rev. **34**, 553 (1929); **36**, 383 (1930); **39**, 616 (1932).

Theory of the Photo- and Electrodisintegration of Be^9 †

EUGENE GUTH AND CHARLES J. MULLIN
University of Notre Dame, Notre Dame, Indiana

(Received February 14, 1949)

Cross sections for the photo- and electrodisintegration processes at relatively low energies have been calculated as a function of energy on the basis of a simple model of the Be^9 nucleus in which a neutron is assumed to move in the potential well provided by the remainder of the nucleus. According to the theory, the disintegration at low energies results primarily from electric dipole transitions from the ground $P_{3/2}$ state to S and D states in the positive energy continuum. Magnetic dipole disintegration does not seem to play an important role. In order to obtain agreement between the theoretical and empirical photo-disintegration cross sections, it seems necessary to make the plausible assumption that the interaction between the prospective photo-neutron and the remaining nucleons of the nucleus is a function of the orbital angular momentum of the system (Majorana interaction). Furthermore, complete neglect of the $P_{3/2}-P_{\frac{1}{2}}$ splitting of the lowest P state leads to an angular distribution of the ejected neutrons which does not agree with the (preliminary) empirical results.

Using the Born-Møller Approximation, the cross section for electrodisintegration has been calculated in terms of the photodisintegration cross section. This method yields a correlation, which is independent of the nuclear model, between the observed photo- and electrodisintegration cross sections.

The theory based upon the simple model described seems adequate for an interpretation of the experimental data.

I. SUMMARY OF EMPIRICAL DATA ON THE DISINTEGRATION OF Be^9 BY LOW ENERGY PHOTONS, ELECTRONS, AND PROTONS

RECENTLY the cross section for the photo-disintegration of Be^9 was measured as a function of energy by Wattenberg and his associates.[1] Their results, as well as the results of other workers, are shown in Fig. 1. (The solid curve in Fig. 1 is a plot of the theoretical cross section derived in Section III of this paper.) It should be noted that the experimental results indicate that the photo-disintegration cross section has a sharp maximum and a minimum in the energy range covered by the data. Probably there is a second maximum beyond the range of these data.

Experimental data giving the cross section for electrodisintegration of Be^9 also are available. The first measurements were made by Collins, Waldman, and Guth[2] who obtained a value of $\sigma_e \cong 10^{-31}$ cm^2 with an electron beam energy of 1.73 Mev. Subsequently, Wiedenbeck,[3] using a thin Be target, determined the cross section as a function of energy in the energy range extending from the threshold to about 3 Mev.

Empirical results on the disintegration of Be^9 with protons have been obtained by Davis and Hafner.[4] These workers studied the energy distribution of protons inelastically scattered on Be^9. Incident proton energies of 4.5 Mev and 7.1 Mev were used, and the protons scattered through 37° were analyzed. The results show a sharp maximum in the energy distribution curve at 2.41 Mev.

The purpose of the present work is to see if the photo- and electrodisintegration data can be explained on the basis of a simple model of the Be^9 nucleus. The theory of the disintegration of Be^9 by protons has been given by Longmire.[5] Only a brief discussion of the correlation between the data on proton disintegration and those on photo- and electrodisintegration is given in this paper.

II. THE MODEL FOR THE Be^9 NUCLEUS

A. The Ground State

Three models for the Be^9 nucleus have been investigated.[6] These are: (1) the Hartree model, (2) the α-particle model ($2\alpha+n$), and (3) an "equivalent two-body model" in which the two α-particles are treated as a unit (Be^8) and the remaining neutron is assumed to move in the field of the Be^8 nucleus. Calculations to determine the ground state and magnetic moment of Be^9 have been carried out on the bases of the Hartree and α-particle approximations.[7-9] These calculations predict a $^2P_{3/2}$ ground state, and that the magnetic moment should lie in the interval $-0.7>\mu>-1.5$ nuclear magnetons.

The molecular beam magnetic resonance method has been applied to the measurement of the magnetic moment of Be^9 by Kusch, Millman, and Rabi.[10] The most reasonable interpretation of the results of these experiments yields $\mu=-1.18$ nuclear magnetons and $j=\frac{3}{2}$. An attempt to determine the angular momentum from hyperfine structure data has been made by Paul;[11] these data favor the value $j=\frac{3}{2}$ but do not exclude $j=\frac{1}{2}$.

The combined results of theory and experiment seem to favor a $P_{3/2}$ ground state, with the $D_{3/2}$ as second choice. The calculations made in this paper are based upon the choice of a $P_{3/2}$ ground state; however, the

† A statement of some of the results of the theory has been given by E. Guth and C. J. Mullin, Phys. Rev. **74**, 833 (1948), and Guth, Mullin, and Marshall, Phys. Rev. **74**, 834 (1948).

[1] Russell, Sachs, Wattenberg, and Fields, Phys. Rev. **73**, 545 (1948). The experimental data given in Fig. 1 were kindly communicated to us by Dr. Wattenberg.

[2] Collins, Waldman, and Guth, Phys. Rev. **55**, 875 (1939).

[3] Marcellus L. Wiedenbeck, Phys. Rev. **69**, 236 (1945).

[4] K. E. Davis and M. Hafner, Phys. Rev. **73**, 1473 (1948).

[5] Conrad L. Longmire, Phys. Rev. **74**, 1773 (1948); and thesis, University of Rochester, 1948. The authors wish to thank Dr. Longmire and Professor Marshak for communicating their results to us.

[6] For a brief summary of the models investigated for Be^9 see E. Guth and C. J. Mullin, Phys. Rev. **74**, 832 (1948).

[7] E. Feenberg and E. Wigner, Phys. Rev. **51**, 95 (1937).

[8] M. E. Rose and H. A. Bethe, Phys. Rev. **51**, 205 (1937).

[9] Robert G. Sachs, Phys. Rev. **55**, 825 (1939).

[10] Kusch, Millman, and Rabi, Phys. Rev. **55**, 666 (1939).

[11] W. Paul, Zeits. f. Physik **117**, 774 (1941).

empirical data probably can be explained also on the basis that the ground state is a $D_{3/2}$ state.

B. The Equivalent Two-Body Model

Attempts to calculate the disintegration cross sections on the basis of either the Hartree approximation or the α-particle approximation lead, of course, to laborious computations. For this reason a simpler yet creditable model of the Be^9 nucleus is desirable. In the Be^9 nucleus one neutron is loosely bound, having a binding energy of about 1.63 Mev,[12] compared to the 8–10-Mev average binding energy per particle. Guth[13] first pointed out that this would lend credence to the simple two-body model in which the neutron is regarded as moving in the potential field of the Be^8 nucleus. Although the Be^8 nucleus is unstable, breaking down into two α-particles, the unstability is only 116 kev;[14] and the lifetime of Be^8 is long compared to the time required for the ejection of a neutron from Be^9. Consequently, it may be expected that the two-body model is a reasonable approximation for the explanation of at least the coarse features of the disintegration process at low energies where only neutron ejection occurs. At higher energies competing processes, involving the ejection of a proton or an α-particle ($Be^9 \rightarrow He^5 + He^4$) may be expected.[15] For the description of these processes, and for an accurate description of the properties of the Be^9 nucleus (e.g., magnetic moment), a more accurate model is required.[16]

C. The Be^8-Neutron Interaction

In the present work the Be^8-neutron interaction for a given eigenstate of the system is assumed to be of the central field (non-tensor) type; for simplicity, this central interaction is represented by a spherical potential well. If the interaction is solely of the "ordinary" type, one well should describe the interaction for all the eigenstates of the system. If, on the other hand, the interaction is partly of the exchange type, the interaction energy may be expected to be a function of the orbital angular momentum of the system and of the orientation of the spin of the neutron. Since the Be^8 nucleus presumably has spin zero, it seems likely that the resultant of the interaction between the spin of the neutron and the spins of the Be^8 nucleons is small and plays a role only in the "fine structure" of the energy levels corresponding to a given value of the orbital angular momentum. Majorana-type forces, on the other hand, may be large; thus, the well depth and the well radius may be a function of the orbital angular momentum or at least of parity.

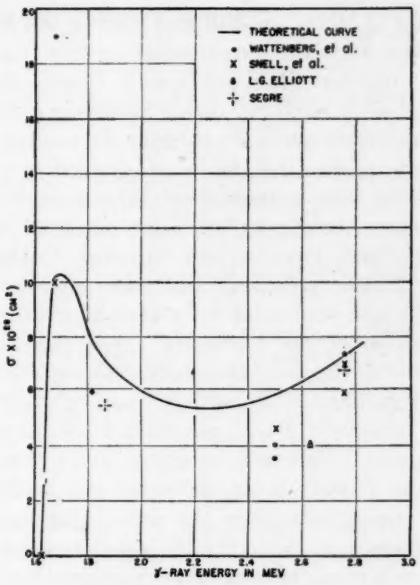

FIG. 1. Photo-disintegration cross sections for Be^9.

The assumption that the Be^8-neutron interaction is of the "ordinary" type, requiring only one well to describe the interactions for all states of the system, has been employed by Mamasachlisov[17] in formulating a theory of the electrodisintegration of Be^9. The disintegration is attributed to an electric dipole transition from the ground P state to an S state in the positive energy continuum. Mamasachlisov's results, which were based in part on the results of Bethe and Peierls[18] for the electrodisintegration of the deuteron, appeared to give good agreement with the experimental measurements of Collins, Waldman, and Guth at 1.73 Mev. However, the results of Bethe and Peierls used by Mamasachlisov were marred by two algebraic errors which were subsequently corrected by Wick.[19] The correction of these errors reduced Mamasachlisov's theoretical cross section

[12] The calculations in this paper are based upon the value 1.63 for the binding energy of the neutron. This value was determined by Collins, Waldman, and Guth (reference 2). More recent measurements on the binding energy of the deuteron by R. E. Bell and L. G. Elliott (Phys. Rev. **74**, 1552 (1948)) yield a value of about 1.67 Mev for the binding energy of the neutron in Be^9. Use of this latter value would not greatly alter our results for the total cross section, but may, of course, alter the angular distribution of the photo-neutrons by a measureable amount at some γ-ray energies.

[13] Eugene Guth, Phys. Rev. **55**, 411 (1939).

[14] The instability was first shown by E. Glückauf and F. A. Paneth, Proc. Roy. Soc. **A165**, 229 (1938). The value 116 kev is due to Arthur Hemmendinger, Phys. Rev. **73**, 806 (1948).

[15] The $\gamma - p$ reaction for Be^9 has been observed by Ogle, Brown, and Conklin, Phys. Rev. **71**, 378 (1947) and Phys. Rev. **73**, 648 (1948); the threshold for proton ejection is about 18 Mev. The threshold for the ejection of an α-particle ($Be^9 \rightarrow He^6 + H^4$) and the threshold for the $Be^9 \rightarrow \alpha + \alpha + n$ process should be about 5 Mev.

[16] T. Schmidt (Zeits. f. Physik **106**, 358 (1937)) has used the two-body model to explain the magnetic moments of nuclei. As expected, the representation is better for medium and heavy nuclei than it is for light nuclei. Inclusion of the exchange current contribution to the magnetic moment yields only a small correction to Schmidt's results. A general theoretical discussion of the magnetic moments of nuclei has also been given by Margenau and Wigner (Phys. Rev. **58**, 103 (1940)). Assuming the ground state of Be^9 to be a $P_{3/2}$ state, the measurements of Kusch, Millman, and Rabi (reference 10) yield a result for the magnetic moment which falls above the lower limits set by these theories, and which is, therefore, consistent with the results obtained from these theories.

[17] V. I. Mamasachlisov, J. Phys. U.S.S.R. **7**, 239 (1943).

[18] H. A. Bethe and R. Peierls, Proc. Roy. Soc. **A148**, 146 (1935).

[19] G. C. Wick, Ricerca Scient. **11**, 49 (1940). See also B. Peters and C. Richman, Phys. Rev. **59**, 804 (1941).

by a factor of about one-half and led to a less favorable comparison with the experimental result. Caldirola[20] tried to improve Mamasachlisov's theory by introducing, *ad hoc*, a magnetic dipole transition between the $P_{3/2}$ ground state and a $P_{\frac{1}{2}}$ state in the positive energy continuum; again all states were assumed to be eigenstates of the same potential well. However, if the $P_{3/2}$ and $P_{\frac{1}{2}}$ states belong to the same potential well, the magnetic dipole cross section vanishes. Caldirola apparently did not notice this and, using approximations, obtained a non-zero value for a vanishing integral.

Interaction of the "ordinary" type has also been applied to the theory of the photo-disintegration of Be^9 by Mamasachlisov,[21] Borsellino,[22] and Schlögl.[23] These workers consider a $P \rightarrow S$ transition. Unfortunately the virtual level of the S state belonging to the same well as the ground P state is far too broad and occurs at too high an energy to explain the rather sharp maximum which occurs just above the threshold in the empirical cross section *versus* energy curve. Furthermore, it seems that *two* transitions are required to explain the maximum, minimum, and subsequent rise in the experimental curve (Fig. 1).

It should be noted that the assumption that the Be^8-neutron interaction is entirely of the "ordinary type" contradicts the assumption that the ground state is a P state. For if the S states belong to the same well as the P states, the lowest lying bound level should be an S state. Furthermore, application of the Pauli principle to the external neutron and those in the α-particles makes it seem likely that the effective potential is deeper for P states than it is for S and D states. Because of these considerations, and since the positive energy states belonging to the potential well used to describe the ground state have virtual levels which (1) are far too broad and (2) do not occur at the proper energy values

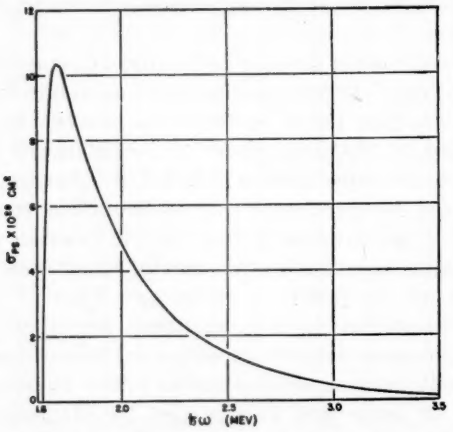

FIG. 2. Photo-disintegration cross sections due to the $P \rightarrow S$ transitions.

[20] P. Caldirola, J. de phys. et rad. 8, 155 (1947).
[21] V. I. Mamasachlisov, Physik. Zeits. Sowjetunion **9** (1936).
[22] A. Borsellino, Nuovo Cimento 5, No. 4 (1948).
[23] F. Schlögl, Zeits. f. Naturforschung **3a**, 229 (1948). Schlögl also considers the possibility that the ground state may be an S state.

to explain the empirical data, it seems necessary to assume that the Be^8-neutron interaction is of a type which depends upon the orbital angular momentum (or at least upon parity) and upon the orientation of the spin of the neutron. In the spherical potential well approximation, this type of interaction is introduced schematically by assuming the well depth to be a function of orbital angular momentum and spin orientation. The spin interaction results in a "fine structure" splitting of the levels corresponding to a given value of the orbital angular momentum. Thus, presumably, the ground P state is split into $P_{3/2}$ and $P_{\frac{1}{2}}$ levels, with the $P_{3/2}$ level as the ground state. This inverted order of the splitting would be expected if the spin interaction is of the relativistic spin-orbit type. Although there is no conclusive experimental evidence for the splitting of the lowest P state in Be^9, it is reasonable to assume this splitting to be approximately the same as the known splitting of similar levels in other light nuclei. In He^5 the ^2P splitting is about 250 kev[24] and appears to be normal —the ground state being a $P_{\frac{1}{2}}$ state. Dancoff[25] has shown that this splitting may be understood on the basis of tensor forces. In Li^7 an excited state has been found 478.5 kev above the ground state.[26] The ground state for Li^7 is believed to be a $P_{3/2}$ state. Until recently it has been assumed that the excited state 478.5 kev above the ground state is the $P_{\frac{1}{2}}$ member of the P doublet, the 478.5 kev separation probably being due to relativistic spin orbit coupling.[27] This interpretation has been successfully applied, for example, in the interpretation of the experimental data on the K-capture transitions $Be^7 \rightarrow Li^7$ and $Be^7 \rightarrow Li^{7*}$.[28] An analysis of the $B^{10}(n, \alpha)Li^7$ reaction, using the recently measured[29] value $I=3$ for the nuclear spin of B^{10}, leads Inglis[30] to favor the interpretation that the ^2P splitting is so small that it has not been resolved, and that the observed excited state is an unresolved $^2F_{7/2, 5/2}$. The magnitude of the ^2P splitting in Be^9 is not of great importance in the present work, in which it will be assumed only that the splitting is of sufficient magnitude that practically all the Be^9 nuclei are initially in the $j=\frac{3}{2}$ state. Complete neglect of the ^2P

[24] H. Staub and H. Tatel, Phys. Rev. **58**, 820 (1940); H. Staub and W. E. Stephens, Phys. Rev. **55**, 131 (1939).
[25] S. M. Dancoff, Phys. Rev. **58**, 326 (1940).
[26] The value 478.5 kev is due to L. G. Elliott and R. E. Bell, Phys. Rev. **74**, 1869 (1948). The excited state was found by L. H. Rumbaugh and L. R. Hafstad, Phys. Rev. **50**, 681 (1936). Six reactions which leave Li^7 in a low lying excited state are known. These reactions have been summarized by W. Hornyak and T. Lauritsen, Rev. Mod. Phys. **20**, 191 (1948).
[27] David R. Inglis, Phys. Rev. **50**, 783 (1936) and Phys. Rev. **56**, 1178 (1939). See also G. Breit and J. R. Stehn, Phys. Rev. **53**, 459 (1938), and Charles Kittel, Phys. Rev. **62**, 109 (1942). The most recent theoretical considerations seem to indicate that relativistic spin-orbit coupling does not produce large splitting; the origin of the nuclear doublets is not understood quantitatively at present. See S. Hanna and D. R. Inglis, Phys. Rev. **75**, 1767 (1949); D. R. Inglis, Phys. Rev. **75**, 1767 (1949).
[28] C. Breit and J. K. Knipp, Phys. Rev. **54**, 652 (1938). See also Emil Jan Konopinski, Rev. Mod. Phys. **15**, 209 (1943).
[29] Gordy, Ring, and Burg, Phys. Rev. **74**, 1191 (1948). See also M. Goldhaber, Phys. Rev. **74**, 1194 (1948).
[30] David R. Inglis, Phys. Rev. **74**, 1876 (1948).

splitting seems to lead to an incorrect angular distribution for the neutrons obtained in the (γ, n) process (see Section III-*D*). In Section III-*E* it is shown that magnetic dipole transitions play a negligible role in the disintegration process if the ^2P splitting does not exceed 500 kev.

SYMBOLS USED IN THE TEXT

i: initial eigenstate of the system
f: final eigenstate of the system normalized on the energy scale
m: rest mass of the electron
M: mass of neutron
μ: reduced mass of neutron $\cong \frac{8M}{9}$
r: radius vector from Be^8 to neutron
z: $r\cos\theta$
α_n, β_n: spin eigenvectors for the neutron
σ_n: Pauli spin vector for the neutron
μ_n: magnetic moment of neutron
ϵ: binding energy for the ground state
E: energy of the neutron
$Y_{l,m}(\theta, \phi)$: normalized surface harmonic
$j_l(x)$: spherical Bessel function of order l:

$$j_l(x)=\left(\frac{\pi}{2x}\right)^{\frac{1}{2}}J_{l+\frac{1}{2}}(x)$$

$V_{l,j}$: well-depth describing the Be^8-neutron interaction in the state with quantum numbers l (orbital angular momentum) and j (total angular momentum)
V_2: average well depth for the $D_{3/2}$, $D_{5/2}$ states

$$\alpha=\left[\frac{2\mu}{\hbar^2}\epsilon\right]^{\frac{1}{2}},\quad k=\left[\frac{2\mu}{\hbar^2}E\right]^{\frac{1}{2}},$$

$$\beta=\left[\frac{2\mu}{\hbar^2}(V_{1,3/2}+E)\right]^{\frac{1}{2}},$$

$$\gamma=\left[\frac{2\mu}{\hbar^2}(V_{0,\frac{1}{2}}+E)\right]^{\frac{1}{2}},$$

$$\xi=\left[\frac{2\mu}{\hbar^2}(V_2+E)\right]^{\frac{1}{2}},$$

$$\eta=\left[\frac{2\mu}{\hbar^2}(V_{1,\frac{1}{2}}+E)\right]^{\frac{1}{2}}.$$

III. CROSS SECTION FOR PHOTO-DISINTEGRATION

A. General Considerations

Photo-disintegration of Be^9 results when photons incident upon the nucleus cause the neutron to be excited from the ground state to states of positive energy. In general, the photons may produce photoelectric and photomagnetic transitions. In first approximation, only electric dipole and magnetic dipole transitions need be considered at low energies. Since the resultant spin interaction between the loosely bound neutron and the nucleons of Be^8 seems to be small, the well depth used to describe the Be^8 neutron interaction is only slightly dependent upon the orientation of the neutron spin; consequently, the cross section for magnetic dipole transitions is small, and, in first approximation, only electric dipole transitions need be considered. (Later, in part *E* of this section, magnetic dipole transitions will be considered.) Using a ground P state, the selection rule

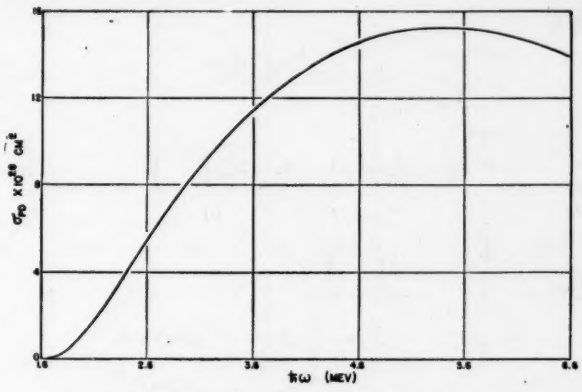

FIG. 3. Photo-disintegration cross sections due to the $P\rightarrow D$ transitions.

$\Delta l=\pm 1$ for electric dipole transitions permits $P\rightarrow S$ and $P\rightarrow D$ transitions.

The cross section for electric dipole disintegration of Be^9 is given by

$$\sigma=(64\pi^2/81)(e^2/\hbar c)\hbar\omega\sum|\langle f|z|i\rangle|^2, \tag{1}$$

where the summation is to be extended over all non-vanishing matrix elements. Assuming the spin interaction to be small and of a central (non-tensor) type, the eigenstates f, i are described by the quantum numbers E (energy), j, m_j, and l. The eigenfunctions are

$$\psi(l, j=l+\tfrac{1}{2}, m_j)=\frac{R_{l,j}(r)}{(2l+1)^{\frac{1}{2}}}\{(l+\tfrac{1}{2}+m_j)^{\frac{1}{2}}Y_{l,m_j-\frac{1}{2}}(\theta,\phi)\alpha_n+(l+\tfrac{1}{2}-m_j)^{\frac{1}{2}}Y_{l,m_j+\frac{1}{2}}(\theta,\phi)\beta_n\}, \tag{2a}$$

$$\psi(l, j=l-\tfrac{1}{2}, m_j)=\frac{R_{l,j}(r)}{(2l+1)^{\frac{1}{2}}}\{(l+\tfrac{1}{2}-m_j)^{\frac{1}{2}}Y_{l,m_j-\frac{1}{2}}(\theta,\phi)\alpha_n-(l+\tfrac{1}{2}+m_j)^{\frac{1}{2}}Y_{l,m_j+\frac{1}{2}}(\theta,\phi)\beta_n\}. \tag{2b}$$

The matrix element $\langle f|z|i\rangle$ of Eq. (1) is different from zero only if $\Delta l=\pm 1$, $\Delta j=0, \pm 1$, $\Delta m_j=0$.

B. Cross Section for the $P\rightarrow S$ Transition

Using the potential well approximation, the Be^8-neutron interaction for the ground $P_{3/2}$ state is described by

$$V=-V_{1,3/2}\quad r\leqslant r_0,$$
$$V=0\quad r\geqslant r_0.$$

The four initial states are given by Eq. (2a). For these states

$$R_{1,3/2}(r)=A_1 j_1(\beta r)\quad r\leqslant r_0,$$
$$R_{1,3/2}(r)=B_1\frac{(1+\alpha r)}{r^2}e^{-\alpha(r-r_0)}\quad r\geqslant r_0, \tag{3}$$

with

$$B_1=-\frac{A_1}{\alpha^2}\sin\beta r_0, \tag{4a}$$

$$\beta r_0\cot\beta r_0=1+(1+\alpha r_0)\left(\frac{\beta}{\alpha}\right)^2, \tag{4b}$$

$$\frac{A_1^2 r_0}{2\beta^2}\left\{1+\left[(2+\alpha r_0)\left(\frac{\beta}{\alpha}\right)^4+(1+\alpha r_0)\left(\frac{\beta}{\alpha}\right)^2-1\right]\frac{\sin^2\beta r_0}{(\beta r_0)^2}\right\}=1. \tag{4c}$$

Using $\epsilon=1.63$ Mev, and assuming $r_0=5\times10^{-13}$ cm, Eq. (4b) gives $V_{1,3/2}=12.16$ Mev. Equations (4a) and (4c) then determine A_1 and B_1.

The final S states are obtained from Eq. (2a) with

$$R_{0,\frac{1}{2}}=A_0 j_0(\gamma r), \qquad r\leqslant r_0,$$
$$R_{0,\frac{1}{2}}=\left(\frac{2}{\pi}\frac{\mu k}{\hbar^2}\right)^{\frac{1}{2}}\frac{\sin[k(r-r_0)+\delta_0]}{kr} \qquad r\geqslant r_0, \tag{5}$$

where

$$A_0\sin\gamma r_0=\frac{\gamma}{k}\left(\frac{2}{\pi}\frac{\mu k}{\hbar^2}\right)^{\frac{1}{2}}\sin\delta_0, \tag{6a}$$

$$A_0\cos\gamma r_0=\left(\frac{2}{\pi}\frac{\mu k}{\hbar^2}\right)^{\frac{1}{2}}\cos\delta_0. \tag{6b}$$

For the $P\rightarrow S$ transition, these equations yield

$$\sum|\langle f|z|i\rangle|^2=|R_{ps}|^2/9, \tag{7}$$

where

$$R_{ps}=\int_0^\infty R_{0,\frac{1}{2}}{}^* R_{1,3/2} r^3 dr,$$

and, thus,

$$\sigma_{ps}=(64\pi^2/729)(e^2/\hbar c)\hbar\omega|R_{ps}|^2. \tag{8}$$

From Eqs. (3), (4), (5), and (6)

$$R_{ps}=\frac{B_1\alpha^2[(2/\pi)(\mu k/\hbar^2)]^{\frac{1}{2}}}{r_0(k^2+\gamma^2\cot^2\gamma r_0)^{\frac{1}{2}}}\times\left\{\frac{2+2(\beta^2/\alpha^2)(1+\alpha r_0)-r_0^2(\gamma^2-\beta^2)}{(\gamma^2-\beta^2)^2}+\frac{\alpha r_0(2+\alpha r_0)+k^2r_0^2}{(\alpha^2+k^2)^2}+\left[-\frac{2+[(\gamma^2-\beta^2)/\alpha^2](1+\alpha r_0)}{(\gamma^2-\beta^2)^2}+\frac{3+\alpha r_0+(k^2/\alpha^2)(1+\alpha r_0)}{(\alpha^2+k^2)^2}\right]\cdot\gamma r_0\cot\gamma r_0\right\} \tag{9}$$

with B_1 given by Eq. (4).

The cross section given by Eq. (8) contains the well depth $V_{0,\frac{1}{2}}$ as an adjustable parameter.[31] The choice $V_{0,\frac{1}{2}}=3$ Mev yields the curve shown in Fig. 2. The cross section for the $P\rightarrow S$ transition gives a sharp maximum* just above the threshold and is in fairly good agreement with the experimental measurements made for energies just above the threshold (Fig. 1).

C. Cross Section for the $P\rightarrow D$ Transition

The wave functions for the final $D_{3/2}$ and $D_{5/2}$ states are given by Eq. (2). The gradual rise beyond 2.5 Mev in the cross section *versus* energy curve is presumably due to the $P\rightarrow D$ transition. The gradualness of this rise indicates that the resonance D levels are broad. If the resonance D levels are broad, and if the $D_{5/2}-D_{3/2}$ splitting is not unexpectedly large, a good approximation is obtained by using the same (average) well to describe the $D_{3/2}$ and $D_{5/2}$ states. (This means that in the evaluation of σ_{PD} we set $V_{2,3/2}=V_{2,5/2}=V_2=$average well depth describing the Be^8-neutron interaction in the D-state.) Using this approximation,

$$R_{2,3/2}=R_{2,5/2}=R_2=A_2 j_2(\xi r),$$
$$R_{2,3/2}=R_{2,5/2}=R_2=\left(\frac{2}{\pi}\frac{\mu k}{\hbar^2}\right)^{\frac{1}{2}}\frac{(3-k^2r^2)\sin[k(r-r_0)+\delta_2]-3kr\cos[k(r-r_0)+\delta_2]}{k^3r^3}, \tag{10}$$

with

$$A_2=\left(\frac{2}{\pi}\frac{\mu k}{\hbar^2}\right)^{\frac{1}{2}}\left(\frac{\xi}{k}\right)^3\times\frac{(3-k^2r_0^2)\sin\delta_2-3kr_0\cos\delta_2}{(3-\xi^2r_0^2)\sin\xi r_0-3\xi r_0\cos\xi r_0}, \tag{11a}$$

$$\frac{(3-k^2r_0^2)\sin\delta_2-3kr_0\cos\delta_2}{(3-\xi^2r_0^2)\sin\xi r_0-3\xi r_0\cos\xi r_0}=\left(\frac{k}{\xi}\right)^2\frac{\sin\delta_2-kr_0\cos\delta_2}{\sin\xi r_0-\xi r_0\cos\xi r_0}; \tag{11b}$$

thus for the $P_{3/2}\rightarrow D_{3/2}$ transition

$$\sum|\langle f|z|i\rangle|^2=\frac{|R_{PD}|^2}{250}\int\{[4|Y_{22}|^2+|Y_{21}|^2]+\tfrac{1}{9}[2|Y_{20}|^2+3|Y_{21}|^2]\}d\Omega \tag{12a}$$

$$=\frac{|R_{PD}|^2}{45}; \tag{12b}$$

[31] Since the well depth and well radius are not independent parameters, the same well radius, $r_0=5\times10^{-13}$ cm, has been used for all wells.

* The choice $V_{0,\frac{1}{2}}=3$ Mev for the depth of the S-well yields a bound level at $E\cong-100$ kev. This level acts as a *resonance* level,

and for the $P_{3/2}\rightarrow D_{5/2}$ transition

$$\sum|\langle f|z|i\rangle|^2=\frac{|R_{PD}|^2}{125}\int\{2[4|Y_{21}|^2+|Y_{22}|^2]+3[3|Y_{20}|^2+2|Y_{21}|^2]\}d\Omega \quad (13a)$$

$$=\frac{|R_{PD}|^2}{5}, \quad (13b)$$

where

$$R_{PD}=\int_0^\infty R_2^* R_{1,3/2} r^3 dr.$$

The term in the first bracket on the right-hand side of each of the Eqs. (12a) and (13a) represents the contribution from the $|m_j|=\frac{3}{2}$ states; the term in the second bracket represents the contribution from the $|m_j|=\frac{1}{2}$ states. Adding the contributions from the $P_{3/2}\rightarrow D_{3/2}$ and the $P_{3/2}\rightarrow D_{5/2}$ transitions, the cross section for transition to the D doublet is

$$\sigma_{PD}=\frac{128}{729}\pi^2\frac{e^2}{\hbar c}\hbar\omega|R_{PD}|^2. \quad (14)$$

From Eqs. (3), (4), (10), and (11)

$$R_{PD}=\frac{B_1[(2/\pi(\mu k/\hbar^2))^{\frac{1}{2}}}{\{k^2r_0^2(3QP+k^2r_0^2)^2+(3QP+k^2\xi r_0^3\cot\xi r_0)^2\}^{\frac{1}{2}}}$$
$$\times\left\{k^2r_0^2\left[\frac{2k^2(1+\alpha r_0)-\alpha^2r_0^2(\alpha^2+k^2)}{(\alpha^2+k^2)^2}-\frac{2(1+\alpha r_0)\xi^2-\alpha^2r_0^2(\xi^2-\beta^2)}{(\xi^2-\beta^2)^2}\right]\right.$$
$$+k^2r_0^2Q\left[\frac{(\alpha^2+k^2)(1+\alpha r_0+3(\alpha^2/k^2))+2\alpha^2}{(\alpha^2+k^2)^2}-\frac{(\xi^2-\beta^2)(1+\alpha r_0+(\alpha^2/\xi^2))+2\alpha^2}{(\xi^2-\beta^2)^2}\right]$$
$$\left.+3PQ\left[\frac{2k^2(1+\alpha r_0)-\alpha^2r_0^2(\alpha^2+k^2)}{(\alpha^2+k^2)^2}\right]\right\}, \quad (15)$$

where $Q=1-\xi r_0\cot\xi r_0$ and $P=1-\xi^2/k^2$. The cross section σ_{PD} contains the well depth $V_2(=V_{2,3/2}=V_{2,5/2})$ as an adjustable parameter. However, on the basis of a Majorana interaction, it may be expected that the well depth should be a function of parity rather than orbital angular momentum. For this reason, the choice $V_2=V_{0,\frac{1}{2}}=3$ Mev has been made. With this choice, Eq. (14) yields the curve shown in Fig. 3.

maximizing the wave function inside the well; this resonance level is responsible for the sharp maximum in σ_{pn}. The photoelectric disintegration cross section of the deuteron has a *broad* maximum because the outgoing P-wave is a free wave.

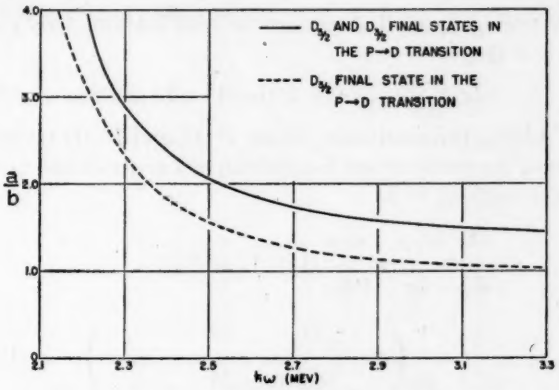

FIG. 4. Angular distribution of the photo-neutrons as a function of energy.

D. Total Cross Section for Photoelectric Disintegration

Angular Distribution of the Photo-Neutrons

In the dipole approximation, the total cross section for photoelectric disintegration is given by

$$\sigma=\sigma_{PS}+\sigma_{PD}. \quad (16)$$

The partial cross sections σ_{PS} and σ_{PD} are given by Eqs. (8) and (14). For the case $V_{0,\frac{1}{2}}=V_2=3$ Mev, the partial cross sections may be obtained from Figs. 2 and 3. For this case the resulting total cross section is plotted as the solid curve in Fig. 1. From these figures it may be seen that the $P\rightarrow S$ transition is predominant for energies near the threshold, whereas the $P\rightarrow D$ transition plays the predominant role for energies somewhat above 2.5 Mev.

In the range of energy for which the $P\rightarrow S$ transition is primarily responsible for the disintegration, the angular distribution of the ejected neutrons should be that characteristic of an S wave—spherically symmetric. In the range of energy in which the $P\rightarrow D$ transition is important, the angular distribution of the D neutrons must be taken into consideration. The angular distribution of the neutrons ejected into D states may be obtained from Eqs. (12a), (13a), and (1). The $P_{3/2}\rightarrow D_{5/2,3/2}$ cross section for ejection of a neutron into unit solid angle at θ is

$$\frac{d\sigma_{PD}}{d\Omega}=\frac{d}{d\Omega}(\sigma_{P_{3/2}\rightarrow D_{3/2}}+\sigma_{P_{3/2}\rightarrow D_{5/2}})$$
$$=\frac{\sigma_{PD}}{100\pi}(17+24\cos^2\theta). \quad (17)$$

The angle, θ, between the direction of the outgoing neutron and the direction of polarization of the incident radiation may be expressed in terms of the angle, Θ, between the direction of the outgoing neutron and the direction of propagation of the incident photon beam, and an angle, χ, giving the direction of polarization of the incident radiation:

$$\cos^2\theta=\cos^2\chi\sin^2\Theta.$$

Averaging over-all directions of polarization, $\langle\cos^2\chi\rangle_{Av}=\frac{1}{2}$, and

$$(d\sigma_{PD}/d\Omega)=(\sigma_{PD}/100\pi)(17+12\sin^2\Theta). \quad (18)$$

Adding the results due to the $P\rightarrow S$ and $P\rightarrow D$ transitions, the cross section for ejection of a neutron into unit solid angle at Θ is

$$\frac{d\sigma}{d\Omega}=\frac{\sigma_{PS}}{4\pi}+\frac{\sigma_{PD}}{100\pi}(17+12\sin^2\Theta)$$

$$=\frac{1}{4\pi}\left(\sigma_{PS}+\frac{17}{25}\sigma_{PD}+\frac{12}{25}\sigma_{PD}\sin^2\Theta\right). \quad (19)$$

The distribution is, thus, of the general form

$$d\sigma/d\Omega=a+b\sin^2\Theta, \quad (20)$$

where a and b are, of course, functions of energy. From Eq. (19)

$$\frac{a}{b}=\frac{25}{12}\frac{\sigma_{PS}}{\sigma_{PD}}+\frac{17}{12}. \quad (21)$$

The values of σ_{PS} and σ_{PD} may be calculated from Eqs. (8) and (14). For the special case that $V_{0,\frac{1}{2}}=V_2=3$ Mev, the values of σ_{PS} and σ_{PD} may be taken from Figs. 2 and 3; The resulting values for a/b are shown in Fig. 4 (solid curve). For energies just above the threshold, $\sigma_{PS}\gg\sigma_{PD}$, and the distribution is spherically symmetric; this is in agreement with the measurements of Goloborodko and Rosenkewitch[32] who found the neutrons ejected with very low energies to have a uniform angular distribution. Hamermesh and Wattenberg[33] find $a/b\cong 1.5$ at 2.76 Mev. The theoretical value obtained from Fig. 5 is $a/b=1.65$ at this energy.

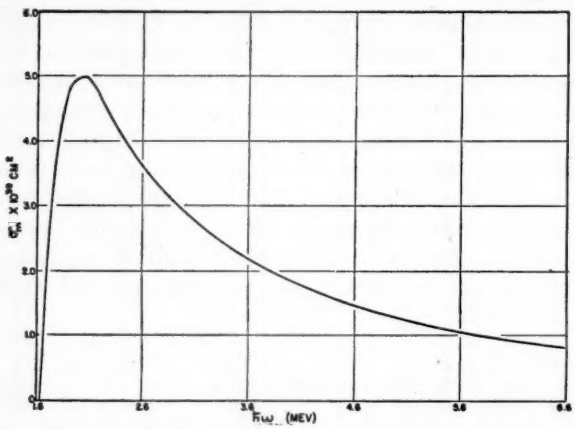

FIG. 5. Cross section for magnetic dipole disintegration.

If the splitting of the levels corresponding to a given orbital angular momentum into $j=l\pm\frac{1}{2}$ components is neglected entirely, so that the ground state has coincident $P_{3/2}$ and $P_{\frac{1}{2}}$ levels, the wave functions are

$$\psi_{E,l,m}=Y_{l,m}(\theta,\phi)R_{E,l}(r). \quad (22)$$

These wave functions lead to the same total cross section obtained with the wave functions given by Eq. (2). However, the angular distribution obtained from the wave functions given by Eq. (22) is

$$d\sigma/d\Omega=1/8\pi\{2\sigma_{PS}+\sigma_{PD}+\tfrac{3}{2}\sigma_{PD}\sin^2\Theta\}. \quad (23)$$

This gives the value

$$\frac{a}{b}=\frac{2}{3}\left(1+\frac{2\sigma_{PS}}{\sigma_{PD}}\right). \quad (24)$$

At 2.76 Mev, this yields $a/b=0.72$, which compares very unfavorably with the measured value of $a/b=1.5$.

Of course, another reasonable alternative is to assume that the $P_{3/2}\rightarrow D$ transition which is responsible for the rise observed beyond 2.5 Mev in the σ *versus* $\hbar\omega$ curve (Fig. 1) occurs to only one of the $D_{5/2}$, $D_{3/2}$ components. On the basis of relativistic spin orbit coupling, the $D_{5/2}$ level should occur at a lower energy than the $D_{3/2}$. The assumption that the $D_{5/2}$ level is the one primarily responsible for the $P_{3/2}\rightarrow D$ transition in the energy range of the observed data produces little change in the total cross section; actually $\sigma_{PD_{5/2}}=(9/10)\sigma_{PD}$, where σ_{PD} is given by Eq. (14). However, the angular distribution becomes

$$d\sigma/d\Omega=1/4\pi\{\sigma_{PS}+\tfrac{3}{5}\sigma_{PD_{5/2}}+\tfrac{3}{5}\sigma_{PD_{5/2}}\sin^2\Theta\}, \quad (25)$$

or

$$\frac{a}{b}=1+\frac{5}{3}\frac{\sigma_{PS}}{\sigma_{PD_{5/2}}}. \quad (26)$$

A plot of Eq. (26) for the special case $V_{0,\frac{1}{2}}=V_2=3$ Mev is given in Fig. 4 (dashed curve).

E. Magnetic Dipole Disintegration

The cross section for magnetic dipole disintegration is

$$\sigma_m=(4\pi^2/\hbar c)\hbar\omega\sum|\langle f|\mu_z|i\rangle|^2, \quad (27)$$

where the summation is to be extended over all non-vanishing matrix elements. μ_z is the component of the magnetic dipole moment of the Be^9 system along the direction of the magnetic vector of the incident radiation. The magnetic dipole moment is

$$\boldsymbol{\mu}=(e\hbar/2Mc)(\mu_n\boldsymbol{\sigma}_n+(1/18)\mathbf{L}). \quad (28)$$

The first term on the right-hand side gives the magnetic moment of the loosely bound neutron, and the second term gives the magnetic moment due to the orbital motion of the Be^8 around the center of gravity. In terms

[32] T. Goloborodko and L. Rosenkewitch, Physik. Zeits. Sowjetunion **11**, 78 (1936). See also J. Chadwick and M. Goldhaber, Proc. Roy. Soc. **A151**, 479 (1935).

[33] B. Hamermesh and A. Wattenberg, Phys. Rev. **75**, 1290(A) (1949). The value $a/b=1.5$ was obtained in a preliminary measurement. In more recent measurements B. Hamermesh, M. Hamermesh, and A. Wattenberg (scheduled for publication in Phys. Rev. Aug. 15, 1949) obtained $a/b=1.22$. E. P. Meiners (private communication) has obtained the value $a/b=1.15\pm0.07$. A more complete discussion of the theory of the angular distribution, in which the dependence of a/b upon the binding energy of the neutron is considered, has been given by C. J. Mullin and E. Guth (to be published in Phys. Rev. August 15, 1949).

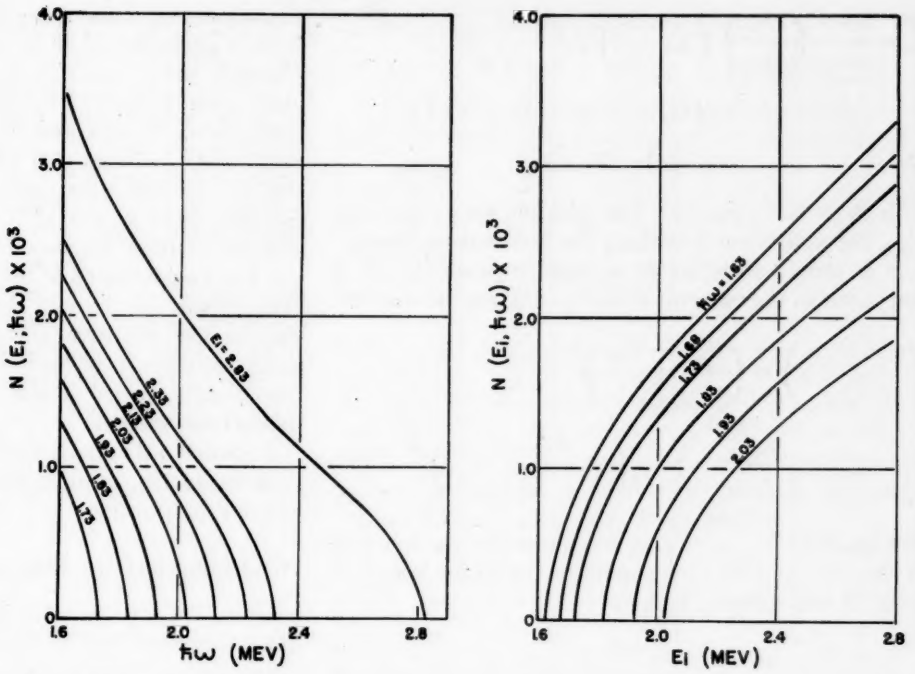

FIG. 6. Number of photoelectric quanta as a function of $\hbar\omega$ and E_i.

of the total angular momentum, $\mathbf{J}=\mathbf{L}+\frac{1}{2}\boldsymbol{\sigma}$,

$$\mu_z=\frac{e\hbar}{2Mc}\left(\mu_n-\frac{1}{36}\right)+\frac{e\hbar}{2Mc}\cdot\frac{1}{18}J_z. \tag{29}$$

Assuming the spin interaction to be relatively small and of a central (non-tensor) type, the eigenstates f, i are given by Eq. (2). For these eigenstates, J_z is a constant of the motion, and the matrix elements involving J_z vanish. Consequently,

$$\sigma_m=4\pi^2\left(\frac{e^2}{\hbar c}\right)\left(\frac{\hbar}{2Mc}\right)^2 \times\left(\mu_n-\frac{1}{36}\right)^2\hbar\omega\sum|\langle f|\sigma_{nz}|i\rangle|^2. \tag{30}$$

Since the initial states are $P_{3/2}$ states, the orthogonality of the angular functions involved in f, i, requires that the final states be $P_{\frac{1}{2}}$ states if the matrix elements in Eq. (30) are to be different from zero. Obtaining f, i from Eq. (2),

$$\frac{d\sigma_m}{d\Omega}=\frac{16\pi^2}{27}\left(\frac{e^2}{\hbar c}\right)\left(\frac{\hbar}{2Mc}\right)^2 \times\left(\mu_n-\frac{1}{36}\right)^2\hbar\omega|R_{PP}|^2\{|Y_{10}|^2+2|Y_{11}|^2\}, \tag{31}$$

and

$$\sigma_m=\frac{16\pi^2}{9}\left(\frac{e^2}{\hbar c}\right)\left(\frac{\hbar}{2Mc}\right)^2\hbar\omega|R_{PP}|^2, \tag{32}$$

where

$$R_{PP}=\int_0^\infty R_{1,3/2}{}^*R_{1,\frac{1}{2}}r^2dr.$$

The radial function $R_{1,3/2}$ is given by Eqs. (3) and (4). The radial function $R_{1,\frac{1}{2}}$ is

$$R_{1,\frac{1}{2}}(r)=A_{\frac{1}{2}}j_1(\eta r), \qquad r\leqslant r_0,$$
$$R_{1,\frac{1}{2}}=\left(\frac{2}{\pi}\frac{\mu k}{\hbar^2}\right)^{\frac{1}{2}}\frac{\sin[k(r-r_0)+\delta_{\frac{1}{2}}]-kr\cos[k(r-r_0)+\delta_{\frac{1}{2}}]}{k^2r^2} \qquad r\geqslant r_0, \tag{33}$$

with

$$A_{\frac{1}{2}}=\frac{\eta^2}{k^2}\left(\frac{2}{\pi}\frac{\mu k}{\hbar^2}\right)^{\frac{1}{2}}\frac{\sin\delta_{\frac{1}{2}}-kr_0\cos\delta_{\frac{1}{2}}}{\sin\eta r_0-\eta r_0\cos\eta r_0}, \tag{34a}$$

$$\sin\delta_{\frac{1}{2}}=\frac{kr_0}{\{(kr_0)^2+[1-(k^2/\eta^2)G]^2\}^{\frac{1}{2}}}, \tag{34b}$$

$$G=1-\eta r_0\cot\eta r_0.$$

R_{PP} may be determined by straightforward integration, which gives[34]

[34] A different formula for the integral must be applied for the case $\eta=\beta$. The integration shows that the cross section does not become large for this case; in fact, this point fits on the curve obtained from (35) by excluding the point $\beta=\eta$. The same procedure must be applied to Eqs. (9) and (15); however with these equations, the singular point occurs for energies far outside the range of interest to us.

$$\sigma_m=\frac{16\pi}{9}\frac{e^2}{\hbar c}\left(\frac{\hbar}{2Mc}\right)^2\left(\mu_n-\frac{1}{36}\right)^2 B_1{}^2\cdot\frac{k^3}{\alpha^2+k^2}$$
$$\cdot\frac{(1+\alpha r_0+(\alpha^2/\eta^2)G)^2[(\alpha^2+k^2/\beta^2-\eta^2)+1]^2}{(kr_0)^2+(1-(k^2/\eta^2)G^2)} \quad (35)$$

with B_1 given by Eq. (4). The equation for σ_m contains $V_{1,\frac{1}{2}}$, the well depth describing the Be^8-neutron interaction in the $P_{\frac{1}{2}}$ state, as an adjustable parameter. The last factor in the numerator of Eq. (35) may be written:

$$\left(\frac{\alpha^2+k^2}{\beta^2-\eta^2}+1\right)^2=\left(\frac{V_{1,3/2}-V_{1,\frac{1}{2}}}{E+\epsilon}\right)^2$$
$$\times\left(1-\frac{V_{1,3/2}-V_{1,\frac{1}{2}}}{E+\epsilon}\right)^{-2}. \quad (36)$$

The quantity $V_{1,3/2}-V_{1,\frac{1}{2}}$ is determined by the splitting of the $P_{3/2}$ and $P_{\frac{1}{2}}$ components of the *lowest* bound P level. If this splitting is small

$$\frac{V_{1,3/2}-V_{1,\frac{1}{2}}}{E+\epsilon}\ll 1,$$

and

$$\left(\frac{\alpha^2+k^2}{\beta^2-\eta^2}+1\right)\cong\left(\frac{V_{1,3/2}-V_{1,\frac{1}{2}}}{E+\epsilon}\right)^2. \quad (37)$$

Consequently, if the $P_{3/2}-P_{\frac{1}{2}}$ splitting of the lowest P level is neglected, that is, if the same well is used to represent the $P_{3/2}$ and $P_{\frac{1}{2}}$ states, σ_m vanishes. A reasonable upper limit for the splitting of the $P_{3/2}$ and $P_{\frac{1}{2}}$ components of the lowest bound P level is 500 kev (see Section II C). Using $\epsilon=1.63$ for the binding energy in the $P_{3/2}$ ground state, and using a 500 kev splitting, Eq. (4b) gives $V_{1,3/2}=12.16$ Mev and $V_{1,\frac{1}{2}}=9.84$ Mev. The use of these values should give an upper limit for σ_m. The magnetic dipole cross section obtained by using these values for the well depths is shown in Fig. 5. It may be seen that over the energy range for which the basic assumptions of the theory are valid the magnetic dipole cross section is much smaller than the electric dipole cross section.

Equation (31) shows that the neutrons obtained by photomagnetic disintegration should have a uniform angular distribution.

IV. CROSS SECTION FOR ELECTRODISINTEGRATION

Since the electrodisintegration is accomplished by quanta emitted by the incident electrons, the electrodisintegration cross section, σ_e, may be expressed in terms of the photo-disintegration cross section, $\sigma(\hbar\omega)$. Guth[14] applied this method to the calculation of the electrodisintegration cross section for Be^9 for energies just above the threshold and obtained a value which agrees reasonably well with the value observed at 1.73

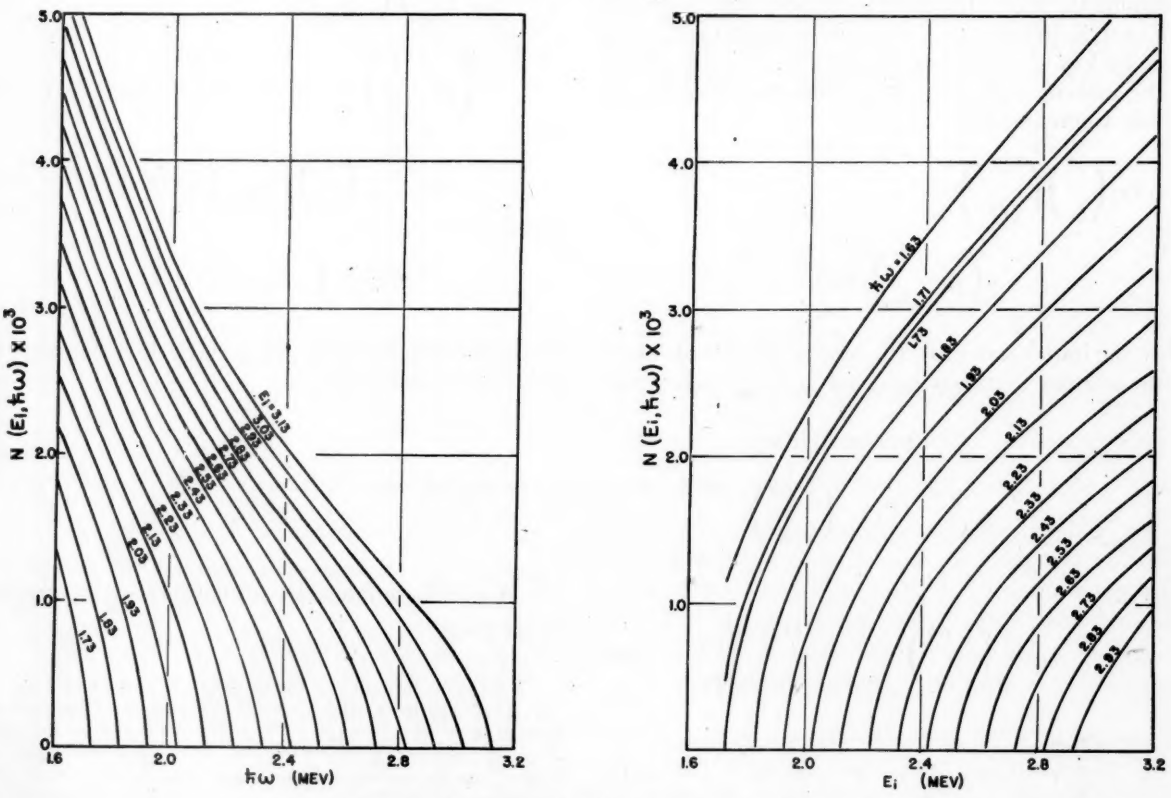

FIG. 7. Number of photomagnetic quanta as a function of $\hbar\omega$ and E_i.

Mev.[2] In the present paper, σ_e will be calculated in terms of $\sigma(\hbar\omega)$ in the energy interval for which only dipole disintegration is important. This procedure, in addition to providing a theory of the electrodisintegration process, yields a correlation between the measured photo-disintegration and electrodisintegration cross sections; this correlation is based upon quantum electrodynamics and is not subject to specific assumptions about the nuclear model employed.

If $\sigma(\hbar\omega)$ is the cross section for photo-disintegration with photons of energy $\hbar\omega$, and $N(E_i, \hbar\omega)$ is the number of photons (per unit energy interval) with energy $\hbar\omega$ by which the action of the field of the electron may be represented in producing the disintegration process, then

$$\sigma_e(E_i)=\int_{\epsilon}^{E_i}\sigma(\hbar\omega)N(E_i,\hbar\omega)d(\hbar\omega), \qquad (38)$$

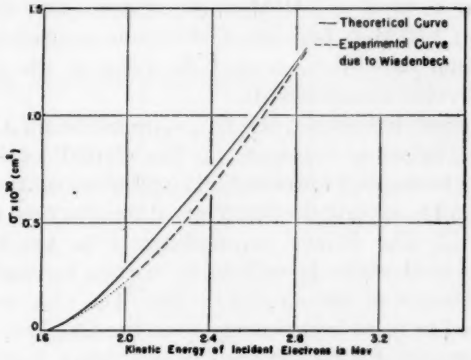

FIG. 8. Electrodisintegration cross sections for Be^9.

where E_i is the kinetic energy of the incident electrons. $N(\hbar\omega, E_i)$ may be evaluated by quantum electrodynamics.[35] For photoelectric disintegration

$$N_e(E_i,\hbar\omega)=\frac{2}{\pi}\frac{e^2}{\hbar c}\frac{1}{\hbar\omega}\left\{\frac{(E_i+mc^2)^2+(E_i-\hbar\omega+mc^2)^2}{2E_i(E_i+2mc^2)}\times\ln\left[\frac{E_i(E_i-\hbar\omega)+mc^2(2E_i-\hbar\omega)+\{E_i(E_i-\hbar\omega)(E_i+2mc^2)(E_i-\hbar\omega+2mc^2)\}^{\frac{1}{2}}}{mc^2\hbar\omega}\right]-\left[1-\frac{\hbar\omega}{E_i}\left(1+\frac{E_i-\hbar\omega}{(E_i+2mc^2)}\right)\right]^{\frac{1}{2}}\right\}, \qquad (39)$$

and for photomagnetic disintegration,

$$N_m(E_i,\hbar\omega)=\frac{2}{\pi}\frac{e^2}{\hbar c}\frac{1}{\hbar\omega}\left\{1-\frac{\hbar\omega}{2E_i}\left[1+\frac{E_i-\hbar\omega}{(E_i+2mc^2)}\right]\right\}\cdot\ln\left\{\frac{E_i(E_i-\hbar\omega)+mc^2(2E_i-\hbar\omega)+[E_i(E_i-\hbar\omega)(E_i+2mc^2)(E_i-\hbar\omega+2mc^2)]^{\frac{1}{2}}}{mc^2\hbar\omega}\right\}. \qquad (40)$$

These formulas are derived from the Møller potentials; since the procedure is equivalent to the use of the Born approximation, the formulas (39) and (40) can be expected to yield valid results only if the momentum transferred to the nucleus by the electrons is small compared to their total momentum. However, in view of the difficulties involved in obtaining expressions which are valid for electron energies near the threshold, the formulas (39) and (40) will be applied over the entire energy range covered by the empirical data. Plots obtained from Eqs. (39) and (40) are given in Figs. 6 and 7.

Since the magnetic dipole cross section is negligibly small, only photoelectric disintegration need be considered. Using Eqs. (8), (14), (16), and (39), σ_e may be determined from Eq. (38). The integration cannot be done in closed form in an elementary manner, but numerical evaluation may be carried out readily. Again using the values $V_{1,3/2}=12.16$ Mev, $V_{0,\frac{1}{2}}=V_2=3$ Mev, Eq. (38) yields the electrodisintegration cross section shown as the solid curve in Fig. 8; the dotted curve is a plot of Wiedenbeck's experimental results.

V. DISCUSSION

The results derived in the preceding sections show that the simple two body model of the Be^9 nucleus is adequate for an interpretation of the currently available data on the photo- and electrodisintegration of Be^9. There remains for discussion the correlation between the data on photo- and electrodisintegration and those on disintegration by protons. The sharp maximum observed[4] at 2.41 Mev in the energy distribution of the protons inelastically scattered on Be^9 has been interpreted by Longmire[5] as being due to a $P_{3/2}\rightarrow D_{5/2}$ transition. If this interpretation is correct, this sharp maximum should appear also in the photo-disintegration cross section *versus* energy curve. Unfortunately, the photo cross section has not been measured in the im-

[35] C. Møller, Ann. d. Physik **14**, 531 (1932). See also L. Rosenfeld, *Nuclear Forces* I (Interscience Publishers, New York, 1948), pp. 138–141. The use of the Born approximation to evaluate the number of virtual quanta has been treated in a general way by M. Lax and H. Feshbach (to be published soon). The authors wish to thank Drs. Lax and Feshbach for communicating their results to us.

mediate vicinity of 2.41 Mev, the nearest γ-ray energy being at 2.50 Mev. Because of its extreme sharpness, the maximum may have escaped detection in the photo cross section measurements.

Longmire has chosen the $D_{5/2}$ state as the final state for the following reasons: (1) The virtual levels belonging to states of lower orbital angular momentum are too broad to explain the sharpness of the observed maximum. (2) The D level is presumed to be the lowest energy level which is sufficiently narrow to meet the requirements of the empirical data. The $D_{5/2}$ level is assumed to be of lower energy than the $D_{3/2}$ level; this is to be expected on the basis of relativistic spin-orbit coupling. (3) The matrix elements corresponding to a change of the angular momentum of the incident proton by more than one unit are small. Longmire chooses the well describing the Be^8-neutron interaction in the $D_{5/2}$ state in such a way that the virtual $D_{5/2}$ level is extremely narrow. Unfortunately, the theory of the photodisintegration of Be^9 seems to require that the $D_{5/2}$ level be a broad level centered at an energy considerably higher than 2.41 Mev. A reasonable solution to this problem is to assume the sharp maximum in the proton scattering data to be due to a $P \rightarrow F$ transition. On the assumption that the Be^8-neutron interaction is partly of a Majorana type, it is not at all unreasonable to have the F level at a lower energy than the D level. Furthermore, even though the matrix elements for the $P \rightarrow F$ transition may be small for most energies, a sharp resonance at the narrow F level could result in the sharp maximum observed.

ACKNOWLEDGMENT

The authors wish to thank Mr. G. S. Colladay for the computation of most of the numerical results used in the paper.

PHYSICAL REVIEW VOLUME 76, NUMBER 2 JULY 15, 1949

The (α,n) Cross Section of Boron*

R. L. WALKER**
University of California, Los Alamos Scientific Laboratory, Los Alamos, New Mexico
(Received March 21, 1949)

The differential cross section for the $B^{10,11}(\alpha,n)N^{13,14}$ reactions was measured as a function of the alpha-particle energy up to an energy of 5.3 Mev. To determine this cross section, the number of neutrons emitted by boron under alpha-particle bombardment was measured by comparison with a calibrated Ra-α-Be source in a graphite column.

Resonances were observed at alpha-particle energies of 1.8, 2.5, 4.2, 4.9 Mev. Poor resolution may explain why other resonances found by Maurer and by Fünfer were not observed.

I. INTRODUCTION

NEUTRONS are produced when alpha-particles strike boron, by the two reactions:

$$B^{11}+He^4=N^{14}+n \qquad Q\approx+\ .28 \text{ Mev.}$$
$$B^{10}+He^4=N^{13}+n \qquad Q\approx+1.2 \text{ Mev.}$$

Reasons are given by Bonner and Mott-Smith[1] and by Maurer[2] for believing that only a small fraction of the neutrons from boron (of the order of one-tenth) arise from B^{10}. Thus the principal neutron yield from boron under alpha-particle bombardment is probably due to the first reaction above.

Maurer[2] and Fünfer[3] have studied the $B^{10,11}(\alpha,n)N^{13,14}$ reactions at different alpha-particle energies for the purposes of locating resonances, determining upper limits for their widths and determining the level spacing of the intermediate nucleus for the first reaction, N^{15}.

In the present work an absolute measurement of the cross section for the $B^{10,11}(\alpha,n)N^{13,14}$ reactions was made by determining the number of neutrons emitted from a thin boron target upon which are incident a known number of alpha-particles of variable energy.

II. EXPERIMENTAL ARRANGEMENT

The conventional arrangement shown in Fig. 1 was used as a means of controlling the energy of the alpha-particles striking the boron target. Alpha-particles from polonium coated on the small central sphere, 5 mm in diameter, lose a part of their energy in nitrogen gas before striking the thin boron target coated on the inside of two hemispherical iron spinnings, 7.5 cm in diameter. By changing the pressure of nitrogen in the chamber one can control the energy of the alpha-particles when they reach the boron.

The assembly shown in Fig. 1 was placed in a graphite column containing a sensitive BF_3 proportional counter, in order that the number of neutrons emitted by the

* This paper is based on work performed at Los Alamos Scientific Laboratory of the University of California under contract No. W-7405-eng-36 for the Manhattan Project.
** Now at Cornell University, Ithaca, New York.
[1] T. W. Bonner and L. M. Mott-Smith, Phys. Rev. **46**, 258 (1934).
[2] W. Maurer, Zeits. f. Physik **107**, 721 (1937).
[3] E. Fünfer, Ann. d. Physik **35**, 147 (1939).

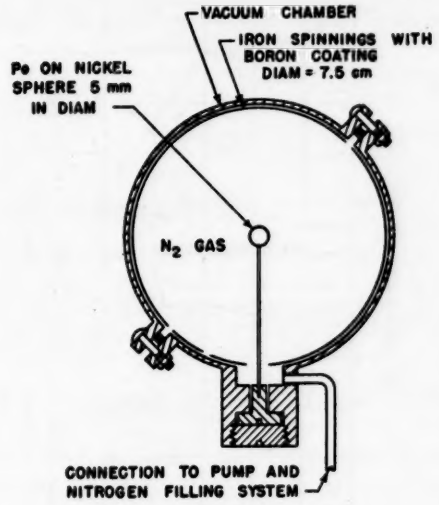
VACUUM CHAMBER
IRON SPINNINGS WITH BORON COATING DIAM = 7.5 cm
Po ON NICKEL SPHERE 5 mm IN DIAM
N_2 GAS
CONNECTION TO PUMP AND NITROGEN FILLING SYSTEM

FIG. 1. Experimental arrangement of the alpha-particle source and the boron target.

boron might be measured as a function of the nitrogen pressure in the chamber. The neutron measurement will be described later.

Data on the polonium sources and the boron targets used are collected in Tables I and II. The polonium sources were made by Mr. Leonard Treiman of Dr. Martin's group at Los Alamos. The sources were placed in the nitrogen atmosphere of the chamber immediately after the polonium was deposited in order to avoid oxidation, and all the data were taken within one or two days thereafter. The sources were then returned to Mr. Treiman, who measured their strengths by a calorimeter method.

The boron layers were coated on the iron hemispheres by Mr. Glenn Barbaras and Dr. W. P. Jesse at the Metallurgical Laboratory of the University of Chicago. In the process both sides of the hemispheres were coated. Since only the total amount deposited could be found by weighing, the weight of boron on the inside surface, as shown in Table II, involves an estimate that 55 percent of the total weight was on the inside.

TABLE I. Data on the polonium sources.

Po source	Strength when made (curies)	Thickness (curies/cm²)	Thickness (cm air equivalent)*
1	1.55	1.96	0.11
3	0.48	0.61	0.033

* Using 4.2 for the atomic stopping power of polonium relative to air for alpha-particles of energy near 5 Mev.

TABLE II. Data on the boron targets.

Boron layer	Total weight of boron on inside surface (mg)	Thickness (mg/cm²)	Equivalent air thickness* (cm air)
"Thicker boron"	56	0.31	0.33
"Thinner boron"	31	0.18	0.18

* Using 0.94 for the atomic stopping power of boron relative to air.

III. ALPHA-PARTICLE ENERGY. RESOLUTION

The alpha-particle energy corresponding to a given pressure of nitrogen in the chamber was found from the range-energy relation given by Holloway and Livingston[4], assuming the atomic stopping power of nitrogen relative to air to be 0.99.

The resolution was limited by the spread in the energies of the alpha-particles resulting from the finite thickness of the boron target, the thickness of the polonium source, the straggling of the energy loss, and the differences in the geometrical path lengths through the nitrogen gas. In Table III are listed estimates of the loss of resulution from these causes. The effect of the source thickness was calculated assuming the polonium layer to be pure and of uniform thickness. The energy spread in Table III is such that, under the assumed conditions, about 85 percent of the alpha-particles emitted have energies differing from the maximum energy by less than the amount listed.

IV. NEUTRON MEASUREMENT

The chamber containing the *Po* source and boron target was placed on the axis of a large graphite column (approx. 5×5×9 feet) with a sensitive BF_3 proportional counter about 58 cm away from the chamber,

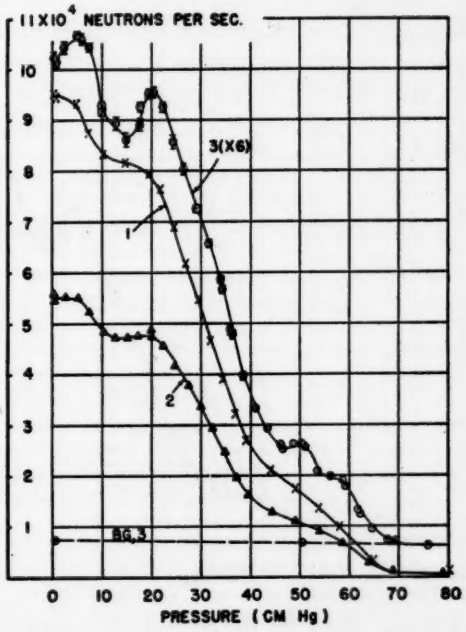

FIG. 2. Number of neutrons emitted in the $B^{10,11}(\alpha,n)N^{13,14}$ reactions as a function of the pressure of nitrogen in the chamber. Curve 1: *Po* source No. 1 and "thicker" boron target. Curve 2: *Po* source No. 1 and "thinner" boron target. Curve 3: (ordinates multiplied by 6): *Po* source No. 3 and "thinner" boron target. The background for curve 3 is shown by the curve marked *BG*,3.

[4] M. G. Holloway and M. S. Livingston, Phys. Rev. **54**, 18 (1938).

TABLE III. Estimates of the loss of resolution from various causes.

Alpha-particle energy (Mev)	Energy spread due to source thickness (Mev)		Straggling of energy loss (Mev)	Energy loss in boron target (Mev)		Energy spread due to differences in path lengths (Mev)
	Po source No. 1	Po source No. 3		"Thicker boron"	"Thinner boron"	
1	0.5	0.13	0.11	0.72	0.41	0.32
2	0.5	0.13		0.60	0.34	0.24
3	0.5	0.13		0.46	0.26	0.14
4	0.5	0.13		0.40	0.22	0.07
5	0.5	0.13	0.03	0.32	0.18	0.01

also on the axis of the column. With this separation between the neutron source and slow neutron detector, the counting rate is relatively insensitive to the primary energy of the neutrons emitted by the source, being approximately proportional to the number of neutrons emitted per second (see Appendix). Assuming this proportionality to be exact, the neutron measurement is easily made absolute by observing the counting rate of the BF_3 counter when the polonium alpha-particle source is replaced by a Ra-α-Be neutron source of known strength. In this way, the number of neutrons emitted from the boron under alpha-particle bombardment was measured as a function of the pressure of nitrogen in the chamber. Data are shown in Fig. 2 for three combinations of *Po* source and boron target, corresponding to different energy resolutions. The probable error in the absolute calibration of the Ra-α-Be source used as a standard was about 5 percent.[5]

Background of neutrons from impurities in the Po source, from the nitrogen gas, or from the iron hemispheres upon which the boron was deposited, was measured by replacing the boron coated hemispheres with uncoated iron ones. Background from possible polonium contamination on the boron target was measured by removing the *Po* source, and counting the neutrons still present. These measurements include, of course, the background of the counter when no source is present in the graphite column. The background from all causes was small as may be seen in Fig. 2.

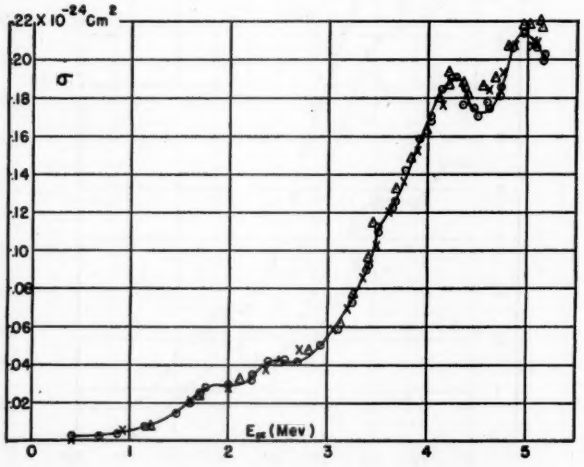

FIG. 3. Cross section for the $B^{10,11}(\alpha,n)N^{13,14}$ reactions as a function of the alpha-particle energy. The curve has been drawn through data obtained with the best resolution, i.e., with *Po* source No. 3 and the "thinner" boron target (circles). Also shown are data obtained with *Po* source No. 1 and the "thinner" boron target (triangles), and with *Po* source No. 1 and the "thicker" boron target (crosses).

[5] O. R. Frisch and R. L. Walker, Los Alamos Declassified Report LADC-155 (1945).

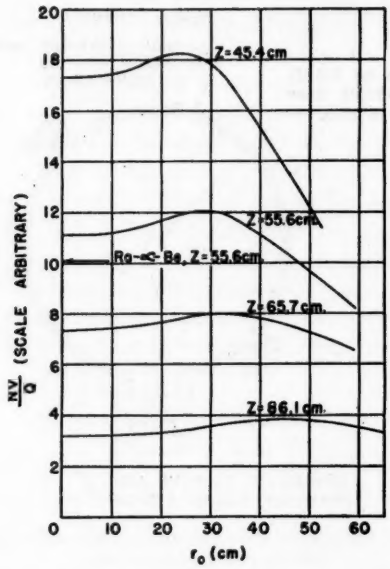

FIG. 4. Flux of thermal neutrons as a function of the parameter r_0 of the source function. Z is the distance from the source along the axis of the graphite column. The arrow marked "Ra-α-Be" indicates the value of nv/Q calculated from a measured distribution q for one Ra-α-Be source, at $z=55.6$ cm.

V. THE CROSS SECTION

In Fig. 3 is shown the cross section for the $B^{10,11}(\alpha,n)N^{13,14}$ reactions as a function of the alpha-particle energy. The energy is the average energy of alpha-particles in the boron layer, taking into account energy losses in the *Po* source and in the boron layer, as well as in the nitrogen gas. Because of poor resolution, the cross section shown in Fig. 3 at a given energy is, of course, an average over a small energy interval determined by the resolution width. The cross section is:

$$\sigma = I/NS$$

where I is the number of neutrons emitted per second, S is the number of alpha-particles striking the boron per second, and N is the thickness of the target in boron atoms/cm^2.

The alpha-particle energies corresponding to the four resonances suggested by curve 3 of Fig. 2. are listed in Table IV. For comparison are listed the eight resonances observed by Maurer[2] and those resonances observed by Fünfer[3] with *ThC'* alpha-particles, which lie below 5.3 Mev.

The fact that fewer resonances were observed in the present experiment than were found by Maurer and by

TABLE IV. Energy of the alpha-particles at resonance.

Present paper	Maurer*	Fünfer
1.8 Mev	1.90 Mev	
2.5	2.68	2.65 Mev
	3.15	3.25
	3.59	3.60
4.2	4.26	4.10
	4.55	4.45
	4.85	4.73
4.9	5.02	5.08

* These energies, which differ slightly from those listed by Maurer, were found from Maurer's ranges using the newer range-energy relation given by Holloway and Livingston.[4]

Fünfer may be due to the relatively poor resolution indicated in Table III.

From the cross section, σ, as a function of the alpha-particle energy shown in Fig. 3, the total neutron yield from *Po* alpha-particles on a thick boron target has been calculated. The result is, for the thick target yield:

19 neutrons per 10^6-*Po* alpha-particles.

This is in good agreement with the value of 22 neutrons per 10^6-*Po* alpha-particles measured directly by Roberts[6] and 19 neutrons per 10^6-*Po* alpha-particles found by Segrè and Wiegand.[7]

An estimate of the probable error in the cross-section shown in Fig. 3 is about 20 percent.

ACKNOWLEDGMENTS

I am indebted to Mr. Glen Barbaras and Dr. W. P. Jesse for making the boron layers; to Mr. Leonard Treiman and Professor Don Martin for making the polonium sources; and to Professor H. H. Barschall for suggesting the experiment, and interest in its progress.

APPENDIX

The use of thermal neutron measurements in a graphite column to obtain the approximate ratio of the strengths of two neutron sources, even though their energies may be different, is based upon an analysis which may be qualitatively outlined as follows:

As is well known, if a "point" source of fast neutrons is placed in a large graphite block, the neutrons will be slowed down by successive collisions with carbon nuclei until they reach thermal energies. Thereafter, they will diffuse in the graphite until they either are absorbed or escape from the block.

The distribution of thermal neutrons in the graphite column will depend upon the primary energy of the neutron source, because the higher the primary energy, the farther the neutrons will spread out from the source during the slowing down process. A measure of this spreading out may be obtained from the elementary age theory of the slowing down process.[8,9] According to age theory, if a point source of neutrons of a single energy is placed in an infinitely large block of graphite, the spatial distribution of neutrons just reaching thermal energies, or the density of "nascent thermal neutrons," $q(\mathbf{r})$ is a Gaussian,

$$q(\mathbf{r}) = (Q/\pi^{\frac{1}{2}} r_0^3) e^{-r^2/r_0^2}$$

where Q is the total number of neutrons emitted per second by the source. The parameter r_0 is larger, the higher the primary energy of the neutrons. ($r_0 = 2\tau^{\frac{1}{2}}$ where τ is the neutron "age"). In a finite, but large, column such as used in the present experiment, the distribution $q(\mathbf{r})$ is slightly different from the Gaussian given above, since it must satisfy boundary conditions that the neutron density vanish at the effective sides of the block. However, the age theory result[8] is characterized by the same parameter $r_0 = 2\tau^{\frac{1}{2}}$ which appears in the simple Gaussian distribution for an infinite block.

$q(\mathbf{r})$ is important in calculating the distribution of thermal neutrons in the graphite column, since $q(\mathbf{r})$ is the distributed source of thermal neutrons in the graphite. The distribution of thermal neutrons may be found by solving the steady state diffusion equation with source function $q(\mathbf{r})$:[8]

$$-D\nabla^2 n(\mathbf{r}) + (1/T) n(\mathbf{r}) = q(\mathbf{r})$$

where $n(\mathbf{r})$ is the density of thermal neutrons at position $\mathbf{r}$, D is the diffusion constant, and T is the mean life of the thermal neutrons in graphite. The boundary conditions are that $n(\mathbf{r})$ vanish at the effective sides of the block.

By solving this equation using the age theory result for $q(\mathbf{r})$, one may calculate the flux, nv, of thermal neutrons at any point in the graphite, as a function of the parameter r_0 in the source function, $q(\mathbf{r})$. The results of such a calculation are shown in Fig. 4 for four different distances from the source on the axis of the graphite column used in the present experiment.

By choosing a distance from the source for which the curve is as flat as possible over a large range in r_0, one may assume that the density of thermal neutrons at this position will be approximately porportional to the total source strength, Q, and will be insensitive to the primary energy of the neutrons.

For the distance between source and detector, $z \approx 58$ cm, used in this experiment, the thermal flux curve is seen to be flat within about 10 percent for parameters $r_0 \leqq 45$ cm. Unfortunately it is not possible to say that this corresponds to a definite primary energy of the neutrons. According to the age theory approximation, $r_0 = 42$ cm for neutrons of 4 Mev primary energy, in graphite, and increases only slowly with further increase in primary energy. However, if the actual distribution arising from a source of 4-Mev neutrons were expressed empirically by a sum of two or three Gaussian terms, one of them would probably have a parameter, r_0, considerably larger than 42 cm. It is felt, nevertheless, that the thermal neutron flux at $z \approx 58$ cm varies with the primary neutron energy by less than ten to fifteen percent over the energy range of the neutrons produced in the present experiment.

Since a Ra-α-Be source (having a neutron spectrum extending to quite high energies) was used as a standard in the present experiments, it is of interest to compare with the curves of Fig. 4 the thermal neutron flux produced by a Ra-α-Be source. The distribution of nascent thermal neutrons, $q(\mathbf{r})$, from various Ra-α-Be sources have been measured experimentally so that the flux of thermal neutrons may be calculated with fair accuracy. The result for one particular Ra-α-Be source at a distance $z = 55.6$ cm is indicated in Fig. 4. Since the flux from this source is seen to be 10 or 15 percent below that calculated for a source with small r_0, the value of the boron (α,n) cross section may be too high by about this amount, except near the high energy end.

[6] J. H. Roberts, Manhattan Project Report MDDC-731 (1944).
[7] E. Segrè and C. Wiegand, Manhattan Project Report MDDC-185 (1944).
[8] E. Fermi, Neutron Physics (Los Alamos Lecture Notes) MDDC-320 (1946).
[9] R. E. Marshak, Rev. Mod. Phys. **19**, 185 (1947).

The (α, n) Cross Sections of Beryllium, Magnesium, and Aluminum

I. HALPERN*
University of California, Los Alamos Scientific Laboratory, Los Alamos, New Mexico
(Received March 21, 1949)

The (α, n) cross sections in beryllium, magnesium, and aluminum were measured by counting the number of neutrons emitted from fairly thin targets of these elements for a given incident flux of alpha-particles. The energy of the alpha-particles was variable up to the full energy of polonium alpha-particles, 5.3 Mev.

I. INTRODUCTION

THE (α, n) cross sections in beryllium, magnesium, and aluminum were measured by the method described in the preceding paper by R. L. Walker.[1] A thin polonium alpha-source was mounted at the center of a spherical chamber onto the inner surface of which the target material was evaporated. The neutrons emitted by the target were slowed down and counted in a graphite block, and it was possible to vary the energy of the alpha-particles striking the target by adjusting the pressure of the gas that filled the chamber. The gas chosen for this purpose was nitrogen, because nitrogen reacts with neither source nor target materials and also because it has a low (α, n) cross section.

II. THE SOURCES AND TARGETS

The polonium alpha-sources were prepared by Mr. L. Treiman, who also determined their strength. The strengths of the several sources that were used are listed in Table I, together with their equivalent thicknesses in centimeters of air for polonium alpha-particles. The target thicknesses were determined by weighing and also are given in the table.

It was unfortunately necessary to use thicker sources and targets with the magnesium and aluminum than it was with the beryllium. The (α, n) cross sections in these heavier elements are considerably lower than they are in beryllium, mainly because of the increased effect of coulomb repulsion of the alpha-particles. It is a weakness of all such experiments, in which natural sources are used, that with heavier targets the resolution must be compromised for reasons of intensity. In general, it would be desirable to increase rather than to decrease the resolution, because of the closer-level spacing in heavier elements.

From Table I, it is seen that the targets were all made thicker than were the sources. This was done in order to introduce about the same energy spread in the sources and targets. Although the alpha-particles enter the targets nearly perpendicularly, their average path length in the source is roughly three times the thickness of the source. The width of the alpha-particle energy distribution introduced into the beryllium measurement by the thickness of both source and target was about 6 percent of the energy of the polonium alpha-particles; whereas, in the magnesium and aluminum measurements, it was about 13 percent.

Only a negligible additional energy spread was introduced by the non-uniformity of the source and target thickness. There was, however, another somewhat serious cause of resolution loss; namely, the finite size of the small nickel sphere onto which the polonium was plated. The alpha-particle path lengths through the chamber differ by as much as the radius of the nickel sphere. The relative energy spread $\Delta E/E$ introduced by this effect becomes rapidly larger at the low-energy (high-pressure) points, both because of the decrease in E and because of the increase in ΔE as the pressure is raised. Fortunately, only with beryllium were points taken at low enough energies for this loss in resolution to be comparable to that due to source and target thickness. Finally, there was a resolution loss caused by the natural straggling of the alpha-particles. However, this loss was smaller than any of those already mentioned.

III. NEUTRON COUNTING

The neutrons produced in the disintegrations were counted by placing both the disintegration chamber and a detector of thermal neutrons in a large graphite block. This method of neutron counting is described in detail by R. L. Walker.[1] It has the advantage that it can be made to permit neutron-counting rates that are fairly independent of the initial neutron energy. This allows the determination of strengths of neutron sources by calibration against standardized sources that need not have the same neutron-energy spectrum. The standard source used in this experiment was a radium-beryllium source whose neutron emission was known to approximately 5 percent.

The energy independence, or "flatness," of the

TABLE I. Source and target thickness.

Target material	Target thickness mg/cm²	Target thickness cm air equiv.*	Source strength when made (curies)	Source thickness cm air equiv.*
Beryllium	0.22	0.17	0.496	0.05
Magnesium	0.50	0.32	1.14	0.10
Aluminum	0.63	0.38	1.14	0.10

* The full range of polonium alpha-particles is 3.84 cm.

* Now at Massachusetts Institute of Technology, Cambridge, Massachusetts.

[1] R. L. Walker, Phys. Rev. (to be published).

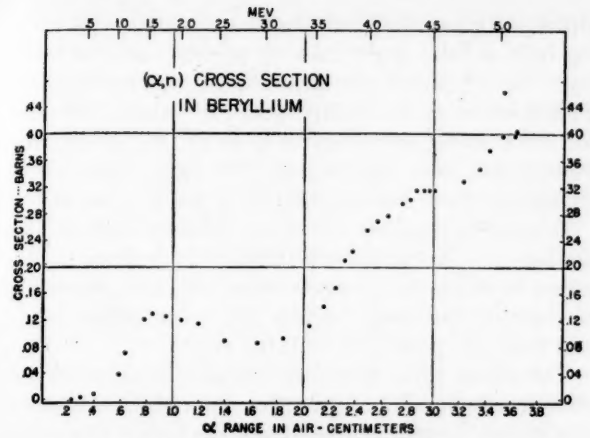

FIG. 1. (α, n) cross section in beryllium.

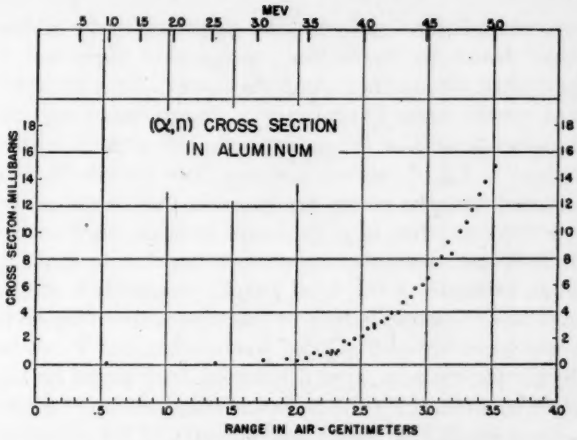

FIG. 3. (α, n) cross section in aluminum.

graphite-block method of neutron detection arises somewhat as follows. The fast neutrons that are emitted by a source in graphite are slowed down by collisions until they reach thermal energies, and then they diffuse until they are captured or leak out of the graphite. If a detector of thermal neutrons is placed in the graphite at a fixed distance from the source, the sensitivity of such a detector will in general depend upon the initial neutron energy. Very fast neutrons would get too far from both the source and the thermal-neutron detector before slowing down enough to be counted efficiently.

On the other hand, neutrons with energies near thermal would be slightly absorbed by capture in the carbon before reaching the detector. Neutrons of some intermediate energy would count with maximum efficiency; and, in the neighborhood of this maximum, the response of the neutron-counting system would be essentially energy independent. In fact, a detailed calculation shows that this maximum is very flat, especially on the low-energy side. For example, for the source-to-detector spacing used in the present experiment, neutrons with initial energies from a fraction of a volt to about 4 Mev could be expected to count within 10 percent of maximum efficiency. If the distance from the source to the detector were increased, this energy region of flat response would also increase, but the absolute counting rate would be reduced. A compromise must be made between flatness and intensity. In the present experiment, the necessary compromise is probably more serious in the magnesium and aluminum measurements than it is in the beryllium measurement. This is mainly because the neutron spectra from the polonium-beryllium measurement and radium-beryllium standard source are probably not too different. However, there is a considerable number of rather high-energy neutrons (about 10 Mev) from both of these sources that are not counted efficiently, probably leading to an overestimate of the cross sections of magnesium and aluminum.

A proportional counter filled to 20-centimeter mercury pressure of boron trifluoride was used as the thermal-neutron detector. The pulses of the detector were amplified and fed through a pulse-height discriminator to a scaler and recorder.

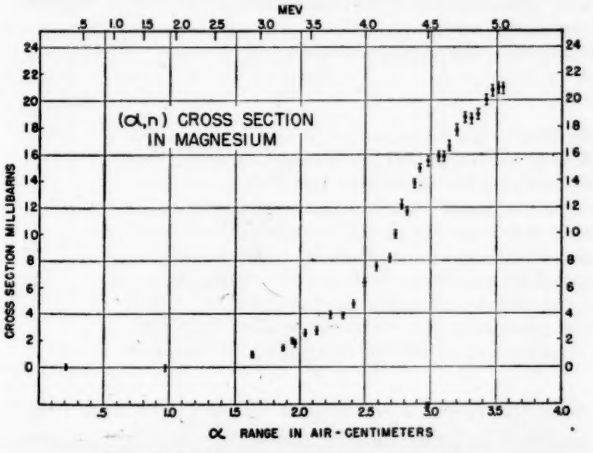

FIG. 2. (α, n) cross section in magnesium.

IV. RESULTS

The (α, n) reaction on beryllium was one of the earliest nuclear reactions found to exhibit resonances. An excitation curve was first given by Bernardini.[2] Subsequent

TABLE II. Neutrons per million polonium alpha-particles.

Authors	Type of target	Particles counted	Beryllium (0.61)	Magnesium (1.4)	Aluminum (1.5)
J. Roberts[6]	Thick	Neutrons	77	1.3	0.7
E. Segrè and C. Wiegand[7]	Thick	Neutrons	73	—	—
A. Szalay[8]	Thick	Positrons (from the residual nucleus)	—	—	0.22
This work	Thin	Neutrons	50	0.5	0.25

[6] J. H. Roberts, Manhattan District Report CN. 1190.
[7] E. Segrè and C. Wiegand, LADC 61.
[8] A. Szalay, Zeits, F. Physik 112, 29 (1939).

[2] G. Bernardini, Zeits. F. Physik 85, 557 (1933).

curves[3–5] all showed essentially the same shape as the curve drawn by Bernardini, except that there was a systematic discrepancy along the energy axis of the type that would seem to indicate a disagreement on the stopping powers of the gases used. The present curve, plotted in Fig. 1, agrees with the later curves. If it is assumed that the lowest resonance in this curve can be described in terms of a resonance formula, such as the Breit-Wigner formula, it becomes possible to make a rough estimate of the total angular momentum of the level in C^{13} corresponding to this resonance. This level would have odd-half angular momentum, but it can be shown, for example, that a value of $J=\frac{1}{2}$ would be too small to account for the observed cross section.** From a consideration of yields and energies of the neutrons and gamma-rays observed in the decay of the C^{13}, it appears that values of J higher than 5/2 are unlikely. The total angular momentum of the observed level is therefore probably either 3/2 or 5/2.

Figures 2 and 3 show the results for magnesium and aluminum. (It should be remarked that in all three figures, the height of the zero ordinate above the abscissa represents the constant background that had to be subtracted from the data.) The statistical errors based on the number of counts are indicated for magnesium, where they were the largest. Because of the poor resolution, no resonances are readily apparent in either the magnesium or aluminum curves. The cross section given for magnesium is for the normal isotopic mixture. The (α, n) reaction in the most abundant isotope Mg^{24}, however, is too endoergic to be possible with polonium alpha-particles. Mg^{25} and Mg^{26} have abundances totaling only a little more than 20 percent, and probably both contribute to the observed (α, n) cross section. Therefore, in terms of Mg^{25} and Mg^{26} alone, the cross section is about five times as large as that given. Aluminum has only one isotope; therefore, there is no ambiguity about the assignment of the cross section.

In order to compare the values obtained for the cross sections in this article with those of previous experiments in which thick targets were used, it is convenient to convert thin-target results into thick-target yields, and these are presented in Table II.

The above table gives the number of neutrons per million polonium alpha-particles reported by a number of authors. In parentheses below the target element is given the atomic stopping power in relation to air that was used in the conversion of the thin-target results. The discrepancies that appear in the table are rather large compared with the errors that might otherwise be assigned to the individual measurements, and it is therefore not readily apparent how these discrepancies may be explained.

[3] J. Chadwick, Proc. Roy. Soc. 142A, 1 (1933).
[4] T. Bjerge, Proc. Roy. Soc. 164A, 243 (1938).
[5] E. Stuhlinger, Zeits. F. Physik 114, 185 (1939).
** The author is indebted to Dr. D. C. Peaslee for pointing this out.

ACKNOWLEDGMENTS

The author is indebted to Mr. L. Treiman for his careful preparation and calibration of the polonium sources used in this measurement and also to Dr. R. L. Walker for the preparation of much of the original instrumentation. I wish also to thank Professor H. H. Barschall for suggesting this measurement and for his continued interest in the work.

This paper is based upon work performed at the Los Alamos Scientific Laboratory of the University of California under Contract No. W 7405-eng-36 for the Manhattan Project.

PHYSICAL REVIEW VOLUME 76, NUMBER 2 JULY 15, 1949

The Clustering of Ions and the Mobilities in Gaseous Mixtures

ALBERT W. OVERHAUSER
Department of Physics, University of California, Berkeley, California
(Received March 14, 1949)

It is shown by direct analysis that the deviations from Blanc's law for mobilities of ions in mixtures of gases observed when a strongly polarizable gas is mixed with one less polarizable cannot be ascribed to a statistical clustering effect as proposed by Loeb. Analysis involving the assumption that the ion undergoes labile clustering of the simplest type indicates that the observed results can be completely accounted for within the realms of simple theory. Thus assuming that the active gas can attach a single molecule to the ion and that this attachment molecule may be detached with different probabilities by collisions with the two types of gas molecules leads to an equation for the resultant mobilities which will cover practically all cases observed. The forces assumed can be dielectric but may also be secondary valence or van der Waals' forces. It is indicated how, with appropriate experimental procedures possible under modern techniques, most of the constants required for the solution of the equation can be directly determined or computed.

FOR many decades controversy raged as to whether gaseous ions were molecular clusters of large radii or charged single molecules retarded in their motion by dielectric forces with the gas. These forces were usually assumed to be attractive and of the inverse fifth power type, their effect being to increase the effective collision

radius of the ion. The discussions were indecisive because little could be said about the binding forces of the proposed clusters and the conditions necessary for their formation. It was assumed that a cluster would form and be stable if $-2u_r/3kT>1$, where u_r is the potential energy of a gas molecule at a distance r from the ion equal to the sum of the radii of the molecule and the ion. If one assumes the inverse fifth power law to hold even at distances of the order of 10^{-8} cm, then $u_r=-(D-1)e^2/8\pi Lr^4$, where D is the dielectric constant of the gas and L is the Loschmidt number. This criterion is, of course, quite arbitrary, but it would appear to be correct in a qualitative way.

Investigations over the years established certain points very clearly. In many gases the ions do not attach molecules as long as the gas is pure and at room temperature. Notable examples of such behavior are the alkali ions in the inert gases. However, it was found from aging and mixture studies that ions have strong affinities for certain types of gaseous molecules and selectively attach these to form stable complex ions of relatively few atoms. These ions in some cases resemble well-known ion complexes observed in solution. The experimental observations indicated that when such clustering occured, the attachment was rapid, causing a discrete change in the mobility, and hence the size of the ion. There was no evidence of a gradual or successive change in mobility or size.

Studies of ion mobilities in mixtures of certain gases showed deviations from the behavior to be expected on simple theory. The drift velocity of an ion in a gas due to an electric field X is $v=kX$. The constant of proportionality k is called the mobility of the ion. The mobility, which depends upon the natures of the ion and the gas, is found to be inversely proportional to the density of the gas. Thus, in general, one may write $1/k=QN$, where N is the number of molecules per unit volume and Q is a constant. It is useful to define a constant K called the reduced mobility, which is the mobility if the gas is at atmospheric pressure. Thus, $1/K=QL$, where L is the Loschmidt number.

Assume a gas to be composed of N_A molecules of a

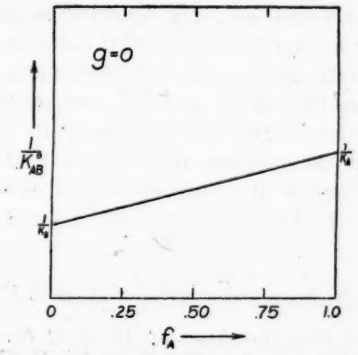

FIG. 1. Calculated reciprocal mobilities in arbitrary units against mole fraction of attaching gas. Clustering coefficient $g=0$. Blanc's law holds.

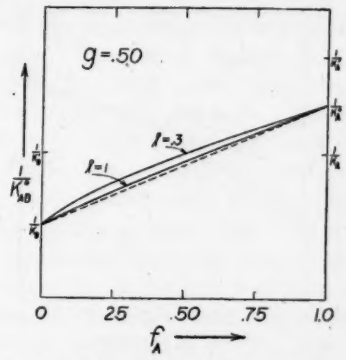

FIG. 2. Calculated reciprocal mobilities in arbitrary units against mole fraction of attaching gas. Same scale as in Fig. 1, with $g=0.5$ and two values of l. Low values of l indicate low dissociating action of neutral gas. Blanc's law is dashed curve. Note intermediate value of quasi-clustered ion in pure attaching gas.

gas A with a constant Q_A and N_B molecules of a gas B with a constant Q_B. Then, if mixing gases A and B does not change the nature of the ions, the mobility of an ion in the mixture will be given by $1/k_{AB}=Q_AN_A+Q_BN_B$. This result follows from the principle that for an ion of a given drift velocity, the rate of transfer of momentum to one component of the gas is independent of the presence of the other component. If we let f_A and f_B be the mole fractions of A and B molecules ($f_A=N_A/(N_A+N_B)$), then the reduced mobility in the mixed gas is given by: $1/K_{AB}=f_A/K_A+f_B/K_B$. This is Blanc's law. Since $f_A+f_B=1$, $1/K_{AB}$ is a linear function of f_A as shown in Fig. 1.

Studies of ion mobilities in mixtures containing one constituent of high dielectric constant showed deviations from the anticipated form given by Blanc's law. The deviation from the linear curve of $1/K_{AB}$ against f_A with gases like NH_3 or HCl was convex upward as in Fig. 3, indicating that $1/K_{AB}$ increased more rapidly with f_A than the increase in concentration warranted. Since these effects were observed when gases of high dielectric constant were mixed with gases of low dielectric constant, P. Debye suggested that this action might be similar to the statistical clustering which he was then applying to ions in solutions. On this basis, E. U. Condon suggested a theory which was applied in approximate form by L. B. Loeb.[1] In what follows, however, it will be shown that statistical clustering properly accounted for cannot explain deviations from Blanc's law.

The studies of Tyndall, Powell[2,3] and their associates at Bristol on mobilities at very low temperatures and in gaseous mixtures containing polar and polarizable molecules gave results which were quite revealing. They first showed that for common gases of low dielectric

[1] For general background see L. B. Loeb, *Fundamental Processes of Electrical Discharge in Gases* (John Wiley and Sons, Inc., New York, 1939), p. 42 ff.

[2] R. J. Munson, A. M. Tyndall, and K. Hoselitz, Proc. Roy. Soc. (London) **A172**, 28–54 (1939).

[3] H. G. David and R. J. Munson, Proc. Roy. Soc. **A177**, 192 (1941); see also reference 1, p. 65 ff.

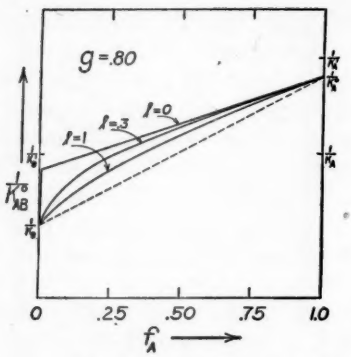

FIG. 3. Analogous to Fig. 2 with $g=0.8$ and 3 values of l. Note the progressive changes relative to Fig. 2. Blanc's law dashed.

constant clustering could occur if temperatures were sufficiently low.[2] It was further shown that if the ion were small and the gas molecule a large polarizable entity, such as Li^+ ions in Xe, clusters of one to a very few atoms could form even at room temperatures.[2] These results gave the first clear evidence of the type of attachment to be expected when $-2u_r/3kT>1$. In interpreting their results in mixtures the Bristol group concluded that the statistical clustering concept of Loeb was in error.[3] They qualitatively inclined toward another concept of the ion cluster for their interpretation of the deviations from Blanc's law. This involved the concept of a cluster which changes its size owing to association and dissociation as the ion moves, a consequence to be expected when $-2u_r/3kT\sim1$. Such an ion can be called a labile ion cluster in contrast to the fixed and statistical clusters of history. In what follows, it will be formally proved that the statistical clustering in the gaseous phase is inapplicable and that a labile cluster theory quantitatively explains all the results on mobilities in mixtures.

In order to discuss the effect of statistical clustering in relation to Blanc's law, we may proceed as follows. The presence of the ionic charge in the gas changes the density of molecules in the neighborhood of the ion because of the force field. This change in density near the ion is given by the Boltzmann law as $\exp(\beta)$, where $\beta=-u/kT$, u being a potential of the order of magnitude of u_r. The equation for the mobility as a function of density then becomes $1/k=QN\exp(\beta)$. Thus the expression for Q is no longer $Q=1/KL$, but is:

$$Q=1/KL\exp(\beta).$$

If one now considers the mobility of a given ion in a mixture of two gases A and B, the amount of clustering of A molecules about the ion is in general different from the amount of clustering of the B molecules. The expression for the mobility in the mixture must be modified as follows: $1/k_{AB}=Q_AN_A\exp(\beta_A)+Q_BN_B\exp(\beta_B)$, where β_A and β_B are the β's appropriate to the given ion in the gases A and B. Introducing the new values of Q_A and Q_B we infer the value of K_{AB} as: $1/K_{AB}=f_A/K_A+f_B/K_B$. This is again the Blanc law. It is seen that with a proper use of the concentration factors, the statistical clustering factors drop out because they are already present in the expressions for $1/K_A$ and $1/K_B$. Although statistical clustering does occur and causes the observed mobilities to be somewhat lower than may first be expected from a solid elastic sphere model of the gas, the net effect is only to demand a renormalization of the Q's.

The formation of stable ion clusters also fails to explain deviations from Blanc's law. For example, let an ion combine with a molecule of an active gas A to form a stable cluster. Then, in mixtures with an inactive gas B, $1/K_{AB}$ is a linear function of f_A, as shown in Fig. 4, except in the neighborhood of $f_A=0$. The anomaly near $f_A=0$ is due to the fact that the ion does not attach an A molecule immediately unless there is a sufficient number of A molecules present. In the pure gas B no attachment takes place.

There remains but one alternative. One must assume that the ions involved are labile and can change their average nature continuously with concentration. In the original investigations Loeb and others used mixtures of gases like H_2 and NH_3.[4] H_2, having a low dielectric constant D_B, does not attach itself to the ion, whereas NH_3, having a large dielectric constant D_A, can associate with the ion to form a cluster. Since addition of several molecules to form an A cluster is unlikely from experimental evidence, it is best to consider a relatively simple model for study.

We will first consider the effect of labile cluster formation in a pure active gas A. We will assume that in drifting through the gas, an ion I can combine with one molecule of gas A to form a new ion $I'=I+A$. We will further assume that as the new ion I' drifts through the gas, it can dissociate as a result of molecular impacts, and become again the ion I. Thus, as the ion wanders through the gas, it spends part of its time as I and the remaining time as I'. Such actions are possible if the ratio $-2u_r/3kT\sim1$, a condition that is not unlikely in the light of the studies of the Bristol group on temperature dependence of mobilities.[2]

The individual ions I and I' will have different mobilities, k_A and k_A', and corresponding reduced mobilities, K_A and K_A'. The observed mobility of the ion will not be equal to either of these values, but to a value k_A^0, such that $k_A'<k_A^0<k_A$. In order to determine k_A^0 as a function of k_A and k_A', one must know the fraction of the distance that the ion drifts as I or I'.

Let x be the average total distance that the ion drifts as I, and x' the average total distance that the ion drifts as I'. Then, the observed reduced mobility is given by:

$$1/K_A^0=x/(x+x')K_A+x'/(x+x')K_A'.$$

[4] L. B. Loeb, Proc. Nat. Acad. Sci. **12**, 35, 42, 677 (1926); L. B. Loeb, and L. DuSault, Proc. Nat. Acad. Sci. **13**, 511 (1927); **14**, 192, 384 (1928); L. B. Loeb and K. Dyk, Proc. Nat. Acad. Sci., **15**, 146 (1929); L. B. Loeb, Phys. Rev. **35**, 184 (1930); A. M. Tyndall and L. R. Phillips, Proc. Roy. Soc. **A111**, 577 (1926).

Let us define a new quantity g as the clustering coefficient of ion I in gas A, given by: $g=1/(1+x/x')$. The previous expression can then be written as

$$1/K_A^0=(1-g)/K_A+g/K_A'.$$

We must now evaluate g in view of the mechanisms assumed for clustering.

Let μ_A be the probability per collision that the ion I will change to I' in collisions with the gas A. Let ν_A be the probability per collision that the ion I' will dissociate to form I as a result of impacts with the gas. The quantities μ_A and ν_A will depend upon the temperature and upon the nature of the molecules involved. We will assume for the present that they are independent of the density of the gas. Let $\bar{x}$ be the mean distance that the ion I drifts in the direction of the field X before it associates to form I', and $\bar{x}'$ the mean distance that I' drifts before it dissociates to I.

The collision frequency of I with A molecules is $Z_A=\bar{c}_A\sigma_A N_A$, where $\bar{c}_A$ is the mean relative velocity, and σ_A is the cross section for the collision. The time spent in traversing 1 cm in the field direction is: $t_A=1/kX=Q_AN_A/X$. Therefore:

$$\bar{x}=1/Z_At_A\mu_A=X/\bar{c}_A\sigma_AQ_AN_A^2\mu_A.$$

Similarly, with the primed symbols relating to the corresponding quantities for I', we have:

$$\bar{x}'=X/\bar{c}_A'\sigma_A'Q_A'N_A^2\nu_A.$$

Therefore,

$$p=x/x'=\bar{x}/\bar{x}'=\frac{\bar{c}_A'\sigma_A'Q_A'\nu_A}{\bar{c}_A\sigma_AQ_A\mu_A},$$

so that g becomes: $g=1/(1+p)$.

Since p is independent of N_A, so is g. This result implies that $1/k_A^0$ is proportional to N_A in active gases as well as in inactive gases. Theoretically, this conclusion follows from the assumption that μ_A and ν_A are independent of N_A. The dissociation probability ν_A is, plausibly, independent of N_A, since one would expect that the dissociation mechanism involves only simple collisions. In order for association to occur, there must be some means of carrying away the binding energy of the cluster. Such action can occur if the process of association involves a three body collision. The association probability μ_A may then depend upon the density of the gas, and in the latter case, we would have $\mu_A=\alpha N_A$. This relation implies that $1/k_A^0$ is not proportional to N_A. Such a non-linear dependence of mobility on density has not been reported; but the proportional law has not been under suspicion, and has never been verified for active gases. Clarification of this question appears possible only by recourse to experiment. In the discussion of mobilities in a mixture of active and inactive gases, we will treat μ_A as a constant.

In a mixture of an active gas A and an inactive gas B we assume that B forms no cluster with I, that is, $\mu_B=0$. However, collisions of $I'=I+A$ with B molecules can dissociate I' to give I. Let ν_B be the dissociation probability for impacts with B molecules. In general ν_B will be different from ν_A. Now, in the mixed gas the ions I and I' will have different mobilities: $1/k_{AB}=Q_AN_A+Q_BN_B$ and $1/k_{AB}'=Q_A'N_A+Q_B'N_B$.

In analogy with what has gone before, if y represent the average total distance that the ion drifts as I in the mixture, and y' the distance covered as I', then the observed mobility k_{AB}^0 in the mixture is given by:

$$1/k_{AB}^0=y/(y+y')k_{AB}+y'/(y+y')k_{AB}'.$$

For the ion I, the time to drift 1 cm in the field direction is $t=1/k_{AB}X=(Q_AN_A+Q_BN_B)/X$. The collision frequency of I with A molecules is again: $Z_A=\bar{c}_A\sigma_AN_A$. These expressions lead to the value of $\bar{y}$, the mean distance that I drifts before forming a cluster as: $\bar{y}=X/(Q_AN_A+Q_BN_B)\bar{c}_A\sigma_AN_A\mu_A$.

For the ion I' we have

$$t'=1/k_{AB}'X=(Q_A'N_A+Q_B'N_B)/X.$$

For collisions with gas A, $Z_A'=\bar{c}_A'\sigma_A'N_A$; and for collisions with gas B, $Z_B'=\bar{c}_B'\sigma_B'N_B$. It may be noted that $\bar{c}_A'$ and $\bar{c}_B'$ are different since these quantities are the relative velocities. Accordingly, we have for $\bar{y}'$:

$$\bar{y}'=1/(Z_A'\nu_A+Z_B'\nu_B)t'.$$

Thus, one can write:

$$\frac{y}{y'}=\frac{\bar{y}}{\bar{y}'}=\frac{(Q_A'N_A+Q_B'N_B)(\bar{c}_A'\sigma_A'N_A\nu_A+\bar{c}_B'\sigma_B'N_B\nu_B)}{(Q_AN_A+Q_BN_B)\bar{c}_A\sigma_AN_A\mu_A}.$$

From this equation and the expression for k_{AB}^0 we can find the expression for K_{AB}^0, the reduced mobility as observed in the mixed gas. Letting $N_A+N_B=L$, we obtain:

$$\frac{1}{K_{AB}^0}=\frac{\left(\frac{f_A}{K_A}+\frac{f_B}{K_B}\right)\left(\frac{f_A}{K_A'}+\frac{f_B}{K_B'}\right)\left[f_A+(f_A+lf_B)\frac{K_A'}{K_A}\left(\frac{1-g}{g}\right)\right]}{\left(\frac{f_A}{K_A}+\frac{f_B}{K_B}\right)f_A+\left(\frac{f_A}{K_A'}+\frac{f_B}{K_B'}\right)(f_A+lf_B)\frac{K_A'}{K_A}\left(\frac{1-g}{g}\right)}.$$

This expression is seen to be a function of the mole fractions, the reduced mobilities of the ions I and I' in gases A and B, and two characteristic constants g and l.

The quantity g is the clustering coefficient of I in the pure gas A, as has already been discussed. g can have values from $g=0$ for no clustering to $g=1$, the con-

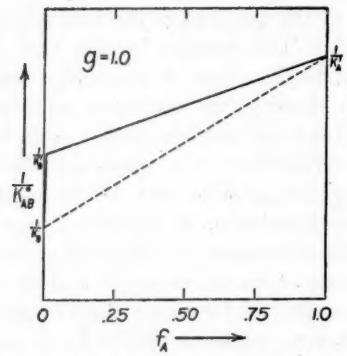

FIG. 4. Analogous to Figs. 2 and 3 with $g=1$. Note that clustering is completed at low values of mole fraction of attaching gas, and that the mobilities of both extremes refer to the ion I'. Blanc's law dashed.

dition for the formation of stable clusters. The quantity l is a dissociation parameter, and is a measure of the relative dissociation abilities of gas A and gas B. It is given by the relation $l=\sigma_B'\bar{c}_B'\nu_B/\sigma_A'\bar{c}_A'\nu_A$. l can have any positive value. In general, unless the gases have very disparate masses, or cross sections, l will be close to unity.

The curves shown in Figs. 1, 2, 3, and 4 illustrate the final result for appropriate relative values of K_A, K_A', K_B, K_B', and for several values of g and l. In Fig. 1, with $g=0$, i.e. no clustering, one has the conventional Blanc's law, as would be expected. When g is 0.5, as in Fig. 2, a slight curvature is apparent, the deviation being greater for smaller values of l. When the clustering coefficient is 0.8, Fig. 3, the bowing is quite marked.

It may be noted that when $l\sim 0$, $1/K_{AB}^0$ rises sharply at $f_A=0$, and then increases almost linearly to its maximum value $1/K_A^0$. Such a small value for the dissociation parameter means that the B molecules have little effect in the dissociation process, so that clustering is not suppressed by large concentrations of gas B. This condition may be realized when the inactive gas B is of low molecular weight, e.g. H_2; for then, the impacts delivered to the heavy clustered ions I' by the light B molecules are small, causing relatively few dissociations.

Finally, when $g=1.0$, $1/K_{AB}^0$ behaves like a Blanc's law curve for I' ions in the mixture, except for a small range of values at $f_A=0$. References to papers by Loeb, Tyndall, and Powell, and others will show the striking similarity between the observed curves and those computed, indicating that even this simple theory accounts well for the experimental results.

One might believe that with six parameters at his disposal, a theoretical curve could be found to fit almost any set of data. Five of these constants, however, can be established independently. From the complete mobility equation of Langevin,[3] the constants K_A, K_A', K_B, and K_B' can be computed. In many practical cases K_B can be measured directly, and K_A can be computed from the equation:[5]

$$K_A=0.235\left(\frac{1+M/m}{(D-1)M_0}\right)^{\frac{1}{2}}.$$

Here, M_0 is the molecular weight of gas A. The studies of Tyndall and Powell have substantiated this expression for the reduced mobility of an ion I in a gas A where the effect of dielectric attractive forces predominates over that of solid elastic collisions. However, this equation cannot be expected to hold for the clustered ions I', where the collisions will play a greater role, owing to the increased size of the ion. It was the application of this expression to K_A^0 that inclined the Bristol group to postulate multimolecular clusters, a concept at variance with the results of aging experiments.

There is a possibility that K_A and K_A' may be measured directly. If apparatus of good time resolution is applied, and mobility measurements are made over distances of the order of $\bar{x}$ and $\bar{x}'$, then a mobility spectrum will be obtained with K_A and K_A' as the upper and lower limits.

With K_A and K_A' known, measurement of K_A^0 determes g immediately:

$$g=(1/K_A^0-1/K_A)/(1/K_A'-1/K_A).$$

The remaining parameter l can then be determined by measurements in the mixed gas and subsequent comparison with computed curves. The theory is therefore open to verification. It is hoped that the concept of clustering here advanced will make possible a more complete interpretation of experimental data.

In conclusion, the author takes pleasure in acknowledging his indebtedness to Professor L. B. Loeb, whose course in discharge through gases prompted the investigation, and who was most generous with his encouragement and aid in preparing the manuscript.

[5] See reference 1, p. 62 ff.

The Role of the Cathode in Discharge Instability*

LEONARD B. LOEB
Department of Physics, University of California, Berkeley, California

(Received March 14, 1949)

It is shown that a highly stressed conditioned cathode in a gas will, by positive space charge action, produce an autocatalytic increase in current through a chain reaction leading to complete breakdown. Depending on conditions in the circuit this common tendency will explain a number of phenomena. In pure free electron gases, the discharge has a negative characteristic and must be controlled by external resistance or else lead to an arc. In the presence of adequate low field regions and moderate negative ion formation, a current controlled by the internal space charge resistance of the system results. Where negative ion formation is heavy and low field regions exist, the discharge will choke itself off and be intermittent. In cases where there are large electrically elastic columns of ionized gas at lower pressure that can be swept by ionizing potential waves, as in glow discharges, the cathode instability leads to pulsations or moving striations and is the cause of setting up and sustaining plasma oscillations. Among the consequences of such action where intermittent or pulsed discharges occur, there will be a Faraday dark space and perhaps striations. Faraday dark spaces will occur only where cathode instabilities cause current fluctuations and should not be observed in more stable discharges.

THE circumstance that in relatively high fields the negative carriers are mobile free electrons, while the positive carriers are the more sluggish gaseous ions, leads inevitably to conditions which can make the cathode region a source of instability in many gaseous discharges. Such instabilities now appear to be much more common than heretofore suspected. They manifest themselves in peculiar phenomena whose nature and common origin have remained obscure. Thus, for instance, one would hardly suspect that the following phenomena had a common origin, to wit: (a) the equality of onset thresholds of some positive and negative coronas, (b) the breakdown of some gaps directly to power arcs, (c) the transitions from Townsend discharge to glow discharges, (d) the transitions of some glow discharges to power arcs, (e) the negative resistance characteristics of many arcs and some corona discharges, (f) the appearance of periodically interrupted pulsed coronas, (g) the existence of the Faraday dark space and the appearance of striations in some otherwise seemingly, steady direct current discharges, (h) the appearance of sustained plasma oscillations of a wide range of frequency from megacycles to microwave frequencies in some discharge tubes.

It is the purpose of this paper to indicate a basic common origin and to associate it with the asymmetry of carrier nature and cathode function. If one regards a highly stressed region near the *anode* of an electrode system at a pressure leading to ionization by electron impact, it will be noted that the electrons and electron avalanches of $e^{\int \alpha dx}$ electrons created by Townsend ionization in the high field regions converge toward the anode. The ionization increases exponentially as the electrons approach the anode. The electrons reaching the anode are relatively rapidly absorbed, leaving behind a space charge of positive ions moving relatively slowly outward. Especially at higher pressures, with the proper geometrical field conditions, in gases having a high absorption coefficient and capable of photo-ionization by high energy photons created by the avalanches, a self-propagating discharge streamer sometimes leading to breakdown can materialize. In, however, a large variety of conditions near the threshold, this action is not possible. The net result of the ionization by converging avalanches is the creation of an outwardly moving positive space charge near the anode, which will in greater or lesser degree control the discharge current by acting as an internal space charge limiting resistor. In some discharge regions such as corona just above onset, space charges will even choke off the discharge as in the Geiger counter regime. Thus, while under some extreme conditions and primarily at higher potentials, a breakdown can initiate as a streamer from the anode, in a majority of cases the removal of electrons leaves behind a positive space charge which acts to limit and control the current, thus preventing transition and breakdown until much higher potentials are reached.

The situation with the negative electrode is quite the opposite, as will readily be seen in what follows. Electrons leaving the highly stressed cathode surface at appropriate pressures will move outward from the cathode ionizing cumulatively as they leave the cathode. In so doing, they soon reach regions of lower field strength where the rate of ionization rapidly falls off owing to the decreased field and consequent rapidly decreasing value of Townsend's first coefficient α. Thus, despite the exponential increase of electrons in the avalanches, the rate of ionization rapidly declines to inappreciable values. The electrons of high mobility leave behind a distribution of positive ions which, sparse near the cathode, increases to a peak at some distance from the cathode, and decreases to a very few at the point where the rate of electron ionization has fallen to negligible dimensions. This positive ion space charge converges on the cathode. In doing so it acts to

* The basic studies that have made this generalization possible have been supported by ONR funds.

augment the field next to the cathode surface in a measure consistent with its density. These space charges can thus act only to augment the field near the cathode and thus enhance the ionization of subsequent electron avalanches. That is, cathode action has inherent in itself a potentially autocatalytic character. Under proper conditions, such action can lead to a chain reaction and catastropic breakdown. The cathode is thus a potential source of instability.

The realization of this instability involves secondary ionizing processes which are especially propitious at the cathode in the lower pressure ranges. For photons created by the avalanches reaching the cathode can liberate photoelectrons from the *metal surfaces* in much greater quantity than is the case for the *photoelectric ionization of the gas* by photons in the neighborhood of the anode. Furthermore, at higher fields, the positive ions whose ionizing potential is above the work function of the surface can liberate electrons from it by positive ion impact. Their efficiency increases rapidly with the field strength. If now the condition of the surface is such that the primary avalanches of $n_0e^{\int \alpha dx}$ electrons can create enough positive ions and photons effectively to augment the incoming positive ion space charge, the basis for the initiation of a catastrophic chain reaction is at hand. Such action once it starts is enhanced by still another effect. In general, fields at the cathode surface are fairly high when breakdown at cathodes starts. Appropriate positive ion densities approaching the surface can increase these fields by an order of magnitude or more. If these fields reach appropriate magnitudes, the ordinary Townsend ionization, represented by the coefficient α, and the use of the expression $e^{\int \alpha dx}$ is no longer valid. In such electrical fields the electrons cease to remain in equilibrium with the field as Townsend's mechanism requires. Thus, the Townsend ionization is replaced by the more efficient Morton-Johnson[1] ionization processes. The primary ionization function is therefore replaced by functions which may be greater by a factor of several hundred percent as observed by Morton and Johnson. This further augments the density of positive ion space charge and further increases the rate of the chain reaction. Thus, there is present with any given cathode and gas a potential instability of considerable effectiveness.

Whether such instability develops in a given combination of electrodes fields, pressure, and gases depends critically on the condition of the cathode surface, the positive ion types, and the electrical fields. Too little is known today about the secondary electron liberation, especially by positive ion bombardment to permit one to be specific. The secondary emission by photoelectric ionization at the cathode is always present for metal surfaces, but it is questionable whether by its magnitude it alone can yield the autocatalytic breakdown described above. It is, however, very likely from the data yielded by recent observations[2,3] that at appropriately high fields the field intensified currents, i.e., $n_0e^{\int \alpha dx}$, yielded by n_0 externally produced electrons from the cathode will evolve into a self-sustaining Townsend discharge. This will set in with potentials and fields at the cathode satisfying the condition $\eta\theta g/\alpha e^{\int \alpha dx}=1$. Here η is the number of active photons produced per electron in the avalanche, g is a geometrical factor determining what fraction of these reach the cathode, and θ is the chance that these will lead to the emission of a secondary electron. The resulting avalanches produce enough positive ions to render the discharge self-sustaining. It is inadequate to yield the positive ion space charge leading to the chain reaction and indefinite increase in current is controlled by negative space charge resistance in the low field regions. Such currents will rapidly increase with potential largely owing to the increase of $\int \alpha dx$. They still may not produce enough positive ions to yield an adequate space charge effect.

Now the high fields at the cathode are such that above the threshold in many discharges the positive ions striking the cathode have been observed to sputter or blast atoms of the cathode from the surface.[4] At the lower fields existing in the Townsend discharge region, these same ions are certainly capable of cleaning the cathode surfaces of oxide and of gas films. If oxygen or chemically active gases are present, these gases will strive to reform the films by diffusion. Such films are known to alter and frequently to increase the work function of the pure metal surface.[5] Increased work function or other action will lower both θ and the γ for secondary electron liberation by positive ion bombardment. If then, as the potential of the cathode is made more negative, the Townsend discharge current reaches such a density of positive ion bombardment as with adequate duration to clean up the surface, the cathode will end up as a clean surface. It will thus reach a condition of low work function and high θ or γ. On the appearance of high secondary emission, the chain reaction can set in and the condition of instability is achieved. A cathode under such circumstances will find itself highly "overvolted," since γ and θ can increase by an order of magnitude or more on the clean surface. The achievement of such clean-up by the low order Townsend discharge initiated on a dirty surface by photoelectric action and possibly by a γ of low value, will depend on a number of factors. These are the nature of the surface, its initial condition, the nature and pressure of contaminating gas present, and the geometry of the field affecting the current density of positive ion bombardment and its energy of bombardment. All these factors have been observed to determine

[1] P. L. Morton, Phys. Rev. **70**, 358 (1946); G. W. Johnson, Phys. Rev. **73**, 284 (1948).

[2] W. N. English and L. B. Loeb, J. App. Phys. **20**, 707 (1949).
[3] Charles G. Miller, Ph.D. Thesis, University of California, 1949.
[4] Hudson, Loeb, Bennett, and Kip, Phys. Rev. **60**, 714 (1941).
[5] G. L. Weissler and R. W. Kotter, Phys. Rev. **73**, 538 (1948).

the nature and clean-up of the surface in the course of recent studies.[2,3] Once the potential of the cathode is such as to produce the clean surface, then the threshold of the appearance of one of the many possible phenomena to be expected with the overvolted clean surface and the attendant chain reaction can be expected.

The manifestations possible with such a surface are varied and may now be listed and discussed.

1. If the gas is very pure and of a type that does not attach electrons and form negative ions, it is to be expected that clean-up will follow in time, depending on the initial soiling of the cathode surface, once the threshold of the low order Townsend discharge is reached. Thus, breakdown and Townsend threshold occur at nearly the same potential. Breakdown will be far more rapid the higher the potential above the Townsend threshold, as then the increased value of $e^{\int \alpha dx}$ will produce more intense bombardment and more rapid clean-up. Once the surface is clean, the chain reaction sets in and the breakdown develops into a power arc, unless there is a current limiting resistor in the outer circuit. If the gap has a long low field region and the gas is clean, there is a chance that the electron space charge in the low field regions may act to limit the discharge. Transitions from a Townsend discharge to an electron space charge limited current 1000-fold greater at constant potential have been observed by G. L. Weissler[6] in negative point corona in pure N_2 and H_2. With shorter gaps, C. G. Miller,[3] with N_2 and H_2 in a concentric cylindrical corona gap found that the discharge went to arc over unless he used an external limiting resistor. Here the currents jumped from 10^{-10} ampere on clean-up to 10^{-2} ampere or more.

2. If gases like O_2 are present in the N_2, then negative ion formation with oxides of nitrogen, O_2 molecules, and O atoms takes place. Under these conditions, the enormous burst of electrons from the chain reaction builds up such a heavy space charge of slowly moving *negative* ions in the lower field regions as to reduce the fields at the cathode to values where cumulative ionization is no longer possible.[7] The discharge then terminates until the space charge of negative ions is cleared by the field when a new discharge can start. The discharge is, therefore, an interrupted discharge of the Trichel pulse type. The magnitude and duration of the pulses depend on the rate of negative ion formation and electron liberation. In such cases the negative pulse onset, or "breakdown," is higher in negative potential than the Townsend threshold as the larger Townsend current is needed to clean up the surface.[2] The pulse onset is lower the higher and the more convergent the field at the cathode and the lower the pressure of O_2.

3. In such discharges the maximum luminosity occurs at the height of the pulse. The enormous burst of ionization liberates electrons so rapidly compared to their removal in the lower field region, that even before much attachment to ions has occurred, the discharge will show not only a Crookes dark space and a negative glow but a Faraday dark space as well. In the stationary low order Townsend discharge, calculation of the rate of ionization would lead one to infer only the presence of the Crooke's dark space and the negative glow. Thus, it seems likely that the appearance of the Faraday dark space in discharges is not a property of the steady Townsend discharge. Instead it is caused by a transient, unstable regime where overproduction of electrons in one phase produces a second region of high potential gradient beyond the negative glow. This is a condition in which the electrons pile up so heavily in the low field region as to possibly hold back positive ions and to produce a steep gradient with the outward lying more positive portions of the discharge. This has recently been strikingly confirmed by observations by H. W. Bandel[8] that for large points and lower pressures the intermittent Trichel pulses give way through a fluctuating corona to a steady direct current discharge of higher value. The higher potentials, broader fields, and low pressures prevented the choking action of the negative space charge by reducing attachment, thus terminating Trichel pulses. When this occurs the Faraday dark space disappears and the positive column becomes diffuse and general, shading into the negative glow.

4. It is possible that the intense electron liberation leading to enormous current increase will be accompanied by a compressive effect on the cathode regions of the discharge.[7] Such compression results from the distortion of the equipotential surfaces between regions of discharge along the axis and the surrounding regions of no discharge. This so concentrates the current that the current densities observed in the low boiling point metal vapor arcs of in excess of 10^5 amperes per cm^2 are achieved. Under such conditions the intense local surface heating leads to a disruption of the surface in the form of vapor jets. It begins to be assumed that such jets in part cause the peculiar wandering of the cathode spots in these arcs. This action constitutes a different type of disturbance of the discharge, to wit, by a destruction of the surface also owing to the chain reaction. It in turn also acts to limit the discharge. Actually both in coronas and arcs such confined discharges are able to carry only a limited current. Thus, increased current resulting from lowered external resistance is achieved only by the appearance of multiple spots as has been observed in corona studies and in Hg arcs by Froome.[9] Incidentally, it appears that in arcs where the current is controlled by external resistors, one does not have the pulsating instability resulting from the overproduction of electrons. Thus so far only the Crookes dark space and negative glow have been observed in arcs. The Faraday dark space is absent.

[6] G. L. Weissler, Phys. Rev. **63**, 96 (1943).
[7] L. B. Loeb, J. App. Phys. **19**, 882 (1948).
[8] H. W. Bandel, work currently in progress, University of California.
[9] K.D. Froome, Proc. Phys. Soc. London **60**, 424 (1948).

5. Under appropriate conditions of low pressure together with an extensive gaseous path length yielding a high controlling internal resistance, one has the glow discharge. With a steadily applied potential, these discharges appear to the eye to be thoroughly stable, steady discharges. They have a positive resistance characteristic. They show a Crookes dark space, a negative glow, and a Faraday dark space. In some cases the Faraday dark space is followed by other dark spaces in the striated discharge with stationary striations. Until very recently such discharges have been assumed to be stable and steady. To the writer at least there was no satisfactory explanation of the reason for the appearance of the Faraday dark space or striations which appeared as some sort of standing potential wave pattern. Very recently G. H. Dieke and T. Donahue[10] have studied the steady glow discharge by means of a photomultiplier tube and oscilloscope. These studies revealed that what to the eye appears as a *steady glow* is in reality a seething mass of pulsations of a most complicated form. Negative striations initiate near the negative glow and travel toward the anode. Positive striations start from the anode region and move towards the cathode but with a different velocity. These striations interfere and impede each other's progress as they move. The striations may be regular in time or the oscillations may be quite confused. Their frequencies range from 10^3 per second to 10^5 per second. The fluctuations in light intensity, at a point ranging from zero to the maximum value, are accompanied by oscillations in potential across the tube of some percent and synchronize with the fluctuations of light intensity where these are regular. It is Dieke's belief that a truly steady d.c. glow discharge is rare indeed. Where it occurs the Faraday dark space should sensibly be absent.

The oscillations are difficult to explain unless there is some cause for instability inherent in the glow discharge. They become a logical consequence of the situation once an overvolted or unstable cathode condition is assumed. In such discharges, as the initial glow discharge builds up on application of the potential, it begins as a Townsend discharge with a low secondary coefficient at the cathode. Once the cathode is cleaned up, the tube is overvolted and the autocatalytic breakdown begins. In this case, however, the long gaseous column yields the limiting resistor in the tube that prevents arc over. In fact, the tube as a whole has a positive resistance characteristic since energy derived from the gradient is required to maintain the long conducting luminous positive column. Electron attachment at these pressures usually does not throttle the discharge as in the more confined and less uniform gradients of the corona. In addition, a column of ionized gas has distinctly elastic and even resonant electrical properties and can thus be set into oscillation by electrical disturbances caused by instability. Plasma oscillations have long been recognized in ionized plasma. The ionic plasma oscillations have frequencies of the order of 10^5 cycles and up, depending on ion mass and density. Electronic plasma oscillations can occur at the lower pressures and these have frequencies in the microwave region.

One can picture the occurrences of the lower frequency oscillations observed by Dieke and Donahue as follows. As the cathode cleans up, the autocatalytic breakdown begins. There is a rapid overproduction of electrons in the negative glow. This builds up a steep gradient of potential relative to the positive column. It also holds back some of the positive charge in the Crookes dark space. The withholding of positive ions temporarily reduces the fall of potential in the cathode fall and slows the autocatalytic increase in positive ions and secondary electrons. Eventually the gradient between negative glow and positive column reaches such a value that a potential wave sweeps from this up the preionized positive column, ionizing as it goes. This is the negative striation of Dieke. Such potential waves have been produced in long tubes by Snoddy and Beams[11] with impulse potentials and are known in lightning discharge. Their velocity depends on the steepness of the potential gradient and on the density of ionization of the plasma. Once this wave of ionization has started towards the anode, the excess electron charge in the negative glow is reduced. The positive ions are released and the potential gradient at the cathode in the Crooke's dark space again begins to build up. When this is again at the value to overvolt the gap, the process repeats. The frequency of this oscillation will depend on pressure current density, overvolting, etc. When the negative voltage pulse from the cathode has reached the region of the anode fall, it produces a burst of ionization and a "reflected" wave of excess positive ionization, the positive striation of Dieke sweeps toward the cathode with, however, a different velocity. There are thus a succession of negative striations passing from negative glow to the anode, and of positive striations passing from anode towards the cathode, disappearing when they reach the negative glow. If these have the proper frequency and synchronize with instability pulsations in the Crookes dark space, then the regular oscillations observed by Dieke appear. If, however, they interfere destructively, the confused hash observed by Dieke results. There are a large number of modes of stable oscillations depending on the character of the discharge, the gases used, the pressure, length of tube, and current conditions. Under more special conditions the same cathode instabilities will call forth plasma oscillations at higher frequency. Emeleus and Armstrong[12] as well

[10] G. H. Dieke and T. Donahue, Gaseous Discharge Conference, Brookaven, New York, Oct. 27–29, 1948; also ONR Report.

[11] Snoddy, Dieterich, and Beams, Phys. Rev. **50**, 469 (1936); **52**, 739 (1937); F. H. Mitchell and L. B. Snoddy, Phys. Rev. **72**, 1202 (1947).

[12] E. B. Armstrong and T. R. Niell, Nature **160**, 713 (1947); **163**, 59 (1949).

as Wehner,[13] by properly arranging the electrode disposition at very low pressures, were able by regenerative methods to produce electron plasma oscillations in the microwave region. On the basis of this picture, striations and the nature of and function of the Faraday dark space become clear. The Faraday dark space is connected with the cathode instability and represents the transient dark phase of the region between glow and column while the potential builds up. Since in other phases of oscillation it does not exist, the dark space is never completely dark. It is dark compared to the negative glow and positive column.

In the glow discharge it may be noted that the behavior of the discharge is determined largely by the electrically resonant properties of the tube, the function of the cathode instability being to furnish the driving force. That is, unless the cathode is in a state to furnish more complete breakdown by a chain reaction, the energy is not available for setting into motion the oscillations occurring. It is this important role of the cathode instability which has up to the present been lacking for an adequate explanation of these phenomena.

[13] G. Wehner, submitted for publication Rev. Sci. Inst. (1949).

PHYSICAL REVIEW VOLUME 76, NUMBER 2 JULY 15, 1949

Angular Distribution of Photo-Neutrons from Deuterium* †

EDWIN P. MEINERS, JR.
Department of Physics, Washington University, St. Louis, Missouri
(Received March 21, 1949)

A study has been made, using 2.76 Mev Na^{24} gamma-rays, of the angular distribution of photo-neutrons from deuterium under approximately ideal conditions of low neutron scattering from the general surroundings into the detector. Results were obtained for two general methods of neutron detection, a BF_3 chamber and the Szilard-Chalmers reaction on $Ca(MnO_4)_2$. Assuming the neutron distribution to have, in the barycentric system, the form $I(\theta)=a+b\sin^2\theta$, the values of a/b obtained are 0.212 ± 0.008 for the first method and 0.203 ± 0.040 for the second, giving as a weighted average 0.211 ± 0.008. From this, the ratio of the photomagnetic cross section to the photoelectric cross section is calculated to be 0.317 ± 0.012.

I. INTRODUCTION

THE theory of photo-disintegration[1] of the deuteron predicts that for gamma-rays of energy appreciably smaller than about 50 Mev,[2] the distribution of photo-neutrons from deuterium should have, in the barycentric coordinate system, the angular distribution represented by $a+b\sin^2\theta$, θ being the angle between the direction of the photon incident on the deuteron and the direction of the neutron leaving the nucleus. This distribution is the combination of essentially two types of interactions, customarily referred to as the photoelectric effect, leading to the $\sin^2\theta$ term, and the photomagnetic effect, leading to a spherically symmetric distribution. Theory also predicts that for gamma-ray energies close to the threshold, which for deuterium is 2.237 Mev,[3] the photomagnetic effect predominates and thus the distribution should be isotropic. As the photon energy is increased, the photoelectric contribution becomes increasingly important and the distribution goes over into that represented by $b\sin^2\theta$.

Early research workers[4–6] showed quite readily that, for gamma-rays from ThC″ and radium, the distribution of photo-neutrons is anisotropic. However, due to either poor geometry, poor statistics, or both they were not able to show that the distribution found was actually a combination of a $\sin^2\theta$ part plus a spherically symmetric part. Myers and Van Atta,[7] using x-rays from a Van de Graaff electrostatic generator, which gave a continuous spectrum with a maximum energy of 2.43 Mev, first proved the existence of the photomagnetic component. They found the distribution was predominately isotropic as is to be expected for energies so near the threshold. Halban,[8] and Graham and Halban,[9] using the 2.62 Mev gamma-ray from RaTh, made a careful study of the relative intensities of photo-neutrons emitted in the 0°, 45°, and 90° directions with respect to the direction of the gamma-ray, obtaining the result: $a/b=0.26\pm0.08$. By means of a qualitative argument, based on the effect of neutron scattering within the heavy water sphere, an upper

* Assisted by the joint program of ONR and AEC.
† Part of dissertation to be presented to the graduate school of Washington University in partial fulfillment of the requirements for the degree of Doctor of Philosophy.
[1] See, for instance, H. A. Bethe and R. F. Bacher, Rev. Mod. Phys. 8, 124 (1936).
[2] M. E. Rose and G. Goertzel, Phys. Rev. 72, 749 (1947).
[3] R. E. Bell and L. G. Elliott, Phys. Rev. 74, 1552 (1948).
[4] J. Chadwick and M. Goldhaber, Proc. Roy. Soc. A151, 479 (1935).
[5] J. Chadwick, N. Feather, and E. Bretescher, Proc. Roy. Soc. A163, 366 (1937).
[6] J. R. Richardson and L. Emo, Phys. Rev. 53, 234 (1938).
[7] F. E. Myers and L. C. Van Atta, Phys. Rev. 61, 19 (1942).
[8] H. Halban, Nature 141, 644 (1938).
[9] G. Graham and H. Halban, Rev. Mod. Phys. 17, 297 (1945).

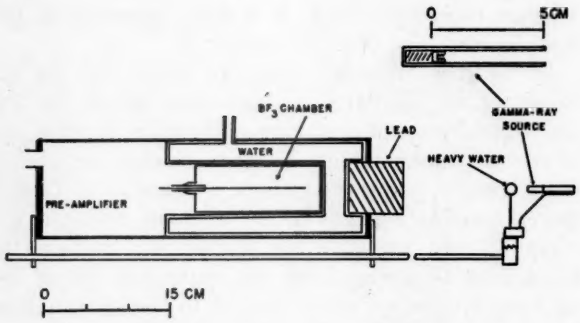

FIG. 1. Diagrammatical representation of the arrangement of the BF_3 chamber and source. The chamber was cadmium covered.

limit of $a/b=0.29$ was set, indicating that their value of 0.26 might be too high within the limits of their precision. Unfortunately, this experiment was performed in a room with the apparatus only 80 cm above the floor for which the scattering of neutrons from the floor, walls and ceiling must have been appreciable and for which it is very difficult to make a reliable correction.

Recently, Lassen,[10] using Na^{24} gamma-rays, showed that the angular distribution is given very closely by an $a+b\sin^2\theta$ law. He detected the photo-protons in deuterium filled proportional counters and measured the pulse-size distribution for different angles of the gamma-ray beam with respect to the axis of the proportional counters. He finds his results are best fitted by the curve: $I(\theta)/I(90)=a+b\sin^2\theta$ with a/b equal to 0.22 ± 0.04, a value which is less than that of Graham and Halban, as it should be, due to the higher photon energy.

Note added in proof: This result has recently been corrected [N. O. Lassen, Phys. Rev. **75**, 1099 (1949)], yielding a somewhat lower value of a/b (0.18 ± 0.04).

This experiment was undertaken for the purpose of measuring a/b for the photo-neutrons ejected from deuterium by the action of Na^{24} gamma-rays under conditions for which there should be practically no correction necessary due to the scattering of neutrons from the surroundings into the detector.

II. THE EXPERIMENTAL METHOD

The experimental method is essentially the same as that used by Graham and Halban. The neutron detector used (see Fig. 1) consisted of an ionization chamber 6 cm in diameter by 15 cm long, filled to atmospheric pressure with enriched boron trifluoride, and surounded by a water jacket, the walls of which were made of Lucite. A lead plug, 6.3 cm thick by 6 cm in diameter, was inset in the end facing the source to shield the chamber from direct gamma-radiation. It was found necessary to do this to reduce the gamma-ray background noise to the point where neutron pulses could be easily detected. A pre-amplifier was mounted directly behind the chamber. The detector, thus constructed, was surrounded with a cadmium cover to help prevent the detection of any neutrons other than those coming directly from the source. The over-all dimensions of this detector are 11.5 cm in diameter by 40 cm long.

The source was mounted on the end of a piece of $\frac{5}{16}$-inch diameter aluminum tubing which was fastened directly to the under side of the detector and along its axis. On the far end of this tubing was attached the mechanism for holding a small glass-walled sphere filled with heavy water mounted on the end of a piece of aluminum rod $\frac{1}{8}$ inch in diameter by 4 cm long. Spheres of three different diameters (0.95, 1.27, and 1.50 cm) were employed. The spheres have wall thicknesses of about 0.5 cm. To this mechanism was also attached, on a small arm, the gamma-ray source. By means of strings running along the aluminum tubing to the rear of the chamber, the gamma-ray source could be rotated through certain fixed angles. The neutron source to detector distance could be set at will and was usually kept between 50 and 80 cm. (The solid angle subtended by the chamber was between 0.041 and 0.016 steradian.) This setup was then suspended from a horizontal rod at the top of a frame tower on the roof of the Washington University Physics Building and was thereby held at a height of 16 feet above the roof, which was the nearest massive object.

Tests of the background due to scattering were made by observing the variation from an inverse square law for a 20 mg Ra-Be source. No detectable variation was obtained out to a distance of 100 cm from the chamber along its axis. That the scattering effect at this height is truly negligible was confirmed by measuring the counting rate as a function of the distance of the source-detector combination from the ground. It is readily seen (see Fig. 2) that 16 feet is certainly enough to reduce, to a negligible amount, the back-scattering of Ra-Be neutrons.

The Na^{24} sources were prepared by the Washington

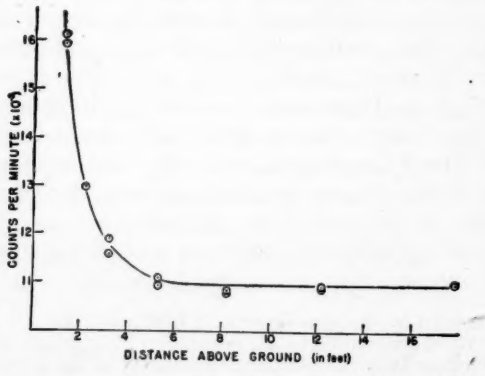

FIG. 2. A plot of the counting rate for the BF_3 chamber *versus* the height of the chamber-source combination from the ground. The chamber was suspended horizontally and a 20 mg Ra-Be source was attached to it, by an aluminum rod, so that it was 6 inches from the front face of the chamber.

[10] N. O. Lassen, Phys. Rev. **74**, 1533 (1948).

University cyclotron by bombarding metallic sodium with deuterons (for about 2000 microampere hours) and then scraping a thin layer off the surface. This active sodium was put into a brass tube 6 cm long by 6 mm inside diameter with a 1 mm wall-thickness (see Fig. 1). A brass plug 6 mm long was forced in behind the sodium to keep it in position. The plug was drilled and threaded in one end so that the finished source could be picked up and handled conveniently on the end of a long rod. The sources, thus prepared, ranged in initial activity from 700 to 1200 mc. It is assumed that this activity is uniformly distributed throughout the volume of the sodium. This assumption, although not critically tested, is probably valid since only the active region of the target was scraped and since considerable mixing took place as a result of the way the sodium was packed in the tube.

The distance between the gamma-ray source and the heavy water sphere was kept small compared to the distance between the sphere and the neutron detector. The reasons for this geometrical arrangement are essentially those given by Graham and Halban and hence will not be repeated here.

As an alternative method for studying the distribution of photo-neutrons, the detector just described was replaced by a device which detected neutrons by means of the Szilard-Chalmers reaction in calcium permanganate solution. The procedure is that worked out by Dodson, Goldblatt, and Sullivan.[11] The detection apparatus for this case (see Fig. 3) consisted of two cadmium covered glass chambers 33 cm long by 8.3 cm in diameter and of 1350 cc volume. These containers filled with 2.4 M $Ca(MnO_4)_2$ solution, were supported horizontally on an aluminum framework with axes at right angles to each other and with the front faces of each 24.5 cm from the center of a heavy water sphere. (The solid angle subtended by the detector at the sphere was about 0.090 steradian.) The gamma-ray source was supported by a small rod near the sphere so that its axis was along that of one of the chambers. This whole apparatus was then hoisted 14 feet above the ground by means of a cable running from the Washington University Physics Building to a tree 300 feet away, thus securing adequate isolation from the ground or walls of the building. After 8-hour irradiation periods, the permanganate solution from each container was filtered separately through asbestos, the residues washed, and then dissolved in hot 1.5N HNO_3 containing 10 cc of 3 percent H_2O_2. MnO_2 was reprecipitated by adding 5 g of $KBrO_3$ and boiling. The solutions were then filtered and the filter papers which held the residues were made into cylindrical foils which could be easily slipped around a thin walled counter tube and counted.

[11] R. W. Dodson, M. Goldblatt, and J. H. Sullivan, Los Alamos Scientific Laboratory Report, MDDC 344.

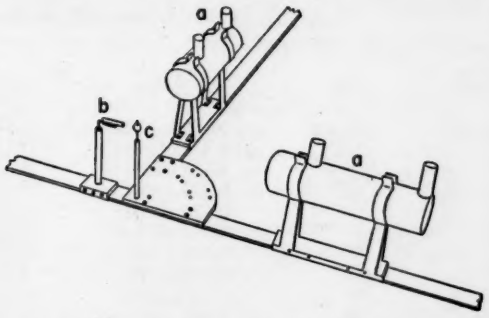

FIG. 3. Diagrammatical representation of the arrangement used for determining the angular distribution by the Szilard-Chalmers reaction in $Ca(MnO_4)_2$ solution. a is a cadmium covered glass chamber containing $Ca(MnO_4)_2$ solution, b is the gamma-ray source, and c is the heavy water sphere. The supporting framework is made of aluminum.

III. THE EXPERIMENTAL RESULTS

(a) BF_3 Chamber

In taking data with the BF_3 chamber, there were several somewhat complicating factors that had to be taken into account. The chamber had a natural background of about 5 c.p.m. which, in the presence of a one curie Na^{24} source, was usually increased to about 12 c.p.m. (due to building up of gamma-ray pulses in the chamber and probably, to some extent, due to the natural D_2O content of the water jacket). The maximum counting rate at 90° ranged usually about 30 c.p.m. above background. At the same time it was found very difficult to reproduce exactly, each time, the position of the heavy water sphere, although once in position, it retained this position very well. In view of these considerations, the data were taken in groups, each group giving a value of the ratio $I_{90°}/I_{0°}$, and the data of alternate groups consisting of either of the two following series of measurements.

$$B,\ S(0°),\ S(90°),\ S(90°),\ S(0°),\ B,$$
$$B,\ S(90°),\ S(0°),\ S(0°),\ S(90°),\ B,$$

B stands for background obtained by removing the heavy water sphere, $S(0°)$ for zero angle between the line from the center of the gamma-ray source to the center of the heavy water sphere and the line from the sphere to the detector, and $S(90°)$ stands for 90° between these lines. The backgrounds were counted for periods ranging between 1 and 2 hours and the others 40 minutes each. The results, thus obtained, were corrected for decay of the Na^{24} source and for background. If a count in any one group was suspected as being false (due to weather conditions, microphonics, etc.) the entire group containing this count was discarded. A summary of these results is given in Table I. The errors quoted are the standard errors due to the number of counts taken.

It is necessary to make several corrections to the data. In the first place, scattering of neutrons inside the heavy water spheres will tend to increase the value of

TABLE I. Summary of experimental results with the BF_3 chamber.

Sphere diameter	d*	$I(0°)/I(90°)$	$[I(0°)/I(90°)]_c$**	$\langle\cos^2\psi\rangle$	$\langle\sin^2\theta\rangle$	a/b	Weight
0.95 cm	51 cm	0.336±0.022	0.240±0.034	0.026	0.052	0.201±0.045	4
0.95	51	0.352±0.038	0.256±0.052	0.026	0.052	0.215±0.070	2
0.95	55	0.323±0.042	0.227±0.054	0.011	0.022	0.221±0.072	1
0.95	64	0.323±0.013	0.227±0.025	0.011	0.022	0.221±0.034	8
1.27	76	0.373±0.025	0.242±0.037	0.023	0.046	0.206±0.050	3
1.27	59	0.379±0.009	0.248±0.021	0.025	0.050	0.208±0.028	5
1.27	51	0.358±0.047	0.227±0.059	0.017	0.034	0.204±0.079	1
1.27	51	0.370±0.025	0.239±0.037	0.025	0.050	0.195±0.050	2
1.27	51	0.407±0.023	0.276±0.035	0.037	0.075	0.207±0.047	1
1.50	76	0.391±0.046	0.235±0.058	0.017	0.035	0.223±0.078	5
1.50	51	0.391±0.011	0.235±0.023	0.014	0.029	0.222±0.031	4
1.50	51	0.366±0.017	0.210±0.029	0.014	0.029	0.189±0.039	2

* d is the distance from the center of the sphere to the front face of the detector.
** $I(0°)/I(90°)$ corrected for scattering of neutrons inside the sphere.

$I_{0°}/I_{90°}$. Also, the sources and spheres are of finite size and thus subtend finite and, due to the geometrical arrangement, not negligible solid angles to each other.

To correct for the effect due to scattering of neutrons inside the heavy water spheres, the raw data for each of the three spheres were averaged separately and the best linear plot *versus* the sphere radius (r) made. The point where this line crosses the r axis (0.237±0.012), gives, then, a sort of average value of $I_{0°}/I_{90°}$ which is uncorrected for geometry. The correction for geometry has to be made however, on each value of $I_{0°}/I_{90°}$ separately since the corrections differ for the different spheres and sources used. Thus the effect due to scattering was subtracted from each set of data and the geometrical corrections were applied.

To obtain the geometry correction, it is assumed that the solid angle subtended by the neutron detector at the heavy water sphere is small compared with the solid angle subtended between the sphere and the gamma-ray source. Then make the following definitions:

$$\langle\sin^2\theta\rangle=\int\int\int d\tau d\tau' \sin^2\theta/r^2 \Big/ \int\int\int d\tau d\tau'/r^2$$

and similarly for $\langle\cos^2\psi\rangle$. $d\tau$ and $d\tau'$ are elements of volume in the gamma-ray source and the heavy water sphere respectively, and r is the distance between them. θ and ψ are the angles between the directions of propagation of the gamma-ray and the neutron produced (which enters the detector) for the 0° and 90° cases. The ratio a/b will then be given by

$$\frac{a}{b}=\frac{I(0°)/I(90°)(1-\langle\cos^2\psi\rangle)-(1+2\delta)(\langle\sin^2\theta\rangle)/(1-\delta)}{1+2\delta-I(0°)/I(90°)}$$

where

$$\delta=\hbar\omega/[(4M_pc^2)(\hbar\omega-\epsilon)]$$

$\hbar\omega$ being the energy of the incident gamma-ray in the laboratory system and ϵ the binding energy of the deuteron. δ is a small correction term to account for the fact that the experiment is performed in the laboratory system, whereas theory predicts the simple $a+b\sin^2\theta$ law in the barycentric coordinate system. The values of a/b have been calculated by the above method for each case and are also given in Table I (column 7). It should be noted that there is no significant trend in these values of a/b with the size of the heavy water sphere. It is thus assumed that the effect due to neutron scattering within the spheres is now negligible. Then taking the weighted average (weight factor = number of groups) of the data, the final value of a/b is 0.212 ±0.008. The error is based on the standard statistical error due to the number of counts taken plus estimated errors due to the correction for neutron scattering within the spheres. According to theory this leads to the following for the ratio of the photomagnetic cross section to the photoelectric cross section:

$$\sigma_m/\sigma_e=3/2(a/b)=0.318\pm0.012.$$

This value, obtained by measuring neutrons, is in excellent agreement with that of Lassen, who measured the photo-protons. That this is so, gives us considerable confidence in the reliability of both methods and their freedom from unsuspected errors.

It should be noted here that undoubtedly corrections should also be made for the fact that all data were not taken for the same source to detector distance. In effect, data were being compared which originated from experiments performed under somewhat different geometrical conditions. However, a correction of this nature appears to be small in comparison with the statistical deviations of the data taken at any one setting of the source to detector distance (see Table I). In view of this fact, no attempt has been made to make this correction, but all data taken (within the limits 50–80 cm) have been treated equally.

It might be added, by way of conclusion of this section, that it was attempted to find $I_{90°}/I_{0°}$ for a heavy water sphere only 5 mm in diameter. The observable neutron intensities for this case, even in the presence of a one curie Na^{24} source, were less than half the background intensity and the statistical accuracy thus so low that the results cannot be given any serious weight.

(b) Szilard-Chalmers Reaction

The method just described possessed two distinct disadvantages. The BF_3 chamber had a natural background which was increased by the presence of a gamma-ray source. At the same time, it was found to be extremely difficult to eliminate entirely microphonics, voltage breakdown, etc. under all weather conditions. The weather thus became a major problem.

These particular difficulties were overcome by using containers filled with $Ca(MnO_4)_2$ solution as neutron detectors. The results so obtained (see Table II) are, however, not without their own sources of error. The major source of error here is due to the scattering of neutrons from one chamber to the other and from the supporting framework. An attempt was made to correct for this by using a 20 mg Ra-Be source under approximately ideal conditions (only one chamber present and relatively little supporting mechanism), and under the conditions used for the actual experiment. This correction was made even more difficult due to the fact that the reproducibility of extraction of the active manganese by the Szilard-Chalmers method was hard to attain from one run to another, even though reproductibility of the ratio of results obtained using two chambers at the same time was quite good (about 5 percent variation). It should be noted that the intensity at the 0° position requires a relatively larger correction than that at the 90° position. The correction finally arrived at amounts to a decrease in the 0° intensity of 27 percent and a decrease in the 90° intensity of 14 percent.

The geometry corrections, due to finite sizes of source and sphere were applied as previously described and values for a/b obtained also are shown in Table II. The average value of a/b from the above is 0.203 ± 0.040 where the error quoted is based to a large extent on estimates made of the reproducibility of the method and the correction factors. Although it is to be noted that the errors are rather large, the value of a/b is nevertheless in substantial agreement with that obtained by the previous method.

TABLE II. Summary of results with the Szilard-Chalmers reaction.

Sphere diameter	$I(0°)/I(90°)$	$[I(0°)/I(90°)]_c$*	$\langle\sin^2\theta\rangle$	$\langle\cos^2\psi\rangle$	a/b
0.95 cm	0.452	0.233	0.052	0.026	0.184
1.27	0.500	0.251	0.040	0.020	0.227
1.50	0.519	0.251	0.062	0.031	0.192
1 50	0 500	0 230	0 034	0 017	0 207

* $I(0°)/I(90°)$ corrected for neutron scattering from supports, between chamber, and within the heavy water sphere.

IV. SUMMARY

A determination of the ratio of the neutrons in the 0° and 90° positions for the reaction $D+\gamma\rightarrow p+n$ has been made using Na^{24} gamma-rays and approximately ideal conditions of low neutron scattering. Assuming the neutron intensity, as a function of angle, to have the form $I(\theta)=a+b\sin^2\theta$, in the barycentric system, the values of a/b obtained by the two different methods are 0.212 ± 0.008 for the BF_3 chamber and 0.203 ± 0.040 for the method using the Szilard-Chalmers reaction. The weighted average of these is 0.211 ± 0.008, giving for the ratio of σ_m/σ_e, 0.317 ± 0.012. Using the value for the total cross section of the photodisintegration of deuterium by Na^{24} gamma-rays ($[15.6\pm1.0]\times10^{-28}$ cm^2), recently obtained by Wilson, Collie, and Halban,[12] one obtains,

$$\sigma_m=3.8\pm0.3\times10^{-28},\quad \sigma_e=11.8\pm0.8\times10^{-28}.$$

Work is nearing completion on the angular distribution of photo-neutrons from beryllium using both Sb^{124} and Na^{24} gamma-rays.

V. ACKNOWLEDGMENTS

The author would like to express his appreciation to Dr. F. Rasetti for suggesting this problem and for his invaluable aid in its initial phases. He would also like to thank Mr. L. Slack and Mr. D. Smith for their help in constructing the apparatus and taking the data, Professor E. Feenberg and Professor H. Primakoff for their aid and discussion of the theoretical problems involved, and Professor A. L. Hughes for his stimulating discussions and continued support of this work. He is indebted to the Washington University cyclotron crew for the preparation of the Na^{24} sources.

[12] R. Wilson, C. H. Collie, and H. Halban, Nature **163**, 245 (1949).

Straggling of Electrons near the Critical Energy

L. EYGES*
The University, Birmingham, England
(Received March 31, 1949)

The straggling of electrons caused by loss of energy by radiation and collision is discussed. The paper is essentially in three parts. In Section III we have found the "straggling probability" for an electron that loses energy only by radiation, and give curves corresponding to various approximations to the expression for the radiative cross section. In Section IV collision loss is also taken into account and a formal expression for the straggling probability is found in the form of a series whose terms decrease rapidly for energies not too small and not too large thickness. No proof of the convergence is given however and, in fact, for very small energies the terms increase and some higher order terms become infinite at zero energy. In Section V some remarks are made on the small "showers" initiated by a particle of energy near the critical energy.

INTRODUCTION

WE shall be mainly concerned in this paper with the behavior of an electron with energy of order of the critical energy, when incident on matter. Such an electron, of energy E_0, cannot itself penetrate a distance t greater than E_0/β, where β is the critical energy.[1] For E_0 less than β, t is automatically less than one. Of course, an electron can make itself felt at larger distances than E_0/β by pair-production by its radiated quanta, i.e., by producing a small "shower," but at small thicknesses and for a considerable range of energy the main contribution to such a "shower" will be due to the straggling of the original electron. It is the main burden of this paper to calculate this straggling, although some remarks on the effect of photons are made in the last section.

It will appear that our solution can be used only for thicknesses which are not too large and energies not too far from the initial energy. The restriction on thickness is not too serious, since we have seen that for an initial energy equal to the critical energy, one is never interested in the original electron for thicknesses greater than unity. Also, the restriction that the energy be close enough to the initial energy has one redeeming feature; for this case we can to some extent take into account the variation of the radiation cross section with energy by using an expression appropriate to some average of the initial energy and the energy considered.

There has been at least one other attempt to calculate the small showers initiated by an electron of order of the critical energy. This is due to Bhabha and Chakrabarty,[2] who claim to have found a solution of the general shower equations, including the effect of collision loss. As a special case of their results they derive an expression for the energy spectrum at small thicknesses, which purports to hold for incident particles with energy of the order of the critical energy. Their expression is in the form of a series in t in which terms of order t^3 and higher are dropped as negligible. For $t=0.1$ and some energy values, however, the term in t^2 is as much as 300 times as large as the linear term;[3] the dropping of higher order terms is thus quite suspect, and the expressions they give for small thickness cannot be considered as a correct solution.

The present paper is essentially in three parts. In Section III we have discussed the "straggling probability" for electrons which lose energy only by radiation, and investigated how this probability depends on the expression for the radiative cross section. In the next section we have extended this to the case where electrons lose energy by constant collision loss as well. Finally, in Section V we have considered the effect of photons and pair production.

II. THE DIFFUSION EQUATION

Let $\pi(E,t)dE$ be the probability that an electron which loses energy by radiation and by collision loss has energy in the range E to $E+dE$ at thickness t. Then $\pi(E,t)$ satisfies the well-known diffusion equation[4]

$$\frac{\partial\pi(E,t)}{\partial t}=-\int_0^1\left[\pi(E,t)-\frac{1}{1-v}\pi\left(\frac{E}{1-v},t\right)\right]\varphi(v)dv-\beta\frac{\partial\pi(E,t)}{\partial E}. \quad (1)$$

Here $\varphi(v)dvdt$ is the probability that in the thickness dt the electron emits a photon which has a fraction between v and $v+dv$ of the electrons energy. The first term on the right-hand side of (1) describes the decrease in $\pi(E,t)$ due to electrons initially in the interval (E,dE) which leave it by radiation, the second describes the increase in $\pi(E,t)$ due to electrons of energy greater than E which enter the interval (E,dE) by radiation, and the last term takes account of collision loss.

* U. S. AEC post-doctoral research fellow.

[1] We measure lengths in radiation lengths, as usual, and take β, the critical energy, to be also the (constant) energy loss per radiation length.

[2] H. J. Bhabha and S. K. Chakrabarty, Proc. Roy. Soc. **A181**, 267 (1943) and Phys. Rev. **74**, 1352 (1948).

[3] This was pointed out to me by Professor H. A. Bethe. See Table IX, p. 299 in the first paper of reference 2.

[4] See B. Rossi and K. Greisen, Rev. Mod. Phys. **13**, 240 (1941).

If we apply the Mellin transform

$$M(s,t)=\int_0^\infty E^s\pi(E,t)dE \tag{2}$$

with the inverse transform

$$\pi(E,t)=\frac{1}{2\pi i}\int_{\delta-i\infty}^{\delta+i\infty}E^{-(s+1)}M(s,t)ds \tag{3}$$

to (1), we are led to the equation

$$\partial M(s,t)/\partial t=-A(s)M(s,t)-\beta sM(s-1,t), \tag{4}$$

where

$$A(s)=\int_0^1[1-(1-v)^s]\varphi(v)dv. \tag{5}$$

The contour in (3) should lie to the right of all singularities of the integrand.

III. STRAGGLING WITHOUT COLLISION LOSS

We will first consider an electron that loses energy only by radiation, and add a subscript zero to the function $\pi(E,t)$ to denote this. Then $\pi_0(E,t)$ satisfies Eq. (1) with β set equal to zero, and the corresponding equation for the transform $M(s,t)$ is

$$\partial M(s,t)/\partial t=-A(s)M(s,t). \tag{6}$$

The solution of (6) which corresponds to the boundary condition of one electron of energy E_0 incident at $t=0$ is

$$M(s,t)=E_0^s e^{-A(s)t}. \tag{7}$$

The straggling function is then given by:

$$\pi_0(E_0,E,t)dE=\frac{dE}{E_0 2\pi i}\int_{\delta-i\infty}^{\delta+i\infty}\left(\frac{E_0}{E}\right)^{s+1}e^{-A(s)t}ds. \tag{8}$$

The integral probability $\Pi_0(E,t)$ i.e., the probability that the electron has energy *greater* than E at t is

$$\Pi_0(E_0,E,t)=\frac{1}{2\pi i}\int_{\delta-i\infty}^{\delta+i\infty}\left(\frac{E_0}{E}\right)^s\frac{e^{-A(s)t}}{s}ds. \tag{9}$$

It is convenient to introduce the new variable $y=\ln(E_0/E)$ and write:

$$\pi_0(y,t)e^{-y}dy=\frac{e^{-y}}{2\pi i}dy\int_{\delta-i\infty}^{\delta+i\infty}e^{ys-A(s)t}ds, \tag{10}$$

$$\Pi_0(y,t)=\frac{1}{2\pi i}\int_{\delta-i\infty}^{\delta+i\infty}\frac{e^{ys-A(s)t}}{s}ds. \tag{11}$$

We will carry out calculations for three different expressions for $\varphi(v)$, which are good approximations in different energy ranges. They are:

$$\varphi_1(v)=1/v, \tag{12a}$$

$$\varphi_2(v)=-b[(1-v)^a/\ln(1-v)], \tag{12b}$$

$$\varphi_3(v)=(4/3)(1-v)/v. \tag{12c}$$

In $\varphi_2(v)$ the constants a and b are to be considered as parameters which can be chosen to fit the correct functions at various energies. In Fig. 1 are plotted the approximate expressions given above, along with the correct expressions for various energies in air.

The expressions for the functions $A(s)$ corresponding to the three cases (12) are:

$$A_1(s)=\Psi(s)+C, \tag{13a}$$

$$A_2(s)=b\ln[1+(s/1+a)], \tag{13b}$$

$$A_3(s)=-(4/3)+(4/3)(\Psi(s+1)+C), \tag{13c}$$

where $\Psi(s)$ is the logarithmic derivative of the factorial functions i.e.,

$$\Psi(s)=d/ds(\ln s!),$$

and $C=0.5772\cdots$ is the Euler-Mascheroni constant.

Bethe and Heitler have shown[5] by other reasoning that the straggling function corresponding to the expression for φ_2 given above, and in particular for the special case $a=0$, is

$$\pi_{02}(E_0,E,t)dE=\frac{dE}{E_0}\frac{[\ln(E_0/E)]^{bt-1}}{(bt-1)!}. \tag{14}$$

It is easy to derive this result. If we use Eqs. (9) and (13b) we get

$$\pi_{02}(E_0,E,t)dE=\frac{(1+a)^{bt}}{2\pi i}\frac{dE}{E_0}\int_{\delta-i\infty}^{\delta+i\infty}\frac{e^{y(s+1)}}{(s+a+1)^{bt}}. \tag{15}$$

Completing the contour in (15) by an infinite semi-circle in the left half plane and evaluating the residue at the singularity $s=-(1+a)$ gives

$$\pi_{02}(E_0,E,t)dE=\frac{dE}{E_0}(1+a)^{bt}\left(\frac{E}{E_0}\right)^a\frac{[\ln(E_0/E)]^{bt-1}}{(bt-1)!} \tag{16}$$

which for $a=0$ is just the Bethe-Heitler result.

The expressions for π_{01} and π_{03} are got from (10) and (13) and are,

$$\pi_{01}(y,t)e^{-y}dy=\frac{dye^{-Ct}}{2\pi i}\int_{\delta-i\infty}^{\delta+i\infty}e^{sy-t\Psi(s)}\cdot ds, \tag{17a}$$

$$\pi_{03}(y,t)e^{-y}dy=\frac{dy}{2\pi i}e^{(1-C)t-y}\int e^{sy-(4/3)\Psi(s)t}ds. \tag{17b}$$

We have changed the variable of integration from $s+1$ to s in the last integral. The integrals in these two ex-

[5] H. Bethe and W. Heitler, Proc. Roy. Soc. **A146**, 83 (1934).

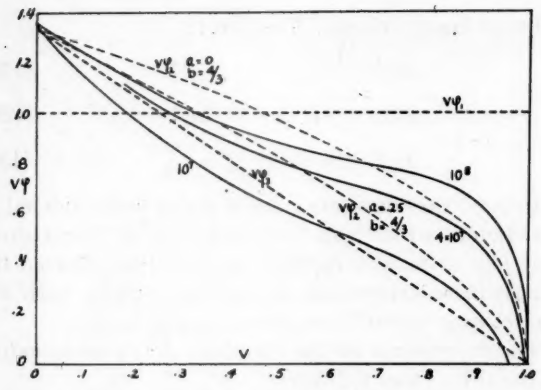

FIG. 1. The approximate expressions for the radiative cross section given by Eqs. (12) are plotted as dotted lines and the correct expressions for various energies in air as solid lines.

pressions are of exactly the same form and since for all $y>0$ and $t>0$, $sy-\Psi(s)t$ has a more or less sharp minimum on the real axis they can be evaluated by the saddle point method. One gets

$$\frac{1}{2\pi i}\int_{\delta-i\infty}^{\delta+i\infty} e^{sy-t\Psi(s)}ds \approx \frac{e^{s_0y-t\Psi(s_0)}}{(-2\pi\Psi''(s_0)t)^{\frac{1}{2}}}, \tag{18}$$

where s_0 is defined by

$$[d\Psi(s)/ds]|_{s=s_0}=y/t.$$

Curves for various t are plotted in Fig. 2.[6] Before discussing them we will discuss briefly the accuracy of the saddle-point method.

There are two indirect checks on this accuracy. If one evaluates $\pi_{02}(y, t)$ by the saddle-point method it is easy to show that the result is equivalent to replacing $(bt-1)!$ in the exact expression (14) by the first term in its Stirling approximation, i.e., by the expression $(2\pi)^{\frac{1}{2}}e^{-bt}(bt)^{\frac{1}{2}-bt}$. For $bt=2$, 1, 0.5, 0.25, the Stirling approximation gives too low a value by 4, 8, 16, 31 percent, respectively. Thus the saddle-point method fails for small t, which is not surprizing, since for $t=0$ there is no saddle-point at all. Since the behavior of the integrand in all three expressions for $\pi_0(y, t)$ is rather similar, although the exact functional form is different, one would suspect that if the saddle-point method is adequate for $\pi_{02}(y, t)$ it will be adequate for the other expressions. Moreover, one should have from the normalization condition

$$\int_0^\infty e^{-y}\pi_0(y, t)dy=1$$

and for the larger values of t this can be seen to be true to a few percent from Fig. 2.

Even though for given y, the saddle-point method for the differential spectrum becomes less accurate for small t, the integral spectrum defined by (11b) is quite accurate for all t. We have

$$\Pi_0(y, t)=\frac{1}{2\pi i}\int_{\delta-i\infty}^{\delta+i\infty}\exp[sy-A(s)t-\ln s].$$

Evaluation by the saddle point method gives

$$\Pi_0(y, t)\approx\frac{1}{(2\pi)^{\frac{1}{2}}}\frac{\exp[s_0y-A(s_0)t-\ln s_0]}{(-A''(s_0)t+(1/s_0)^2)^{\frac{1}{2}}}, \tag{19}$$

where $y-A'(s_0)t-(1/s_0)=0$.

We should have $\Pi_0(y, 0)=1$. Putting $t=0$ in these equations one gets

$$\Pi_0(y, 0)=e/(2\pi)^{\frac{1}{2}}\approx 1.08. \tag{20}$$

Thus there is only 8 percent inaccuracy even for $t=0$. For larger t the saddle-point method should be even more accurate, for the reasons given above in connection with the differential spectrum.

Let us now consider the differential spectrum plotted in Fig. 2. We see that for small y, i.e., energies close enough to the initial energy, π_{03} is considerably greater than π_{01} or π_{02}. This is simply a reflection of the fact that $\varphi_3(v)$ drops off much more quickly for large v than $\varphi_1(v)$ or $\varphi_2(v)$ and hence gives more weight to small energy losses. For large y, $e^{-y}\pi_0$ is always small, of course; moreover the values given by the three expressions differ widely from one another. This is because large y corresponds to an electron which has low energy and therefore probably emitted a quantum containing an appreciable fraction of its energy. But we see from Fig. 1 that for this case, i.e., for v close to unity, the expressions for the radiation probability differ widely, hence it is not surprising that the expressions in Fig. 2 should also differ widely for large y. The integral straggling function is plotted in Fig. 3.

IV. STRAGGLING WITH COLLISION LOSS

In this section we will consider the straggling of an electron which loses energy both by radiation and ionization. We denote by $\pi_\beta(E, t)$ and $\Pi_\beta(E, t)$ the differential and integral straggling functions. $\pi_\beta(E, t)$, and its Mellin transform, which we call $M_\beta(s, t)$, satisfy Eqs. (1) and (2). The boundary condition for one electron of energy E_0 at $t=0$ is:

$$M_\beta(s, 0)=E_0^s. \tag{21}$$

If we make the substitution

$$M_\beta(s, t)=e^{-A(s)t}N(s, t), \tag{22}$$

Eq. (4) becomes:

$$e^{D(s)t}\frac{\partial N(s, t)}{\partial t}=-\beta sN(s-1, t), \tag{23}$$

where $D(s)=A(s-1)-A(s)$. The expressions for the

[6] For making these calculations a useful table of the factorial function and its derivatives is: Tracts for Computers No. 1, Eleanor Pairman, *Tables of the Digamma and Trigamma Functions* (Cambridge University Press, London, 1919).

functions $D(s)$ corresponding to the expressions (13) for the functions $A(s)$ are:

$$D_1(s)=-1/s, \tag{24a}$$

$$D_2(s)=b\ln(s+a/s+a+1), \tag{24b}$$

$$D_3(s)=-4/3(s+1). \tag{24c}$$

We will be interested mainly in not very large t, as was stated in the introduction. Now if we put $t=0$ in the exponent of (23), the solution of the resulting equation, remembering the boundary condition, which now reads $N(s,0)=E_0^s$, is just $(E_0-\beta t)^s$. For non-vanishing t we therefore look for a solution of (23) in the form

$$N(s,t)=(E_0-\beta t)^s\cdot P(s,t), \tag{25}$$

where $P(s,t)$ is a power series in t with coefficients functions of s, i.e.,

$$P(s,t)=\sum_{n=0}^{\infty}c_n(s)t^n, \tag{26}$$

in which we must have $c_0(s)=1$ to satisfy the boundary condition. If we put (25) into (23) we get for $P(s,t)$

$$\left(\frac{E_0}{\beta}-t\right)\frac{\partial P(s,t)}{\partial t}-sP(s,t)=-sP(s-1,t)e^{-D(s)t}. \tag{27}$$

If we now put (26) into (27) and successively equate the coefficients of powers of t on either side of (27), we get for coefficients up to $c_4(s)$

$$c_1(s)=0, \tag{28a}$$

$$c_2(s)=(\beta/2E_0)sD(s), \tag{28b}$$

$$c_3(s)=(\beta^2/E_0{}^2 3!)[(s+2)D(s)-(s-1)D(s-1)]-(\beta/E_0 3!)sD^2(s), \tag{28c}$$

$$c_4(s)=\frac{\beta}{E_0}\frac{s+3}{4}c_3(s)+\frac{\beta}{E_0}\frac{s}{4}\left(\frac{D^3(s)}{3!}+D(s)c_2(s-1)-c_3(s-1)\right), \tag{28d}$$

In the last equation we have, for simplicity, expressed $c_4(s)$ in terms of $c_3(s)$ instead of expressing it directly in terms of $D(s)$.

If we reassemble $M_\beta(s,t)$ using (22) and (25) we get the general expression for π_β

$$\pi_\beta(E_0,E,t)dE=\frac{dE}{E_0-\beta t}\frac{1}{2\pi i}\int_{\delta-i\infty}^{\delta+i\infty}e^{-A(s)t}\times\left(\frac{E_0-\beta t}{E}\right)^{s+1}\left(\sum_{n=0}^{\infty}c_n(s)t^n\right)ds. \tag{29}$$

We will see later that the series under the integral sign converges quite well for small t and E close enough to E_0; under these conditions the term in t^2 is small. If we now compare (29) with (8) and remember that $c_0(s)=1$, we see that the first and *dominant term for* $\pi_\beta(E,t)$ *is just the spectrum for straggling without collision loss in which* E_0 *is replaced by* $E_0-\beta t$. Also, the next term is of order t^2 since $c_1(s)$ is zero. This result holds for any $\varphi(v)$.

In calculating higher order terms the coefficients $c_n(s)$ depend of course on the expression $\varphi(v)$ chosen for the radiation cross section. Because of the rather simpler form of $D(s)$ for the functions $\varphi_1(v)$ and $\varphi_3(v)$, the coefficients $c_n(s)$ for these two functions are also simpler than for the function $\varphi_2(v)$, and we shall confine our attention from now on to the two former functions. For thicknesses and energies for which the higher order terms are not only small, but also negligible, the straggling function corresponding to $\varphi_2(v)$ may be quite useful, however, since it is an explicit formula, and the two adjustable coefficients in $\varphi_2(v)$ enable one to fit the correct cross sections fairly well over a considerable range of energies.

From Fig. 1 we see that $\varphi_1(v)$ is a rough approximation to the correct expressions for the radiation cross section near the critical energy in the lightest elements, i.e., around 10^8 ev and $\varphi_3(v)$ a fair approximation near the critical energy in the heaviest elements, i.e., around 10^7 ev. The first few coefficients are, remembering $c_0(s)=1$ and $c_1(s)=0$

$\varphi_1(v)$:

$$c_2(s)=-\beta/2E_0, \tag{30a}$$

$$c_3(s)=-(\beta^2/3E_0{}^2)-(\beta/3!E_0 s), \tag{30b}$$

$$c_4(s)=-\frac{\beta^3}{4E_0{}^3}+\frac{\beta^2}{12E_0{}^2}+\frac{\beta^2}{4!E_0{}^2}\left(\frac{s}{s-1}-\frac{3}{s}\right)-\frac{\beta}{4!E_0 s^2}. \tag{30c}$$

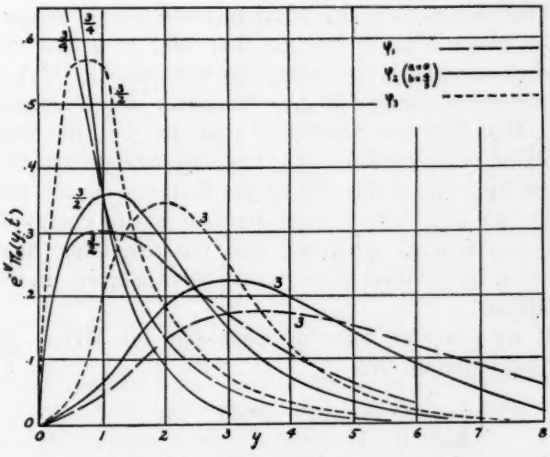

FIG. 2. Differential straggling functions for an electron that loses energy by radiation only. The numbers attached to the curves are thickness in radiation units. $y=\ln(E_0/E)$.

$\varphi_3(v)$:

$$c_2(s)=-(2\beta/3E_0)(s/s+1), \tag{31a}$$

$$c_3(s)=-\frac{2}{9}\frac{\beta^2}{E_0^2}\left(1+\frac{s}{s+1}\right)-\frac{8}{27}\frac{\beta}{E_0}\frac{s}{(s+1)^2}. \tag{31b}$$

Let us consider $\varphi_1(v)$. Denoting the *integral* straggling function for this case by $\Pi_{\beta 1}(E_0, E, t)$, introducing the new variable z,

$$z=\ln(E_0-\beta t/E), \tag{32}$$

and using the expressions (30) we see that up to terms in t^3 we have:

$$\Pi_{\beta 1}(z, E_0, t)=\Pi_{01}(z, t)\left(1-\frac{\beta t^2}{2E_0}-\frac{\beta^2 t^3}{3E_0^2}\right)-\frac{t^3\beta}{3!E_0}\int_0^z \Pi_{01}(z, t)dz. \tag{33}$$

The integral in the last term in (33) is just an alternate way of writing

$$\frac{1}{2\pi i}\int_{\delta-i\infty}^{\delta+i\infty}\frac{\exp[zs-A(s)t]}{s^2}ds.$$

Since a particle can be found at thickness t only if $E_0>\beta t$, we see that the terms in parentheses in (33) decrease quite rapidly for t not too large. It is the integral in the last term in (33) (and similar integrals in the expressions for the higher order $c_n(s)$) that, as stated previously, limit our solution to energies not too far from the initial energy. This can be seen if we remember that for large z, i.e., small E, $\Pi_{01}(z, t)$ is constant, so that the integral diverges. For values of E for which the integral is small compared with the dominant term, we assume that (33) is a correct approximate expression.

This limitation on the solution can be seen in another way. From Eq. (2) we see that $M(s, t)$ is the s'th energy moment of the straggling function, i.e., $M(1, t)$ is the mean energy, $M(2, t)$ the mean square energy, etc. $M(0, t)$ is the number of particles, i.e., the total probability for a particle of any energy to be present at t. Even for $t<E_0/\beta$ this will be less than one since a particle can e.g., lose a large fraction of its energy in emitting a hard quantum, and the remaining small fraction by collision loss after a short distance, and so disappear.

If we put $s=0$ into the expression for $M(s, t)$, we get for terms up to t^3

$$M(0, t)=1-\frac{\beta t^2}{2E_0}-\frac{t^3}{3}\frac{\beta^2}{E_0^2}-\frac{\beta t^3}{6E_0 s}\Big|_{s=0}.$$

The last term is infinite so that one can attach no meaning to this expression.* Similarly, $c_4(s)$ contains a term $1/(s-1)$ so that $M(1, t)$ is also infinite, and in general the higher moments will diverge due to singularities in the higher coefficients $c_n(s)$. From the argument above we see, however, that these divergences really come from energies near zero, so that if we use our distribution function for energies sufficiently greater than zero, it converges and is probably correct. We would like to emphasize, however, that we have not provided a formal proof of this.

To illustrate the above points we have plotted in Fig. 4 the effect of contributions of various powers of t to the total function for $t=1$ and $E_0=2\beta$. One can see that for large z the higher order terms become increasingly important. There is however a considerable range of energy of physical interest for which the terms up to t^3 or even t^2 give a good approximation to the total result.

The remarks made above concerning the function $\Pi_{\beta 1}$ apply equally to the function $\Pi_{\beta 3}$ corresponding to the radiation cross section $\varphi_3(v)$. The integrals involved can all be evaluated by the saddle-point method. Since one can see directly the essential difference in the numerical results for $\Pi_{\beta 1}$ and $\Pi_{\beta 3}$ by comparing their

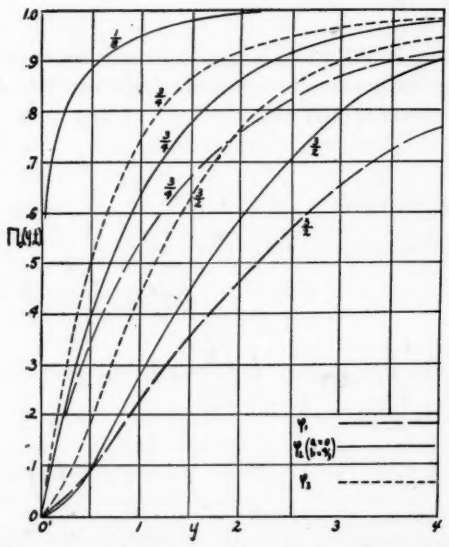

FIG. 3. Integral straggling functions for an electron that loses energy by radiation only. The numbers attached to the curves are thicknesses in radiation units. $y=\ln(E_0/E)$.

* It may be however that the quadratic term is correct, since one can derive it independently in the following way, due to Professor Peierls. If we integrate Eq. (19) with respect to E from 0 to E_0 one gets (using $\varphi_1(v)$),

$$\partial\Pi_{\beta 1}(0, t)/\partial t=-\beta\pi_{\beta 1}(0, t).$$

Now for small t we can get $\pi_{\beta 1}(0, t)$ by putting the value for $t=0$, i.e., $\delta(E_0-E)$, in the right-hand side of (19). This gives

$$\frac{\partial\pi_{\beta 1}(E, t)}{\partial t}=\int_0^1\frac{1}{1-v}\delta\left(E_0-\frac{E}{1-v}\right)\frac{dv}{v}=\frac{1}{E_0-E}.$$

Therefore, $\pi_{\beta 1}(0, t)=t/E_0$. Thus, using the first equation

$$\Pi_{\beta 1}(0, t)\approx 1-(\beta t^2/2E_0).$$

dominant terms (see Figs. 2 and 3) we have not computed $\Pi_{\beta 3}$ numerically any further.

V. DISCUSSION

The straggling function derived in the last section does not describe completely what happens when a low energy electron falls on matter, since it neglects the electron pairs produced by the radiated photons, as well as the Compton electrons. We shall not treat the latter here, but discuss briefly the effect of pair-production.

One can, of course, supplement the diffusion equation (1) by terms that describe pair-production, thus getting the ordinary shower equations, and again apply Mellin transforms, but then a solution for the transformed equations of the form found in the last section does not seem possible. This form is

$$M(s, t)=e^{-A(s)t}(E_0-\beta t)^s P(s, t), \tag{34}$$

where $P(s, t)$ is a power series in t. It is a mathematical consequence of (34) that at thickness t a particle cannot have energy greater than $E_0-\beta t$, and that there can be no electrons at thicknesses greater than E_0/β. These statements are obviously correct physically when one does not consider pair production, but not otherwise. With pair production, electrons of any energy can in principle be created at any thickness, since photons, of course, do not suffer collision loss.

It seems clear that for small thicknesses, and for energies E less than $E_0-\beta t$, where there is an appreciable probability for the original electron to be present, the relative effect of pair production will be small, except perhaps for very low energies where the straggling function of the preceding section breaks down anyway. This is made plausible, e.g., by the results of Bhabha and Heitler.[7] These authors consider the solution of the general cascade equations when collision loss is neglected. Their solution is written in the form of a series, the terms of which contain integrals over the straggling function. The nth term of their series has the physical meaning that it corresponds to an electron produced by n photon intermediaries. If one looks at their graphs one sees, e.g., that for $t=0.7$, $E=E_0e^{-3}$ the effect of photons is to increase the probability that a particle of energy greater than E is present by about 30 percent. It is also true that the main effect from photons in Bhabha and Heitler's theory comes from $n=1$, a result we would also expect when collision loss is taken into account.

Finally, some remarks on the evaluation of the integrals in the higher order terms of the straggling function may be helpful in practical computations.

[7] H. J. Bhabha and W. Heitler, Proc. Roy. Soc. **159**, 432 (1937).

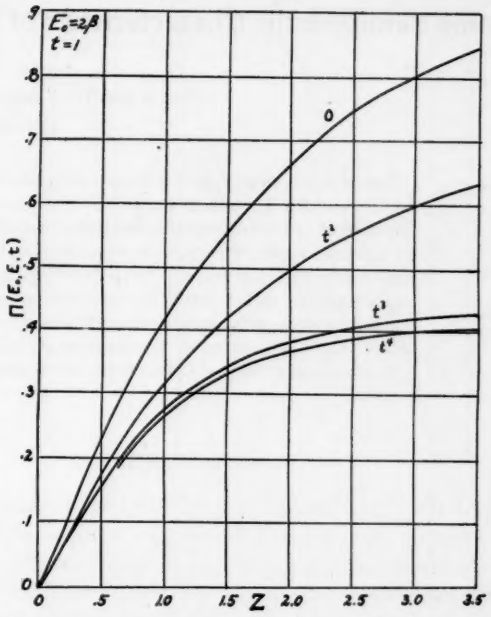

FIG. 4. Illustrating the effect of including higher powers of t in the integral straggling function $\Pi_\beta(E_0, E, t)$, for $E_0=2\beta$, $t=1$ and $\varphi(v)=\varphi_1(v)$. The curve marked 0 corresponds to taking only the constant term $c_0(s)$ in the series (26), that marked t^2 corresponds to taking $c_0(s)+c_1(s)t^2$, etc. $Z\equiv\ln(E_0-\beta t/E)$. For $E_0=2\beta$, $t=1$, $Z=\ln\beta/E$.

Integrals of the form

$$\frac{1}{2\pi i}\int_{\delta-i\infty}^{\delta+i\infty}\frac{\exp[ys-A(s)t]}{s^n(1+s)^m}ds\equiv I(n, m, y, t) \tag{35}$$

occur, where n and m are small integers. These can be evaluated by the saddle-point method directly, but it is often convenient to use the relations

$$I(n+1, m, y, t)=\int_0^y I(n, m, y', t)dy',$$

$$I(n, m+1, y, t)=\int_0^y e^{y'}I(n, m, y', t)dy'.$$

It is also possible to break the integrand in (36) into partial fractions and evaluate each of the resulting integrals separately. For a considerable range of values of y and t however, it will be found possible to consider $s^n(1+s)^m$ slowly varying and take it out from under the integral sign, particularly since great accuracy is not required in the higher order terms. With a few simple considerations like these the evaluation of the higher order terms can be effected quite quickly.

It is a pleasure to thank Professor R. E. Peierls for several stimulating discussions and the United States AEC for a post-doctoral research fellowship during the tenure of which this work was done.

Some Semimetallic Characteristics of the Photoelectric Emission from As, Sb, and Bi

L. APKER, E. TAFT, AND J. DICKEY
General Electric Research Laboratory, Schenectady, New York

(Received March 31, 1949)

Spectral and energy distributions were determined for photoelectrons from crystalline evaporated layers of As, Sb, and Bi. The relative numbers of electrons ejected from states near the Fermi level were obtained by the method of interchangeable emitters. In each case, the result was several times smaller than that expected for a simple metal. Structure was observed in the energy distribution function $N(\nu, E)$ for Sb. These effects were attributed qualitatively to an overlapping of energy bands like that assumed in the conventional model for semimetals. Data could be analyzed conveniently with the aid of the function $N(\nu, E)/E$ previously applied to semiconductors. Spectral distributions, relatively insensitive in form to deviations from metallic behavior, could be fitted by Fowler plots. Work functions so determined differed by less than 0.1 ev from the following values derived from energy measurements: As, 4.72 ev; Sb, 4.60; Bi, 4.34.

I. INTRODUCTION

PREVIOUS studies have dealt with the photoelectric emission from several elementary semiconductors.[1] The electronic energy structures of these materials had readily measurable effects on the character of both the energy and the spectral distributions of the photoelectrons. On the other hand, distribution functions for different types of metals have shown no appreciable differences in form. The emission from elements as unlike as sodium and tungsten, for instance, can be specified near the threshold by the well-known results that Fowler and DuBridge have derived from considerations of the Sommerfeld model.[2] The volume properties of the semimetals indicate that the energy structures of these substances are in an intermediate class. It is perhaps interesting to ask, then, if any clear-cut evidence of this is to be found in the external photoelectric effect. Techniques based on Millikan's method of interchangeable emitters[1] permit a convenient attack on such a problem. Results so obtained on the series As, Sb, and Bi are given in this paper.

II. EXPERIMENTAL DETAILS

The eight photo-tubes used were like those described in reference 1. Bi was investigated in three, Sb in two, and As in three. These elements were deposited from the vapor on substrates of Ni, Mo, Pt, Cb, fused quartz, graphite, or Ni-Fe alloy. Commercial grade Bi was used in one tube; all other samples were spectrographically standardized materials obtained from Johnson, Matthey Company, Ltd. They were evaporated from graphite crucibles, from Ta boats, or, in the case of As, from Pyrex distillation trains. Ionization gauges indicated pressures of $<5\times10^{-8}$ mm Hg after the seal-off except in tubes containing As; here the amorphous form of the element was present with a vapor pressure apparently of the order of 10^{-6} at 300°K. Miss Eileen Alessandrini kindly took electron diffraction data on the emitters after they had been removed from the tubes.

Because of difficulties met in working with As, complete data including electron diffraction photographs were taken on only one surface. This sample was deposited directly in crystalline form. On cool substrates, As normally condenses as a semiconducting amorphous layer.[1] Films of this type, on Ta or graphite, were heated by focused radiation from a one-kilowatt tungsten lamp. The characteristics thereupon ceased to be typical of a semiconductor and approached those described here. When the tubes were opened, the surfaces oxidized before electron diffraction data were obtained. Thus, there was no proof that the samples had crystallized, although it is reasonable to assume that this happened.[3] Results for As must be presented, therefore, as tentative. For Sb and Bi, data were checked for reproducibility on two or more surfaces in each tube. At $h\nu=5.80$ ev, the photoelectric yield varied by less than a factor of two from surface to surface and by less than 1 percent over any single surface. Neither spectral nor energy distributions showed measurable variations in form.

Other experimental details have been given previously.[1,2]

III. DISCUSSION OF RESULTS

Current-voltage characteristics are given in Fig. 1. Overlapping is avoided by setting the curves coincident at the saturation points V_s rather than at the more significant point V_0, the "stopping potential for 0°K." (Symbols in this paper are the same as in reference 1.) The abscissa $V-V_s$ is thus equal to $-E/e$, where E is the kinetic energy of the photoelectrons after emission. Initial energies ϵ may be obtained from the equation $\mu-\epsilon=h\nu-\varphi-E$, where μ is the Fermi level. Work functions determined from the relation $\varphi=h\nu-e(V_s-V_0)$ were 4.34 ev for Bi, 4.60 for Sb, and 4.72 for As.

As shown explicitly in Fig. 1, the characteristic for Bi lies well below that for a simple metal with the same

[1] Apker, Taft, and Dickey, Phys. Rev. **74**, 1462 (1948); E. Taft and L. Apker, Phys. Rev. **75**, 344 (1949).
[2] Apker, Taft, and Dickey, Phys. Rev. **73**, 46 (1948), and cited papers.
[3] R. Suhrmann and W. Berndt, Zeits. f. Physik **115**, 17 (1940).

work function. Sb and As gave similar results. For all of these semimetals, therefore, the relative numbers of photoelectrons originating in states near the Fermi level were considerably smaller than for simple metals. In Fig. 2 this is also apparent from the behavior of $N(\nu, E)/E$.[4] This function, which has been of value in analyzing data on semiconductors,[1] was interpreted as being roughly proportional to $s(\nu, \epsilon)n(\epsilon)f(\epsilon)$, where s is an excitation probability, n is the density of states, and f is the Fermi factor; ϵ, as mentioned above, is the energy of the electrons before excitation. Several properties of As, Sb, and Bi have been treated with the aid of a simple model in which the valence electrons occupy two energy bands that overlap each other slightly.[5] In order of magnitude, the amount of overlap is 1 ev, and the Fermi level μ lies in this region of encroachment. Under these conditions, s and n may undergo relatively rapid variations near μ, and structures like those in Fig. 2 may result. The curves contrast strikingly with the smooth characteristics typical of semiconductors, for which n (and almost certainly s) depend monotonically on ϵ near

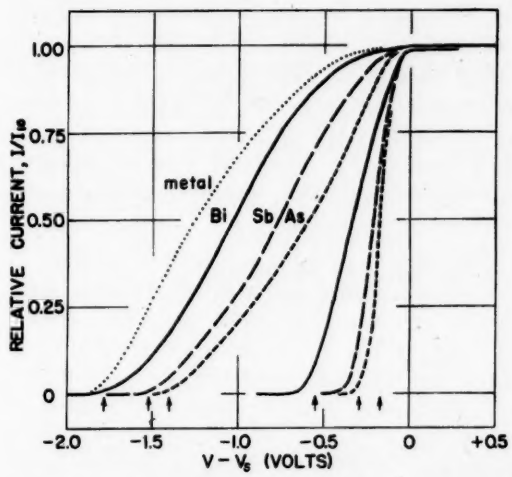

FIG. 1. Current-voltage characteristics for crystalline semimetals at 300°K. Curves are normalized with $I/I_{10}=1$ at $V=+10$ volts. Abscissas are $V-V_s$ and saturation points are coincident. For the three curves at the right, $h\nu=4.89$ ev; for the others, $h\nu=6.12$. Arrows mark values of V_0-V_s found from data on reference metals. The dotted curve is for a simple metal with $\varphi=4.34$ ev; it may be compared directly with the adjacent characteristic for Bi. Experimental errors are not visible on this scale. At $V=1000$ and $h\nu=6.12$, $I/I_{10}=1.02$ for Bi and Sb, and 1.03 for As.

[4] Here N is the energy distribution function. To make a quantitative comparison, one may contrast the semimetals with simple metals having the same yields at $h\nu=6.12$ ev. Then at $h\nu-\varphi-E=0$, the value of N/E for the semimetals is lower by a factor of about two than N/E for the metals. If the semimetals are compared with metals having the same N/E at $h\nu-\varphi-E=1.0$ ev, the discrepancies at the Fermi level are even larger.

[5] For references and discussion, see Frederick Seitz, *The Modern Theory of Solids* (McGraw-Hill Book Company Inc., New York, 1940); A. H. Wilson, *Semi-Conductors and Metals* (Cambridge University Press, London, 1939); N. F. Mott and H. Jones, *The Theory of the Properties of Metals and Alloys* (Oxford University Press, London, 1936). For recent work on Sb, see S. H. Browne and C. T. Lane, Phys. Rev. **60**, 895 (1941); K. Rausch, Ann. d. Physik **6**, 190 (1947).

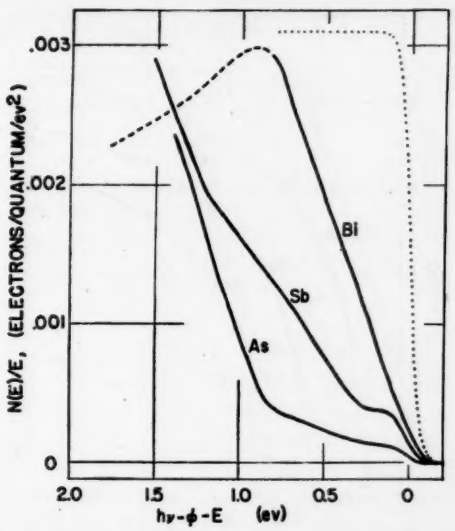

FIG. 2. $N(E)/E$ for 300°K and for $h\nu=6.12$ ev. The dashed portion of the Bi characteristic is discussed in the text. The dotted curve shows the Fermi factor (arbitrarily normalized at 0.0031), which is characteristic of a simple metal on this type of plot. For metals having the same yields as As, Sb, and Bi at $h\nu=6.12$ ev, the appropriate Fermi factors are normalized at 0.00017, 0.00043, and 0.0013, respectively.

the edge of the single band involved. By assuming that s does not depend strongly on ϵ, one may obtain the form of nf from N/E.[6] Although such an argument is probably not applicable in detail to semimetals, the density of states derived on this basis is relatively low near μ—a result to be expected from the simple model.

Perhaps the most interesting feature in Fig. 2 is the plateau for Sb near $h\nu-\varphi-E\sim0.2$ ev. While the values of N/E decreased by a factor of 1.8 as $h\nu$ increased from 5.80 to 6.71 ev, the location and shape of the plateau did not change. One concludes that the form of $s(\nu, \epsilon)$ did not depend on ν, and that two groups of initial energy states having dissimilar properties were separated by the point $h\nu-\varphi-E=\mu-\epsilon\sim0.3$ ev. If the bottom of the upper band had this location, nf would have a form somewhat like that shown in the figure.

It is interesting also that the curve for Bi has a maximum. This peak shifted from $h\nu-\varphi-E\sim0.7$ to 0.9 ev as $h\nu$ varied from 5.42 to 6.12 ev; at $h\nu=6.71$, it disappeared but a plateau was still evident. To indicate the variable portion of the curve, a dashed line is used in the figure. It should be noted that when E falls below a few tenths of an electron volt, the process of determining N/E is no longer reliable. (The curves shown are terminated at the point for which $E=0$.) Experimental errors in E may become appreciable, and patch fields due to surface non-uniformity may produce effects like those just described.[1] For these reasons, we attach less

[6] For metals, of course, this is known to be justified; moreover, n is nearly constant and the result is practically identical with f as shown by the dotted curve in Fig. 2. When the top of the occupied band of a semiconductor is a few tenths of an electron volt below μ, f is so nearly unity at 300°K that it need not appear explicitly.

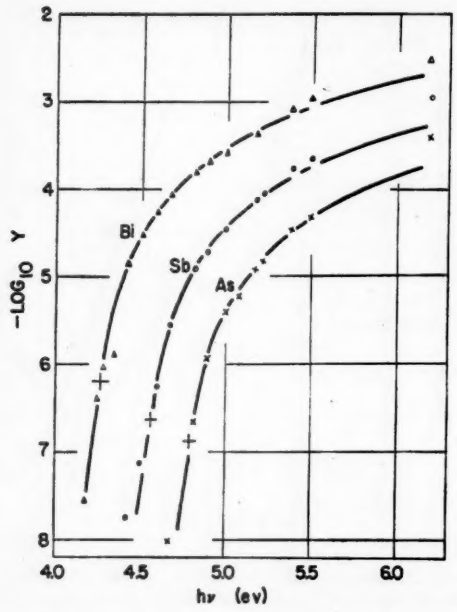

FIG. 3. Spectral distribution of the yield Y (in electrons/quantum) at 300°K. Curves through the experimental points are computed from Fowler's equation. Work functions determined from these plots are: Bi, 4.26 ev; Sb, 4.56; As, 4.79.

significance to the maximum for Bi than to the plateau for Sb.[7] The solid portion of the curve for Bi, however, should be trustworthy.

[7] One may speculate about another result also affected, perhaps, by the uncertainties associated with small values of E: In the order Bi to As, the curves in Fig. 2 exhibit progressively wider regions in which N/E is relatively low. This is consistent with the increasing energy gaps expected at the boundaries of the important Brillouin zones (reference 5).

Thus, the photoelectric energy distributions given here for As, Sb, and Bi show evidence of irregular initial energy spectra. In contrast, no such effect is observable in the spectral distributions of Fig. 3. For all three semimetals, the results may be fitted within experimental error by Fowler plots. The data for Bi are in excellent agreement with previous work by Jupnik.[8] The work function found for Bi by this method is lower than that obtained from energy data by almost 0.1 ev. For Sb and As, the discrepancies are smaller and doubtless not significant.

It is not surprising, of course, that spectral distributions are comparatively insensitive to deviations from metallic behavior. Such deviations show up directly in the energy distributions, but appear only in integrated form in spectral data. In the latter case, too, the effects may be distorted by the dependence of s on ν. Further, the experimental errors in measured radiation intensities are large compared to those in current-voltage characteristics. This is reflected in the scatter shown by spectral data even when they are plotted logarithmically.

The semimetals become relatively close-packed on melting, and irregularities due to their unusual crystal structures disappear.[9] Hence, the energy distributions given here should become metallic in character when the materials liquefy. Gallium, which may also show this effect, is particularly interesting from an experimental point of view since it has a convenient melting point and a low vapor pressure.

[8] H. Jupnik, Phys. Rev. **60**, 884 (1941).

[9] N. F. Mott, Proc. Roy. Soc. **A146**, 465 (1934); see also reference 5.

Resonance Scattering of Protons by Aluminum

R. S. BENDER,* F. C. SHOEMAKER, S. G. KAUFMANN, AND G. M. B. BOURICIUS
University of Wisconsin, Madison, Wisconsin

(Received April 5, 1949)

The elastic scattering of protons by aluminum at energies near the 985-kev [based on the 440-kev Li(p,γ) voltage scale] resonance has been studied, with the use of the homogeneous proton beam available from the Wisconsin pressure generator equipped with the 90° electrostatic analyzer. The variation in the scattering yield with proton energy agrees qualitatively with the prediction of the Breit-Wigner formula. On the assumption of S-scattering, the data indicate a natural resonance width of the order of 100 volts.

INTRODUCTION

IN the course of tests on the Wisconsin 90° electrostatic analyzer,[1] runs were taken over gamma-ray resonance levels in several elements. The preparation of good thin targets turned out to be the main experimental difficulty, and aluminum targets seemed to be the easiest to make. Because of this, the best data were obtained from the 985-kev $Al^{27}(p,\gamma)Si^{28}$ level, and an attempt was made by Bender, Shoemaker, and Powell[2] to determine the natural width of this resonance. It was necessary to correct for the effect of energy spread in the proton beam and the effect of target absorption thickness. A resonance width of 300±50 volts was obtained on the basis of the following assumptions: (a) the surfaces of the analyzer plates were sufficiently accurate that the energy spread of the proton beam could be calculated from the slit widths, (b) the aluminum target film was perfectly uniform, (c) the effects of oxidation of the aluminum film were negligible, and (d) the effects of straggling in the target film could be neglected. It should be noted that all of the neglected effects would cause the above figure to be larger than the true width, so that this result had to be taken as reliable only as far as the upper limit is concerned.

During a visit to this University in the spring of 1947, E. P. Wigner emphasized the desirability of experimental data on elastic resonance scattering. The Breit-Wigner theory of nuclear resonance predicts a variation from Rutherford scattering near a resonance, in form similar to the optical dispersion near an absorption band. In order that this variation shall not be excessively reduced by averaging over a range of energies, the energy spread of the proton beam and target absorption thickness cannot greatly exceed the resonance width. An aluminum film thin enough for resonance experiments must be supported, and the large number of protons scattered by a heavy backing material, such as is commonly used for gamma-ray work, would completely mask those scattered by the target film. Professor Wigner pointed out that protons scattered into the backward direction from a backing of lower atomic weight than the target would all have lower energy than those scattered by the target, and suggested that it might be possible to make use of this energy difference so that only the desired protons would be recorded.

EXPERIMENTAL METHOD AND RESULTS

The energy difference available for the separation of the scattered protons, of course depends on the atomic weight of the backing material. It would seem that the best choice would be the lightest material available, but, as will be seen later, an aluminum film has a surface film of oxide, so that one must be able to separate the protons scattered by oxygen from those scattered by aluminum. The energy of a proton scattered in the backward direction by an aluminum nucleus is about 86 percent of the bombarding energy, and a proton scattered in the same direction by an oxygen nucleus is about 78 percent of the bombarding energy. Thus, there is a difference of about 9 percent for the separation. This is well within the capabilities of a simple focusing magnetic analyzer.

Figure 1 shows a plan view of the apparatus used. An aperture, $\frac{1}{8}''\times\frac{1}{4}''$, limited the cross section of the incident proton beam, so that the illuminated area on

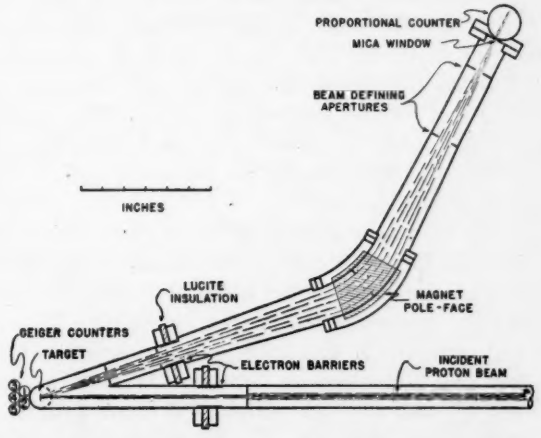

FIG. 1. Plan view of the apparatus used for the resonance scattering experiment. The focusing magnetic analyzer was used to separate the protons scattered by the aluminum from those scattered by the lighter target backing.

* Now at the University of Pittsburgh, Pittsburgh, Pennsylvania.

[1] Warren, Powell, and Herb, Rev. Sci. Inst. 18, 559 (1947).

[2] Bender, Shoemaker, and Powell, Phys. Rev. 71, 905 (1947).

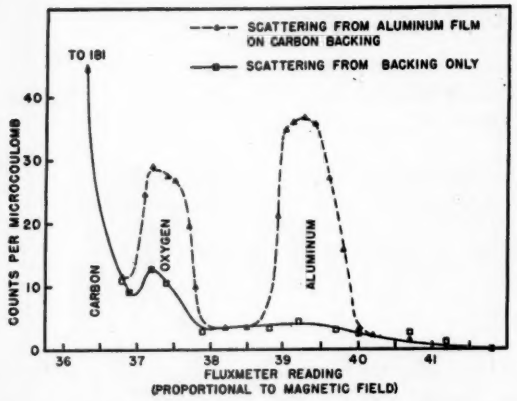

FIG. 2. Momentum spectrum of the scattered protons. The incident proton energy was kept constant at a value well away from the resonance while these data were taken. The three groups of protons were scattered by aluminum, oxygen, and carbon, respectively.

the target formed the entrance slit of the magnetic analyzer. Other apertures were spaced at intervals along the path of the scattered protons to avoid secondary small angle scattering from the walls of the vacuum chamber. The gap between the pole-faces of the magnet was adjusted with iron shims so that the focusing error was less than $\frac{1}{32}''$ in the image plane. The opening into the counter was intentionally made wider than the image formed by the magnet, so that the counting rate would not vary with small fluctuations in the magnetic field.

Scattered protons were counted by a proportional counter consisting of a $1\frac{1}{2}''$-diameter brass tube with a coaxial 0.003-in. molybdenum wire supported at both ends by Stupakoff Kovar-glass insulators. Protons entered through a $\frac{1}{4}\times\frac{1}{2}$-in. opening in the side, made vacuum tight by a 1.6-mg/cm² mica window sealed on with a thermoplastic (Gelva V-7, obtained from the Shawinigan Products Company). The counter was filled to a total pressure of 15 cm Hg with tank argon (99.6 percent pure) with 2 percent CO_2 added. The operating potential was 570 volts, which provided a gas amplification of about 20. The proton pulses were amplified by a Los Alamos Model 100 amplifier and were counted by a scale of 64 and mechanical recorder. The pulses were twenty times the noise level, and very uniform in size so that the discriminator on the scaler could be set to give zero background.

Gamma-rays were counted by five Radiation Counter Laboratories Geiger-Mueller tubes connected through a coincidence circuit to another scaler. Referring to Fig. 1, counter (1) was connected in coincidence with (3) and (4), and counter (2) was operated in coincidence with (4) and (5). Coincidences between (1) and (5) and between (2) and (3) were eliminated to minimize the background counting rate. To maximize the counting efficiency, the counters were placed as close as possible to the target, with a millimeter of lead in between.

To provide for beam current integration, the target chamber was insulated from the remainder of the apparatus by Lucite disks to form a Faraday cage. Electrons released by the proton beam striking the target or defining aperture were prevented from passing into or out of the target chamber by guard cylinders maintained 300 volts negative by a battery. The current was integrated by causing it to charge an eight-microfarad polystyrene condenser to a potential of ten volts, measured by a string electrometer. For proton currents of the magnitude used in this experiment, 0.05 to 0.5 microampere depending on the energy spread of the beam, the combination of a short period electrometer and high quality condensers appears to be an unusually reliable and convenient current integrator.

Targets were prepared by evaporating aluminum onto strips of spectroscopically pure carbon, which had been polished by rubbing with another piece of the same material. Beryllium was also tried for target backings, but all available samples had large amounts of heavy impurities, which gave an excessive amount of background scattering. Another advantage of carbon over beryllium as a target backing is that the gamma-ray yield proved to be much lower. Previous results[2] showed that if targets were maintained at a temperature of about 250°C and a liquid air trap was used between the target and oil diffusion pump during bombardment, there was no detectable surface contamination. Accordingly, the targets were mounted on a heated support. This support was arranged so that it could be moved by a rod through a Wilson seal, so that targets could be changed without breaking the vacuum.

Figure 2 illustrates the behavior of the magnetic analyzer. In taking these data, the incident proton

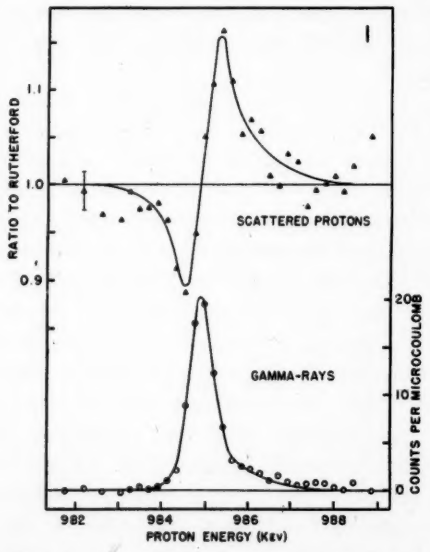

FIG. 3. Data from run *1* showing resonance scattering and absorption of protons by aluminum. The scattered proton yield at energies distant from the resonance was assumed to be Rutherford scattering. The curves were drawn to give an apparent fit with the experimental points without reference to the theory. The absolute energy position is based on the 440-kev Li(p,γ) standard.

energy was kept constant at a value well away from the resonance, and proton counts were recorded as a function of magnetic field. Results of two of these runs are shown, one taken with a carbon-backed aluminum target, and the other using as the target a region on the carbon which had been shielded from the aluminum during the evaporation. On the curve taken with the aluminum target, three groups of protons are evident. The group having the highest energy was scattered by the aluminum. The next group appears at a magnetic field setting corresponding to scattering by oxygen. Since this group has appreciable intensity only in the run taken with the aluminum target, and since it has the character of scattering from a thin target, it is assumed that it is due to oxidation of the aluminum film. The group next lower in energy has a continuous spectrum extending to the low energy limit of the counter, set by the stopping power of the mica window. The upper energy limit and thick target character identify this group as scattered by the carbon backing. For the thinnest targets used, the intensities of the aluminum and oxygen groups correspond to scattering by Al_2O_3, the common oxide of aluminum. Thicker targets show a relatively less intense oxygen group, indicating that these films were not completely oxidized. The curve taken with the bare carbon target shows the presence of heavy impurities, and in addition a slight surface layer of oxygen.

Five runs were made with different target thicknesses and proton beam energy spreads, recording both gamma-ray counts and proton counts as the energy of the incident proton beam was varied. By use of a flip coil and fluxmeter, the field in the magnetic analyzer was kept at the value to accept the protons scattered by the aluminum. Figures 3 and 4 show two of these runs. In plotting these data, a background of about 10 percent, due to heavy impurities in the target backing, was subtracted from the scattered proton yield. Also, a background of about 10 counts per microcoulomb, due to gamma-radiation from the thick carbon target backing, and a time dependent background amounting to around two counts per microcoulomb, were subtracted from the gamma-ray yield. These corrections were measured for every target. The scattered proton yield at energies relatively distant from the resonance was assumed to be Rutherford scattering. The run shown in Fig. 4 was taken with a thicker target and a larger proton energy spread than the one shown in Fig. 3. This shows up in an increased gamma-ray yield, a broader gamma-ray peak, and a relatively smaller effect of the resonance on the proton scattering.

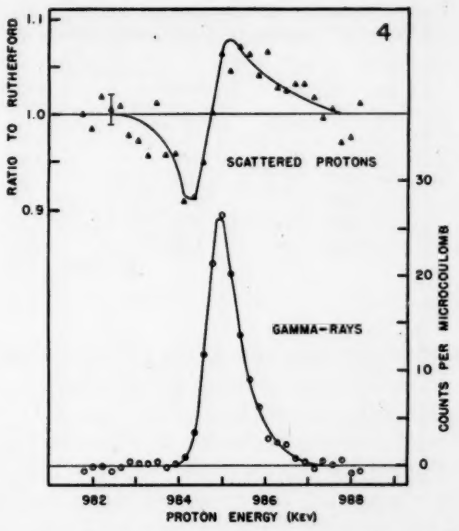

FIG. 4. Data from run *4*. A larger target thickness and proton energy spread were used for this run than for run *1* shown in Fig. 3. Note that the gamma-ray peak is wider and more intense, and that the effect of the resonance on the proton scattering is smaller.

DISCUSSION OF RESULTS

The observed scattering variation has the form predicted by the Breit-Wigner theory. The decrease from Rutherford scattering on the low energy side of the resonance, predicted by the theory, is caused by destructive interference between the coulomb and resonance scattering amplitudes.

An attempt was made to use this data to determine the width of this level. The lack of angular distribution data makes necessary some assumption about the orbital angular momentum of the scattered protons. In this discussion, the assumption is made that only zero orbital angular momentum is important. The formula for the cross section for scattering of particles with spin has been worked out explicitly only for this case. Bethe[3] gives this formula, which, after substituting constants fixed by the experimental arrangement, reduces for this resonance to:

$$\sigma/\sigma_0 = 1 + 0.078(2J+1)(0.85+2x)/(1+x^2),$$

where σ is the differential elastic scattering cross section, σ_0 is the Rutherford scattering cross section, J is the total angular momentum quantum number for the compound nucleus, $x = 2(E-E_r)/\Gamma$, E is the proton energy, E_r is the proton energy for resonance, and Γ is the total width of the resonance. The constants shown in this formula were computed on the assumption that the partial width for proton re-emission is large compared to the width for gamma-ray emission. This assumption is justified by the following argument. Brostrom *et al.*,[4] by measurements of absolute gamma-ray yield, have shown that the smaller of these widths is about 15 volts. If the total width were not very much larger than this, no variation in scattering would have been observed with the resolving power available, so that one of the partial widths must be large compared to 15 volts. If the large one were the gamma-ray width,

[3] H. A. Bethe, Rev. Mod. Phys. **9**, 69 (1937). (Formula 625, p. 176.)

[4] Brostrom, Huus, and Tangen, Phys. Rev. **71**, 661 (1947).

TABLE I. Determination of the natural width of the 985-kev $Al^{27}(p,\gamma)Si^{28}$ resonance (S-scattering assumed).

Run	Width of gamma-ray peak (electron volts)	Amplitude of the scattering variation	Natural width (electron volts) $J=2$	$J=3$
1	690	26%	154	103
2	760	21%	120	84
3	810	16%	95	68
4	880	17%	120	86
5	550	25%	103	68
		Averages	118	82

the values of the constants in the above formula would be so small that the variation in scattering, even with perfect resolution, would be smaller than that observed.

When this formula is plotted, it gives a curve similar to the optical anomalous dispersion curve, dipping on the low energy side to 0.64, and rising on the high energy side to 1.83, for $J=3$. For $J=2$, the dip is to 0.74 and the rise to 1.59.

While the variation in scattering near the resonance as shown in Figs. 3 and 4 is of the form represented by this formula, the amplitude is not as large. This is due to the fact that the resolving power was insufficient, resulting in an effective averaging of the scattering over an energy region considerably larger than the resonance width. Therefore, not all of the assumptions made in the analysis of the gamma-ray results in reference 2, as listed in the introduction to this paper, are valid. Among the possibilities for explanation of the invalidity of one or more of these assumptions are: (a) an almost unmeasurable conicity of the electrostatic analyzer deflection plates would increase the energy spread of the proton beam appreciably, (b) the thermal agitation of the atoms in the target[5] assuming Maxwellian motion, would cause a perfectly homogeneous million-volt proton beam to have an effective energy spread of about 140 volts (Note: Because this combines with the energy spread of the proton beam approximately as the square root of the sum of squares, it contributes only from 10 to 20 percent to the energy spreads used.), (c) Figure 2 shows that the targets were oxidized so that their effective thickness was increased by as much as a factor of two, and (d) electron microscope photographs of evaporated aluminum films[6] show a crystalline structure, instead of a uniform distribution, which could increase the energy loss in the target by a completely unknown amount, as one would expect this crystallization to depend on the nature of the backing material.

In view of these uncertainties, the following method was used to estimate the resonance width. For each run a value was found for the energy spread and for the target thickness, which would account for the observed width of the gamma-ray peak if the natural resonance width were 50 volts. This computation was repeated for assumed natural widths of 75 volts, 100 volts, and 150 volts. The method used was essentially that developed by J. L. Powell for the analysis of the gamma-ray work in reference 2. Next, for each of these assumed natural widths, the effect of the corresponding energy spread and target thickness on the amplitude of the scattering variation was calculated, assuming that Bethe's formula would give the correct scattering if the resolving power were infinite. Of course, the gamma-ray data are capable of fixing only one of these experimental parameters, but since the energy spread and target thickness enter symmetrically into both the gamma-ray and scattering calculations, one of them can be assumed to have a reasonable fixed value and the other can then be determined. If the energy spread is assumed to be that given by the electrostatic analyzer slit widths, corrected for the effect of thermal agitation of the target atoms, the target thicknesses required to account for the observed width of the gamma-ray peaks are found to be about twice as large as those calculated on the assumption of a uniform film of aluminum, corrected for oxidation. A comparison of these calculated amplitudes with the observed scattering variation gives, by interpolation, a first approximation to the natural resonance width. These results, combined with Brostrom's[4] measurement of the radiation width, were then used to recompute the constants in the scattering formula. The analysis of the data was then repeated to give a better approximation to the width. This result clearly depends on the angular momentum quantum number of the compound nucleus, which could be either 2 or 3 for S-scattering of protons by aluminum. The results are shown in Table I.

The S-wave barrier penetrability is 0.005 if 4.5×10^{-13} cm is used for the nuclear radius. Combined with the width indicated by the present data, this gives approximately 15 kev for the width without barrier.

ACKNOWLEDGMENTS

The authors wish to express thanks to Professor R. G. Herb for making the electrostatic generator available for this experiment and for his advice and assistance in the course of the work, to Mr. J. N. McGruer and Mr. G. G. Wiseman for their assistance in the construction of the apparatus used, and to Mr. D. C. Ralph for his help in taking some of the data. Thanks are especially due Professor E. P. Wigner for suggesting this experiment, and for helpful discussions regarding the results. The University Computing Service, directed by Professor H. K. Arnold of the Mathematics Department, was of great assistance in the numerical work involved in the analysis of the data. This work was supported financially by the Wisconsin Alumni Research Foundation.

[5] H. A. Bethe, Rev. Mod. Phys. 9, 140 (1937).
[6] C. E. Hall, J. App. Phys. 19, 198 (1948).

Total Cross Section Measurements for Fast Neutrons

C. K. BOCKELMAN, R. E. PETERSON, R. K. ADAIR, AND H. H. BARSCHALL
University of Wisconsin, Madison, Wisconsin

(Received April 11, 1949)

The total cross sections of Zr, Ag, In, Sb, I, Ta, and Pb have been measured as a function of neutron energy in the energy range from 20 kev to 1600 kev. A spread in energy of 30 kev was used up to 200 kev, and a spread of 70 kev above this energy. Indications of structure were found in Zr and Pb. The results are compared with the predictions of the statistical theory.

INTRODUCTION

ON the basis of statistical theory, Feshbach, Peaslee, and Weisskopf[1] have made calculations to find approximate expressions for the total neutron cross section as a function of neutron energy up to 1 Mev. When the results of the calculations were compared with the total cross sections for photo-neutrons measured by Fields *et al.*,[2] there appeared to be qualitative agreement. The comparison, however, was made difficult by the wide spacing in energy of the experimental results. Further, in order to permit a test of the theory, it is necessary that the experimental energy spread be much larger than the average distance between nuclear energy levels. It was not clear that this was the case for the photo-neutrons. An attempt was made previously at this laboratory to test the theory by measuring the total cross sections of Fe, Ni, and Bi with a resolution of about 150 kev.[3] Only in the case of Fe could agreement be obtained by appropriate choice of the parameters entering into the theory. The discrepancy in Ni was attributed to the presence of a strong resonance occurring at 15 kev, and in Bi the closed shell structure of the nucleus might make the theory inapplicable. In the present experiments, a survey of several medium-heavy and heavy nuclei was undertaken to investigate the validity of the statistical theory.

Since the previous work showed strong effects of resonances in Ni, only heavier elements were chosen for this study. The choice of the particular elements used was based on their availability and the desire to cover a wide range of atomic numbers.

PROCEDURE

Neutrons were produced by bombarding a Li film by protons accelerated by the electrostatic generator. A sufficient energy spread of the neutrons was obtained by using a Li target which had a stopping power of 60 kev for the protons. Up to neutron energies of 200 kev, observations were carried out in a direction making an angle of 115° with respect to the incident protons. For measurements at this angle, the spread in energy of the neutrons is about 30 kev. Above 200 kev, the observations were made in the forward direction with respect to the protons. In this case the resolution is about 70 kev.

The neutrons were detected in a proportional counter filled with $B^{10}F_3$ [4] and covered by Cd sheet. Cross sections were determined by simple transmission experiments as described previously.[5]

The samples used were circular disks, 1.75 in. in diameter, machined or cast from pure metal, except in the cases of Sb and I where the powdered material was tightly packed into brass containers. Table I shows a list of the samples used.

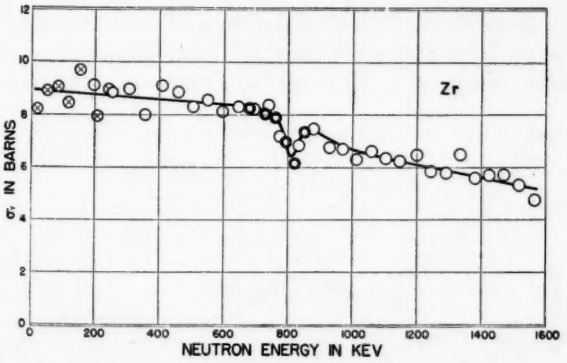

FIG. 1. The total cross section of zirconium as a function of neutron energy. Encircled crosses represent data taken at 115° with respect to the incident protons, the other symbols measurements in the forward direction. Single and double circles show two separate runs.

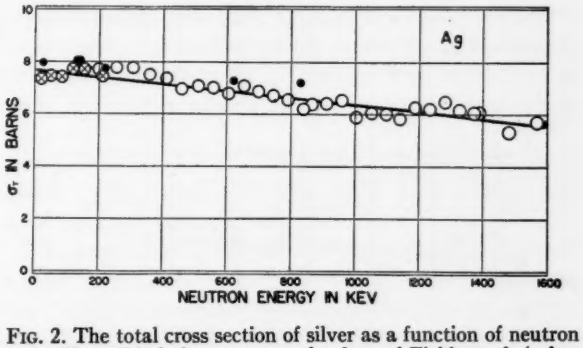

FIG. 2. The total cross section of silver as a function of neutron energy. The solid circles represent the data of Fields *et al.* (reference 2).

[1] Feshbach, Peaslee, and Weisskopf, Phys. Rev. **71**, 145 (1947).
[2] Fields, Russell, Sachs, and Wattenberg, Phys. Rev. **71**, 508 (1947).
[3] Barschall, Bockelman, and Seagondollar, Phys. Rev. **73**, 659 (1948).
[4] Furnished by the Isotopes Branch of the AEC.
[5] Adair, Barschall, Bockelman, and Sala, Phys. Rev. **75**, 1124 (1949).

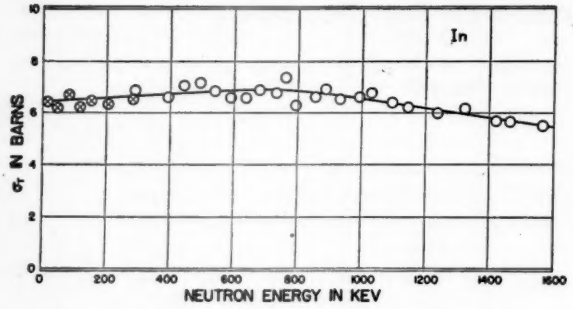

FIG. 3. The total cross section of indium. Encircled crosses represent data taken at 115° with the 1.25-cm thick sample, while the open circles show measurements taken in the forward direction with the 2.42-cm sample.

RESULTS

The results of the measurements are shown in Figs. 1–7 as plots of the total cross section in barns against neutron energy in kev. All cross sections were corrected for scattering into the detector and for background. As the neutron energies cover an appreciable

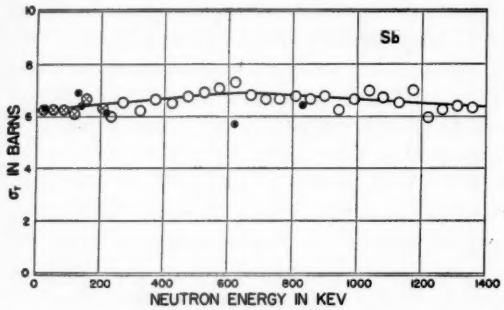

FIG. 4. Total cross section of antimony.

energy interval, the median values of each energy interval are plotted. Encircled crosses indicate measurements taken at 115° with respect to the proton beam, while the open circles represent data taken in the forward direction. The height of the symbols is approximately equal to the statistical error of the measurements.

For each element several runs were taken over the complete energy range. In some instances, the manner in which the curve was drawn through the experimental points was influenced by the results of runs not shown

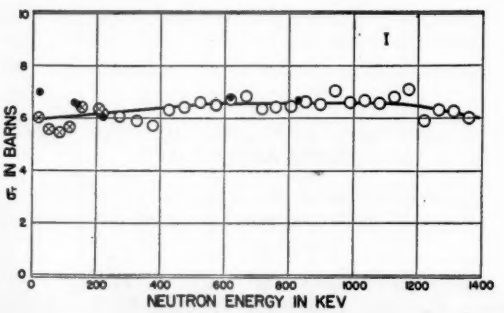

FIG. 5. Total cross section of iodine.

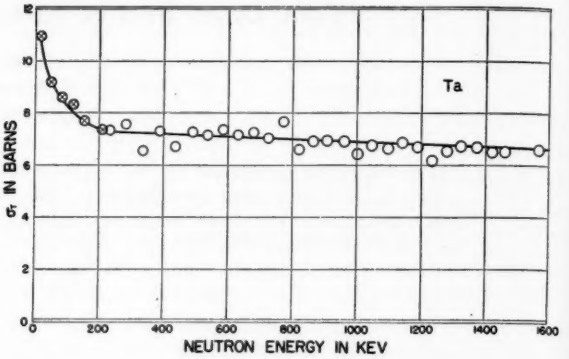

FIG. 6. Total cross section of tantalum.

in the figures. Wherever available, the results of Fields *et al.*,[2] using photo-neutron sources, are indicated by solid circles.

DISCUSSION

According to the statistical theory, the total cross section should be a monotonic function of energy, increasing slowly as the energy decreases. The present measurements do not show this increase at low energies except in the case of Ta and Pb where the increase is more rapid than predicted by theory. A reason why the measurements might give too small a cross section at low energies was suggested by Feshbach and Weisskopf.[6] According to the theory, most of the rise at low energies is due to the effect of averaging over many resonances, the peaks of which reach higher values in this region. For medium-heavy nuclei, these resonances would be expected to be quite sharp and to have separations in energy of many times their widths. If this is the case, the experiment will not yield a cross section corresponding to the average over the resonances, since even a considerably thinner sample would be completely opaque to the neutrons which have energies close to the resonance energy. This argument does not help, however, to explain the behavior of Ta and Pb. There is other evidence

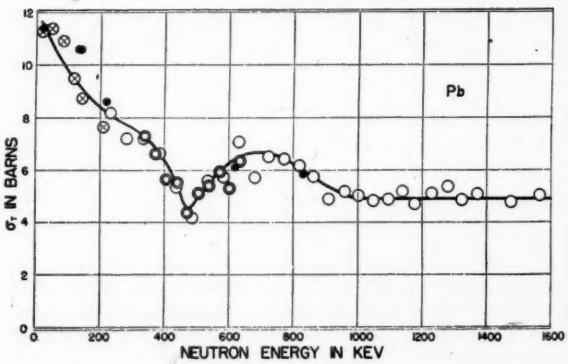

FIG. 7. Total cross section of lead. Up to a neutron energy of 1080 kev, measurements were made with the 1.90-cm thick scatterer. Above this energy the 3.18-cm sample was used. Double circles show a second run.

[6] Private communication.

that Pb has relatively few levels so that the statistical theory might not be applicable, just as in the case of Bi.

Two of the elements investigated, Zr and Pb, show deviations from a smooth variation of the cross section with energy. These anomalies were quite reproducible and are shown in two typical runs in Figs. 1 and 7. It is somewhat surprising to find structure in heavy elements, considering the poor resolution used. Evidence for such a structure in Pb had previously been found by Bretscher and Murrell.[7] In view of the fact that the anomalies have the shape of dips rather than peaks, one might suspect that they could be caused by inelastic scattering. As the energy of the primary neutrons becomes just sufficient to produce the final nucleus in an excited state, low energy neutrons will be emitted from the scatterer, and the detector used will detect these neutrons with high efficiency. This effect would result in a decrease of the observed cross section. It does not appear likely, however, that this explanation could account for the observations. It is known[8] that at these energies the cross section for inelastic scattering, at least in the case of Pb, is very small (not more than 0.3 barn), and only three percent of the scattered neutrons will reach the detector in the geometry used. Furthermore, because of the wide spread in energy of the primary neutrons, only a very small fraction of the scattered neutrons will have energies in the range in which the sensitivity of the counter is very high.

TABLE I. Samples used in transmission experiments.

Element	Atomic weight	Thickness (cm)	Number of atoms/cm² ×10⁻²⁴
Zr	91	1.27	0.0551
Ag	108	1.27	0.0746
In	115	1.25	0.0471
In	115	2.42	0.0923
Sb	122	3.18	0.0657
I	127	3.18	0.0723
Ta	181	1.27	0.0705
Pb	207	1.90	0.0630
Pb	207	3.18	0.1081

It is interesting to note that the most abundant isotopes of both Zr and Pb have closed neutron shells[9] (50 and 126 neutrons, respectively), and might, therefore, be expected to have broad and widely spaced levels. It is planned to investigate, with better resolving power, the energy regions in which the anomalies were observed.

The authors wish to thank Mr. R. L. Henkel for assistance in the experiments. This work was supported by the Wisconsin Alumni Research Foundation and by the AEC.

[7] Bretscher and Murrell, quoted Goldsmith, Ibser, and Feld, Rev. Mod. Phys. **19**, 259 (1947).
[8] Barschall, Battat, Bright, Graves, Jorgensen, and Manley, Phys. Rev. **72**, 881 (1947).
[9] M. G. Mayer, Phys. Rev. **74**, 235 (1948).

PHYSICAL REVIEW VOLUME 76, NUMBER 2 JULY 15, 1949

Measurements on Radioactive Krypton Isotopes from Fission after Mass-Spectrographic Separation

J. KOCH, O. KOFOED-HANSEN, P. KRISTENSEN, AND W. DROST-HANSEN
Institute for Theoretical Physics, University of Copenhagen, Denmark
(Received April 4, 1949)

Radioactive isotopes of krypton resulting from fission of uranium have been separated in a mass-spectrograph. The half-lives and the relative fission yields of the isotopes Kr^{85}, Kr^{87}, and Kr^{88} have been measured. The maximum energies of the β-particles from Kr^{85} and Kr^{87} have been checked by absorption. It has been shown that Kr^{88} emits soft β-particles and an intense γ-radiation. This result combined with other measurements indicates that the β-spectrum of Kr^{88} is complex.

INTRODUCTION

AMONG the radioactive nuclei formed in neutron-induced fission of uranium there are many krypton isotopes.[1,2] By using mixtures of these isotopes several radioactive periods have been isolated, either from the analysis of complex decay curves[3] or by the application of less direct methods.[4] The mass-numbers of the radioactive isotopes could be determined with considerable certainty from such experiments.

The present note describes experiments which were carried out with some long-lived krypton isotopes after they had been separated by means of the mass-spectrograph of this Institute.[5] This procedure is a crucial test of the assignment of activities to mass-numbers and,

[1] Plutonium Project, Rev. Mod. Phys. **18**, 513 (1946).
[2] G. T. Seaborg and J. Perlman, Rev. Mod. Phys. **20**, 585 (1948).
[3] A. H. Snell, Phys. Rev. **52**, 1007 (1937). W. Seelmann-Eggebert and H. J. Born, Naturwiss. **31**, 59 (1943). E. P. Clancy, Phys. Rev. **60**, 87 (1941).
[4] G. N. Glasoe and J. Steigman, Phys. Rev. **58**, 1 (1940).
[5] J. Koch and B. Bendt-Nielsen, Kgl. Danske Vid. Sels. Mathfys. Medd. **21**, No. 8 (1944). J. Koch, Phys. Rev. **69**, 238 (1946).

TABLE I. Half-lives of krypton isotopes. (a) Measurements with pure isotopes. (b) Measurements according to reference 2.

Isotope	Half-life (a)	Half-life (b)
Kr^{88}	2.77 hr.	2.8 hr.
Kr^{87}	1.30 hr.	1.25 hr.
Kr^{85}	4.36 hr.	(4–4.6) hr.

moreover, it offers the possibility of determining the half-lives and relative fission yields with some precision. Due to the strong activity of each isotopic sample this technique, in principle, also permits a closer study of the β-spectrum of the different krypton isotopes, but in lack of a β-spectrograph only the maximum energy of the β-particles could be checked by absorption.

Our interest has been especially devoted to the question whether γ-rays are emitted in the decay of Kr^{88}. The closer knowledge of the decay scheme of this isotope is in itself of course of some interest. It is, however, of primary importance to the interpretation of the recoil experiments with Kr^{88}, carried out by Jacobsen and Kofoed-Hansen.[6] The consequences which may be drawn from such experiments regarding the type of the coupling in β-decay have been discussed in more detail elsewhere.[7]

EXPERIMENTAL PROCEDURE

Ten kilograms of powdered uranium oxide, mixed with a small portion of ammonium carbonate, were placed in a glass container which was surrounded by a few centimetres of paraffin. After having evacuated the container, the tube leading to the pumps was closed by turning a stopcock. The uranium container was inserted between the coils of the cyclotron magnet, as close to the $(D+Be)$ neutron source as possible, and then heavily irradiated for about three hours. The inert gases emanating from the uranium compound were pumped off by means of a Toepler pump, using the gases given off by the ammonium carbonate (NH_3, CO_2, and H_2O) as a carrier of the activity, and concentrated in a volume of about 100 cm^3. After having added a great amount of normal krypton, the gas mixture was introduced to the capillary ion source of the mass-spectrograph. These operations were carried out quickly, so that the separation of the isotopes could be started about half an hour after stopping the cyclotron. The technique of collecting gaseous isotopes by bombarding a metal with energetic ions has already been described elsewhere.[8] In the present case, the collector was built of a stack of brass plates, which were mounted as shown in Fig. 1, and which divided the mass range in question into fifty steps. By means of this arrangement it was possible after mass-spectrographic separation to investigate the radiation from the individual parts of the collector without being disturbed by any radiation originating from active atoms deposited in the neighborhood. The use of a fluorescent screen of crown glass, mounted on top of the collector, permitted the adjustment of the intensity and resolving power of the mass-spectrum of the stable krypton isotopes before operation and the observation of the beams during the time of collection. While the isotopes were being collected, either Kr^{82}, Kr^{83}, or Kr^{84} was focused on a wire. In front of the collector a shutter was inserted, which was opened magnetically as soon as good operating conditions were established. After running the mass-spectrograph for about one hour, the collector was quickly removed from the apparatus in order to study the active deposits.

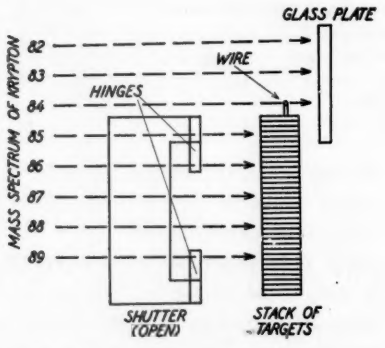

FIG. 1. Detail of mass-spectrograph. Arrangement for the collection of radioactive krypton isotopes. Thickness of each target 1.5 mm.

RESULTS

Mass Determination and Relative Fission Yields

The distribution of radioactivity along the stack of collector plates is plotted in Fig. 2, showing three clearly resolved peaks. From visible marks on the collector plates, due to the sputtering action of the beams of stable krypton isotopes, these peaks can be identified to belong to Kr^{85}, Kr^{87}, and Kr^{88}. The figures of the diagram have been corrected for radioactive decay

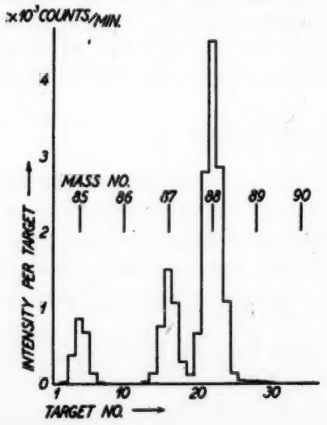

FIG. 2. Mass-spectrum of some radioactive krypton isotopes.

[6] J. C. Jacobsen and O. Kofoed-Hansen, Phys. Rev. **73**, 675 (1948).

[7] O. Kofoed-Hansen, Phys. Rev. **74**, 1785 (1948).

[8] J. Koch, Nature **161**, 566 (1948).

during the time of measurement, and they refer to the situation 2.5 hr. after stopping the neutron bombardment from the cyclotron. The dispersion per mass unit is found to be about 9 mm and the breadth of the peaks about 3 mm.[9] This breadth is somewhat smaller for Kr^{85} than for Kr^{88} due to a slight change in the focusing properties of the mass-spectrograph along the mass scale.

Because of the relatively long time interval between the termination of the neutron irradiation and the radioactive measurements, there was no possibility of finding the short-lived Kr^{89} (2.5 m) or its successor Rb^{89} (15.4 m). The faint activity (~1 percent of Kr^{88}) at the mass number 89 probably originates from $(Kr^{88}H)^+$ ions, which may be formed in the ion source due to the presence of hydrogen in the gas mixture. A search for the 2-hr. isomer of mass number 83 also gave a negative result. This, however, is in agreement with the facts that the number of atoms of this isomer, formed in fission, is relatively very small, and that the radiation mainly consists of γ-rays which have only a low efficiency for being detected by the counter. Also the 10-yr. Kr^{85} isomer could not be observed here.

The half-lives of the isotopes Kr^{85}, Kr^{87}, and Kr^{88} were determined by following the decrease in activity of the strongest isotopic samples for about 24 hr. These decay curves are shown in Fig. 3 and the resulting half-lives are listed in Table I together with the hitherto accepted values. The accuracy here obtained is estimated to be about 2 percent.

The calculation of the total number of atoms of the different krypton isotopes decaying per unit time (see Fig. 2) makes it possible to determine the course of the curve of fission yields in the mass region in question. It is well known that the constant production of a radioactive substance during the time T, followed by a decay during the time t, leads to a number of atoms of the substance N which is given by

$$N=(y/\lambda)[1-\exp(-\lambda T)]\exp(-\lambda t), \qquad (1)$$

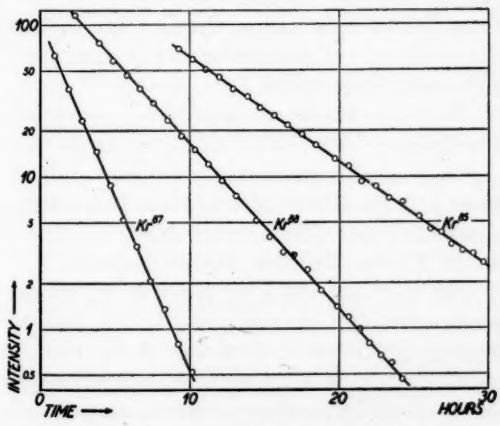

FIG. 3. Decay curves of Kr^{88}, Kr^{87}, and Kr^{85}.

[9] The breadth is defined as twice the standard deviation when approximating the measured curve by a Gaussian distribution.

TABLE II. Fission yields in relation to the production of Kr^{88}.

Isotope	y_{rel} (measured)	y_{rel} (by interpolation)
Kr^{88}	100	100
Kr^{87}	70±15	78
Kr^{85}	33±10	44

where y is the yield of production per unit time, and λ is the decay constant. The application of this formula for the determination of the relative fission yields (y_{rel}) of the isotopes in question is permitted, since all the predecessors are short-lived ($\leqslant$3 m).[10] In the case of Kr^{88} it must, however, be remembered that this isotope is in equilibrium with its successor Rb^{88}, having a half-life of 17.8 m. For Kr^{88} the expression (1) must therefore be multiplied by a factor

$$1+\lambda_{Rb}/(\lambda_{Rb}-\lambda_{Kr}). \qquad (2)$$

The average values of y_{rel} for two series of measurements are given in Table II and compared with values taken from the course of the known fission yield curve (see reference 1). The agreement is satisfactory, considering the presence of irregularities during the time of irradiation with neutrons, from which the large error mainly arises. The rather low value listed for Kr^{85} is partly due to the fact that the contribution of the long-lived Kr^{85} isomer has been neglected.

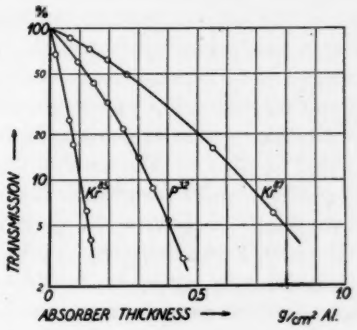

FIG. 4. Absorption curves of Kr^{87}, Kr^{85}, and P^{32}. The curves have been corrected for the thickness of the counter window.

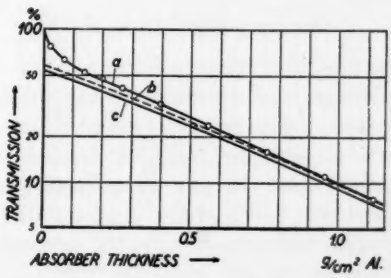

FIG. 5. *a*, Absorption curve for Kr^{88}+Rb^{88} in equilibrium. *b*, Absorption curve for Rb^{88}, normalized so as to fit curve *a* for thick absorbers. *c*, Absorption curve for Rb^{88}, representing the contribution from this isotope to the course of curve *a*.

[10] N. Sugarman, J. Chem. Phys. **17**, 11 (1949).

TABLE III. Maximum energies of β-rays from Kr^{87} and Kr^{85}.

Isotope	Max. energy in Mev (measured)	Max. energy in Mev (reference 2)
Kr^{87}	3.2 ±0.3	4
Kr^{85}	0.75±0.1	0.85–0.94

Beta-Ray Energies

The maximum energies for the β-rays from Kr^{85} and Kr^{87} were simply estimated by measuring the absorption in aluminum, neglecting the existence of γ-rays from these isotopes, which give rise to only a small error. These absorption curves are shown in Fig. 4, together with an absorption curve for P^{32}, which was taken for comparison. The unknown ranges of the β-particles from the two krypton isotopes were determined relative to the range of the β-particles from P^{32}. The corresponding β-energies, which are listed in Table III together with former values, were derived from Feather's formula.

The absorption curve for the radiations from the mixture of Kr^{88} and Rb^{88} in equilibrium has also been measured and has been compared with the absorption curve for the radiations from pure Rb^{88} (Fig. 5, curves *a* and *b*). For this purpose, samples of Rb^{88} were collected on a set of collector plates, which were mounted in a bulb containing radioactive krypton, and which was connected to a negative potential.[4,6] In carrying out the absorption experiments, special precaution was taken to ensure the same geometrical arrangement. An analysis of the absorption curve *a* clearly shows that the main number of Kr^{88} atoms decay with a maximum energy of about 0.5 Mev. The maximum energy of the only hitherto known group of β-particles from Kr^{88} is reported to be 2.43 Mev.[6,11] The small difference in the slope of the curves *a* and *b* for absorbers of thicknesses larger than the range of the low energy group is probably due to the presence of the group of 2.43 Mev. From the present experiments, however, it cannot definitely be concluded that this group exists; but as far as one may rely on the conclusion from the above mentioned measurements on the existence of the 2.43-Mev group, it is seen that the decay scheme of Kr^{88} is complex.

Gamma-Rays from Kr^{88}

The demonstrated group of short range β-particles from the decay of Kr^{88} indicates the existence of a γ-ray group having an energy of about 2 Mev. A special experiment was designed with the purpose of finding this radiation. Due to the disturbing effect of the γ-radiation from Rb^{88}, which is in equilibrium with Kr^{88}, it was necessary to liberate the krypton from the samples collected in the mass-spectrograph. This was carried out in vacuum by means of induction heating, with the result that not only the krypton was given off, but also a great amount of other gases being occluded in the brass collectors. Using these gases as carrier of the activity, the gas mixture was first compressed by means of a Toepler pump, and then transferred to a small glass vessel filled with mercury and having the bottom turned upwards. A counter was mounted above the vessel and lead absorbers were interposed in order to eliminate β-rays.

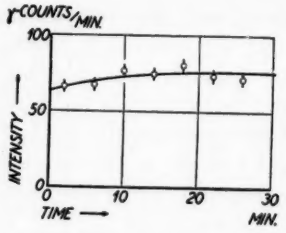

FIG. 6. Time dependence of gamma-ray intensity from a sample which at time zero consists of pure Kr^{88}.

Under these conditions, the curve of Fig. 6 was measured, showing the change of γ-rays intensity with time. The extrapolation of this curve to time zero, which corresponds to the time of inlet of active gas into the vessel, clearly shows the presence of γ-rays which must originate from pure Kr^{88}. The further course of the curve is governed by the decay of Kr^{88}, combined with the production and decay of the γ-active isotope Rb^{88}. The full-drawn curve in the figure corresponds to the expression

$$a\cdot\exp(-\lambda_{Kr}\cdot t)-b\cdot\exp(-\lambda_{Rb}\cdot t), \qquad (3)$$

where $a=109$ and $b=47$. The measurements of Fig. 6 could be repeated several times by replacing the glass vessel by another one. The active gas mixture was sucked over into the Toepler pump during this procedure.

The presence of an intense γ-radiation from Kr^{88} implies that the absorption curve for the mixture of Kr^{88} and Rb^{88} (see Fig. 5*a*) must be somewhat above the absorption curve for pure Rb^{88} in the case of very thick absorbers. The more exact position of this Rb^{88} curve, in relation to the curve *a*, can be determined by applying considerations leading to the expression (2). Curve *c* in Fig. 5 is constructed on this basis. Any further conclusions which may be drawn from the relative adjustment of the curves *a* and *c* must, however, be taken with considerable reservation, since we have no evidence that the efficiency of the counter is the same for low as for high energy β-particles.

This fact and the above-mentioned possibility of a complex β-decay of Kr^{88} show that any closer interpretation of the recoil experiments with Kr^{88}, which were mentioned in the Introduction, must be postponed at the present time. The further study of the decay scheme of Kr^{88} is, therefore, highly desirable.

We wish to thank Professor Niels Bohr for his never-failing interest and encouragement. We also wish to express our gratitude to Professor J. C. Jacobsen for valuable discussions. Furthermore, our thanks are due Mr. B. Madsen for putting a counter equipment at our disposal, Mr. K. O. Nielsen and Mr. S. Møller-Holst for their help in the work with the cyclotron and the mass-spectrograph, respectively.

[11] G. L. Weil, Phys. Rev. 62, 229 (1942).

The Molecular Spectrum of Hydrogen. The Fulcher Bands of TH and T_2

G. H. DIEKE AND F. S. TOMKINS
Argonne National Laboratory, Chicago, Illinois*
(Received April 11, 1949)

The spectra of TH and T_2 were photographed under high dispersion. The analysis of the $3p^3\Pi \rightarrow 2s^3\Sigma$ bands of these molecules is presented and the constants of the two states given.

I. INTRODUCTION

THE spectrum of the hydrogen molecule is now fairly well known.[1] Nevertheless, a further study of its spectrum is highly desirable because of the fundamental nature of the hydrogen molecule as the simplest of all molecules.

Among the known regularities in the H_2 spectrum are some the interpretation of which is little or not at all understood. These are chiefly due to levels with both electrons excited or to levels which, because they interact with other levels, have a highly irregular structure. The information concerning those that can be extracted from the H_2 spectrum alone is not sufficient to get a clear picture. It is fortunate that the hydrogen molecule exists in several isotopic species which differ only in the mass of the nuclei. The molecules HD and D_2 that contain deuterium have been studied successfully and the information obtained from them has proved very valuable.[2–4] More recently the radioactive isotope tritium with mass three has become available, which offers the possibility of studying the spectra of TH, TD, and T_2. This doubles the empirical material for the study of the structure of the hydrogen molecule.

It is well known that the results of all theoretical calculations for a system as complex as the hydrogen molecule can be obtained only in approximation formulas, which are usually expressed as series. This is true, for instance, for the vibrational and rotational energies which are given by the well-known formula

$$E(V, K)=\Sigma_{l,n}\, Y_{l,n}(V+\tfrac{1}{2})^l K^n(K+1)^n, \qquad (1)$$

where V and K are the vibrational and rotational quantum numbers respectively, and $Y_{l,n}$ constants which can be expressed in terms of the constants occurring in the potential energy of the molecule.

The usual procedure is to express the energies found empirically from the spectrum by the formula (1) and thus obtain the constants $Y_{l,n}$ which can then be used to obtain certain features concerning the structure of the molecule. This procedure is legitimate only if the expression (1) converges rapidly so that a few terms suffice to represent the energy satisfactorily. For this the situation is particularly bad in H_2 and a reasonable convergence can only be expected for the lowest values of V and K and even then the convergence is not very good, so that a number of terms is required. These can be obtained from the empirical data only by going to fairly high values of V and K where the convergence is so bad that the formula is practically useless. This presents a dilemma which makes it very difficult to obtain reliable constants for H_2 with the help of the spectroscopic data and formula (1).

The use of the isotopic species makes it possible to overcome this difficulty. With certain restrictions the rotation-vibration energies of all isotopic species are given by (1) where the constants $Y_{l,n}$ of the various molecules are related to each other by simple known expressions. The heavier the molecule the better is the convergence. For this reason D_2 is better for the computation of the molecular constants than H_2, and T_2 is even better than D_2. There is one additional fact which makes the calculation of the molecular constants much more reliable if several isotopic species are available. As many independent empirical energy differences are required as the number of desired constants $Y_{l,n}$. For instance, if the six constants $Y_{1,0}$, $Y_{2,0}\cdots Y_{6,0}$ are wanted, six vibrational differences are required, which would involve all vibrational quantum numbers from zero to six. As mentioned before, for H_2 the convergence of the formula would be bad except for $V=0$ or 1 and even in T_2 no satisfactory convergence would exist for $V=6$. If, however, instead of the six differences in *one* molecule, one for each of the six molecules is used, the levels need only involve tkose with $V=0$ and $V=1$, where the convergence is satisfactory. Much more reliable results can thus be expected.

By the reasons just set forth and others, we were convinced that considerable effort was justified to obtain the spectra of the hydrogen molecules containing tritium. The present paper deals with the general procedure by which the spectra were obtained and then deals with the so-called Fulcher bands, one of the most extensive band systems in the molecular spectrum of hydrogen.

II. EXPERIMENTAL PROCEDURE

The preliminary work was done with a sample having about 35 percent T and 65 percent H. Samples of higher tritium content were obtained later.

* The work on which this paper is based was begun jointly at the Argonne National Laboratory. It is being continued as a collaborative effort between the Argonne National Laboratory and the Johns Hopkins University under a contract with the AEC.

[1] For a general review of the H_2-spectrum up to 1934, see O. W. Richardson, *Molecular Hydrogen and Its Spectrum* (Yale University Press, New Haven, 1934).

[2] G. H. Dieke and R. W. Blue, Phys. Rev. **47**, 261 (1935).

[3] G. H. Dieke, Phys. Rev. **48**, 606 (1935); **50**, 797 (1936).

[4] G. H. Dieke and M. N. Lewis, Phys. Rev. **52**, 100 (1937).

TABLE I. The $3p^3\Pi \rightarrow 2s^3\Sigma$-band system of TH.

The *intensities* in column I are photographic densities multiplied by 100, taken from uncalibrated plates. Different regions of the spectrum are not necessarily on the same scale.

Blends are designated in the appropriate column as follows:

x: Line appears abnormally broad or diffuse and is probably not single.

y: Intensity appears too high. Another line must coincide with it.

z: Known blend with another classified line.

A means that the coinciding line is a H_2 line.

D means that it is a TH line.

F means that it is a T_2 line.

c: Because of confusion with other lines no reliable density reading can be obtained.

	P-branch			*Q*-branch			*R*-branch		
K	ν	*I*	Blends	ν	*I*	Blends	ν	*I*	Blends
				0→0 Band					
0	—	—		—	—		16 688.48	180	
1	—	—		16 643.92	200*		723.39	200	
2	16 554.59	133		633.34	200*	*z, AF*	753.03	200*	
3	501.07	200*		618.30	200*		777.21	180	
4	443.34	200*		598.30	200*		795.72	126	
5	381.80	200*		573.54	200*		808.48	70	
6	316.61	151		544.15	200		815.39	22	
7	248.06	111		510.20	130		816.45	8	
8	176.41	66		471.94	57				
9	101.85	26		429.40	85	*z, F*			
				0→1 Band					
0	—	—		—	—		14 605.40	31	
1	—	—		14 562.42	43		642.33	56	
2	14 477.08	6		555.88	64		675.55	68	
3	428.82	6		546.15	67		705.02	67	
4	378.25	4		533.28	*c*		730.63	51	*y*
5	325.52	2		517.27	30		752.18	33	
6	270.74	3		498.33	8		769.65	71	*yy*
7				476.49	3		782.76	8	
				1→0 Band					
0	—	—		—	—		18 538.20	122	*y*
1	—	—		18 493.38	132		570.00	109	
2	18 404.48	16		480.01	145		594.79	114	
3	347.69	28		460.02	160		612.52	109	
4	285.16	22		433.52	103		623.05	90	
5	217.19	15		400.59	68		626.28	47	
6	144.00	9		361.54	19		622.02	27	
7				316.37	20				
				1→1 Band					
0	—	—		—	—		16 455.44	170	
1	—	—		16 412.25	200*		488.88	200*	
2	16 326.95	109		402.40	200*		517.23	200*	
3	275.46			387.65	200*		540.28	200	*z, F*
4	219.99	155		368.34	200*		557.92	165	
5	160.89	150		344.30	200*	*z, F*	569.92	81	
6	098.16	116		315.88	170	*x, z*	576.14	45	
7	032.06	155	*z, F*	282.69	107	*z, F*			
8	15 962.99	62		245.62	18				
9	890.88	13							
				1→2 Band					
0	—	—		—	—		14 464.14	36	
1	—	—		14 422.68	32		499.33	64	
2	14 340.84	5		416.33	48		531.11	80	
3	294.53	8		406.87	43		559.40	78	
4	245.96	32	*y*	394.33	22		583.98	60	
5	195.39	10		378.83	10		604.51	29	
6	142.91	*c*		360.54	22	*z, D*	621.08		
7	088.69	3		339.34	8	*z, D*			
8	032.83	2							
				2→1 Band					
0	—	—		—	—		18 220.62	15	
1	—	—		18 177.62	29		250.38	15	
2	18 092.12	3		164.21	51		273.04	12	
3	037.02	10		145.17	61		287.59	7	
4	17 975.84	8		119.39	30		289.94	4	
5	908.14	10		087.46	13				
6	830.21	5		049.52	25	*y*			
7				005.28	5	*z, F*			

TABLE I.—*Continued.*

	P-branch			*Q*-branch			*R*-branch		
K	ν	*I*	Blends	ν	*I*	Blends	ν	*I*	Blends
				2→2 Band					
0	—	—		—	—		16 229.38	128	
1	—	—		16 188.12	165		260.81	175	*z, F*
2	16 106.11	62		178.54	200*		287.02	125	
3	056.14	96		164.28	200*	*z, F*	306.75	116	
4	001.84	94		145.48	165		315.88	170	*x, z*
5	15 942.70	86		122.11	125				
6	875.01	47		094.30	70				
7				062.24	29				
				2→3 Band					
0	—	—		—	—		14 360.54	42	*z, D*
1	—	—		14 287.75	47		390.06	23	
2	14 209.15	10		281.58	67		414.89	18	
3	*164.28	16		272.42	64		430.98	3	
4	116.75	26*c*		200.27	57				
5	065.94	25		245.28	51*c*				
6	008.24	20		227.46	11				
7				206.98	7*c*				
8				183.90	2				
				3→2 Band					
0	—	—		—	—		17 912.91	12	
1	—	—		17 871.30	39		942.02	15	
2	17 789.59	4		858.66	44		964.68	14	
3	737.27	9		839.76	36		980.62	10	
4	679.55	17		814.67	29		989.62	5	
5	616.60			783.65	11				
6				746.67					
7									
				3→3 Band					
0	—	—		—	—		16 010.99	162	*z, F*
1	—	—		15 970.99	102		041.74	77	
2	15 892.74	65		961.77	130		067.80	85	
3	845.42	57		947.96	115		088.86	86	
4	794.44	80		929.61	87		104.53	37	
5	739.90	57		906.92	59		114.54	34	*y*
6	681.83	32		879.94	30		117.92	12	
7	620.18	155		848.86	9				
8	554.46	85							
				3→4 Band					
0	—	—		—	—		14 196.31	26	
1	—	—		14 158.08	47		228.76	41	
2	14 083.13	8		152.15	59		258.17	60	
3	040.79	25		143.30	58		284.15	39	
4	13 996.38	21		131.58	36		306.42	19	
5	950.02	17		117.08	32*c*		324.61	6	
6	901.71	15		099.91	12		339.34	8	*z, D*
7	851.47	7		080.14	18	*z, F*			
8				057.90	30	*z, F*			
	4→3 Band			4→4 Band			4→5 Band		
1	17 574.15	12		15 761.13	35		14 034.20	46	
2	561.84	19		752.22	53		028.44	110	*z, F*
3	543.47	175	*yz, D*	738.83	44		019.95	56	
4	519.11	190	*y, F*	721.03	29		008.73	37	
5	488.94	18		699.10	15		13 394.82	26	
6				672.99	5		978.48	13	*z*
7				642.89	2		959.35	4	
				5→5 Band			5→6 Band		
1				15 558.86	46		13 916.87	31	
2				550.21	70		911.40	41	
3				537.25	59		903.29	49	
4				520.06	75	*y, A*	892.61	25	
5				498.81	21		879.31	17	
6				474.36	10		863.29	14	*z, F*
7							844.75	5	
8							823.52	6	

* Line overexposed, density unreliable.

The discharge tube was of a type described before.[5] It was made entirely of quartz and immersed in running water. Graded quartz to Pyrex seals connected it with the vacuum system. The horizontal part was silvered and the observations made end on. This kind of tube will easily stand 1.5A discharge current. The electrodes were aluminum in one tube, nickel in another one.

The gas was admitted through a palladium valve to the tube. Palladium transmits *H* more readily than *T* and therefore the initial part of the sample admitted through palladium has a lower tritium concentration than the supply and the later part is considerably higher in tritium content. Our set-up did not lend itself readily to a quantitative determination of the separation factor. The initial tritium concentration obtained from the 35

[5] G. H. Dieke and R. W. Blue, Phys. Rev. **47**, 261 (1935).

TABLE II. The $3p^3\Pi \rightarrow 2s^3\Sigma$-band system of T_2. (See caption of Table I for interpretation of symbols under blends.)

K	ν	I	Blends	ν	I	Blends	ν	I	Blends
				0→0 Band					
0	—	—		—	—		16 706.43	115	
1	—	—		16 683.72	150		723.77	170c	
2	16 638.73	2		678.59	139		738.66	27	
3	611.38	200*		671.00	200*		750.93	175	
4	581.69	12		660.87	69		760.48	68	
5	549.80	111		648.25	200*		767.26	160	
6	515.74	13		633.34	200*	z, D	771.42	21	
7	479.68	140		615.79	148		772.76	66	
8	441.37	84		595.96	36				
9	401.36	145		573.54	200*	z, D			
10	359.50	29		549.35	62	y			
11				522.92	16				
				0→1 Band					
0	—	—		—	—		15 212.55	6	
1	—	—		15 190.59	42		230.62	57	
2	15 146.98	3		186.84	16		246.84	17	
3	121.48	18		181.10	77		260.99	43	
4	094.37	5		173.54	25		273.08	8	
5	065.63	36		164.10	94		283.07	28	
6	035.36	7		152.79	25		290.95	7	
7	003.63	25		139.98	135	y	296.78	11	
8	14 970.44	29	y	124.82	22		300.51	2	
9	936.05	9					301.90	5	
				1→0 Band					
0	—	—		—	—		18 034.17	4	
1	—	—		18 011.48	10		050.33	10	
2				005.28	5		063.60	3	
3	17 938.05	4		17 995.83	29		073.43	17	
4	906.85	3		983.34	4		080.26	6	
5	872.41	8		967.88	27		083.49	8	
6									
7				933.73	4				
8									
9									
				1→1 Band					
0	—	—		—	—		16 540.32	130	z, D
1	—	—		16 518.35	114		557.24	121	
2	16 474.74	27		513.39	28		571.67	13	
3	448.09	147		505.92	200*		583.48	125	
4	419.27	69		496.00	39		592.73	7	
5	388.15	180		483.63	180		599.25	72	
6	355.07	83		468.91	19		603.14	30	y
7	319.86	150		451.82	97		604.33	20	
8	282.69	107	z, D	432.40	60				
9	243.65	94		410.70	160				
10	202.74	53							
11	159.98	40		360.75	43				
				1→2 Band					
0	—	—		—	—		15 093.07	20	
1	—	—		15 071.75	135		110.69	108	
2	15 029.27	6		068.12	75		126.31	30	
3	004.61	88		062.41	180		139.98	135	z, F
4	14 978.23	29		055.00	64		151.76	26	
5	950.33	102		045.71	160		161.55	105	
6	920.79	68	z, D	034.69	44		169.00	13	
7	890.02	80		021.93	112		174.48	39	
8	857.76	20		007.40	16				
9				14 991.22	66				
10				973.34	9				
11				954.04	15				
				2→1 Band					
0	—	—		—	—		17 825.39	11	
1	—	—		17 803.28	37		841.55	35	
2	17 758.93	6		797.12	8		854.29	9	
3	732.37	18		787.91	88		863.91	34	
4	701.87	5		775.71	10		870.31	12	
5	668.53	24		760.43	67		873.52	21	
6				742.29	6				
7				721.15	30				
8									
9									
				2→2 Band					
0	—	—		—	—		16 378.33	40	
1	—	—		16 356.60	190		394.90	153	
2	16 314.56	21		351.74	114		408.84	162	
3	288.82	128		344.30	200*	z, D	420.43	170	
4	260.81	175	z, D	334.69	111		429.31	85	
5	230.63	150		322.59	200*		435.63	125	
6	198.43	150	z, F	308.17	70		439.36	17	
7	164.28	200*	z, D	291.34	150		440.57	103	y
8	128.09	17		272.35	26				
9	090.12	55		251.12	77				

TABLE II.—*Continued.*

K	ν	I	Blends	ν	I	Blends	ν	I	Blends
				2→3 Band					
0	—	—		—	—		14 976.61	53	
1	—	—		14 955.53	200*		993.79	200	
2	14 914.70	12		951.89	109		15 009.04	180	z, D
3	890.79	108		946.40	200*		022.37	180	
4	865.28	40		939.14	126		033.72	56	
5	838.17	145		930.10	200*		043.09	172	
6	809.58	34		919.28	74		050.45	23	
7	779.58	105		906.73	200		055.76	70	
8	748.26	46		892.52	25		059.05	9	
9	716.13	10		876.67	82		060.29	18	
10				859.22	9		059.46	5	
11				840.20	23		056.56	12	
12				819.62	5		051.70	5	
13				797.32	15		044.76	4	
				3→2 Band					
0	—	—		—	—		17 620.86	4	
1	—	—		17 599.52	63		636.26	37	
2	17 557.58	86	zz, F	593.53	17		648.57	5	
3	530.16	21		584.50	138		657.83	39	
4	500.47	4		572.38	52	y	663.99	5	
5	468.08	14		557.58	86	z, F	666.99	24	
6									
7									
8									
9									
				3→3 Band					
0	—	—		—	—		16 219.16	25	
1	—	—		16 198.43	150	z, F	235.13	100	
2	16 157.27	5		193.62	70		248.67	24	
3	132.17	90		186.48	170		259.81	96	
4	104.92	30		176.92	64		268.44	20	
5	075.59	95		165.04	141		274.48	59	
6	044.17	38		150.88	53				
7	010.99	162	z, F	134.51	99				
8				115.87	10				
9				095.02	29				
				3→4 Band					
0	—	—		—	—		14 862.18	61	
1	—	—		14 842.06	200*	z, F	878.81	200	
2	14 802.17	24		838.50	200*	z, F	893.57	86	
3	778.84	152		833.13	200*		906.49	200*	
4	754.00	52		826.11	160		917.50	68	
5	727.68	158		817.15	200*		926.56	160	
6	699.92	39		806.74	200	zy			
7	670.83	111	z, F	794.31	175				
8				780.53	104	z, F			
9				764.94	82				
10				747.90	13				
				4→3 Band					
0	—	—		—	—				
1	—	—		17 399.96	41		17 435.42	35	
2						c			
3	17 332.41	55	y	385.36	98		452.82	66	
4				373.65	12				
5	268.55	23							
6									
7									
				4→4 Band					
0	—	—		—	—				
1	—	—		16 043.78	67		16 079.13	50	
2				039.13	31		091.67	11	
3	15 979.10	27		032.06	155	z, D	099.52	68	
4	952.04	7		022.71	21				
5	920.72	21		010.99	162				
6				15 997.21	12				
7				981.39	30				
				4→5 Band					
0	—	—		—	—		14 750.96	51	
1	—	—		14 731.50	200*		766.83	200	
2	14 692.64	15		727.98	125		780.53	104	z, F
3	669.87	150		722.74	200*		790.21	129	
4	645.13	89		715.77	148	z, F			
5	618.70	200		707.13	200*				
6				696.82	76				
7				684.84	152				
8				671.27	34				
9				656.13	56				
10				639.48	8				
11				621.32	34				

percent sample was only about 20 percent. (Some of this may have been due to dilution due to hydrogen being released from the electrodes or the walls on the tube.) The final portion had a tritium concentration of about 55 percent. The most useful pictures so far were made with a 77 percent sample which showed the HT and T_2

TABLE II.—*Continued.*

K	ν	I	Blends	ν	I	Blends	ν	I	Blends
				5→5 Band					
0	—	—		—	—		15 912.38	86	
1	—	—		15 892.71	200*	z, D	927.40	150	
2	15 835.96	40		888.17	90		940.08	51	
3	830.21	170		881.35	200*	z, F	950.14	12	
4	804.50	100		872.16	c				
5	776.65	140		860.72	175				
6				847.17	53				
7				831.43	148				
8				813.76	63				
				5→6 Band					
0	—	—		—	—		15 642.89	46	
1	—	—		14 623.91	190		658.44	175	
2	14 586.31	9		620.51	90		670.83	111	z, F
3	564.39	110		615.40	200		684.32	170	
4				608.61	150				
5	516.18	120	z, F	600.14	190				
6				590.06	43				
7				578.40	103				
8				565.13	22				
9				550.40	28				
10				534.19	75	y			
	6→6 Band			6→7 Band			7→8 Band		
1	15 745.36	73		14 519.49	102		14 418.56	35	
2	740.86	25		516.07	120	z, F	415.32	12	
3	734.13	112		511.18	154		410.43	94	z, F
4	724.84	42		504.59	44		404.14	13	
5	714.14	103		496.36	130		396.07	58	
6				486.54	14		386.57	6	
7				475.18	40		375.56	21	
8				462.25	7		363.00	2	
9				447.93	6	z, F	349.13	3	
	8→9 Band			9→10 Band			10→11 Band		
1	14 321.42	21		14 228.29	14		14 139.71	7	
2	318.19	3		225.29	2		136.88	2	
3	313.56	37		220.76	22		132.56	14	
4	307.36	6		214.76	3		126.86	2	
5	299.58	40		207.34	19				
6	290.40	3		198.53	2				
7	279.77	11		188.24	6				
8									
9	254.22	1							

* Line overexposed, density unreliable.

bands well developed with the H_2 band very much weakened.**

After an initial run, the first tube with aluminum electrodes showed only the atomic silicon lines as impurity lines. Mercury that was initially present disappeared gradually. If atomic silicon is present, which evidently originates from some disintegration of the quartz by the discharge, it is expected that the SiH bands might appear. Their presence is not obvious. They lie, however, in a region where the hydrogen lines are very crowded. It would be possible to say with certainty whether the SiH bands were present weakly only after this part of the spectrum has been measured and analyzed.

TABLE III. Rotational differences of the $2s^3\Sigma$-state.

K	V=0	1	2	3	4	5	6	7
				$F(K+1)-F(K-1)$				
				TH				
1	133.84	128.51	123.29	118.24	113.25	108.69		
2	222.28	213.40	204.73	196.30	188.03	179.79		
3	309.65	297.20	285.15	273.37	261.74	250.36		
4	395.34	379.48	364.01	348.91	334.02	319.57		
5	479.06	459.78	441.01	422.70	404.64	386.92		
6	560.43	537.88	515.81	494.34	473.26	452.37		
7	638.96	613.23	588.17	563.42				
8	714.60	685.75		630.06				
				T_2				
1	67.69	65.59	63.77	61.90	60.05	58.29	56.58	
2	112.40	109.18	106.09	102.98	99.98	96.98	94.05	91.08
3	157.01	152.44	148.11	143.77	139.60	135.32		
4	201.08	195.33	189.76	184.22	178.80	173.51	168.20	
5	244.68	237.70	230.92	224.16	217.58	211.07		
6	287.02	279.46	271.43	263.51	255.74	248.12		
7	329.91	320.50	311.26	302.18		284.17		
8	371.32	360.76	350.37	329.76				
9	411.84		388.56					

The second tube, with nickel electrodes, was first outgassed in vacuum by heating the electrodes to dull red heat in an induction furnace. In the initial stages this tube showed so strong contamination by CO_2, OH, and related molecules that the H_2 spectrum was completely obliterated. The origin of these impurities was not quite certain. Possibly they originated from the action of hydrogen atoms on stopcock grease present on a stopcock in the vacuum line about one foot away from the tube. That this was probably the case was corroborated by the fact that when the tube was filled with helium the helium spectrum was fairly pure, whereas under the same conditions a hydrogen discharge would start out as a typical H_2 discharge but change in a few minutes into a bluish CO discharge.

After elimination of the stopcock and insertion of platinum asbestos in the line as a catalyzer which would prevent hydrogen atoms from traveling any further, the tube could be cleaned up with helium discharges to drive out remnants of gases present. After this the spectrum would show, besides the atomic silicon lines, only the OH bands very faintly as impurity lines.

The small amounts of tritium available made it important that none of the gas was wasted. The tube with the aluminum electrodes showed a considerable cleanup effect. The pressure would fall rapidly from one millimeter, at which most of the pictures were taken, to below the value where a discharge could be sustained, sometimes within an interval of less than one hour. Unfortunately, time did not permit an investigation of the mechanism by which the gas disappeared. After the initial experiments the tube was operated with argon to drive out hydrogen from the electrodes. This was only partly successful, but the treatment profoundly altered the properties of the tube. The voltage necessary to run the tube with H_2 became higher. Apparently a very considerable amount of argon must have been driven into the electrodes. After the argon treatment the tube was again run with hydrogen. The pressure remained constant now, indicating that no hydrogen was disappearing any more. The spectrum after the argon treatment always showed argon lines in the H_2 spectrum. In the beginning the argon lines, particularly in the near infra-red, were much stronger than the H_2 lines. Repeated new fillings with hydrogen and pumping down to a pressure below 10^{-5} mm between the fillings would not bring any change.[6] The intensity of the argon lines was

** Later results have shown that with a given sample the apparent tritium concentration, determined spectroscopically, may depend very much on the discharge conditions.

[6] A small McLeod gage was used to measure pressures between about 10^{-3} mm and one mm. An ionization gage served to measure pressures below 10^{-3} mm. The ionization gage became useless, of course, once tritium had been admitted to the system, as the

TABLE IV. Constants of the $2s^3\Sigma$-state.

	TH			T_2		
V	B_V	D_V	ω_V	B_V	D_V	ω_V
0	22.363	0.00951		11.2848	0.00271	
1	21.470	0.00924	2082.88	10.9506	0.00231	1493.82
2	20.601	0.00899	1991.28	10.6418	0.00238	1447.23
3	19.756	0.00887	1901.98	10.3290	0.00226	1401.73
4	18.926	0.00880	1814.61	10.0282	0.00224	1256.93
5	18.117	0.00872		9.7230	0.00202	
Y_{10}		2177.01			1541.57	
$-Y_{20}$		47.84			24.47	
Y_{30}		0.502			0.312	
$-Y_{40}$		0.015			0.016	
Y_{01}		22.819			11.4374	
$-Y_{11}$		0.9182			0.3258	
Y_{21}		0.0123			0.00273	
Y_{02}		0.0097			—	
$-Y_{12}$		0.00038			—	

gradually reduced while the tube was operated for many hours with H_2 at high current levels during a period of several weeks, but they never disappeared and were still present with considerable intensity when the tube finally was discarded. During the end of its life this tube again showed a considerable cleanup effect. It would be interesting to investigate whether the reappearance of the cleanup effect was directly connected with the disappearance of the argon from the electrodes.

The tube with nickel electrodes showed only a very moderate amount of cleanup, which was not objectionable.[7]

The technique of obtaining the spectrum of hydrogen containing tritium differs but little from the technique when only H_2 or D_2 are present. While the radioactivity of tritium is considerable, the beta-rays are soft and no activity can penetrate glass. It is, therefore, completely safe to use tritium in a glass container. When pumping was necessary the outlet from the pump was directly led into a ventilating shaft so that not even small amounts of tritium could escape into the room. Neither deuterium nor tritium seems to exchange with the hydrogen contained in stopcock grease. It is, therefore, quite permissible to use stopcocks whenever they can be tolerated for other reasons. Possibly the beta-activity will decompose the stopcock grease, but a possible dilution of the tritium by hydrogen coming out of stopcocks because of this was of no importance for our purposes.

It need hardly be emphasized that any equipment that has contained tritium must be treated with the greatest care, and, if possible, should be discarded afterwards unless all traces of radioactivity can be removed.

III. RESULTS

The molecular spectrum of hydrogen was photographed in the second order of a three-meter grating spectrograph from about 3300A where the discrete spectrum begins to about 8800A. The exposure times ranged from a few seconds to two hours. Under these conditions the spectrum could be obtained with the lines everywhere dense, that is, an increased exposure would not have yielded additional lines. The long wave-length region is an exception and first-order plates were also taken there. In the short wave-length region below about 4800A fourth-order plates were also obtained. The comparison of several sets of plates taken with increasing tritium concentration made it possible to ascertain whether a given line belonged to H_2, HT, or T_2. Eventually, when it will be possible to obtain the spectrum of pure T_2, the identification of the species to which they belong will be considerably simpler. Even in that case the availability of spectra with different concentrations will make it possible to get the necessary information in case of blends which are rather frequent in a spectrum of such complexity. Microphotometer traces of all important plates were taken, with which a good estimate of the intensities could be obtained, even if the plates are not calibrated.

The wave-lengths were measured with a comparator in the usual way.***

It is hoped that, as the wave-length measurements accumulate, a rather complete analysis of the spectra of TH, TD, and T_2 can be given, which will include features which so far have not been elucidated in the H_2 spectrum. Naturally, the completion of this task will take some time, as each of the spectra contains in excess of 10,000 lines. The present paper gives an account of the so-called Fulcher bands of TH and T_2. It is hoped that this will shortly be followed by an analysis of the analogous bands for TD. A detailed comparison of the various molecules will be postponed until the TD data are also available.

Tables I and II present the analysis of TH and T_2, respectively. These bands are due to a $3p^3\Pi \rightarrow 2s^3\Sigma$ transition and lie chiefly in the wave-length region from 5400 to 7200A. The wave numbers should be accurate to within a few hundredths wave numbers for good lines.

The intensities listed in the I column are densities taken directly from representative plates. They are not corrected for changes of plate sensitivity with wave-length and can be regarded as preliminary values only until there is an opportunity to make quantitative measurements. They are, however, considerably better than the usual visual estimates.

It may be said that the degree of certainty with which the classification can be relied on is about the same as for the corresponding H_2 bands or better. This means that there practically cannot be any doubt about most of the lines, with the possible exception of some weak lines near the ends of the branches. The probability of

ionization produced by the tritium radioactivity would upset the calibration completely.

[7] It was later sealed off with tritium at about 2-mm pressure and operated successfully for many additional hours.

*** The earlier measurements were made with the comparator of the Physics Department of the University of Chicago. We wish to thank Drs. R. S. Mulliken and J. R. Platt for making this instrument available to us.

blends that distort the wave-length measurements is fairly high in a complex spectrum that is the superposition of that of three different gases (H_2, TH, and T_2). This situation will be considerably relieved for T_2 when purer tritium samples will become available.

A more complete analysis of all the bands in this region will make a recognition of these blends easier. Finally, when more measurements will have accumulated, a slight revision in the wave-lengths may be expected. All these things may eventually make a recalculation of the constants advisable. Such a revision, however, will not produce any substantial changes in the principal constants.

The chief intensity of the Fulcher bands lies in the sequences where V changes by ±1 or 0. There are fragments of weaker bands with $\Delta V=\pm2$ which, however, are not complete enough to deserve recording.

IV. EVALUATION OF CONSTANTS

The $2s^3\Sigma$-State

The rotational energies of a Σ-state can be represented with sufficient approximation by the usual formula

$$F(K)=BK(K+1)-DK^2(K+1)^2. \quad (2)$$

The differences

$$F(K+1)-F(K-1)=R(K+1)-P(K+1)$$
$$=2(K+1)B-[(2K+1)^3-(2K-3)]D \quad (3)$$

can be directly obtained from the experimental data. Averages are listed in Table III. For the computation of the averages data from other bands which have the same final state were included.

The constants B and D were calculated by a least square method from the first four differences of TH and from the first six differences for T_2. More differences were used for T_2 than for TH because the expression (2) will be a good approximation for higher values of K for T_2. The values of B_v and D_v thus obtained are given in Table IV.

TABLE V. Constants of the $3p^3\Pi$-state.

	TH			T_2		
V	B_V	D_V	ω_V	B_V	D_V	ω_V
0	19.797	0.00810		9.999	0.00213	
1	19.002	0.00797	1851.36	9.701	0.00207	1328.35
2	18.211	0.00794	1766.89	9.412	0.00200	1285.47
3	17.435	0.00787	1684.80	9.129	0.00198	1243.47
4	16.677	0.00772	1604.59	8.846	0.00187	1202.31
5	15.907		1526.30	8.579		1161.78
Y_{10}		1936.93			1372.11	
$-Y_{20}$		43.439			22.135	
Y_{30}		0.459			0.159	
$-Y_{40}$		0.036			0.002	
Y_{01}		20.219			10.150	
$-Y_{11}$		0.823			0.3050	
Y_{21}		0.0080			0.0038	
Y_{02}		0.00812			0.00217	
$-Y_{12}$		0.00008			0.000065	
ν_0		16767.05			16770.61	

The vibrational energy is given by the usual formula

$$E(V)=Y_{10}(V+\tfrac{1}{2})+Y_{20}(V+\tfrac{1}{2})^2$$
$$+Y_{30}(V+\tfrac{1}{2})^3+Y_{40}(V+\tfrac{1}{2})^4+\cdots. \quad (4)$$

The differences between successive vibrational levels for a given K can again be found directly from the observed frequencies. With a knowledge of the rotational constants they can be extrapolated to $K=0$. From these differences

$$E(V)-E(V-1)=Y_{10}+2VY_{20}$$
$$+(3V^2+\tfrac{1}{4})Y_{30}+(4V^3+V)Y_{40}+\cdots,$$

the constants Y_{10} etc. can be obtained. As the convergence of (4) is generally poor except for low values of V it is advantageous to use only as many differences as constants are required.

Finally from

$$B_v=Y_{01}+Y_{11}(V+\tfrac{1}{2})+Y_{21}(V+\tfrac{1}{2})^2+\cdots, \quad (5)$$

and

$$D_v=Y_{02}+Y_{12}(V+\tfrac{1}{2})+\cdots, \quad (6)$$

we obtain the constants $Y_{01}\cdots Y_{11}$, etc.

The $3p^3\Pi$-State

Every Π-state is double. The separation between the two components, Π^- and Π^+ is the Λ-doubling. It has been shown before[8] that the $3p^3\Pi^+$-state is usually irregular due to perturbations by the higher vibrational states of $3p^3\Sigma$. Rotational constants derived from this state would have no simple meaning. On the other hand the $3p^3\Pi^-$-state cannot be perturbed and, therefore, it should be used for the calculation of the rotational constants of the $2p^3\Pi$-state. It gives rise to Q branches only and, therefore, the differences (3) cannot be obtained directly for this state. The procedure for the calculation of the constants is as follows:

The rotational energies of a $p^3\Pi$-state except for a constant are given by

$$F(K)=B[K(K+1)]-D[K^2(K+1)^2-1]^2,$$

which differs from (2) only by the presence of the subtractive *one* in the second term. As the influence of the second term is negligible for small values of K, no appreciable error is made if the one is neglected as compared with $K(K+1)$. If B' and D' are the values of B and D for the $2p^3\Pi$-state and B'' and D'' the same value for the $2s^3\Sigma$-state, the Q branches are given by

$$Q(K)=A-(B''-B')K(K+1)$$
$$+(D''-D')K^2(K+1)^2. \quad (7)$$

The values A (origins of the bands), $B''-B'$ and $D''-D'$ were obtained again by a least square method from the first six lines of each band, and it turned out that (7) represents the Q lines within the limits of the errors of measurement.

[8] G. H. Dieke, Phys. Rev. 48, 610 (1935).

As B'' and D'' are known from Table IV the rotational constants B' and D' for the $2p^3\Pi$-state can be obtained. The vibrational constants of this state are found in a way analogous to that used for $2s^3\Sigma$-state. The constants thus obtained are listed in Table V, which also contains the electronic frequencies of the bands.

V. NUCLEAR SPIN OF TRITIUM

Successive rotational lines in a band of a homonuclear diatomic molecule should alternate in intensities with a ratio $(I+1)/I$ when I is the nuclear spin. No such alternation should occur for a molecule with two different nuclei. None is observed for TH. For T_2 the ratio appears to be 3:1, the same as for H_2. This shows that the spin of tritium is $\frac{1}{2}h/2\pi$. This is in agreement with the findings of Bloch, Graves, Packard, and Spence,[9] who obtained this value by an entirely different method. Only rough intensity measurements are necessary to establish the value of the spin from the band spectrum as it is only necessary to decide whether the ratio is 3:1 or 1.67:1, etc. However, some quantitative measurements have been made more recently which confirm the value 3:1 with considerable accuracy.

VI. PERTURBATIONS AND PREDISSOCIATIONS

The $3p^3\pi^-$-state cannot be influenced by any close lying state because none with the required symmetry can be present. On the other hand the $3p^3\Sigma$-state partly overlaps the $3p^3\Pi$-state and it has the required symmetry for interaction with the $3p^3\Pi^+$-state. This interaction results in a shift of the $3p^3\Pi^+$-state from its unperturbed position. This shift is called Λ-doubling and can be obtained easily from the experimental data, as the unperturbed levels should coincide with the $3p^3\pi^-$-levels. The experimental values for the Λ-doubling are listed in Table VI. The magnitude of the Λ-doubling is

[9] Bloch, Graves, Packard, and Spence, Phys. Rev. **71**, 551 (1947).

TABLE VI. Λ-doubling of the $3p\Pi$-state.

	TH				T_2					
K	$V=0$	1	2	3	0	1	2	3	4	5
1	0.25	0.28	0.12	0.46	0.10	0.07	0.44	0.12	0.01	0.17
2	0.84	0.85	0.22	1.23	0.13	0.11	0.66	0.26	−0.02	0.28
3	1.54	1.66	0.08	2.27	0.27	0.34	0.96	0.52	−0.33	0.51
4	2.37	2.56	−1.21	3.42	0.44	0.51	1.18	0.72	−2.84	0.71
5	3.26	3.58	−7.55	4.46	0.67	0.78	1.48	1.20		
6	4.13	4.46		5.02	0.96	1.03	1.82	1.61		
7	4.90	5.38			1.09	1.28	2.28			
8	5.80	5.96			1.44	1.57	2.65			
9					2.00					
10					2.01					

determined chiefly by two states. The level with the same K and V of $2p^3\Sigma$ has a relatively large influence even though it is fairly distant because the matrix element of the interaction is relatively large. On the other hand, levels with the same K but any value of V may have a strong influence if they are very close. The close approach of such levels does not follow any simple law and, therefore, the influence of such close lying levels appears rather haphazard and accounts for the irregular behavior of the Λ-doubling as function of V. If the levels come very close we have a typical perturbation. Such a perturbation exists for $V=2$ of TH and $V=4$ of T_2.

Beyond a certain limit the $3p^3\Sigma$-level is dissociated which means that no sharp energy levels exist. The $3p^3\Pi^+$-levels that coincide with such dissociated $3p^3\Sigma$-levels take on the properties of the interacting levels. They appear predissociated which means here that the corresponding molecular states disappear before the molecule has had the time to emit the line. This has as consequence that the P and R branches of all bands disappear when the upper state lies beyond the dissociation limit of $3p^3\Sigma$. The data show that this is true for $V=4$ for TH and for $V=6$ for T_2 (see Table VI). The Q branches are unaffected. This can be used to narrow the limits for the dissociation energy of H_2. It is best, however, to postpone a discussion of the details of this until also use can be made of the TD-data.

Coincidence and Absorption Investigation of the Disintegration of Rh^{106}, Sb^{125}, and Pr^{142}

E. T. JURNEY
Indiana University, Bloomington, Indiana
(Received April 6, 1949)

The disintegration of Rh^{106}, Sb^{125}, and Pr^{142} has been studied with the help of conventional absorption and coincidence counting techniques. All three isotopes exhibit complex beta-ray spectra, on the basis of the shapes of their beta-gamma-coincidence plots. A definite gamma-gamma-coincidence rate indicates cascaded gamma-rays in all the disintegration schemes. Corrections for coincidences between gamma-rays and x-rays resulting from internal conversion are discussed for the case of Sb^{125}.

THE coincidence experiments performed in this laboratory principally in conjunction with spectrographic measurements have been continued, as a possible aid in determining disintegration schemes for the active isotopes rhodium 106, antimony 125, and praseodymium 142. The general techniques employed here follow closely those used in previous work and will not be discussed in detail.[1] The counters and associated counting circuits have previously been described.[2] A constant resolving time of 2.0 microseconds was used to obtain the results to be given. The sources used for the investigation were obtained from the Oak Ridge National Laboratory.

1. RHODIUM 106

The 30-sec. Rh^{106} activity grows from 1-yr. Ru^{106}, which emits a single beta-ray group with a maximum energy of approximately 30 kev.[3] W. C. Peacock[4] has measured the energies of the beta- and gamma-rays associated with the decay of Rh^{106} with a magnetic lens spectrograph, and finds two beta-ray groups with maximum energies of 3.55 Mev (82 percent) and 2.30 Mev (18 percent); he finds three gamma-ray lines, of 0.51 Mev, 0.73 Mev, and 1.25 Mev. These measurements, combined with some coincidence experiments, led Peacock to propose the disintegration scheme shown in Fig. 1.

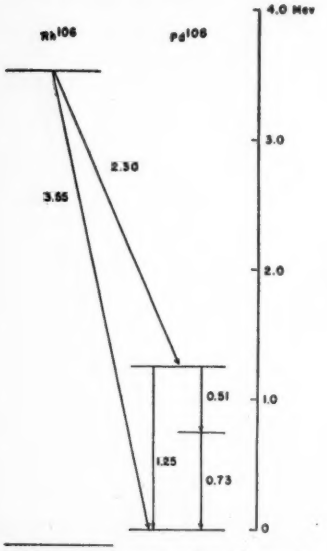

FIG. 1. Disintegration scheme for Rh^{106} as proposed by Peacock (see reference 4).

In the experiments to be described here, a beta-ray absorption curve, taken with aluminum absorbers, and analyzed by the method of Bleuler and Zünti,[5] yielded a maximum energy of 3.50 Mev, with indications of a lower energy group. The energy of the hardest gamma-ray was determined by the coincidence absorption of the Compton recoil electrons produced in an aluminum radiator and was found to be 1.3 Mev. To observe gamma-gamma- and beta-gamma-coincidences, the source was situated between a lead-cathode gamma-ray counter and an end-window beta-ray counter with a 6-mg/cm² mica window. A 1.8-g/cm² aluminum absorber placed before the beta-ray counter served to exclude beta-rays and to provide a radiator for producing secondary electrons when gamma-gamma-coincidences were investigated.

The gamma-gamma-coincidence rate per gamma-ray recorded by the lead counter was $(0.15\pm0.049)\times10^{-3}$, which indicates that at least a pair of gamma-rays is

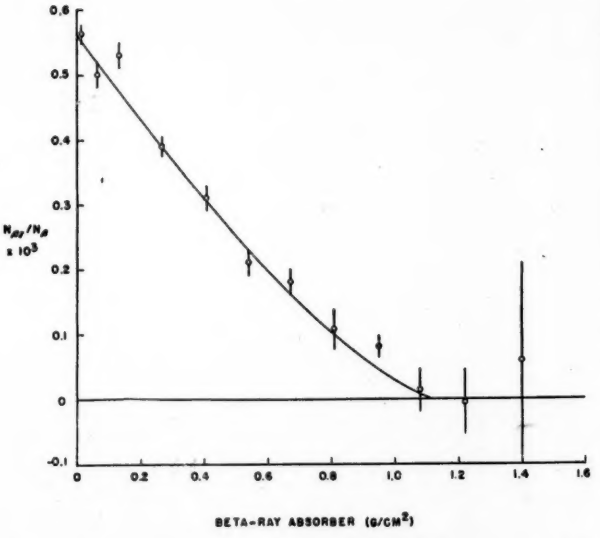

FIG. 2. Beta-gamma-coincidences from the disintegration of Rh^{106}.

[1] For a more complete discussion on coincidence counting procedure, see A. C. G. Mitchell, Rev. Mod. Phys. **20**, 296 (1948).
[2] E. T. Jurney and A. C. G. Mitchell, Phys. Rev. **73**, 1153 (1948).
[3] G. T. Seaborg and I. Perlman, Rev. Mod. Phys. **20**, 585 (1948).
[4] W. C. Peacock, Phys. Rev. **72**, 1049 (1948).
[5] E. Bleuler and W. Zünti, Helv. Phys. Acta **19**, 375 (1946).

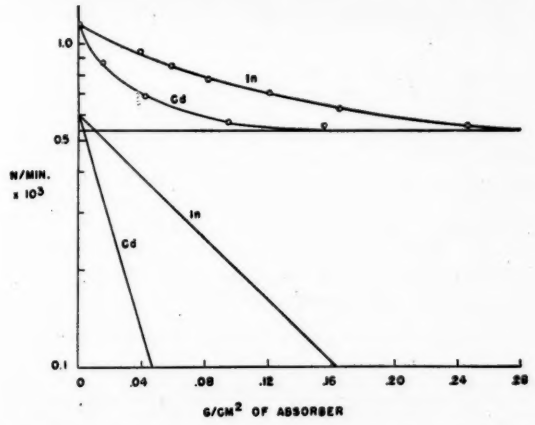

FIG. 3. Critical absorption of characteristic tellurium x-rays in the beta-ray absorption curve for Sb^{125}.

emitted in cascade in some of the disintegrations. The gamma-ray counting efficiency for the beta-ray counter combined with an aluminum radiator is not known, however, and no further information can be inferred from the gamma-gamma-coincidence rate. The beta-gamma-coincidence rate per recorded beta-ray as a function of beta-ray absorber is given in Fig. 2; the curve shows clear evidence of a complex beta-ray spectrum, with a low energy group whose maximum energy is around 2.3 Mev. Above 2.3 Mev no beta-gamma-coincidences are observed, from which fact one concludes that the higher energy group of beta-rays leads directly to the ground state of Pd^{106}. The results presented here are in good agreement with Peacock's proposed disintegration scheme.

2. ANTIMONY 125

Kern, Mitchell, and Zaffarano,[6] using a magnetic lens spectrometer, have found the following beta- and gamma-ray energies associated with the disintegration of Sb^{125}: Beta-ray groups with end-point energies of 0.621 Mev, 0.288 Mev; gamma-ray lines of 0.646 Mev, 0.609 Mev, 0.431 Mev (*I.C.*), 0.174 Mev (*I.C.*), 0.125 Mev, and 0.110 Mev (*I.C.*), in which the symbol (*I.C.*) denotes internal conversion. Friedlander, Goldhaber, and Scharff-Goldhaber[7] report further that a metastable level of approximately two months half-life exists in Te^{125}, and their absorption measurements on the conversion electrons from the delayed gamma-radiation indicate a quantum energy of 120 kev. Kern *et al.*[6] find that the 110-kev line mentioned is delayed.

The absorption and coincidence experiments to be described here are for two cases: (1) with a source which contains the two-month tellurium gamma-ray activity, and (2) with a source which has had chemical separation from tellurium. Identical counter geometries were used in both cases.

In the experiments with the first source, an aluminum absorption curve of the beta-rays appeared to have an end point at approximately 0.7 Mev, with considerable "tailing off" for absorber thicknesses out to about one centimeter. The activity in the "tail" proved to be characteristic K x-radiation from tellurium, following internal conversion of gamma-rays, as shown by the critical absorption curves of Fig. 3. These curves were taken with enough aluminum to stop beta-rays of energies less than 0.300 Mev. The customary beta-gamma-coincidence plot displayed the saddle shape shown in Fig. 4. It seemed likely that a considerable number of coincidences between gamma-rays and x-rays, following internal conversion, were being recorded (at a rate to be symbolized by "$N_{x\gamma}$").

The ratio $N_{x\gamma}/N_x$ should be independent of the absorber thickness placed before the beta-ray counter, which in the present experiments was the only counter capable of recording x-rays. By extrapolation of the x-ray fraction in the total absorption curve, it was possible to arrive at a value for N_x for any absorber thickness. With an absorber made up of 0.270 g/cm² of aluminum and 0.112 g/cm² of lead, it was possible to exclude all the beta-rays and nearly all the x-rays from the beta-counter and thus to arrive at nearly the true value for the ratio $N_{\gamma\gamma}/N_\gamma$, which was found to be $(0.033\pm0.016)\times10^{-3}$. Then, by using enough aluminum absorber to remove the beta-rays, a value for $(N_{x\gamma}+N_{\gamma\gamma})/(N_x+N_\gamma)$ was found, from which, by subtraction, the value of $N_{x\gamma}/N_x$ was secured. It was possible, then, to arrive at the proper value of $N_{\beta\gamma}$ for each absorber thickness by subtracting the $N_{x\gamma}$ rate in addition to the usual chance, cosmic-ray, and gamma-gamma-rates which are subtracted from the total coincidence rate. The true plot of $N_{\beta\gamma}/N_\beta$, as a function of beta-ray absorber thickness, is reproduced in Fig. 5. Because of the fact that many component rates add to give the total coincidence rate, the errors in counting the true beta-gamma-coincidence rate become large.

From Fig. 5 it is apparent that the highest energy group of beta-rays is not emitted in coincidence with a gamma-ray; thus, the transitions associated with that

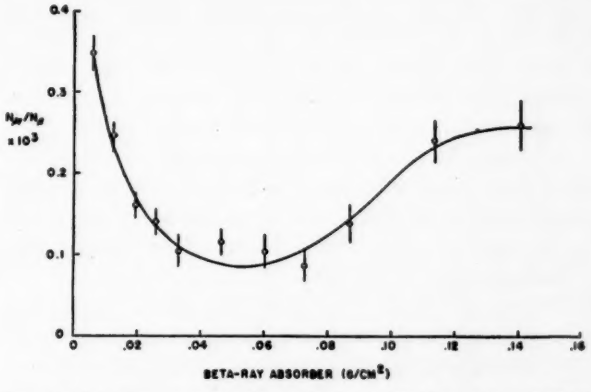

FIG. 4. Beta-gamma-coincidences from the disintegration of Sb^{125}, uncorrected for x-ray-gamma-coincidences.

[6] B. D. Kern, A. C. G. Mitchell, and D. J. Zaffarano, Phys. Rev. 76, 94 (1949).

[7] Friedlander, Goldhaber, and Scharff-Goldhaber, Phys. Rev. 74, 981 (1948).

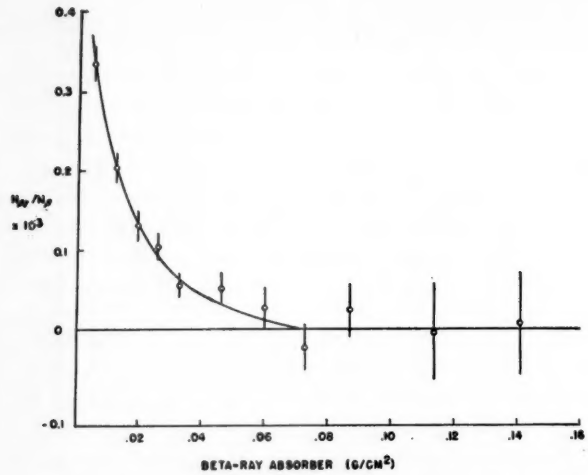

FIG. 5. Beta-gamma-coincidences from the disintegration of Sb^{125}, corrected for x-ray-gamma-coincidences.

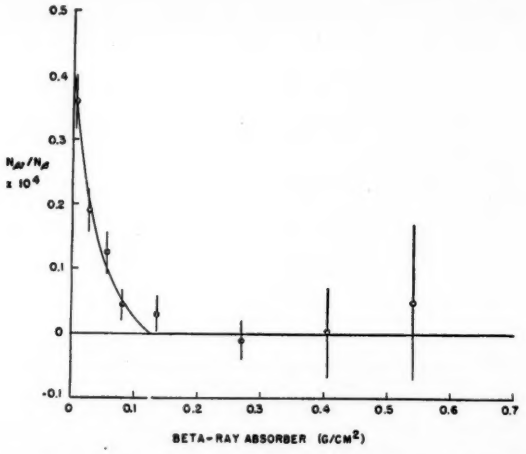

FIG. 6. Beta-gamma-coincidences from the disintegration of Pr^{142}.

group lead either to the ground state of Te^{125} or directly to the known metastable level in Te^{125}. The end point of the highest energy electron group which is in coincidence with a gamma-ray is around 0.25 Mev, within rather large limits of error. Also, the curve gives no indication of coincidences between conversion electrons from the strong 0.436-Mev gamma-ray line reported by Kern *et al.*[6] and other gamma-rays.

Essentially the same results were obtained from similar experiments done with the source which had had two-month Te^{125} gamma-ray activity chemically removed. The low energy beta-ray group end point appeared at 0.24 Mev, and the value of $N_{\beta\gamma}/N_\beta$ was again 0.34×10^{-3} for no absorber before the beta-ray counter. It was not expected that enough of the conversion electrons from the 0.110-Mev gamma-ray could be transmitted by the counter window to have material effect on the shape of the $N_{\beta\gamma}/N_\beta$ *vs.* absorber thickness plot.

3. PRASEODYMIUM 142

Mandeville[8] has reported a series of coincidence and absorption experiments on the radiations from the 19.3-hr.[9] activity of Pr^{142}. His results indicate a complex beta-ray spectrum, with end points of 2.21 Mev and 0.215 Mev, and at least two gamma-rays, the hardest of which has an energy of 1.74 Mev. He also reports gamma-gamma-coincidences and beta-gamma-coincidences which involve only the low energy group.

As a part of the present investigation, the beta-ray end-point energy was found to be 2.52 Mev by absorption in aluminum, and the energy of the hardest gamma-ray was found to be 1.53 Mev by coincidence absorption of Compton recoil electrons.

The rate of counting beta-rays was much higher than that of counting gamma-rays in the usual coincidence arrangement; apparently most of the transitions from Pr^{142} lead directly to the ground state of Nd^{142}. In this same arrangement, the gamma-gamma-coincidence rate was nearly zero, partly because of the low sensitivity of the beta-ray counter for counting gamma-rays. With the source placed between two counters which have lead cathodes, the gamma-gamma-coincidence rate was found to be $(0.10\pm0.075)\times10^{-3}$ per counted gamma-ray. The fraction of 1.53-Mev gamma-rays counted is known to be around 1.2×10^{-3} for the geometry employed; it is not reasonable to suppose the 1.53-Mev gamma-ray to be simply in cascade with a single lower energy gamma-ray, then, for the counter sensitivity for a gamma-ray of the difference energy (approximately 0.7 Mev) is about 0.7×10^{-3}, and for the cascaded pair, one would expect a gamma-gamma-coincidence rate of

$$\frac{N_{\gamma\gamma}}{N_\gamma}=\frac{2\omega^2\epsilon_1\epsilon_2}{\omega(\epsilon_1+\epsilon_2)}=\frac{1.68\times10^{-6}}{1.9\times10^{-3}}=0.89\times10^{-3}.$$

Here $\omega\epsilon_1$ is the fraction of the 1.53-Mev gamma-rays counted, and $\omega\epsilon_2$ is the fraction of the 0.7-Mev gamma-rays counted.

The plot of $N_{\beta\gamma}/N_\beta$ as a function of beta-ray absorber thickness is given in Fig. 6. As was expected, no evidence of coincidence is found between the 2.52-Mev beta-ray group and gamma-rays. A second beta-ray group appears, however, with an end-point energy around 0.35 Mev.

The results, except for some lack of agreement in the energy determinations, agree with Mandeville's findings. It is believed that a careful spectrographic analysis, especially of the gamma-ray spectrum, will have to be made before a complete disintegration scheme can be constructed.

ACKNOWLEDGMENTS

The author takes pleasure in expressing his gratitude to Professor A. C. G. Mitchell for interest and suggestions; this investigation was assisted by the joint program of the ONR and AEC.

[8] C. E. Mandeville, Phys. Rev. **75**, 1287 (1949).
[9] DeWire, Pool and Kurbatov, Phys. Rev. **61**, 564 (1942).

Superconductors in Alternating Magnetic Fields

ROBERT T. WEBBER, J. M. REYNOLDS,* AND T. R. MCGUIRE
*Sloane Physics Laboratory, Yale University,** New Haven, Connecticut*
(Received March 25, 1949)

A simple technique of determining the superconducting transitions of small and irregularly shaped samples of superconducting material is applied to the determination of the transitions and critical magnetic field curves of tin and vanadium. The zero-field transitions and critical field curve for tin agree well with previous determinations. The vanadium was found to have broad transitions in zero magnetic field and critical field slopes of over 4000 gauss per degree. The critical field curve of the vanadium was verified by measurements with a susceptibility balance.

INTRODUCTION

THE measurement of the properties of superconductors through a study of their effect on mutual inductors and self-inductors has been investigated by Shoenberg[1] and Daunt,[2] while Casimir[3] has applied the technique to the determination of the magnetic field penetration depth in superconductors.

Because of the convenience of this method for specimens of small or irregular shapes, it was felt desirable to continue the investigation further.

The apparatus used was very simple. The sample of metal was surrounded as closely as possible with a coil consisting of a few hundred turns of fine wire. This coil formed the secondary of a mutual inductor, and was located in the center of a primary solenoid which was wound on the outside of the helium flask. Using an electron tube oscillator as a source, an alternating current of frequency 250 to 2000 cycles per second was passed through the primary solenoid, and the magnitude of this current adjusted so that the peak magnetic field at the center of the primary solenoid was approximately 0.5 gauss. The signal picked up by the secondary coil was amplified, rectified, and recorded with a Brown recording potentiometer. The primary coil was connected in series with the primary of a standard mutual inductor which allowed the drift in the electronic circuits to be calibrated at intervals during the run.

When the metal sample inside the secondary coil was in the non-superconducting or "normal" state, some or all of the alternating field penetrated the metal, giving a corresponding contribution to the secondary e.m.f. which remained very nearly independent of temperature. However, as the temperature was lowered into the transition region, the alternating field was excluded from the sample, causing the secondary e.m.f. to drop sharply until it reached a small and constant value corresponding to complete superconductivity of the sample.

We define $\Delta E=(E_n-E_s)/E_n$, where E_n is the secondary e.m.f. for the sample in the normal state, and E is the secondary e.m.f. for the sample in the superconducting state. For a first approximation, which will give the maximum ΔE allowed by the geometry of the apparatus, we will assume that the effects of eddy currents in the normally conducting sample are negligible and that the normal metal has unit permeability. For a specimen of spherical shape with the secondary coil wrapped around its equator, the solution is simple, yielding $\Delta E=a^3/R^3$, where a is the radius of the sphere, and R is the coil radius. This formula proved to be correct for vanadium spheres to within the accuracy of the measurement.

A general solution for ΔE must take into account the partial shielding that will occur in the sample in the normal state due to the presence of eddy currents. An argument based on the analysis of Smythe[4] shows, for the spherical case, that the diminution of E_n (or of ΔE), due to eddy currents, will be a function of $a(\omega/\tau)^{\frac{1}{2}}$ where ω is the frequency of the applied field, τ is the resistivity of the metal, and a is the radius of the sphere. The exact nature of this relationship requires the evaluation of some hitherto untabulated modified Bessel functions of half-integral order.

The fact that the ΔE of the vanadium samples agreed quite well with the approximate formula above indicates that the normal resistivity of the metal at

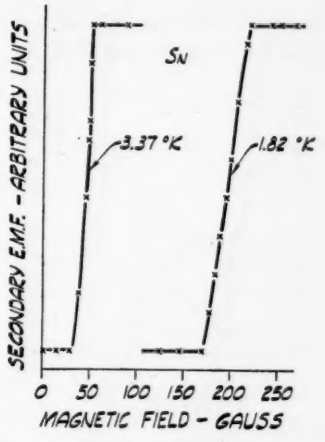

FIG. 1. Typical isothermal transitions of tin.

* Sheffield-Loomis Fellow in Physics.
** Assisted by the ONR.
[1] D. Shoenberg, Proc. Camb. Phil. Soc. **33**, 577 (1937).
[2] J. G. Daunt, Phil. Mag. **24**, 361 (1937).
[3] H. B. G. Casimir, Physica **7**, 887–896 (1940).
[4] William R. Smythe, *Static and Dynamic Electricity* (McGraw-Hill Book Co., Inc., New York, 1939) pp. 396 et seq.

liquid helium temperatures was quite high. The ΔE for tin, on the other hand, was almost an order of magnitude lower.

EXPERIMENTAL RESULTS

(a) Tin

As a check on the alternating field method, a determination was made of the transition and critical fields of a small spheroidal single crystal of spectroscopically pure tin, supplied by Johnson Mathey and Company, London (purity 99.992 percent). The midpoint of the transition in zero steady field occurred at 3.71°K, slightly higher than the accepted value of 3.69°K.[5] The transition width was approximately 0.02°K.

Steady magnetic fields transverse to the direction of the alternating field were supplied by a large pair of Helmholtz coils. Typical isothermal transitions are shown in Fig. 1. When the fields at which the secondary e.m.f. is restored to its normal value were plotted against temperature, we obtained a critical field curve which is identical with that of de Haas and Engelkes.[5]

(b) Vanadium

The superconductivity of vanadium was discovered in 1930 by Meissner and Westerhoff,[6] who observed that the electrical resistance of a sintered rod of this metal vanished at about 4.3°K. Since that time very little further information has been published regarding the properties of this metal at low temperatures, due largely to the difficulty in securing pure samples of a form suitable for measurements.

The samples of vanadium used by us were obtained from the A. D. McKay Company (Sample No. 1, purity 99.8 percent) and from the Vanadium Corporation of America (Sample No. 2, purity 99.7 percent). These samples were polycrystalline in the form of nearly exact spherical solid globules about $\frac{1}{8}$ inch in diameter.

The experimental arrangement was the same as that for the tin sample, with the exception that the steady fields used to obtain the critical field curves were obtained with the use of a large Weiss electromagnet capable of producing fields up to 10,000 gauss.

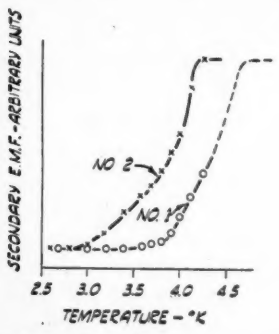

FIG. 2. Zero field transitions of two samples of vanadium.

The transitions of these specimens into superconductivity in zero steady magnetic field are shown in Fig. 2. Both samples exhibited transition ranges approaching a degree of temperature, as compared with the transition ranges of about 0.001° that have been observed in single crystals of pure tin.[7]

Because it exhibited a sharper transition at higher temperatures, Sample No. 1 was chosen for study of the critical field properties. A typical isothermal transition is illustrated in Fig. 3. The rising part of this graph is more or less what might be expected. The secondary e.m.f. remained at a low and constant value until the steady magnetic field reached a magnitude P (which we will call the "penetration field"). Increasing the steady field above P, the secondary e.m.f. rises as more and more of the alternating magnetic field penetrates the metal sample until a field S ("saturation field") is reached at which the sphere is entirely normally conducting. For fields higher than S, the secondary e.m.f. remains a constant.

On lowering the steady field below S, an interesting hysteresis appeared, which had the net effect of leaving the sample as a slightly better shield of the alternating magnetic field than it had been prior to the quenching of the superconductivity by the steady magnetic field. This hysteresis was observed in the vanadium samples at all temperatures for which the critical fields were determined, but was not observed in the tin sample.

The penetration and saturation fields at various temperatures are shown in Fig. 4. The slope of the saturation curve ($dH_c/dT = 4100$ gauss per degree) is much larger than found in any other pure non-alloy conductor. A similar, but less thorough study of the critical fields of our vanadium Sample No. 2 yielded a saturation field slope of about 5000 gauss per degree.

As a further check on the transitions into superconductivity of the vanadium, Sample No. 1, the critical fields were obtained by measuring the magnetic susceptibility of the sample. A modified form of a Hutchison-Reekie[8] balance was used. The so-called Faraday body force was employed in making the measurement,

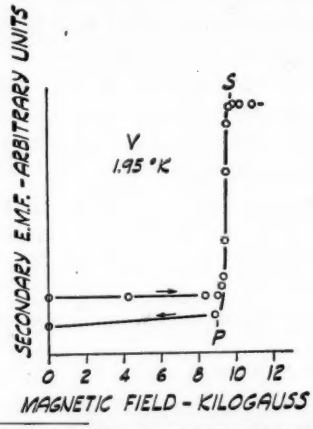

FIG. 3. Typical isothermal transition of vanadium (Sample No. 1).

[5] W. J. de Haas and A. D. Engelkes, Physica **4**, 325 (1937).
[6] W. Meissner and H. Westerhoff, Zeits. f. Physik **87**, 206 (1934).
[7] W. J. de Haas and J. Voogd, Leiden Comm. 214c (1931).
[8] T. S. Hutchison and J. Reekie, J. Sci. Inst. **23**, 209 (1946).

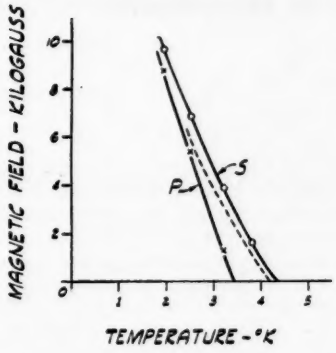

FIG. 4. Critical fields of vanadium (Sample No. 1).

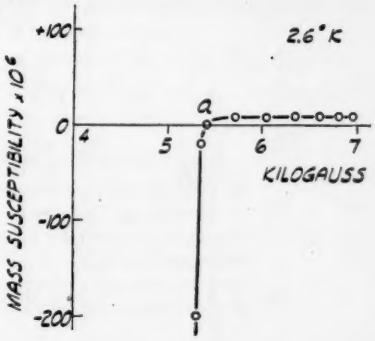

FIG. 5. The susceptibility of vanadium obtained from body force measurements.

wherein the vanadium sample was placed in an inhomogeneous magnetic field (H). The force (F) on the specimen of volume (V) is then given by $\mathbf{F}=[(k-k_0)/2]v\nabla H^2$, where k and k_0 are, respectively, the magnetic susceptibility per unit volume of the specimen and the surrounding medium (the latter being zero in these measurements). The force obtained for different values of H was compared to a standard substance (spectroscopically pure bismuth, purity 99.998 percent).

In Fig. 5, the susceptibility of vanadium at 2.6°K is plotted as a function of the magnetic field. It will be noted that when the field is decreased below 5450 gauss, the sample becomes highly diamagnetic. This is in accordance with the "Meissner effect" in which the field inside a superconductor becomes zero ($B=0$). Consequently, from the relation

$$B=H+4\pi(1-\tfrac{1}{3})I,$$

we obtain

$$I/H=K=-3/8\pi.$$

Thus, we should approach a value $-3/8\pi$ for the volume susceptibility of a pure superconductor of spherical shape. Unfortunately, the measurements could not be carried out to this limit as the balance was not built to measure forces over 100 dynes.

The critical field curve obtained from these susceptibility measurements is shown in Fig. 4 by the dashed line. This curve was obtained by taking the points of inflection of the susceptibility curves (point a, Fig. 5) at temperatures 3.5°, 3°, 2.8°, and 2.6°. It is seen to be in fair agreement with those obtained from the a.c. measurements.

DISCUSSION OF RESULTS

It is evident that the purest vanadium now available shows many of the characteristics of alloy-type superconductors,[9] such as broad transitions in the absence of magnetic field, very high critical fields, and hysteresis. It is quite possible that extremely pure, strain-free specimens of this metal will exhibit much lower critical fields and will otherwise more nearly conform to the behavior of the other pure metal superconductors that have been studied thus far.

It is also apparent that the alternating field technique yields a different view of the intermediate state than do measurements of the resistance and of the susceptibility. It can be easily shown[10] that for a superconducting sample of spherical shape, the magnetic field begins to penetrate the metal when the external applied magnetic field equals $\frac{2}{3}$ the critical field (H_c). As the field is raised from $\frac{2}{3}H_c$ to H_c, the penetration of the metal by the field should increase uniformly. This has been confirmed experimentally by the susceptibility measurements of Shoenberg.[11] Examination of Figs. 1 and 3 shows that the alternating field does not penetrate the metal to any great extent until fields considerably larger than $\frac{2}{3}H_c$ are reached. A similar distortion of the isothermal transitions in hollow cylinders in alternating fields was observed by Daunt.[2] A reasonable explanation of this distortion is that there exist in the intermediate state closed current loops which are still for the most part superconducting, having only a very small section which is resistive.

It has been suggested[12] that such low resistance current loops may exist at the boundary surface between regions in the superconducting and in the normal state.

A general investigation of time effects in the intermediate state is being continued and will be reported in a later issue of this Journal.

---

[9] D. Shoenberg, *Superconductivity* (Cambridge University Press, London, 1938), Chapter 6.
[10] See reference 9, p. 27.
[11] D. Shoenberg, Proc. Roy. Soc. **155**, 712 (1936).
[12] K. Mendelssohn and R. B. Pontius, Physica **3**, 327 (1936).

Wave Equations in the de Sitter Space

SATOSI WATANABE
Tokyo, Japan

(Received February 7, 1949)

The second-order wave equation $\partial^2 u/\partial x_i \partial x^i = 0$ in five-dimensional flat space can reproduce approximately the field hitherto considered in four-dimensional space, if a de Sitter space with the radius R is imbedded in the five-dimensional flat space and the derivative of the wave function u in the direction normal to this de Sitter space is assumed to be equal to imu, where m is a constant proper to the field. Conversely, the ordinary field equations in four-dimensional space can be regarded as valid only for a portion of de Sitter space with the linear dimension, which is small compared with the radius R of the universe. Extensions of these arguments to electromagnetic field and spinor field are also considered.

QUANTUM mechanics of fields and general theory of relativity can be harmonized without interfering with the current principles of either theory as long as the gravitational force is not represented by the metric tensor, i.e., if the latter theory is applied to an empty, homogeneous space. The maximum unification of these two systems without a drastic alteration of their basic methods may therefore be attained by establishing a quantum theory of fields in the de Sitter space. Dirac has indeed shown that the electron wave equation can be generalized to the de Sitter space,[1] however his method of deduction is imbued with many arbitrary supplementary assumptions. The aim of the present paper is to introduce a consistent method which permits a systematic reformulation of all the known field equations in the de Sitter frame of reference.

We take a 5-dimensional flat space,

$$r^2 = g_{ij}x^i x^j = x_i x^i = (x^1)^2 + (x^2)^2 + (x^3)^2 - (x^0)^2 + (x^5)^2, \quad (1)$$

in which the de Sitter space:

$$r^2 = R^2 \quad (2)$$

is imbedded, R being the "radius" of the universe.

We make two fundamental assumptions, from which all the field equations will be automatically deduced:

First, any field quantity should satisfy the second-order wave equation:

$$\partial^2/\partial x_i \partial x^i u = 0. \quad (3)$$

Second, a field quantity differentiated in the direction normal to the de Sitter space should give itself multiplied by i-times a constant m proper to the field ($c = \hbar = 1$):

$$\partial u/\partial r = imu. \quad (4)$$

Alternative assumptions which can equally be used in place of (4) will be discussed later.

The author of this paper introduced some years ago a 5-dimensional formalism in which the fifth coordinate x^5 was regarded as the canonical conjugate of the mass constant.[2] He also discussed some practical consequences which can be drawn from this theory.[3] The following theory, which will be based on assumptions (3) and (4), will become identical with this previous formalism if a small 5-dimensional portion of the space near a point in the de Sitter space is taken into consideration, or in other words if the radius R is considered to be very large.

The differentiation operator $\partial/\partial x_i$ can be expressed in terms of the rotation operators:

$$\pi^{ij} = x^i(\partial/\partial x_j) - x^j(\partial/\partial x_i), \quad (5)$$

which do not go outside the de Sitter space and the operator of differentiation in the normal direction:

$$\pi = r(\partial/\partial r) = x^i(\partial/\partial x^i). \quad (6)$$

Among the ten operators π^{ij}, there are six identical relations of the type

$$x^k\pi^{ij} + x^i\pi^{jk} + x^j\pi^{ki} = 0, \quad (7)$$

so that (5) and (6) make just five independent operators and we have

$$\partial/\partial x_i = 1/r^2(-x_j\pi^{ij} + x^i\pi). \quad (8)$$

The field equations in the de Sitter space will be obtained by substituting (8) into (3) and rewriting π by the assumption (4). Since we have

$$\partial^2/\partial x_i \partial x^i = 1/r^2(\tfrac{1}{2}\pi_{ij}\pi^{ij} + \pi^2 + 3\pi), \quad (9)$$

the second-order wave equation in the de Sitter space becomes

$$(\tfrac{1}{2}\pi_{ij}\pi^{ij} - m^2R^2 + 4imR)u = 0. \quad (10)$$

The linearization of the second-order wave equation in terms of a tensor, as is usual for the electromagnetic or mesonic field, can be done in the following manner:

The field strengths defined by

$$f^{ij} = 1/R^2[x_k(\pi^{jk}u^i - \pi^{ik}u^j) + imR(x^i u^j - x^j u^i)] \quad (11)$$

satisfy the integrability condition,

$$x_l(\pi^{kl}f^{ij} + \pi^{il}f^{jk} + \pi^{jl}f^{ki}) - imR(x^k f^{ij} + x^i f^{jk} + x^j f^{ki}) = 0. \quad (12)$$

[1] P. A. M. Dirac, Ann. Math. **36**, 657 (1935).
[2] Satosi Watanabe, Sci. Pap. I.P.C.R. **39**, 157 (1941). Satosi Watanabe, Sci. Pap. I.P.C.R. **42**, 1 (1944).
[3] Satosi Watanabe, Phys. Rev. **74**, 1864 (1948).

In virtue of the Lorentz condition:

$$(-x^i\pi_{ij}+imRx_i)u^i=0, \tag{13}$$

the field Eq. (10) then becomes

$$(-x^k\pi_{jk}+imRx_j)f^{ij}=0. \tag{14}$$

This set of equations allows for the gauge transformation

$$u'^i=u^i+1/R^2(-x_k\pi^{ik}+imRx^i)\chi, \tag{15}$$

if χ satisfies an equation of the type (10).

The passage to the ordinary Minkowski space is possible for the small region:

$$\left.\begin{array}{l} x^5\approx R \\ |x^\mu|\ll R \quad (\mu=1,2,3,0) \end{array}\right\}. \tag{16}$$

The usual 4-dimensional mesonic equations can then be derived from the equations from (11) to (15) by identifying $f^{5\mu}$ with the mesonic potential v^μ multiplied with im:

$$f^{5\mu}=imv^\mu. \tag{17}$$

The gauge transformation (15) becomes in the region (16)

$$\left.\begin{array}{l} u'^\mu=u^\mu+\partial\chi/\partial x_\mu \\ u'^5=u^5+im\chi, \end{array}\right\} \tag{18}$$

with

$$(\Box-m^2)\chi=0. \tag{19}$$

This entitles us to make u'^5 vanish, so that we may have

$$v^\mu=u'^\mu. \tag{20}$$

This last equality, however, may fail in presence of interaction, whereas (17) is a general relation. Since the gauge transformation (18) leaves the mesonic potential v^μ unchanged, there is in general no gauge transformation for the latter.

The electromagnetic field equations can be obtained, under the condition (16), by simply putting $m=0$ in the equations from (10) to (15). The electromagnetic potential can be identified with the first four components of the 5-dimensional potential and the gauge transformation (18) acquires a 4-dimensional validity. u^5 and $f^{5\mu}$ are completely separated from the electromagnetic field and correspond to a massless c meson.[3]

The linearization of the second-order Eq. (10) for a spinor field can be done, with the help of the Dirac matrices,

$$\tfrac{1}{2}(E_iE_j+E_jE_i)=g_{ij}, \tag{21}$$

by writing

$$E_i(\partial/\partial x_i)\psi=0, \tag{22}$$

which becomes, in consideration of (8) and (4),

$$(-E_ix_j\pi^{ij}+imRE_ix^i)\psi=0. \tag{23}$$

The last equation reduces to the ordinary electron equation under the condition (16).

It will be clear from the above deduction that, in order to obtain the usual 4-dimensional wave equations under the condition (16), we need not necessarily assume (4) but only assume

$$r(\partial u/\partial r)=imR[1+0(1/Rm)]u \text{ for } r=R. \tag{24}$$

Condition (24) is also sufficient for the above theory to become, in the limiting case (16), identical with the 5-dimensional formalism which the author introduced previously.[2]

The quantities which play the role of momentum-energy vector in the above theory are

$$p^\mu=(i/R)\pi^{\mu 5}, \tag{25}$$

which satisfy the commutation relation

$$p^\mu x_\mu-x_\mu p^\mu=-i(x^5/R), \tag{26}$$

which tends to $-i$ as we approach the limiting case (16). The first three components of p^μ are quantized, but the quantum intervals are of the order of $1/R$, which is negligibly small compared with the values of momenta usually intervening in the atomic physics if R is taken from the cosmological determination.

The generalization of the above theory to fields interacting with each other can easily be carried out without introducing any new notion or assumption.

On a Generalization of the Lambda-Limiting Process and the Non-Uniqueness in the Removal of Divergence Difficulties in the Quantum Theory of Elementary Particles*

I. POMERANCHUK
Academy of Sciences of the USSR, Moscow, USSR

(Received March 14, 1947)

A generalized process of the λ-limiting type is established, leading to the elimination of the divergences in the integrals of both the classical and quantum field theories. As a result, however, the process is not unique, and by a suitable choice of the convergence factor the observable quantities, such as the proper mass, may be given any finite value. This indicates either that limiting processes are not capable of solving the basic difficulties in the theory of fundamental particles, or that the necessity for additional postulates of the nature of selection rules.

AS is well known, Wentzel[1] discovered the existence of a certain limiting process which leads to classical field equations without divergence difficulties. Dirac[2,3] gave the quantum version of this process by substituting the usual commutation relations for the Fourier components of the field

$$[a(k), a^+(l)]=\delta_{kl}, \tag{1}$$

by the relations

$$[a(k), a^+(l)]=\delta_{kl}\cos\bar{k}\bar{\lambda}, \quad \bar{\lambda}^2=|\lambda|^2-\lambda_4{}^2<0. \tag{2}$$

The divergence troubles[4] which arise as a result of quantization of the field are not removed by the Wentzel-Dirac λ-process. Dirac[5] therefore suggested that negative probabilities be considered, but these also lead to difficulties in the interpretation of the theory.[3]

It will be shown in the present note that the λ-process can be generalized in such a manner that the divergences in the quantum, as well as in the classical integrals may be removed. A very distinct non-uniqueness then appears, however, which also affects the classical integrals. As in the case of the usual λ-process (2) we shall modify the commutation relationships (1) to read

$$[a(k), a^+(l)]=\delta_{kl}D(k).$$

In order to determine the general expression for D we use the requirement that the function Δ_2 [6–8] should not be introduced into the commutation relations for the field operators. The function D must therefore have the form:

$$D=\sum_n A(\bar{\lambda}_n)\cos\bar{k}\bar{\lambda}_n. \tag{3}$$

The $\bar{\lambda}_n$ are arbitrary four-dimensional vectors. If they satisfy the condition $\bar{\lambda}_n{}^2=|\lambda_n|^2-\lambda_{4n}{}^2<0$ the classical divergencies will vanish (see Eq. (9) below). The quantities $A(\bar{\lambda}_n)$ are subjected to the condition $\sum_n A(\bar{\lambda}_n)=1$. In order to eliminate the uneven[5] divergences we shall attempt to choose the quantities $A(\lambda_n)$ in such a manner that the various terms in the sum (3) lead to results which ultimately cancel out mutually. As an illustration, consider the following example. Let us determine the factor D which removes all even and the first uneven divergence. For this purpose we consider the expression

$$D=(4/3)\cos\bar{k}\bar{\lambda}-\tfrac{1}{3}\cos\tfrac{1}{2}\bar{k}\bar{\lambda}. \tag{4}$$

We change to a coordinate system in which only $\lambda_4\neq 0$. Further assume (for the sake of simplicity) that the rest mass μ of the field quanta equals zero.

$$\int_0^\infty Dkdk=(4/3)\int_0^\infty kdk\cos k\lambda_4 -\tfrac{1}{3}\int_0^\infty kdk\cos\tfrac{1}{2}k\lambda_4=-(4/3)\lambda_4{}^{-2}+\tfrac{1}{3}(2/\lambda_4)^2=0.$$

(See Pauli,[3] page 202.)

In the general form, if we wish to remove the first p uneven divergences, A must satisfy the equalities (if all $\bar{\lambda}_n$ have only λ_4 different from zero):

$$\sum_n A(\bar{\lambda}_n)/\lambda_{4n}{}^{2m}=0. \quad M=1, 2, \cdots, \tfrac{1}{2}(p+1). \tag{5}$$

* This paper, received more than two years ago, is now published although, due to circumstances beyond our control, it has not been possible for the author to have read proof.

[1] B. Wentzel, Zeits. f. Physik **86**, 479, 635 (1933); **87**, 726 (1934).
[2] P. A. M. Dirac, Ann. de l'Inst. Poincaré **9**, 13 (1939).
[3] W. Pauli, Rev. Mod. Phys. **15**, 175 (1943).
[4] I. Waller, Zeits. f. Physik **62**, 673 (1930).
[5] P. A. M. Dirac, Proc. Roy. Soc. **A180**, 1 (1942).
[6] W. Pauli, Rev. Mod. Phys. **13**, 203 (1941).
[7] F. Bloch, Physik. Zeits. Sowjetunion **5**, 301 (1934).
[8] M. Markov, J. Phys. **10**, 333 (1946).

Thus without introducing negative probabilities and by a simple generalization of the λ-process the uneven divergences can be eliminated from the theory.

However, a very distinct non-uniqueness of the theory immediately appears. The condition that the theory be free of uneven divergences can be satisfied also in case (5) is substituted by the condition

$$\lim_{\lambda_{4n}\to 0} \sum_n A(\bar{\lambda}_n)/\lambda_{4n}{}^{2m} = B_m \tag{6}$$

where the B_m's are arbitrary finite numbers.

For, if (4) is replaced by

$$(4/3)\cos\bar{k}\bar{\lambda} - \tfrac{1}{3}[1-\tfrac{3}{4}B\bar{\lambda}^2]\cos\tfrac{1}{2}\bar{k}\bar{\lambda},$$

(B being an arbitrary number), we obtain

$$\int_0^\infty kdk[(4/3)\cos k\lambda_4 - \tfrac{1}{3}(1+\tfrac{3}{4}B\lambda_4{}^2)\cos\tfrac{1}{2}k\lambda_4] = B.$$

This non-uniqueness exists also if the classical (even) divergences are considered. $D(K)$ can be chosen in such a manner that the integrals $\int_0^\infty D(K)K^{2m}dk$ take any finite value. For this purpose, along with the time-like vectors $\bar{\lambda}_n$, space-like vectors $\bar{\mu}_n$ must also be considered:

$$\bar{\mu}_n{}^2 = |\mathfrak{y}_n|^2 - \mu_{4n}{}^2 > 0.$$

Thus, consider the case $m=0$.

$$\int_0^\infty \frac{d\mathbf{k}}{k^2}\cos(\mathbf{k}\mathfrak{y} - k\mu_4) = \frac{2\pi}{\mu}\int_0^\infty \frac{dk}{k}[\sin(\mu-\mu_4)k + \sin(\mu+\mu_4)k].$$

Hence the D-factor which gives the integral $\int_0^\infty Ddk$ any assigned value has the form

$$D = \cos\bar{k}\bar{\lambda} + B/2\pi^2(\mu^2-\mu_4{}^2)^{\frac{1}{2}}\cos\bar{k}\bar{\lambda}. \tag{7}$$

(B being an arbitrary number), and obtain

$$\int_0^\infty (D/k^2)d\mathbf{k} = B(1-\mu_4{}^2/\mu^2)^{\frac{1}{2}}.$$

With $\bar{\mu}$ tending to zero any number between 0 and B can be obtained.

In the general case instead of (3) the following expression for D may be considered

$$D = \textstyle\sum_n \{A(\bar{\lambda}_n)\cos\bar{k}\bar{\lambda}_n + F(\bar{\mu}_n)\cos\bar{k}\bar{\mu}_n\} \times \sum_n \{A_n(0)+F_n(0)\} = 1.\ \ \lambda_n{}^2 < 0.\ \ \mu_n{}^2 > 0. \tag{8}$$

If we wish to obtain any finite value for the even (classical) integrals, D must be subjected to the condition

$$\lim_{|\mathfrak{y}_n|\to 0} \sum_n \frac{F(\bar{\mu}_n)}{|\mathfrak{y}_n|^{2m+1}} = B_{2m+1}. \tag{9}$$

In the case of uneven (quantum) divergence we arrive at the condition

$$\lim \sum_n \left\{\frac{A(\bar{\lambda}_n)(2m+1)!}{\lambda_{4n}{}^{2m+2}} - \frac{\pi}{2}\frac{(2m)!F(\mu_n)}{\mu_n{}^{2m+2}}\right\} = B_{2m+2}. \tag{10}$$

In conclusion it should also be noted that the generalized λ-process of Eqs. (3) and (8) permits one also to sum logarithmically divergent integrals of the type[9]

$$\int_0^\infty dk/(k^2+m)^{\frac{1}{2}}$$

(Pauli,[3] p. 203). Using the relation

$$\int_0^\infty [\cos k\lambda/(k^2+m^2)^{\frac{1}{2}}]dk = -\ln\tfrac{1}{2}m\lambda - \gamma,$$

where γ is Euler's constant, one may, for example, consider the following expression as the D-factor eliminating the logarithmic divergences:

$$D = 2\cos\bar{k}\bar{\lambda} - \cos[a\bar{k}\bar{\lambda}(-\bar{\lambda}^2)^{\frac{1}{2}}]. \tag{11}$$

In the system of coordinates in which $\mathfrak{y}=0$:

$$D = 2\cos k\lambda_4 - \cos ak\lambda_4{}^2;$$

$$\int_0^\infty D/(k^2+m^2)^{\frac{1}{2}} = -\ln\tfrac{1}{2}m - \gamma + \ln a.$$

However, it is easy to choose such a D that, besides (9) and (10), the integral $\int_0^\infty D/(k^2+m^2)^{\frac{1}{2}}$ also takes any finite value.

Thus although the generalized λ-process (3) and (8) permits one to remove all divergences in the theory of fundamental particles, the theory thus obtained turns out to be non-unique; by varying the D-factor various values for the observable quantities (e.g., the proper mass) may be obtained. This non-uniqueness either indicates the invalidity of limiting processes for solving the basic difficulties in the theory of fundamental particles or else points to the necessity of additional postulates or "selection rules."

[9] V. Weisskopf, Zeits. f. Physik **89**, 90 (1934); Phys. Rev. **56**, 72 (1939).

Letters to the Editor

PUBLICATION of brief reports of important discoveries in physics may be secured by addressing them to this department. The closing date for this department is five weeks prior to the date of issue. No proof will be sent to the authors. The Board of Editors does not hold itself responsible for the opinions expressed by the correspondents. Communications should not exceed 600 words in length.

Slow Neutron Cross Sections of the Neodymium Isotopes

DAVID C. HESS, JR., AND MARK G. INGHRAM
Argonne National Laboratory, Chicago, Illinois
May 31, 1949

THE total cross section, i.e., the sum of the absorption and scattering cross sections for neodymium of normal isotopic distribution is 53×10^{-24} cm².[1] If we assume a scattering cross section of 8 barns, the total absorption cross section is 45 barns. The sum of the known activation cross sections is 0.56 barn.[2] Thus one might expect one or more isotopes of large cross section which absorb neutrons to form other stable isotopes of neodymium. In order to locate any such isotope, ten miligrams of neodymium oxide (Hilger Laboratory No. 6783) was submitted to long slow neutron irradiation in a graphite moderated pile. After removal from the pile the sample was allowed to stand for sufficient time to permit most of the induced activities to decay. The isotopic composition of the irradiated sample was then compared with that of normal material. The data obtained is summarized in Table I.

The method of isotopic analysis was as follows. The neodymium oxide was dissolved in $16N$ HNO_3 to produce the nitrate. An aliquot of the solution was then pipetted onto a tungsten ribbon filament and heated in air to form an adherent oxide coat. This filament was then inserted into the source of a 60° direction focussing mass spectrometer. Upon heating, ion currents consisting principally of NdO^+ ions, with very much weaker currents of Nd^+, were detected. Details of the method have been previously published.[3]

For this analysis, normal neodymium and the neutron-irradiated neodymium were introduced alternately into the spectrometer so that an accurate isotopic comparison could be made. The results, tabulated in Table I, are an average of sixty-six individual determinations on two different aliquots of each sample. The comparative values of the cross sections are more reliable than the absolute values. This is due to the fact that with a fixed neutron energy distribution the former depends only on the accuracy of the mass spectrometer measurement, while the latter depends on a knowledge of the integrated flux, or on the absorption cross section for neodymium of normal isotopic composition irradiated under the same neutron flux distribution. The isotopic cross sections given in Table I are computed assuming the flux time obtained from other measurements.[4] Any error in this flux will enter linearly into the cross section and limits given. The cross sections given in brackets are the known activation cross sections.[2]

TABLE I. Isotopic composition of neutron-irradiated neodymium.

Mass No.	Percent abundance normal	Percent abundance bombarded	Net change	Isotopic cross section in 10^{-24} cm²	Contribution to total cross section in 10^{-24} cm²
142	27.13	27.09	−0.04±0.05	<12	<3.5
143	12.20	11.72	−0.48±0.05	240	29.3
144	23.87	24.35	+0.48±0.05	<15	<3.5
145	8.30	8.27	−0.03±0.04	<30	<2.5
146	17.18	17.17	−0.01±0.05	<20 (1.5)	<3.5
147	0.005	<0.005	——		
148	5.72	5.77	+0.05±0.04	<45 (5.5)	<2.5
149	<0.002	<0.002	——		
150	5.60	5.63	+0.03±0.04	<45	<2.5
151	<0.002	<0.002	——		

The data shows that there is one neutron-absorbing isotope in normal neodymium with an isotopic cross section at least six times that of any other isotope. This is the neodymium isotope of mass 143 which by a (n,γ) reaction forms a stable neodymium isotope of mass 144. For the rest of the isotopes it is possible only to assign upper limits to the cross sections. The limits given in the table are tabulated assuming only (n,γ) reactions took place. This is a reasonable assumption since in the graphite of a graphite moderated pile the flux is predominantly slow.

[1] C. Muehlhause, Argonne National Lab., private communication.
[2] 1947 Summary of Nuclear Data, Nucleonics 2, 82 (1948).
[3] Inghram, Hayden, and Hess, Phys. Rev. 72, 967 (1947).
[4] Hayden, Reynolds, and Inghram, Phys. Rev. 75, 1500 (1949).

On the Radius of the Elementary Particle

HIDEKI YUKAWA
*Institute for Advanced Study, Princeton, New Jersey**
June 2, 1949

RECENTLY it was shown[1] that the present theory of quantized fields could be generalized in conformity with the idea of reciprocity proposed by Born[2] to the case, in which field quantities were no longer functions of time and space coordinates alone.[3] The possibility of a theory of such non-localizable fields was illustrated by simple types of scalar neutral zero-mass fields in vacuum. It was further indicated that the theory could be extended to the particle with non-zero rest mass by considering non-localizable fields in five-dimensional space. In this connection, Pais[4] pointed out that the theory of non-localizable fields with non-zero mass could also be formulated in the usual four-dimensional space. In fact, as will be shown in the following paragraphs, the classical rigid sphere model for the electron, which has been believed to be much too classical to be incorporated into quantum theory of fields, can be reproduced as a very simple type of quantized non-localizable fields satisfying postulates of reciprocity.

First we consider a scalar non-localizable field with the mass m satisfying a set of reciprocal commutation relations

$$[x^\mu, p_\nu]=i\hbar\delta_{\mu\nu}, \tag{1}$$
$$[x_\mu[x^\mu, U]]-\lambda^2U=0, \tag{2}$$
$$[p_\mu[p^\mu, U]]+m^2c^2U=0, \tag{3}$$
$$[p_\mu[x^\mu, U]]=0, \tag{4}$$

where x^μ denote contravariant space-time operators with $x^1=x$, $x^2=y$, $x^3=z$, $x^4=ct$, and p_μ $(\mu=1, 2, 3, 4)$ are covariant space-time displacement operators. For any two operators A and B, we write

$$[A, B]\equiv AB-BA. \tag{5}$$

λ is a constant with the dimension of length, which will be interpreted as the radius of the elementary particle described by the field U.[5]

Now the scalar operator U can be expressed as a matrix $(x_\mu'|U|x_\mu'')$ in the representation in which operators x_μ are diagonal. The matrix element $(x_\mu'|U|x_\mu'')$ can alternatively be regarded as a function $U(X_\mu, r_\mu)$ of $X_\mu=\frac{1}{2}(x_\mu'+x_\mu'')$ and $r_\mu=x_\mu'-x_\mu''$. Then (2), (3), and (4) reduce to

$$(r_\mu r^\mu-\lambda^2)U=0, \tag{2'}$$
$$\left(\frac{\partial^2}{\partial X_\mu\partial X^\mu}-\kappa^2\right)U=0, \quad \kappa=mc/\hbar, \tag{3'}$$
$$r^\mu(\partial U/\partial X^\mu)=0. \tag{4'}$$

General form of U satisfying these equations simultaneously is

$$U(X_\mu, r_\mu)=\int\cdots\int (dk)^4(dl)^4\delta(k_\mu k^\mu+\kappa^2)\delta(k_\mu l^\mu)\delta(l_\mu l^\mu-\lambda^2)$$
$$\times b(k_\mu)\exp(ik_\mu X^\mu)\delta(r_1+l_1)\delta(r_2+l_2)\delta(r_3+l_3)\delta(r_4+l_4). \quad (6)$$

δ-functions in (6) are equivalent to restrict two four-dimensional integrations with respect to two vectors k_μ and l^μ to domains satisfying the conditions

$$k_\mu k^\mu+\kappa^2=0, \quad l_\mu l^\mu-\lambda^2=0, \quad k_\mu l^\mu=0. \quad (7)$$

A simple physical interpretation can be given to these restrictions. Suppose that the particle is at rest represented by the plane wave vector $k_1=k_2=k_3=0$, $k_4=\pm\kappa$. In this particular case, the conditions (7) reduce to

$$l_1^2+l_2^2+l_3^2=\lambda^2, \quad l_4=0, \quad (8)$$

which mean that the contribution of the particle at rest to the matrix elements of U is restricted to values of r_μ satisfying

$$r_1^2+r_2^2+r_3^2=\lambda^2, \quad r_4=0. \quad (9)$$

The operator U has a character of the wave amplitude rather than the density itself. However, the density operator, which is quadratic or bilinear in U, has again the matrix elements, which are different from zero only for

$$(r_1/r_2)^2+(r_2/r_2)^2+(r_3/r_2)^2\leqq\lambda^2. \quad (10)$$

Since the above formulation is perfectly relativistic, the whole field U can be regarded as a field theoretical representation of an assembly of elementary particles with the mass m and the radius λ, which move without any change in their form except the Lorentz contraction associated with the change of the proper time axis. Of course, $b(k_\mu)$ should be quantized in the usual way in order to make the correspondence with the particle picture complete.

The above arguments can be extended to the vector field with no essential alteration. The case of the Dirac particle is more interesting. We start from the relations

$$\gamma_\mu'[x^\mu, \psi]+\lambda\psi=0, \quad (11)$$
$$\gamma^\mu[p_\mu, \psi]+mc\psi=0, \quad (12)$$

instead of (2) and (3), where ψ denotes a non-localizable spinor field with four components. γ^μ are well known Dirac matrices

$$\gamma'=i\rho_2\sigma_x, \quad \gamma^2=i\rho_2\sigma_y, \quad \gamma^3=i\rho_2\sigma_z, \quad \gamma^4=\rho_3, \quad (13)$$

forming a four-vector and γ_μ' are also four Dirac matrices

$$\gamma_1'=\rho_3\sigma_x, \quad \gamma_2'=\rho_3\sigma_y, \quad \gamma_3'=\rho_3\sigma_z, \quad \gamma_4'=-i\rho_2, \quad (14)$$

forming a pseudovector.[6] If we again represent ψ by four functions of X_μ and r_μ, we can deduce from (11) and (12) by taking account of the well-known commutation relations between Dirac matrices the result that each of four functions must have the form similar to $U(X_\mu, r_\mu)$ in (6).

Whether a consistent field theory can be constructed by starting from the above model is, of course, an open question, because the introduction of any kind of extended source is almost inevitably accompanied by the departure from the Schrödinger equation. Probably a formalism, which is more or less similar to Heisenberg's S-matrix scheme,[7] will be needed for further developments.

Detailed accounts will be made in later issues of this journal and Progress of Theoretical Physics.

The author wants to express his hearty thanks to Professor Oppenheimer for giving him the opportunity of staying at the Institute for Advanced Study, Princeton, and also to Professor Oppenheimer, Professor Uhlenbeck, and Dr. Pais for stimulating discussions.

* On leave of absence from Kyoto University, Kyoto, Japan.

[1] H. Yukawa, Prog. Theor. Phys. **2**, 209 (1947); **3**, 205, 452 (1948).

[2] M. Born, Proc. Roy. Soc. **A165**, 291 (1938); **A166**, 552 (1938). The idea of reciprocity has been developed since then by Born, Landé, and others in various ways. Very recently, attempts at the problem of masses of elementary particles were made by M. Born, Nature **163**, 207 (1949); H. Green, Nature **163**, 208 (1949).

[3] Non-localizable fields were first considered by Markow, J. Phys. **2**, 453 (1940). More general considerations were made by Born and Peng, Proc. Roy. Soc. Edinburgh **62**, 40, 92, 127 (1944).

[4] The author is indebted to Dr. Pais for informing him of unpublished results.

[5] From the relations (1) and (4), it follows immediately that

$$[x^\mu[p_\mu, U]]=0.$$

[6] λ is not a pure scalar, but a pseudoscalar, which changes sign by reflection. However, the form ot ψ is not altered by the change of sign of λ.

[7] W. Heisenberg, Zeits. f. Physik **120**, 513, 673 (1943); **123**, 93 (1944).

Concerning the High Pressure Allotropic Modification of Cerium*

A. W. Lawson and Ting-Yuan Tang
Institute for the Study of Metals, University of Chicago, Chicago, Illinois
June 1, 1949

CERIUM has long been recognized[1,2] to exist in two variant crystal forms at normal room temperatures and pressures. One structure is face-centered cubic with $a=5.14$A; the other is close-packed hexagonal with $a=3.65$A and $c=5.91$A. In addition, Bridgman[3,4] has reported a high pressure transformation at 12,430 atmospheres which appears to be impurity sensitive, and Trombe and Foex[5] have found dilatometric evidence of a low temperature transformation under certain conditions. Bridgman's[4] latest results on presumably pure cerium indicate an over-all contraction in volume of 16.55 percent at 15,000 atmospheres. Trombe and Foex[5] report a contraction of the order of 10 percent at low temperatures which appears to be associated with an anomaly in the paramagnetic susceptibility.[6] It appears highly probable that both the new phases reported are the same.

Attempts were made to resolve the structure of the low temperature modification from x-ray powder diffraction pictures made at 80°K on pure cerium possessing a face-centered structure at room temperature. This cerium was estimated spectroscopically to contain the following impurities:[7] 0.05 percent Mg, 0.03 percent Si, 0.02 percent Fe, 0.001 percent Cu, 0.001 percent Ag. The instrument used which has a dispersion of 5A/mm was unable to reveal the presence of other rare earths. Unfortunately, we were unable to induce a low temperature transformation in material of this purity. However, no attempt was made to cold-work the metal when it was cold.

Efforts were consequently devoted to obtaining diffraction pictures of the high pressure modification using the beryllium bomb technique developed by Riley and Lawson.[8] Powder patterns, taken at approximately 15,000 atmospheres, reveal as indicated by Table I, that the high pressure modification of the initially face-centered lattice stable at atmosphere pressure is also face-centered cubic! The new structure possesses a lattice constant $a=4.84\pm0.03$A, yielding an over-all volume change at this pressure of 16.5 percent in good agreement with Bridgman. The uncertainty in the result arises largely from the large diameter of the sample ($\frac{1}{32}$ in.) demanded by the mechanical design require-

Table I. Lattice spacings in face-centered cubic cerium* at 15,000 atmospheres.

hkl	$2r$	$2r-\delta$	$d\times10^8$	$a\times10^8$
111	2.02±0.03 cm	1.96 cm	2.75±0.05 cm	4.76±0.09 cm
200	2.30±0.01	2.24	2.42±0.01	4.84±0.02
220	3.23±0.01	3.17	1.71±0.005	4.84±0.02
311	3.78±0.02	3.72	1.46±0.01	4.85±0.03
420	5.14±0.02	5.08	1.077±0.003	4.82±0.02
			Average lattice constant	$a=4.84\pm0.03$

* These spacings were obtained using Mo $K\alpha$ radiation with a camera whose diameter equals 7.57 cm *hkl* are the Miller indices of the reflecting plane, r the radius of the diffraction ring, δ the correction (equal to 0.06 cm) for the thickness of the specimen as determined from similar patterns obtained at atmospheric pressure, d the calculated spacing, and a the calculated lattice constant.

ments of the bomb. Evidence of other lines is present but confused by near coincidence with lines arising from the beryllium. For this reason, they are not included in Table I.

As a result of stimulating conversations with our colleague, W. H. Zachariasen, we propose the following simple model to explain this rather unusual transformation. Cerium, which is the first atom in the periodic table to permit the existence of a $4f$ electron in the free gaseous state, when condensed exhibits the tendency to become perverted from a trivalent to a quadrivalent state. For instance, CeO_2 is the stable oxide. Apparently, the application of 12,000 atmospheres of pressure is sufficient to evoke this transformation and the $4f$ electron is literally squeezed into a $5d$ state. No other model appears capable of explaining the enormous contraction from one closely packed structure to an identical closely packed structure. Quantitatively, this model appears to be supported by the lattice constants observed. Thus, according to W. H. Zachariasen,[9] the ionic radii of trivalent and quadrivalent cerium with a coordination number of 12 should be 1.85 ± 0.01A and 1.71 ± 0.02A, respectively; the lattice constants observed correspond to ionic radii of 1.82A and 1.71 ± 0.02A to which a small correction of about 1.5 percent should be applied for normal compressibility by comparison with the data on lanthanum and praseodymium. If we assume that the phase observed by Trombe and Foex[5] is also a collapsed face-centered structure, the Clapyron equation permits us to make a rough estimate of the energy level separation between the $4f$ and $5d$ states. Such an estimate yields a value of approximately 0.04 ev. In addition, such a change in the electronic configuration of cerium would explain qualitatively the slight decrease in the change of the paramagnetic susceptibility with temperature.[10] Quantitative agreement is not to be expected since the low temperature transformation probably does not go to completion.

The hypothesis proposed above also explains why the transformation, unique to cerium, is absent in lanthanum and praseodymium. In the former, the $5d$ state is known to be the more stable, while in the latter, the $4f$ state is probably sufficiently stable to resist perturbation by pressure in the experimentally available range.

Several related observations deserve mention herein. Below the transformation pressure, the cerium was often partially converted to an alternative form (tentatively identified as a close-packed hexagonal form) which occasionally persisted even at the highest pressures. In view of the lack of reproducibility in the formation of this phase, we believe it to be a metastable form created by the action of unavoidable but variable friction transmitted by the binding cement. Upon sudden release of the high pressure, this form (unmistakably identifiable as close-packed hexagonal) invariably was present and gradually transformed over a period of days to the original face-centered cubic modification. After several weeks the cerium oxidizes and only CeO_2 lines are observed in the diffraction pattern.

In agreement with Bridgman,[4] we observe that below the transformation pressure the compressibility of Ce progressively increases with increasing pressure, accounting for an appreciable fraction (over $\frac{1}{3}$) of the over-all volume change. We believe that this progressive increase in compressibility, terminating in a decisive collapse, is responsible for an increase in amplitude of thermal vibration in the lattice and accordingly explains the anomalous increase of resistance with pressure in Ce, previously reported by Bridgman.[3]

Attempts to produce the transformation in rather impure Ce (containing at least 0.2 percent Fe) existing in the hexagonal modification at atmospheric pressure were unsuccessful.

* This research was supported in part by the ONR under Contract ori-6-20-XX.

[1] A. W. Hull, Phys. Rev. **18**, 88 (1921).
[2] L. I. Quill, Zeits. f. anorg. allgem. Chemie **208**, 273 (1932).
[3] P. W. Bridgman, *The Physics of High Pressures* (G. Bell and Sons, Ltd., London, 1931).
[4] P. W. Bridgman, Proc. Am. Acad. **76**, 55 (1948).
[5] F. Trombe and M. Foex, Ann. d. Chem. **19**, 417 (1944).
[6] F. Trombe, Comptes Rendus **198**, 1591 (1934).

[7] The authors are indebted to Professor Norman Nachtrieb for performing the chemical analyzes.
[8] To be described elsewhere.
[9] Private communication.
[10] C. H. La Blanchetais, Comptes Rendus **220**, 392 (1945).

The Frequency ν_2 in the Infra-Red Spectrum of CH_4

JOHN S. BURGESS
Mendenhall Laboratory of Physics, The Ohio State University, Columbus, Ohio
May 27, 1949

THE infra-red spectrum of methane has been investigated at length by Cooley[1] and Nielsen and Nielsen,[2] and the complex structure of the band ν_4 has been admirably analyzed by Jahn[3] and Childs and Jahn[4] in a series of papers. They accounted for the rotational structure of ν_4 on the basis that there exists a resonance Coriolis interaction between the frequency ν_4 and the optically inactive frequency, ν_2. This analysis has been verified by Shaffer, Nielsen, and Thomas[5] who have presented a theory of the rotation-vibration problem of the tetrahedrally symmetric XY_4 type of molecule complete to second order of approximation.

The Coriolis interaction affects the vibrations somewhat in the following manner. If ν_4 is larger than ν_2, the effective moments of inertia in these states will be, respectively, larger and smaller than the moment of inertia in the normal vibrational state. This should give rise to convergence of the rotational lines in ν_4 toward higher frequencies, and in the frequency ν_2, if it were active, toward lesser frequencies. If, on the other hand, ν_4 is smaller than ν_2, a situation just the reverse of the above should prevail.

The Coriolis perturbation will cause a mixing of the wave functions of the two states so that, if the two frequencies are near enough alike, it should be possible to observe ν_2. This is indeed the case in the molecules SiH_4 and GeH_4 where the two frequencies are separated by 65 cm^{-1} and 114 cm^{-1}, respectively. Tindal, Straley, and Nielsen[6] have reported on the activity of the band ν_2, induced by this Coriolis interaction, for these two molecules. The frequency ν_2 has never been observed in the spectrum of CH_4 principally because it overlaps almost exactly the region of the strong water vapor band. An indication of its existence is nevertheless suggested by the data of Coblentz.[7]

This region has been explored with our vacuum infra-red grating spectrometer, and the band ν_2 has now been observed. The band center has been determined to lie at about 1533.6 cm^{-1} while ν_4 lies at 1305.9 cm^{-1}. The Q branches of these two bands do fold away from each other as is to be expected from the theory outlined above, and the ν_2 band is considerably weaker in intensity.

Complete details of these measurements will be published at a later date.

[1] J. P. Cooley, Astrophys. J. **62**, 73 (1925).
[2] A. H. Nielsen and H. H. Nielsen, Phys. Rev. **48**, 864 (1935).
[3] H. A. Jahn, Proc. Roy. Soc. London **168A**, 469, 495 (1938).
[4] W. H. J. Childs and H. A. Jahn, Proc. Roy. Soc. London **169A**, 451 (1939).
[5] Shaffer, Nielsen, and Thomas, Phys. Rev. **56**, 895, 1051 (1939).
[6] Tindal, Straley, and Nielsen, Phys. Rev. **62**, 151, 161 (1942).
[7] W. W. Coblentz, Pub. Carnegie Inst. Wash., D. C. **I**, 43 (1905).

Note on Measurements of Ambipolar Diffusion in Helium*

MANFRED A. BIONDI AND SANBORN C. BROWN
Research Laboratory of Electronics, Massachusetts Institute of Technology, Cambridge, Massachusetts
June 3, 1949

THE discussion presented in the last paragraph of the article "Measurements of ambipolar diffusion in helium"[1] is in error. The mobility of He^{++} should be $\sqrt{2}$ times the mobility of He^{+} if charge transfer is neglected, and thus would not explain the difference between our measurements and those of Tyndall and Powell. Meyerott[2] has suggested that the theoretical mobility of

He_2^+ agrees with Tyndall and Powell's measured value of 21.4 (cm/sec.) per (volt/cm). The mobility of He^+ in He, neglecting charge transfer, may be determined by the extrapolation of the curve given in Fig. 8 (reference 1) as $\mu_+=26$ (cm/sec.) per (volt/cm). The mobility of He_2^+ should be $\frac{1}{2}\sqrt{3}$ times this value of 22.5 (cm/sec.) per (volt/cm). The agreement between this predicted value and Tyndall and Powell's measured value suggests that they may have measured the mobility of He_2^+. It appears, in any case, that the measurements made by Tyndall and Powell and in our experiment are for two different ions, but the exact identity of the ions in each experiment is not known. Mass spectrographic analysis of our ions is planned.

* This work has been supported in part by the Signal Corps, the Air Materiel Command, and ONR.

[1] M. A. Biondi and S. C. Brown, Phys. Rev. **75**, 1700 (1949).
[2] R. Meyerott, Phys. Rev. **70**, 678 (1946).

Comment on the Nuclear Capture of Negative Mesons

J. BARNOTHY
Barat College, Lake Forest, Illinois
June 7, 1949

A NUMBER of different authors have observed that when negative mesons are stopped in an element with high atomic number the negative mesons do not undergo the normal decay process and it was therefore assumed that they are captured by the nuclei. This interpretation, however, encounters some difficulties because it does not explain the failure to detect stars at the end of such meson tracks.[1] I would like to suggest an explanation to account for the fact that no decay electrons were observed if lead was used as stopping material.

If—and this is rather plausible—the negative meson is captured on a K-shell, then almost the double of the K-shell energy of the meson is needed to liberate the decay electron from the atomic binding. Hence, the decay electron of a meson disintegrating in lead will lose 38.6 Mev of its energy merely in order to be able to get out from the atom. This energy loss is rather considerable, since 54 Mev represents the upper limit of the energy of the decay electrons. It seems rather reasonable to assume that no decay will occur whenever the electron does not obtain an energy sufficient for leaving the K-shell and hence these latter cases might bear the aspect of a nuclear capture leading to no stars at the end of the meson track.

For example, in Retallack's[2] experimental arrangement, where lead plates were placed in the cloud chamber, he observed a total of 27 negative meson tracks stopped in lead. Computing with the same 31 percent probability, experimentally found for positive mesons which can get out of the lead plate and produce a track in the cloud chamber, we would have to expect 8 decay electron tracks, whereas only one was observed. If, however, 38.6 Mev are needed in order that a decay electron should be able to leave the lead atom, and, moreover, we assume a continuous spectrum of the decay electrons between 5 Mev and 55 Mev with a most probable electron energy of about 40 Mev, then we immediately see that out of the 27 negative mesons merely 9 electrons could get out of the lead atom. Moreover, these 9 electrons will have energies between 0 and 15 Mev, hence it is most probable that only about one of them can emerge from the lead plate and produce a track in the cloud chamber.

In order to test the validity of the above given interpretation, it would be of interest to perform cloud-chamber measurements by using as stopping material, for instance, barium, in which case the energy loss of the electron within the atom would amount to 18 Mev, hence we would have to expect a shifting in the energy spectrum of the electrons by 18 Mev toward lower energies.

Our interpretation of the failure to detect decay electron tracks from lead does not, however, explain the apparent shortening of the lifetime of negative mesons in lighter materials (NaF; Al: S) because even for iron the decay electron needs only 3.9 Mev to be released from the meson K-shell, hence this energy loss is quite negligible as compared with the average initial energy of the electron. It remains an open question whether we are confronted, in the apparent lifetime shortening of the negative mesons, with a nuclear capture[3] or with a true decrease of the lifetime occurring in the K-shell.[4] Anyhow, the missing decay electron tracks from lead can no longer be considered as a proof in favor of the nuclear capture conception.

The author would like to point out that similar experiments performed with cloud chambers and by using as stopping materials substances with atomic numbers ranging between sulfur and iron will probably decide between the above-mentioned two alternatives. Because in these materials a quite considerable shortening of the lifetime is to be expected, whereas the energy needed for the electron to leave the K-shell of the meson is still quite negligible.

[1] W. Heisenberg: *Vorträge über kosmische Strahlung* (Berlin, 1943); J. A. Wheeler, Phys. Rev. **71**, 321 (1947).
[2] J. G. Retallack, Phys. Rev. **73**, 921 (1948).
[3] H. K. Ticho and M. Schein, Phys. Rev. **72**, 248 (1947).
[4] G. E. Valley and B. Rossi, Phys. Rev. **73**, 177 (1948).

Spontaneous Decay Rate of Heavy Mesons

L. I. SCHIFF
Stanford University, Stanford, California
May 31, 1949

THE assumption of a direct coupling between heavy (π) and light (μ) mesons that leads to the observed rate of $\pi-\mu$-decay, also explains the observed rate of capture of negative μ-mesons by nuclei as a second-order process.[1] Alternatively, it has been proposed[2] that μ-mesons are directly coupled to nucleons. This latter assumption leads to $\pi-\mu$-decay as a second-order process even if no direct $\pi-\mu$-coupling is postulated.[3] If, in addition, a direct coupling between electrons (e) and nucleons is assumed,[2] $\pi-e$ decay also appears as a second-order process. A comparison of the rates of $\pi-\mu$- and $\pi-e$-decay with observation can therefore be expected to throw some light on the validity of the assumption of direct couplings of μ-mesons and electrons with nucleons.

It is assumed in this note that π-mesons are scalar particles μ-mesons, electrons, neutrinos (ν), neutrons (N), and protons (P) are all Dirac particles, and that all couplings are of the scalar type that involve the Dirac β-operator. The interaction term in the Hamiltonian then has the form

$$H'=G\int\psi_\pi(\psi_P^*\beta\psi_N)d\tau+g_\mu\int(\psi_\nu^*\beta\psi_\mu)(\psi_P^*\beta\psi_N)d\tau + g_e\int(\psi_\nu^*\beta\psi_e)(\psi_P^*\beta\psi_N)d\tau+\text{c.c.} \quad (1)$$

The strength of nuclear forces gives G the approximate value $(4\pi\hbar c^3/3)^{\frac{1}{2}}$. The interaction (1) leads to a reciprocal mean life for decay of a π-meson at rest

$$\frac{1}{\tau_\pi}=\frac{G^2g^2p^2}{2\pi^5m\hbar^5c^5}\left|\int_0^\infty\frac{P^4dP}{(P^2+M^2c^2)^{\frac{1}{2}}}\right|^2. \quad (2)$$

In (2), m is the mass of the π-meson, p is the momentum of the emitted neutrino, M is the mass of the nucleon, and the integration is carried over all intermediate nucleon momenta P. The formula gives $1/\tau_{\pi\mu}$ or $1/\tau_{\pi e}$ according as g is given the value g_μ or g_e. A term $\pm mc$ has been neglected in the energy denominator in comparison with $(P^2+M^2c^2)^{\frac{1}{2}}$.

The divergence of the integral in (2) places any quantitative conclusions drawn from this formula on doubtful ground. Since, however, this integral is the same for the rates of both $\pi-\mu$- and $\pi-e$-decay, it cancels out of their ratio, to give

$$\tau_{\pi\mu}/\tau_{\pi e}=(g_e^2p_e^2/g_\mu^2p_\mu^2); \quad (3)$$

p_μ and p_e are the momenta of the neutrinos emitted in the two modes of decay. If we assume, as suggested by Tiomno and

Wheeler,[2] that g_μ and g_e are likely to be equal, the ratio (3) is approximately equal to 4. If, on the other hand, we adopt their best observational values $g_\mu \cong 10^{-49}$ erg-cm^3 and $g_e \cong 2.2\times 10^{-49}$ erg-cm^3, the ratio is approximately equal to 20. In both cases, there is clear disagreement with recent results at Berkeley,[4] which indicate that the ratio (3) is substantially less than unity.

An estimate for the magnitude of the integral in (2) can be obtained by taking its upper limit to be roughly equal to Mc; this is equivalent to assuming that nucleon theory is valid in the non-relativistic domain, and that relativistic intermediate states can be ignored. Alternatively, the self-energy of a π-meson at rest due to intermediate nucleons can be calculated, and set equal to mc^2. The same integral appears (again with neglect of a factor $-mc$ in the energy denominator), and the values obtained for it in the two ways are approximately the same. When the latter evaluation of the integral is used, and g_μ is taken equal to 10^{-49} erg-cm^3 in order to obtain agreement with the rate of nuclear capture of negative μ-mesons, we obtain $\tau_{\pi\mu} \cong 2.3\times 10^{-9}$ sec., which is in fair qualitative agreement with the observed value.[5] This makes the computed mean life for $\pi - e$ decay much too small to agree with experiment; while the discrepancy could be removed by the assumption of a direct $\pi - e$ coupling that largely cancels the second-order contribution, this is a rather unlikely possibility. Thus, it would seem that the rate of nuclear beta-decay is too large to be consistent with the small rate of $\pi - e$ decay, if either $\pi - e$ coupling[1] or nucleon-electron coupling is assumed by itself.

The interaction (1) also leads to $\mu - e$ decay as a second-order process, but the rate computed in this way is far too small to agree with experiment.

[1] L. I. Schiff, Phys. Rev. **74**, 1556 (1948); A. S. Lodge, Nature **161**, 809 (1948); S. Hayakawa, Prog. Theor. Phys. **3**, 200 (1948); R. F. Christy and R. Latter (to be published).
[2] J. Tiomno and J. A. Wheeler, Rev. Mod. Phys. **21**, 153 (1949); T. D. Lee, M. Rosenbluth and C. N. Yang, Phys. Rev. **75**, 905 (1949).
[3] R. E. Marshak, Phys. Rev. **75**, 700 (1949). R. Latter and R. F. Christy, Phys. Rev. **75**, 1459 (1949).
[4] Private communication.
[5] J. R. Richardson, Phys. Rev. **74**, 1720 (1948).

Production of π-Mesons by High Energy Nucleons*

E. Strick and D. ter Haar
Department of Physics, Purdue University, Lafayette, Indiana
June 6, 1949

In connection with the programs of accelerators under way in this country, it seemed useful to collect as many data as possible about the production of mesons by high energy particles. When looking through the literature we found that for the case where the bombarding particle is a high energy nucleon, two different results had been obtained. Using straightforward third-order perturbation methods, Urban and Schwarzl[1] obtained for the cross section σ:

$$\sigma = 4(g^2/\hbar c)^3(M/\mu)^2(Mc^2/E_0)^2(\hbar/Mc)^2 \log(M/\mu), \qquad (1)$$

where g is the coupling constant, M the mass of a nucleon, μ the mass of the π-meson, and E_0 the energy of the bombarding nucleon. Equation (1) and also the following equations give only the first terms in a series expansion in inverse powers of E_0. This paper was essentially a corrected version of the paper of Nordheim and Nordheim[2] who had arrived at practically the same result, although using an incorrect expression for the perturbation matrix element. As in the following, a charged scalar field was assumed. Independently, the result of Eq. (1) was obtained by us[3] making the same simplifying assumptions.

A different result, however, was obtained by Wang[4] using the Weizsäcker-Williams method. His result was

$$\sigma = K(g^2/\hbar c)^3(M/\mu)(Mc^2/E_0)(\hbar/Mc)^2, \qquad (2)$$

where K is a constant of the order of magnitude unity.

Since it seemed to us that the Weizsäcker-Williams method should give reliable results for high energies, we have performed the third-order perturbation calculations, now retaining all terms. It then turned out that the final result is essentially identical with Wang's formula. Our final result is

$$\sigma = (\pi/8)(g^2/\hbar c)^3(M/\mu)(Mc^2/E_0)(\hbar/Mc)^2. \qquad (3)$$

It is interesting to note that formula (3) does not give an E_0^{-2} dependence as one might expect from dimensional considerations,[5,6] thus indicating a dependence of the matrix element on energy. The difference between formulas (1) and (3) arises from the fact that in the evaluation of the matrix elements, Urban and Schwarzl,[1] as well as the present authors in their preliminary calculations,[3] neglected terms arising from the momentum of the virtual meson which were taken into consideration in the calculations leading to formula (3). Recoil was also taken into account, but this did not influence the final result.

We should like to express our sincere thanks to Professor H. Wergeland for discussions on the subject of this letter. Detailed calculations will be published in a report of the Purdue Synchrotron Project to the ONR.

* Partly assisted by the ONR.
[1] P. Urban and F. Schwarzl, Acta Phys. Austriaca **2**, 368 (1949).
[2] L. W. Nordheim and G. Nordheim, Phys. Rev. **54**, 254 (1938).
[3] E. Strick, Phys. Rev. **76**, 100 (1949).
[4] F. S. Wang, Zeits. f. Physik **115**, 431 (1940).
[5] W. G. McMillan and E. Teller, Phys. Rev. **72**, 1 (1947).
[6] D. ter Haar, Science **108**, 57 (1948).

Note on the Resistivity of Gold at Low Temperatures

C. T. Lane
Sloane Physics Laboratory, Yale University, New Haven, Connecticut
May 25, 1949

As is well known, the wave function of an electron in a perfectly periodic potential field consists of a plane non-attenuated wave, modulated with the period of the potential. In Bloch's model of a solid, the periodicity of this potential is equal to the periodicity of the lattice ions. It follows, therefore, that in such an ideal solid an electron would experience no scattering or in other words the electrical resistivity should be zero.

The above is a fundamental property of an ideal (i.e., rigorously periodic) lattice and is deduced from quantum mechanics without any approximation being involved. If one now inquires as to how closely any real crystal approximates this model, the following modes of departure may be envisaged:

(1) If the situation is such that the states in the lowest Brillouin zone are completely occupied by electrons, and an energy gap between it and the next higher zone exists (no overlap), we should, in the vicinity of absolute zero, have no net current, i.e., the crystal would be an insulator with an infinite resistivity at 0°K.

(2) In the more pertinent case of a monovalent metal such as gold with a half-occupied first zone, departures of the lattice from perfect periodicity can be due to the following: (a) Finite excitation of the Debye waves. This is temperature dependent and will vanish at the absolute zero. (b) Strains and impurities. (c) Crystallite boundaries in polycrystalline material.

These last three will, of course, be temperature independent at low temperatures. Accordingly, as the temperature approaches absolute zero, the resistivity of a conductor should approach zero or at most become temperature independent due to (b) and (c).

In view of all this, the observation made by de Haas, de Boer, and van den Berg[1-3] some years ago that the resistivity of pure gold increased as the temperature was lowered below about 3°K seems exceedingly strange. While all their measurements were made with polycrystalline specimens, even their purest sample (impurity $\sim 10^{-4}$ percent, mainly Cu and Ag) showed a definite minimum in the resistance-temperature curve, although it is true that less pure material gave a more pronounced effect. The

resistance of one specimen continued to rise at temperatures as low as 0.4°K, and, in fact, seemed to be approaching infinity at absolute zero. These authors concluded that the minimum is not due to spurious causes such as gas absorption or unavoidable disturbances caused by the current and potential leads to the specimens.

The only other published measurements on gold appear to be those of Meissner.[4] Here, measurements on gold monocrystals (impurities $\sim 10^{-3}$ percent) showed no minimum down to 1.3°K, a temperature well below the minimum temperature found necessary by the Leiden investigators.

If the effect reported by the Leiden group should prove to be real (i.e., not due to impurities or some similar cause), then it appears that a rather fundamental violation of the basic quantum theory of solids has appeared. Thus, a monovalent substance like gold, where the Fermi surface in the first zone is presumably nearly spherical and far from a zone boundary, approaches the ideal Bloch model closely—the conduction electrons are nearly "free." Presumably, one would then have to go a step further than the present theory of solids and consider the possibility of electron interaction—a mechanism which has sometimes been suggested as responsible for superconductivity.

It seems more plausible to suppose that the effect is of a secondary nature, and in some way connected with the crystallite boundaries in the polycrystalline material. Thus, Meissner's single crystals do not show the effect even though the impurity content of his material was about ten times as large as that used by de Haas and collaborators. It may, of course, be that in the process of growing single crystals, Meissner automatically purified his material—such a process has been used for refining, the impurities being "flushed" to one end of the crystal, and this end then rejected.

It might, therefore, be of interest to re-examine this matter, making use of both single crystal and polycrystalline specimens fabricated from the same material and each having the same impurity content.

[1] de Haas, de Boer, and van den Berg, Physica **1**, 1115 (1934).
[2] W. J. de Haas and G. J. van den Berg, Physica **4**, 683 (1937).
[3] de Haas, Casimir, and van den Berg, Physica **5**, 225 (1938).
[4] W. Meissner, Zeits. f. Physik **38**, 647 (1926).

Magnetic Effects of a Rotating Superconductor*

W. F. Love, R. F. Blunt, and P. B. Alers
The Rice Institute, Houston, Texas
June 8, 1949

It was discovered by Meissner[1] that when a substance goes superconducting in a small magnetic field, the magnetic induction vector $B=0$. What is often observed is a Meissner effect varying anywhere from no effect at all to the complete effect, and this seems to depend on the degree of impurity, geometrical shape, and whether or not the specimen is a single crystal.[2] We have studied the frozen-in magnetic flux of superconducting tin whose total impurity is 0.012 percent. The tin was melted in a vacuum furnace and allowed to cool slowly after the manner of forming a single crystal. Ultrasonic pulses at 10 megacycles per second showed no evidence of flaws. The specimen was in the shape of a cylinder with well-rounded edges, approximately an ellipsoid, and mounted in Textolite such that it could be rotated about its long axis. The rotor of tin was enclosed in a lead shield so that with the lead superconducting, the magnetic field around the tin was not changed by external effects. With the lead housing superconducting, the magnetic field between the lead wall and the normal conducting tin rotor was about 0.01 gauss and remained unchanged (± 0.00005 gauss) with variation in the angular position of the tin rotor. Cooling further, the magnetic field detector, which was placed between the tin rotor and the lead housing, showed the Meissner effect as the tin rotor became superconducting and flux was pushed out of it.

The superconducting tin rotor showed a very pronounced frozen-in flux (incomplete Meissner effect) in that the magnetic field at the detector now varied sinusoidally with the angular position of the rotor. The frozen-in flux threaded through the superconducting tin in an orientation determined by the magnetic field within the lead housing. That is to say, the magnetic moment locked into the superconducting tin was independent of the angular orientation of the rotor with respect to the lead housing when the transition temperature was passed. Thus, there was no special path of impurities or structure flaws through the tin rotor for the frozen flux to choose. The frozen magnetic flux showed no observable relaxation effects over a period of five minutes.

A Meissner effect has been observed when the specimen has been cooled while rotating at 5000 revolutions per minute. On the stopping rotation the specimen showed no frozen flux. The magnetic field was observed to penetrate the rotor (reverse Meissner effect) when the temperature was then raised through the transition point. Magnetic fields were detected by the "magnetic airborne detector," AN-ASQ-3, kindly supplied by the Office of Naval Research.

We may conclude that when a solid ellipsoid of pure tin goes superconducting it may do two things with the magnetic flux which existed within its body. It may eject part of the flux, corresponding to the Meissner effect, by setting up macroscopic currents described by the theory of F. and H. London,[3] and this current does not move with the rotor as it is turned but stays fixed with respect to the external field. The remainder exhibits the intermediate state proposed by Gorter and Casimir[4] wherein magnetic flux is crowded into small regions where the critical field is exceeded, and this flux is supported by annular superconducting currents which we have observed to stay fixed with respect to the rotor. The earlier experiments by Onnes and Tuyn[5] support these conclusions. The authors acknowledge with pleasure the directing guidance of Professor C. F. Squire and the many helpful discussions with Professor W. V. Houston.

* Research supported by the ONR, Contract N6onr-224.
[1] W. Meissner and R. Ochsenfeld, Naturwiss. **21**, 787 (1933).
[2] K. Mendelssohn, Proc. Roy. Soc. **A155**, 558 (1936).
[3] F. and H. London, Proc. Roy. Soc. **A149**, 71 (1935).
[4] C. J. Gorter and H. Casimir, Physica **1**, 305 (1934).
[5] H. K. Onnes and W. Tuyn, Leiden Comm. Suppl. No. 50a.

The Viscosity and Thermal Conductivity of Mixtures of He^3 and He^4

K. S. Singwi and L. S. Kothari
Department of Physics, University of Delhi, India
May 31, 1949

Recently Ter Haar and Wergeland,[1] using Tisza's phenomenological picture of the viscosity of He^4, have estimated the influence of an admixture of He^3 to the He^4 liquid. Their expression for the increase in viscosity due to a fraction x of He^3 in He^4 liquid is

$$\Delta\eta = x(\eta_3^{\text{kin}} - \eta_4^{\text{kin}}) \approx x\eta_3^{\text{kin}}. \quad (1)$$

In deducing (1) the kinetic viscosity of He^4 is neglected in comparison to that of He^3, and also the dynamic viscosity of both He^3 and He^4 is assumed to be the same.

In calculating η^{kin} from the well-known expression

$$\eta^{\text{kin}} = \tfrac{1}{3}\rho\bar{c}\Lambda,$$

these authors have assumed that the mean free path Λ is equal to $m/\sqrt{2}\pi d^2$. This, however, is not justified, since in a degenerate Fermi-Dirac gas the mean free path Λ increases with decreasing temperature because the number of possible collisions is greatly reduced because of the exclusion principle. Indeed, at a temperature T, the possible transitions are limited to the states of the "Maxwell tail" beyond the maximum zero point energy $E_m = (\hbar^2/2M)(3\rho/8\pi M)^{\frac{1}{3}}$: In velocity space such cells roughly fill a spherical cell of radius $v_m = (2E_m/M)^{\frac{1}{2}}$ and thickness

$\Delta v = \Delta E/P_m \sim kT/(2ME_m)^{\frac{1}{2}}$. The mean free path Λ is given by

$$\Lambda \approx \frac{M}{\rho S(\Delta v/v_m)^2} \approx \frac{M}{\rho}\frac{1}{S}\left(\frac{E_m}{kT}\right)^2, \tag{2}$$

where S is the collision cross section.

In a degenerate Fermi-Dirac gas, the coefficients of viscosity η and heat conductivity χ may be written in the familiar form

$$\eta = \alpha_\eta \tfrac{1}{3}\rho v \Lambda_\eta, \tag{3a}$$

$$\chi = \alpha_\chi \tfrac{1}{3}\rho v C_v \Lambda_\chi. \tag{3b}$$

where α's are the numerical factors and v is the mean velocity of the particles. The specific heat C_v per unit mass is given by

$$C_v = \pi^2/2(k^2T/ME_m). \tag{4}$$

Using (2) and (4) in (3) we have

$$\eta_3 = \alpha_\eta \frac{1}{3}\frac{h^5}{2^{5/2}M_3^2}\left(\frac{3\rho_4}{8\pi M_4}\right)^{5/3}\frac{1}{S}\frac{1}{(kT)^2}, \tag{5a}$$

$$\chi_3 = \alpha_\chi \frac{\pi^2}{12}\frac{h^3}{M_3^2}\left(\frac{3\rho_4}{8\pi M_4}\right)\frac{1}{ST}, \tag{5b}$$

where we have taken $\rho_3/M_3 = \rho_4/M_4$.[1]

In the following rough calculation we have assumed $S = \pi d^2$, where $d = 2.9\times10^{-8}$ cm, and have taken α to be equal to unity.* We shall also assume $\rho_4 = 0.145$ g/cc, since the density of He^4 does not change appreciably over the whole range of temperatures for which He^3 constitutes a degenerate gas (the degeneracy parameter $A = 10T^{-\frac{1}{2}}$). In Table I we have given (1) the changes in viscosity for $x = 0.01$ and (2) $x\chi_3$.

TABLE I. Calculated values for the change in viscosity for $x = 0.01$ and for the product $x\chi$

T in °K	1.6	1.8	2.0	2.1	2.2	2.4	3	4
η_4 in μp^2	0.18	0.35	0.80	1.5	15	22	25	28
Ter Haar $\Delta\eta/\eta_4$	0.35	0.18	0.079	0.042	0.0042	0.0029	0.0025	0.0022
Our value $\Delta\eta/\eta_4$	6.4	2.6	0.92	0.44	0.040	0.023	0.013	0.0065
$x\chi_3$ in c.g.s.	58.8	52.3	47.1	44.8	42.8	39.2	31.4	23.5

The values as computed by us are higher than those given by Ter Haar and Wergeland, as is expected. The values are, however, uncertain on account of our lack of exact knowledge of α and S.

It may be noted that the maximum value of heat conductivity of He^4, as determined experimentally, is nearly 300 cal. cm^{-1} $deg.^{-1}$ $sec.^{-1}$ at 2°K; whereas this value for pure He^3, at the same temperature, as computed by us is 4710 c.g.s. units.

Our thanks are due to Professor D. S. Kothari and Professor R. C. Majumdar for their kind interest in this work.

[1] D. Ter Haar and H. Wergeland, Phys. Rev. **75**, 886 (1949).
[2] W. H. Keesom, *Helium*, p. 271.
* In an exact calculation the numerical coefficients α and the collision cross section S will have to be evaluated rigorously. We shall do so in a future paper.

Polarization of Mesons Produced at Threshold in Gamma-Nucleon Collisions

DANIEL B. FEER
The Institute for Advanced Study, Princeton, New Jersey
May 27, 1949

WENTZEL[1] has proposed using the anisotropy in the angular distribution of μ-mesons resulting from the decay of a polarized beam of integral spin mesons to determine the spin of the π-meson. Such a beam can be produced near threshold in nucleon-nucleon collisions; however, as pointed out by Wentzel, precession in strong magnetic fields, which will occur during the π-meson lifetime, which varies by about 10^{-8} sec. will blur the polarization effect, and hence the experiment cannot be performed directly inside a cyclotron tank.

The polarization of mesons produced in gamma-nucleon collisions, as from the gamma-ray beam from a synchrotron, has accordingly been examined. The ratio of the cross sections for production of longitudinal and transverse mesons has been calculated at exact threshold, taken to be mc^2 ($m = \pi$-meson mass) since terms of order m^2/M^2 (M = nucleon mass) are neglected. This quantity has the values shown in Table I. 0 denotes complete

TABLE I.

Field	Coupling	Cross section ratio
Vector	Vector	0
Vector	Tensor	0.4
Pseudovector	Pseudovector	∞
Pseudovector	Dual-tensor	0

transverse polarization, ∞ complete longitudinal polarization. The complete polarization will be reduced by terms of order m^2/M^2, which will be a small effect.

These results, and, in particular, the difference between vector and pseudovector fields, can be simply understood as follows. There are four processes which can produce this effect: a direct interaction coupling the four particles involved, and three others involving the creation of virtual mesons or nucleons and the absorption of the photon. For example, for vector-type coupling, the direct interaction term is of the form,

$$u_n^* o u_p \mathbf{A}\cdot\mathbf{V}, \tag{1}$$

the u's being the nucleon wave function, $\mathbf{A}$ the transverse vector potential, and $\mathbf{V}$ the meson wave function. For a vector field o is the unit operator, and for a pseudoscalar field it is γ_5. Since near threshold, $\gamma_5 = v/c = m/M$, the contribution of the term (1) to the cross section is smaller by m^2/M^2 for pseudovector fields than for vector fields. Thus, while this term will produce transversely polarized mesons of both types, it will not be appreciable for the pseudovector field. A similar investigation of other terms shows that they give mainly longitudinal polarization, which dominates for the pseudovector field.

The corresponding analysis for the vector field with tensor coupling, together with the fact that one must average over the unknown polarization of the incident gamma-rays, verifies the result that only this case does not give complete polarization.

The anomalous magnetic moment of the nucleon will enter only in the one process which involves the photon-nucleon interaction. This term is of the form

$$\lambda(m/M)(e\hbar/mc)u_n^*\boldsymbol{\beta\sigma}\cdot\mathbf{H}u_p;$$

since the photon's momentum is mc, the factor m/M means that this contribution will never be a dominant one.

In an actual experimental situation, one must consider both the internal motion of the bombarded nuclei and the fact that a continuous gamma-ray beam producing mesons with a wide range of kinetic energies is actually used. For mesons with a kinetic energy up to about 20 Mev, the values of v/c involved are of the order m/M; new terms introduced into the matrix elements will be of this order and lead to terms in the cross section of order m^2/M^2, which have been consistently neglected.

It is thus possible to produce near threshold a beam of polarized integral-spin mesons by the synchrotron gamma-ray beam. Since there appear to arise no new depolarizing effects other than those discussed by Wentzel, and since the experiment can be performed outside the tank, thereby eliminating the effect of magnetic fields on Wentzel's experiment, it seems that such an experiment might give useful information on the π-meson spin.

I wish to thank Dr. Oppenheimer for suggesting this problem, and the Institute for Advanced Study for a grant-in-aid-of-research from the AEC.

[1] G. Wentzel, Phys. Rev. **75**, 1810 (1949).

Decay Scheme of Ni^{65}

KAI SIEGBAHN AND AMAL GHOSH
Nobel Institute for Physics, Stockholm, Sweden
June 6, 1949

SWARTOUT, *et al.*,[1] and Conn, *et al.*,[2] have shown that the 2.6^h activity of Ni is due to the mass number 65 and not, as was previously thought, to 63. This isotope, which decays by β- and γ-emission has earlier been studied by absorption methods[3] and also β-spectroscopically.[4] The upper limit of the β-spectrum was determined (abs.) to be 1.9 Mev. The γ-radiation was shown to have an energy of 1.1 Mev according to abs. measurements, and spectrometrically three photo-lines (from a Pb converter) were obtained, corresponding to the γ-energies 0.280, 0.65 and 0.93 Mev.

We have recently studied the decay scheme of this isotope using spectrometer and coincidence technique.[5] The β-spectrum appears to consist of three components with upper limits 0.60 Mev, 1.01 Mev and 2.10 Mev and with relative abundances 29 percent, 14 percent, and 57 percent. The γ-ray energies were found to deviate rather widely from those reported before, and turned out to be 0.37 Mev, 1.12 Mev, and 1.49 Mev from spectrometric measurements. Additional $\beta\gamma$- and $\gamma\gamma$-coincidence measurements support the decay scheme given in Fig. 1. According to this scheme the highest excited level in Cu^{65} can be de-excited *either* by the direct emission of one quantum of 1.49 Mev *or* two of 0.37 Mev and 1.12 Mev in cascade. The fact that these two competing processes occur simultaneously and with roughly the same probability suggests that the very much higher transition probability of the high energy quantum (cross-over transition) gets reduced to almost the same probability as for the 0.37-Mev transition because of selection-rules. From the intensities and energies of the three β-components one would conclude, according to their "*ft*"-values[6] that the softest one is allowed while the other two are first forbidden.

Using GT selection rules for β-decay it is possible to assign a limited number of spin alternatives for the different levels. From the same selection rules the parities of the different states can be (starting with Ni^{65}): even (or odd), even (or odd), odd (or even), odd (or even).

Numerically one can compute that in order to give the same order of magnitude of transition probability for the 0.37- and 1.49-Mev γ-radiation their "effective" l-values have to differ by one unit, e.g., if the l-value of the 0.37-Mev γ-ray is 2 the l-value of the 1.49-Mev γ-ray should be 3. In that case the corresponding decay constants for the two transitions come out to be roughly equal according to Segré-Helmholz[7] formula. One consequence of the γ-selection rules by Dancoff and Morrison[8] is that if the parity changes at a transition, only odd effective l-values can occur (e.g., the l-value, which has to be put into the formula for the decay constant computation, which is the order of the minimum allowed electric multipole), and if the parity remains the same, only even effective l-values occur. In the present case this would mean that the parity of the ground state and the first excited state in Cu^{65} should be opposite, or that of the ground state and the second excited state should be the same, in contradiction to the conclusions drawn from β-selection rules.

If we, for instance, consider the simple case when the second and first excited level and the ground state of Cu^{65} have the spins and parities (7/2, *e*), (5/2, *e*), (3/2, *o*), the following predictions can be made. The 0.37-Mev γ-ray would be expected to consist of 2^2-pole electric and 2^1-pole magnetic radiation. The 1.49-Mev γ-ray would consist of 2^3-pole electric and 2^2-pole magnetic radiation. The effective l-value in the last case is then one unit higher than the former case which explains the simultaneous existence of both these γ-rays. A change of parity of the first excited level in Cu^{65} would, however, require that the β-component going to this level should be second forbidden or allowed which seems difficult to combine with the experimentally found *ft*-value ($8.4 \cdot 10^5$).

The other alternative is to investigate the parity sequence *e*, *o*, *e*. In that case the electric components of the two γ-rays, assuming

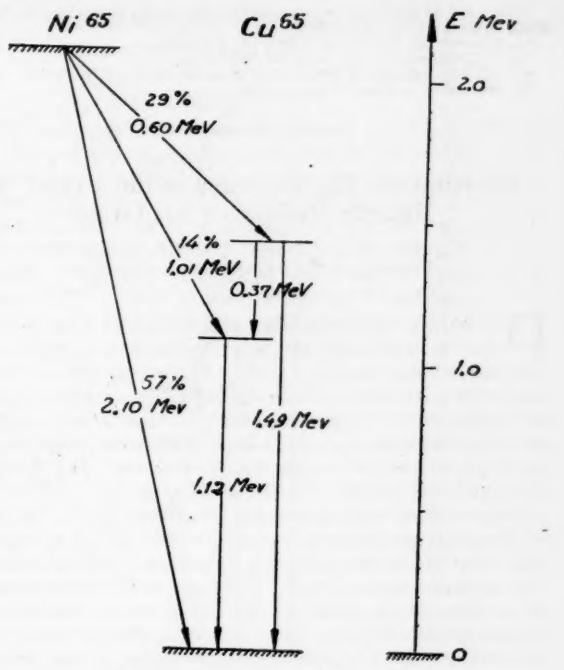

FIG. 1. Decay scheme of Cu^{65}.

the same spin values before, turn out to be 2^1-pole and 2^2-pole, effective l-values 1 and 2, respectively. This combination also fits the transition probability calculation since the difference in effective l-values is 1. In order to get this parity sequence we instead have to require that the β-component going to the ground state is second forbidden, which is only somewhat more probable than in the previous case since its *ft*-value is $3.9 \cdot 10^6$. This assignment is however still far from satisfactory.

If, however, one can allow a deviation of about a factor of 100 in the calculations of the relative radiation probabilities for competing transitions from the same level, then from our values the combination with $l=1$ for both 0.37-Mev and 1.49-Mev γ-rays would also be possible. In that case the β-selection rules regarding the parity would not have to be violated. The nature and multipole order, however, would be the same for both the γ-rays, namely electric dipole and magnetic quadrupole. The corresponding spins are then, starting from the ground state of Cu^{65} : 3/2, 7/2, 5/2. These spin values do not contradict G.T. selection rules.

It has been suggested to us by Professor Lamek Hulthén that selection rules concerning parity perhaps may be more complicated because of spin orbit coupling. If each state can consist of an admixture of *S*, *P*, *D*$\cdots$eigenfunctions (which is very probably the case in H^3 and He^3),[9] the parity has both odd and even character. It is still difficult to know what such parity admixtures can do to selection rules at heavier nuclei, such as Ni and Cu.

A fact of particular interest is that the first excited level in Cu^{65} of 1.12 Mev evidently also is obtained in the Zn^{65} e^+K disintegration, since this isotope is known to emit a γ-ray of just this energy when decaying to Cu^{65}. Hitherto only a few similar cases have been investigated but they can probably be expected to occur rather frequently when looked for. Especially in more complicated schemes such information can be useful to secure the order of emission of several γ-rays.

[1] Swartout, Boyd, Cameron, Keim, and Larson, Phys. Rev. **70**, 232 (1946).
[2] Conn, Brosi, and Sartout, Phys. Rev. **70**, 768 (1946).
[3] J. J. Livingood and G. T. Seaborg, Phys. Rev. **53**, 765 (1938); F. A. Heyn, Physica **4**, 1224 (1937).
[4] A. Guthrie, Phys. Rev. **60**, 746 (1941).

[5] For a full account of the experiments, the reader is referred to Ark. f. Mat., Astr. o. Fysik **36A**, 19.
[6] J. Konopinski, Rev. Mod. Phys. **15**, 209 (1943).
[7] A. C. Helmholtz, Phys. Rev. **60**, 415 (1941).
[8] A. M. Dancoff and P. Morrison, Phys. Rev. **55**, 122 (1939).
[9] L. Rosenfeld, *Nuclear Forces*, p. 405.

Experimental Corroboration of the Theory of Neutron Resonance Scattering

R. K. Adair, C. K. Bockelman, and R. E. Peterson
University of Wisconsin, Madison, Wisconsin
June 3, 1949

DETAILED theoretical investigations have been made on the variations of the cross section with energy near a neutron scattering resonance.[1,2] In particular, the phenomenon of destructive inteference between resonance and potential scattering has been predicted. Until now, however, there has been no definite experimental evidence of this effect. While measuring the total cross section of sulfur, a resonance was observed which shows the effect predicted by theory particularly clearly.

Cross sections were determined from transmission measurements using monoenergetic neutrons from the Li(p,n) reaction. The width of the neutron energy distribution was estimated at 7 kev for measurements made at an angle of 115° with respect to the incident proton beam, and 11 kev for points taken in the forward direction. Measurements were made over an energy range from 16 kev to 250 kev using a procedure similar to that previously described.[3]

The cross section is assumed to represent almost entirely elastic scattering since it is improbable that inelastic scattering will be appreciable at the low energies involved. Further, measurements of the total cross section of sulfur at low energies[4] indicate that neutron capture will probably account for less than 0.1 b at the energies used here.

Figure 1 shows a sharp peak at 111 kev preceded by a dip which is interpreted as caused by destructive interference between resonance and potential scattering. At this energy less than 2 percent of the potential scattering will be due to neutrons of more than zero angular momentum.[5] Therefore, it must be concluded that the resonance is caused by S-neutrons forming a state of S^{33} with spin $\frac{1}{2}$. This compound nucleus is formed from S^{32} which has an isotopic abundance of 95 percent and zero spin.

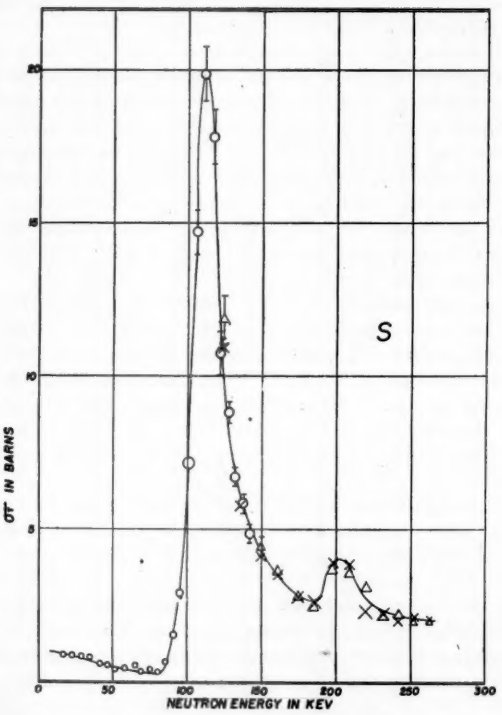

FIG. 1. The total cross section of sulfur as a function of neutron energy. The circles represent data taken at an angle of 115° with respect to the protons incident on the Li target. Other symbols show data taken in the forward direction. The height of the symbols is a measure of the statistical error.

For S-neutrons interacting with a target nucleus of spin zero the Breit-Wigner single level formula, including potential scattering, is expressed by Feshbach, Peaslee and Weisskopf[6] as:

$$\sigma=\frac{4\pi}{k^2}\left|\frac{\Gamma_n/2}{E-E_r+i(\Gamma/2)}+e^{ika}\sin ka\right|^2,$$

where k is the neutron wave number in the center of mass system, a is the nuclear radius $1.4\cdot10^{-13}A^{\frac{1}{3}}$ cm,[7] E_r the resonance energy, and E the energy of the incident neutrons. Γ_n, the elastic scattering width, is taken to be equal to the total width Γ according to the preceding arguments.

The experimental width of the peak is about 19 kev which, by taking into account the effect of the neutron energy spread, yields a natural width of 18 kev. When this value is used for Γ, and E_r is taken as 108 kev, the experimental curve is found to be in good agreement with the theory. The correction for instrumental resolution increases the observed maximum cross section of 19.9±0.9 b at 111 kev to 21.5±1 b, which agrees with the theoretical value of 21.4 b at 111 kev. The theoretical minimum is zero at an energy of 82 kev. The position of the experimental minimum does not contradict this value, and the residual cross section of 0.3 b can be attributed to radiative capture and to the cross section of the other isotopes.

For 1-ev neutrons sulfur has a total cross section of 1.1 b, of which not more than 0.1 b is due to absorption.[4] Neglecting absorption, the potential scattering at low energies should be equal to $4\pi a^2$ or 2.4 b. The low value of the observed cross section can be explained by the effect of the resonance at 108 kev, since destructive interference reduces the theoretical value to 1.1 b at low energies.

There is evidence of a further resonance at 205 kev. The width of this peak is presumably quite small and its effect on the resonance at 108 kev should be negligible.

This work was supported by the Wisconsin Alumni Research Foundation and the AEC.

[1] H. A. Bethe, Rev. Mod. Phys. **9**, 69 (1937).
[2] Feshbach, Peaslee, and Weisskopf, Phys. Rev. **71**, 145 (1947).
[3] Adair, Barschall, Bockelman, and Sala, Phys. Rev. **75**, 1124 (1949).
[4] Rainwater, Havens, Dunning, and Wu, Phys. Rev. **73**, 733 (1948).
[5] Section 5 of reference 2.
[6] Formula 14 of reference 2.
[7] Cook, McMillan, Peterson, and Sewell, Phys. Rev. **75**, 7 (1949).

Scintillations Produced by α-Particles in a Series of Structurally Related Organic Crystals

W. S. Koski and Carl O. Thomas
Department of Chemistry, The Johns Hopkins University, Baltimore, Maryland
May 27, 1949

WE are currently investigating the scintillation properties of a series of structurally related organic crystals, and in view of the fact that one of these crystals possesses a much higher conversion efficiency (number of photons per unit α-particle energy loss) than any other crystal previously reported, we considered it worth while to make a preliminary report of some of our results.

The series under investigation is 1,2-diphenylethane, 1,2-diphenylethylene (stilbene) and diphenylacetylene. The scintillation crystals were prepared by crystallization from a slowly cooling molten mass of the organic material. For purposes of comparison all crystals that were used were of approximately equal thicknesses

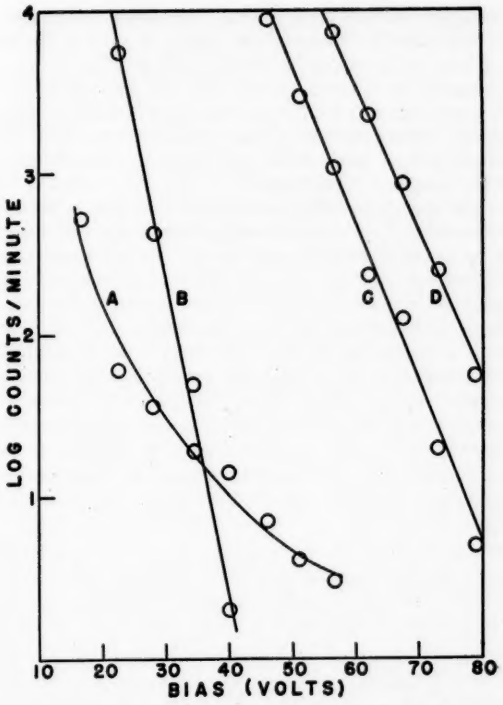

FIG. 1. A plot of net counts/min. *vs.* bias setting in volts for a series of structurally related organic crystals. *A* = average background, *B* = 1,2-diphenylethane, *C* = 1,2-diphenylethylene and *D* = diphenylacetylene.

and were utilized in conjunction with a 931-A photomultiplier tube to count the scintillations produced by alpha-particles from a polonium source. The potential divider and amplifier circuits were similar to those used by Marshall, Coltman, and Bennett.[1] The discrimination of the pulses was made with a Higinbotham[2] amplitude discriminator and the counting was done with a decade scale-of-a-1000 circuit constructed in this laboratory. No refrigeration was used in these experiments.

The results are summarized in Fig. 1 where the log of the counts/min. less background are plotted against discriminator bias in volts. It is clear that the signal to noise ratio increases as one goes from diphenylethane to stilbene and then to diphenylacetylene. The naphthalene curve, if plotted on this scale, would fall in the region between diphenylethane and stilbene and possesses an intermediate slope. It will be noted that diphenylacetylene is about 6 times better than stilbene which is the best material previously reported in the literature.[3]

When these crystals were used for x-ray detection, a similar correlation between conversion efficiency and the unsaturation of the non-benzenoid linkage in the molecules was observed.

In early studies on scintillation properties of crystals there was a tendency to associate these properties with condensed-ring systems, however, the work on stilbene[3] and the present work on diphenylacetylene indicate that conjugation of the multiple bonds is a more determining factor than condensation of rings. This is really not too surprising in view of the numerous correlations that have been observed between certain optical properties of organic materials and the conjugation of double and triple bonds.

In future work it is planned to investigate the spectral distribution of the scintillations, and to further explore the apparent correlation between structure and conversion efficiency.

[1] Marshall, Coltman, and Bennett, Rev. Sci. Inst. **19**, 744 (1948).
[2] Higinbotham, Gallagher, and Sands, Rev. Sci. Inst. **18**, 706 (1947).
[3] Gittings, Taschek, Ronzio, Jones, and Masilun, Phys. Rev. **75**, 205 (1949).

Vacancies and Diffusion in NiAl*

R. SMOLUCHOWSKI AND H. BURGESS
Carnegie Institute of Technology, Pittsburgh, Pennsylvania
May 31, 1949

THE intermetallic compound NiAl (and CoAl) has a CsC-type of structure and is able to dissolve certain excesses of the two elements. It has been shown by Bradley[1] that on the Ni-rich side the extra atoms of nickel substitute for aluminum atoms, while on the other side the extra atoms of aluminum cannot replace the much smaller atoms of nickel and so instead some nickel atoms are missing. A study of diffusion in this compound seemed to be of considerable interest in view of the role of vacancies in the mechanism of diffusion and the possibility of changing their concentration. The concentration of vacancies in metals due to thermal excitation is usually a small fraction of one percent, and so an addition of several percent of aluminum, thus of several percent of vacancies should increase the order of magnitude of the diffusion coefficient. As explained below, a closer examination of the vacancy mechanism shows this conclusion to be incorrect.

Figure 1a shows the cube projection of the ideal NiAl lattice, the rest of the figure shows the three basic kinds of monatomic defects possible in that lattice. A Ni-vacancy, $V(N)$, which is shown in Fig. 1b, is due either to thermal excitation or to an excess of aluminum, and it cannot move by itself because, as mentioned above, the space between the eight Al-atoms is too small to accommodate a central Al-atom. Such a vacancy could move by itself only by an interchange with a second neighbor Ni-atom, which is quite unlikely. In Fig. 1c we have an excess Ni-atom substituting for an Al-atom and finally in Fig. 1d is illustrated an Al-vacancy, $V(A)$, which is due to thermal excitation and which is able to move in the lattice because a Ni-atom can occupy an Al-vacancy and in turn an Al-atom can occupy a Ni-vacancy if not all neighbors of that vacancy are Al-atoms. This is shown in in Figs. 1e and 1f.

There exists an important interchange between these defects. The Al-vacancies moving around can bring into contact a Ni-vacancy with an excess Ni-atom and thus produce a new Al-vacancy, $V(N)+\text{Ni}\rightarrow V(A)$. Of course the opposite is also possible: An Al-vacancy can, with the help of another Al-vacancy, transform itself into a Ni-vacancy plus an excess Ni-atom substituting somewhere for an Al-atom, $V(A)\rightarrow V(N)+\text{Ni}$. These processes alter the balance of vacancies and thus affect the diffusion rate. At the 50:50 composition one expects an excess of $V(N)$ over $V(A)$ and $(V(N)-V(A))$ nickel atoms substituting for Al-atoms. As the concentration of aluminum increases the number of $V(N)$ rapidly increases with a small influence on the number of $V(A)$ (since there are few excess Ni-atoms available) which alone are responsible for diffusion. On the Ni-rich side the number of the excess Ni-atoms increases rapidly and thus many of the $V(N)$ are transformed into $V(A)$ and so the diffusion coefficient should

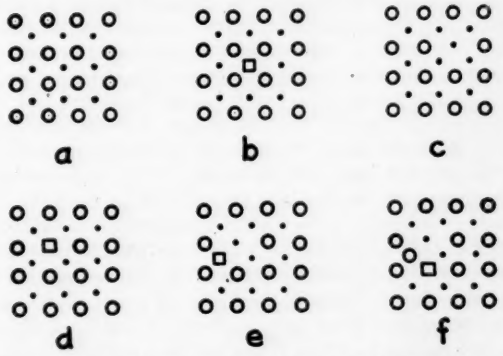

FIG. 1. Atomic configurations in NiAl: (a) perfect lattice at 50:50; (b) Ni-vacancy or excess Al; (c) excess Ni; (d), (e), (f) three positions of an Al-vacancy. Open circles represent Al, dots represent Ni.

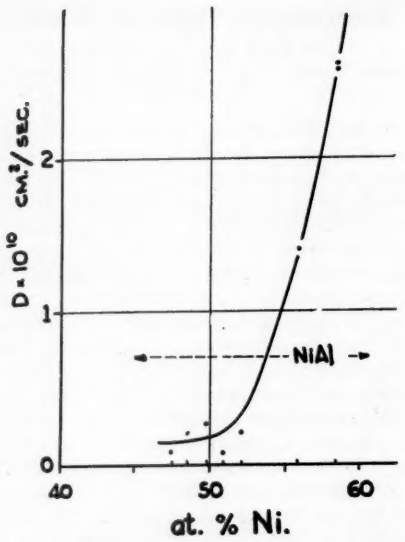

FIG. 2. Diffusion coefficient in NiAl at 1150°C.

increase. The amount of this increase will depend upon the balance between the production and annihilation of $V(A)$.

As illustrated in Fig. 2 experimental results confirm these considerations. Since, at the time the experiments were started, radioactive nickel was not conveniently available, the measurements were made using radioactive cobalt which is known to form a similar compound with aluminum[2] and can substitute for nickel in NiA. Since these alloys are difficult to prepare and on the aluminum-rich side are brittle, a very small quantity of radioactive cobalt was plated on the surface of the sample and the diffusion coefficient computed from the decrease of the activity due to the penetration of cobalt into the samples during 18 hours at 1150°C. The experiment is being repeated with radioactive nickel.

*Research sponsored by ONR.
[1] A. J. Bradley and A. Taylor, Proc. Roy. Soc. **A159**, 56 (1937).
[2] A. J. Bradley and G. C. Seager, J. Inst. Metals **64**, 81 (1939).

Removal of Space-charge in Diamond Crystal Counters

A. G. CHYNOWETH
Wheatstone Physics Laboratory, London, W. C. 2, England
May 26, 1949

IT is well known that a steady decrease in the size of the pulses with time is produced in a crystal counter when subjected to ionizing radiations, owing to the setting-up of space-charge inside the crystal. This space-charge is produced by electrons, and possibly positive holes, being held in electron-traps distributed throughout the crystal. Various authors have neutralized the effect of the space-charge by applying an alternating field across the crystal,[1] the supposed explanation being that during the positive half-cycle, the freed electrons are carried from the surface layers into the body of the crystal where they become trapped; and during the negative half-cycle, positive holes migrate into the crystal where some will re-combine with the trapped electrons while others become trapped themselves. The net effect of a continual repetition of this process is, under favorable conditions, to neutralize the space-charge. It has also been suggested[2] that once a space-charge has been set up, the crystal could possibly be returned to its original state by irradiating it with visible light and heat, after which the counting cycle could be repeated. In a theoretical paper by Newton,[3] the depths of most of the traps in diamond are estimated to be between 0.25 and 0.75 electron-volt, corresponding to photon wave-lengths of approximately 5 mμ and 1.6 mμ, respectively. Thus, irradiation of the specimen with a spectrum extending from about 1 mμ to 10 mμ should be sufficient to de-trap most of the electrons. This spectrum is conveniently produced by a Nernst filament.

In this laboratory, experiments have been performed in which light was focused on to the crystal simultaneously with bombardment by alpha-particles from polonium. It was found that with the Nernst light, no photo-conductivity was detected. The temperature of the crystal was that of the room and was kept fairly constant. The field across the crystal was such that, at high intensities of Nernst irradiation, there was a saturation of counting-rate with applied voltage. Only pulses of height greater than twice the noise-level of the amplifier were recorded. The procedure was to allow the counting-rate to decay to zero while the crystal was in the dark and then, to irradiate it with the Nernst illumination. The following change in counting-rate with time was observed, the curve shown being typical of the many obtained.

Portion OA of Fig. 1 shows the decay prior to irradiation. The illumination was begun at A and the counting-rate rose rapidly, being followed by the peculiar "kink" after which, over the part BC, it gradually approached a saturation. At C, the light was removed and the counting-rate was found to decay exponentially and when it had reached its original value, the whole cycle could be repeated. These curves were plotted for various light intensities and as was to be expected, a curve of saturation counting-rate against light intensity itself showed a saturation for the higher intensities, corresponding to conditions in which a high percentage of the incident alpha-particles was being recorded

The use of radiation of suitable wave-lengths to remove space-charge appeared as satisfactory as the method of field reversal, since, when the latter was carried out, the pulse heights were the same as those reached when the higher intensities of light were used.

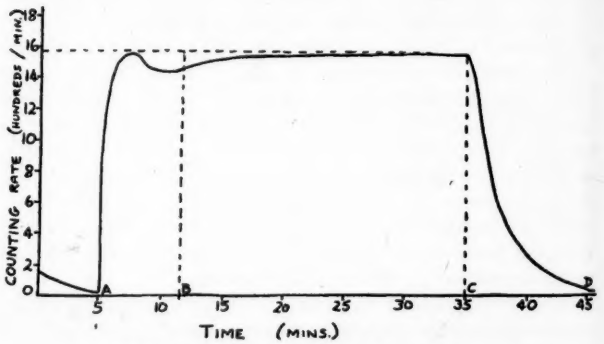

FIG. 1. Variation of counting-rate with time on irradiating the diamond with a Nernst light.

Most of the above experiments were performed on one specimen only, but the behavior of other diamonds differed only in degree.

No simple explanation of the kink in the curve seems forthcoming but it is interesting to note that Newton obtained from theoretical considerations a curve exhibiting the same appearance, though his theory deals with slightly different experimental conditions. It is not clear whether our experiments can be interpreted directly in terms of Newton's curve but this point is being investigated.

[1] L. F. Wouters and R. S. Christian, Phys. Rev. **72**, 1127 (1947). K. G. McKay, Phys. Rev. **74**, 1606 (1948).
[2] R. Hofstadter, Nucleonics (April, 1949).
[3] R. R. Newton, Phys. Rev. **75**, 234 (1949).

Positive Excess of Mesons at 30,000 Feet*

MARCELLO CONVERSI**
Institute for Nuclear Studies, University of Chicago, Chicago, Illinois
May 25, 1949

THE excess of positive particles in the hard component of cosmic rays at airplane altitudes has been measured recently with cloud chamber in a magnetic field[1] and with magnetic lenses.[2] The excess so observed may be due in part to protons and in part to an actual excess of positive mesons. Ordinary mesons can be distinguished from protons without ambiguity taking advantage of their instability. The measure of the ratio of positive to negative mesons can be based then, as already recently suggested,[3] on the fact that in light materials both positive and negative mesons undergo spontaneous decay, while in elements of high atomic number this is true of only the positive ones.[4]

In a series of B-29 flights undertaken at different altitudes and latitudes, experiments with Geiger counters in delayed coincidence have been carried out to investigate the composition of ionizing cosmic rays slowed down after traversing a certain thickness of lead. Preliminary results concerning the excess of positive mesons are here reported. Further results will be published later.

With the apparatus employed four points of the decay curve corresponding to mesons traversing a counter telescope and then stopped in a 10 cm thickness of graphite (C) or sulphur (S) could be simultaneously obtained.[5] Measurements of delayed coincidences with C and S absorbers have been performed: (1) in Chicago with 20 cm Pb placed above the absorber; (2) at China Lake, California (2100 feet) without Pb; (3) in a B-29 flying at 30,000 feet and at an average geomagnetic latitude of about 45° North, with 15 cm Pb. The counting rate of the delayed coincidences, reported in Table I, are corrected for the random coincidences, N_r, listed in the 10th column.

Measurements with C absorber have been performed at China Lake also with 15 and 35 cm Pb. An analysis of all the data obtained in Chicago and at China Lake gives for the lifetime of the meson the value 2.20±0.09 μsec. From the data contained in Table I the most probable exponential curves corresponding to such a lifetime have been drawn for each series of measurements (Fig. 1). By extrapolation to the zero time the numbers N_C and N_S of mesons which are stopped in the two absorbers and then decay into electrons producing delayed coincidences, have been calculated for each series of measurements.

Let k be the ratio of the number of mesons stopped in the C absorber to the number of those stopped in the S absorber. Moreover let ρ be the ratio between the average value of the probability for the decay electrons of mesons stopped in the C absorber to produce a delayed coincidence and the analogous value relative to the S absorber. Then it can be easily shown that the ratio of positive to negative mesons is given by

$$\frac{M_+}{M_-}=\frac{K\rho}{N_C/N_S-K\rho}, \qquad (1)$$

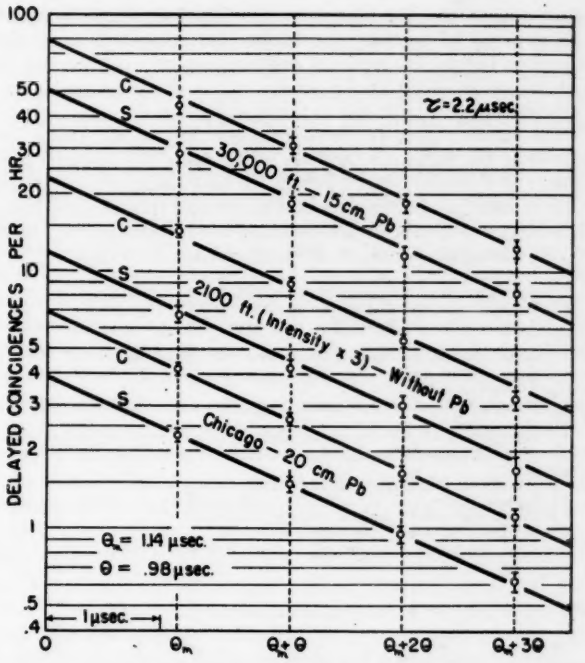

FIG. 1. Decay curves of mesons slowed down in graphite (C) and sulphur (S). Each point is due to the contribution of mesons which disintegrated between the instant t of the corresponding abscissa and $t+\Delta\theta$. $\Delta\theta$ was 2.8 μsec.

under the assumption that *all* negative mesons disintegrate in C and are captured in S. This assumption seems to be reasonable on account of the comparatively large minimum delay θ_m (Fig. 1) and of the experimental dependence of the capture probability of negative mesons upon the atomic number.[6]

The ratio ρ depends in particular on the range of the decay electrons in the two absorbers. An approximate calculation shows, however, that its value does not change appreciably assuming for the energy of the decay electrons values between 25 and 50 Mev, an interval in which the bulk of the decay electrons should be contained.[7] Furthermore the value of ρ can be derived from the data of the first series assuming in Eq. (1) $k=0.91\pm0.03$ (as deduced from direct measurements here not reported and $M_+/M_-=1.24\pm0.05$, as obtained in Rome,[8] for mesons of energy between 320 and 430 Mev, using magnetic lenses. The value $\rho=1.06$ so obtained is in agreement with the calculated one.

The results of the 2nd series give a rough indication of disappearance of the positive excess in the low energy region of the meson spectrum. Such an indication has been found also with cloud chamber at 3500 m.[9]

Since negative π-mesons should be captured in C as well as in S and positive π-mesons disintegrate into ordinary mesons of very

TABLE I. Results of delayed coincidences measurements with graphite and sulphur absorbers.

Series n°	Altitude (feet)	Energy range (Mev)	Absorber	Del. coinc. (per hr.) produced by mesons disintegrating in the time interval. 1.14 to 3.94 μsec.	2.12 to 4.92 μsec.	3.10 to 5.90 μsec.	4.08 to 6.88 μsec.	Duration (min.)	N_r (coinc./hr.)	$\frac{M_+}{M_-}$	$\epsilon=\frac{M_+-M_-}{\frac{1}{2}(M_++M_-)}$
1	600	286–317	C	4.18±0.18	2.64±0.15	1.64±0.10	1.12±0.09	7595	0.021	1.24±0.265	21.5%
		286–320	S	2.31±0.11	1.49±0.09	0.96±0.08	0.63±0.06	10,988	0.023	0.19	
2	2100	16–67	C	4.75±0.19	3.03±0.16	1.81±0.12	1.05±0.09	7720	0.301	0.99±0.22	−1%
		16–71.5	S	2.30±0.15	1.14±0.11	1.04±0.10	0.55±0.08	5990	0.334	0.16	
3	30,000	224–255	C	45.0±2.9	31.2±1.8	18.4±1.4	12.3±1.1	560	9.25	1.54±0.39	42%
		224–258	S	28.7±2.3	18.5±1.2	11.5±1.0	8.2±0.8	770	8.95	0.26	

short range,[10] the increased value of ϵ found at 30,000 feet (3rd series) could be partially due to π-mesons slowed down in the absorber. Indeed, the excess of ordinary mesons would be still 20 percent at 30,000 feet if 13 percent of the delayed coincidences registered with C were due to positive π-mesons.

The author wishes to thank Professor Samuel K. Allison for providing the numerous facilities which made this research possible, and Professor Marcel Schein for his kind hospitality in the Cosmic Ray Laboratory where the experiment has been prepared. It is also a pleasure to acknowledge the cooperation of Major W. A. Gustafson, Mr. C. L. D'Ooge, and the B-29 crew.

* Assisted by the joint program of the ONR and AEC.
** On leave from the University of Rome, Italy.
[1] Adams, Anderson, Lloyd, Rau, and Saxena, Rev. Mod. Phys. **20**, 334 (1948).
[2] Quercia, Rispoli, and Sciuti, Phys. Rev. **74**, 1728 (1948).
[3] Shamos, Levy, and Lower, Phys. Rev. **74**, 1237 (1948); O. Piccioni, private communication.
[4] Conversi, Pancini, and Piccioni, Phys. Rev. **68**, 232 (1945); **71**, 209 (1947).
[5] A complete description of the apparatus, as well as a detailed account of the corrections introduced and a discussion of the results, will be given elsewhere.
[6] H. K. Ticho, Phys. Rev. **74**, 1337 (1948).
[7] Leighton, Anderson, and Seriff, Phys. Rev. **75**, 1432 (1949).
[8] M. Conversi and F. Nappo, unpublished result.
[9] M. Correl, Phys. Rev. **72**, 1055 (1947).
[10] Lattes, Occhialini, and Powell, Nature **160**, 486 (1947).

Measurement of a 2.3×10^{-8}-Second Metastable State in Hg^{198}

W. J. MacIntyre
Sloane Physics Laboratory, Yale University, New Haven, Connecticut*
May 25, 1949

METASTABLE nuclear states of half-lives ranging from a millisecond to 0.65 microsecond have been investigated in detail by De Benedetti and McGowan[1] by the delayed coincidence method. In addition Bittencourt and Goldhaber[2] have reported a $5\pm2\times10^{-8}$ second state of Te^{121} and Stevenson and Deutsch[3] have reported a state of Cd^{111} with a half-life of $8\pm1\times10^{-8}$ second.

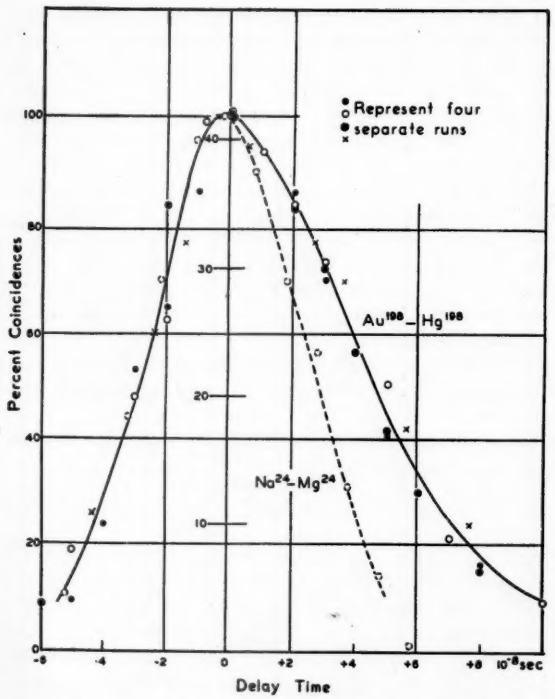

FIG. 1. Coincidence rate *versus* delay curve for Na^{24} and Au^{198} decay. Plus values of delay refer to additions to β-channel. First two sets of data on Au^{198} taken with β-detection by proportional counter and second two by scintillation counter.

By use of detectors and coincidence circuits of combined resolving time of 5.6×10^{-8} second, states of $\beta-\gamma$-coincidences have been investigated in the region of $1-30\times10^{-8}$ second. Determinations on the decay of calcium fluoride and naphthalene crystals as previously reported[4] have shown the measurements possible with the circuits. The long decay time of these phosphors, however, prevent their use and so for a scintillation counter for gamma-detection, polystyrene was selected. When used in conjunction with a 931A and the usual circuits this has a resolving time of 2.8×10^{-8} second[5] and the decay is faster than can be detected with the coincidence circuit used.

For detection of the beta-particles both proportional counters of resolving time of 2.8×10^{-8} second and polystyrene scintillation counters have been used. Results obtained with the polystyrene counter and the proportional counter were identical, thus verifying that the polystyrene decay time is negligible.

In the search for short-lived isomers the isotope was placed between the two counters with an absorber screening the gamma-scintillation counter from the beta-particles. Since the proportional counter has a low efficiency for gamma-rays this results in the proportional counter detecting only the beta-particles and the scintillation counter detecting only the gamma-rays. This is important in the case of cascaded gamma-rays as it proves the data obtained are for $\beta-\gamma$-coincidences and not $\gamma-\gamma$.

The simultaneous stimulation of both counters will result in the familiar resolution curve as the delay time of one channel with respect to the other is varied. Thus identification of isomers is accomplished by searching for departure of the usual symmetric resolution curve to one of asymmetry. The simultaneous stimulation of both counters may be obtained by projecting a beam of beta-particles through the proportional counter into the scintillation counter or by a $\beta-\gamma$-coincidence of a state so fast that no variation of symmetry appears.

Such a state is shown in Fig. 1 for the case of $\beta-\gamma$-coincidences from Na^{24}. Although there is perhaps a slight asymmetry to the traling edge it appears too fast for this equipment to measure and shows the state of Mg^{24} found from Na^{24} decay to be faster than a 2×10^{-8} second half-life. These measurements were obtained with both a proportional counter and polystyrene counter detecting the beta-particles with no variation observed.

In the case of the decay of Au^{198}, as shown also in Fig. 1, a distinct asymmetry is observed. This shows the existence of a lag in the detection of the gamma-rays and consequently a metastable state of the newly-formed Hg^{198}. A compilation of four separate measurements plotted on the figure all show the same asymmetry and approximate decay time.

According to the analysis of Van Name[6] this trailing edge should fall off in value as the exponential of the decay constant, providing the first point is beyond the half-width pulse distribution. The variation of the logarithm of the coincidence against time is shown in Fig. 2 to give a straight line, with half-life 2.3×10^{-8} second. From variations of several curves and the limitation of the range to three half-lives the error is estimated to be $\pm0.2\times10^{-8}$ second.

Previously, Madansky and Wiedenbeck[7] had estimated a state in Hg^{198} of 0.2~0.3 microsecond half-life. Mandeville and Scherb[8] have also investigated Hg^{198} for a possible metastable state by looking for loss in $\beta-\gamma$-coincidences from Au^{198}, while reducing the resolving time of their coincidence circuit from 1.0 microsecond to 0.035 ± 0.002 microsecond and reported no state apparent. De Benedetti and McGowan also reported negative results for the range previously mentioned.

An attempt was made to identify the type of gamma-ray transition by use of Segrè's formula.[9] Using the value of the

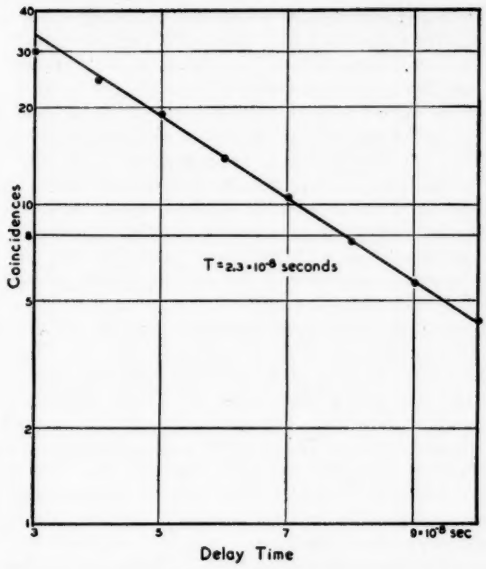

FIG. 2. Semi-logarithmic plot of Au^{198} coincidences *versus* delay time.

gamma-ray energy of 0.41 Mev this predicts a half-life of the order of 1.7×10^{-11} second for electric quadrupole and 1.5×10^{-6} second for electric octupole. The observed value falls between these two values of l equal to 2 or 3 and is thus probably a quadrupole transition.

The writer wishes to thank Professor E. C. Pollard for valuable discussions and encouragement and to Professor H. L. Schultz for discussion of coincidence techniques and circuits involved.

* Assisted by the joint program of the ONR and AEC.
[1] S. De Benedetti and F. K. McGowan, Phys. Rev. **74**, 728 (1948).
[2] P. T. Bittencourt and M. Goldhaber, Phys. Rev. **70**, 780 (1946).
[3] Donald T. Stevenson and Martin Deutsch, Phys. Rev. **76**, 100 (1949).
[4] W. J. MacIntyre, Phys. Rev. **75**, 1439 (1949).
[5] W. J. MacIntyre, Phys. Rev. **75**, 1290 (1949).
[6] F. W. Van Name, Phys. Rev. **75**, 100 (1949).
[7] L. Madansky and M. L. Weidenbeck, Phys. Rev. **72**, 185 (1947).
[8] C. E. Mandeville and M. V. Scherb, Phys. Rev. **73**, 634 (1948).
[9] A. C. Helmholtz, Phys. Rev. **60**, 415 (1941).

Mass Assignment of the 43-Minute Hg Isomer

INGMAR BERGSTRÖM AND SIGVARD THULIN
Nobel Institute for Physics, Stockholm, Sweden
May 31, 1949

THE electromagnetic isotope separator, recently built at our Institute,[1] has been used to determine the mass number of the 43^m activity of Hg. This activity has been known before to be due to an isomeric state and our results, which will be reported here, show that this activity can be uniquely ascribed to mass number 199.

When performing a determination of this kind, one can proceed principally in two different ways. One can either start by irradiation of unseparated Hg and then make the isotope separation of the irradiated sample, whereafter the activity of each mass number is determined, or one can make the separation first and then irradiate the different isotopes separately. In the first case the active isotope assignment will be unique, while the other procedure, though it does not always give an unique answer, may be advantageous when the isotope is very short-lived. In the present case both methods have been used.

One gram Hg was irradiated in a small glass container by fast Be-neutrons from our 6.5-Mev cyclotron for about 2 hours (current 50–100 μa). Immediately after irradiation the container was introduced into the ion source of the separator by means of a vacuum lock device. The mercury ion current was 10–15 μa and the time of separation 40 min., giving about 60 μg stable Hg isotopes. The separation could be started a few minutes after the irradiation in the cyclotron. The Hg spectrum was deposited on a thin Al plate, which could be taken out quickly after a convenient separation time. The Al plate was cut into strips, each corresponding to a mass number and 4 mm wide. The activity of each strip was then measured with a small bell β-counter (background 6 counts/min.). Figure 1 shows the results of such an investigation. On the abscissa axis the mass number scale is given, which is found by the visual deposition on the plate of the stable isotopes. The distance between the centers of two subsequent mass numbers on the plate is 4 mm. According to Fig. 1 the 43^m activity evidently has the mass number 199. The half-life of the activity of this mass number was also checked. Another investigation with better focusing showed an activity of 6 c/m at mass number 199 and no counts above the background for the mass numbers 198 and 200.

In order to investigate different reactions leading to the metastable level in Hg^{199} the previously mentioned second method was used. The stable isotopes of Hg were separated and deposited on a Fe plate, which was cut into strips as mentioned above. The strips were irradiated in the cyclotron and then separately treated with a diluted solution of hydrochloric acid. It was found that the isotope deposits on the strips left the active plates and flowed up to the surface of the solution. The isotopes were then filtered off, washed with water and alcohol and then dried. In this way the activity measurements could be started 10 min. after irradiation. The mass numbers 199 and 200 showed a weak activity above background with a half-life of the order of 40 min. This may mean that both the reaction $Hg^{199}(n,n)Hg^{199*}$ and $Hg^{200}(n,2n)Hg^{199*}$ occur, since earlier investigations have shown that no hydrogen compounds occur in the mass spectrum that can disturb the measurements.

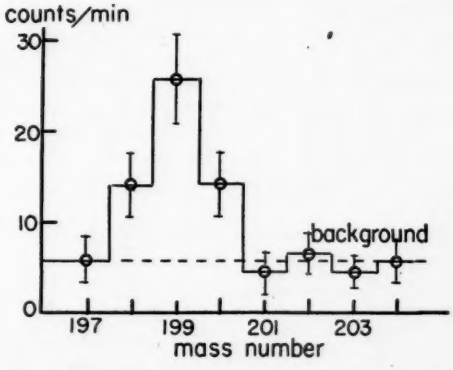

FIG. 1. Histogram showing that activity is to be assigned to mass number 199.

Our mass assignment fits well with the experiments performed by Sherr *et al.*,[2] who observed a 43 min. Hg activity obtained from a (α,n)-reaction on Pt. The mass assignment also explains why the 43 min. activity cannot be produced by a (n,α)-reaction on Pb as shown by Wu and Friedländer,[3] since there is no stable Pb^{202} isotope.

[1] Bergström, Thulin, Svartholm, and Siegbahn, Ark. f. Fysik **1**, 11 (1949).
[2] Sherr, Bainbridge, and Anderson, Phys. Rev. **60**, 473 (1941).
[3] C. S. Wu and G. Friedländer, Phys. Rev. **63**, 227 (1943).

Gamma-Radiation from Light Nuclei under Proton Bombardment

W. A. FOWLER AND C. C. LAURITSEN
Kellogg Radiation Laboratory, California Institute of Technology, Pasadena, California
May 26, 1949

ADDITIONAL studies of the gamma-radiation emitted in the bombardment of light nuclei by protons by several observers during the past year make it advisable to revise data previously summarized on this subject.[1] The revised data are given in Table I and the various changes are discussed in what follows.

The recent determination[2] of 873.5 kev with a probable error of 0.1 percent for the energy at which the first strong resonance in $F^{19}(p\alpha',\gamma)$ occurs, establishes a new and more reliable scale of bombarding energies in nuclear disintegrations with charged particles. The scale previously used was based on the resonance in $Li^7(p\gamma)$ at 440 kev as standard. We have made several comparisons of these two resonances during the past year. Typical results are shown in Fig. 1. A thin ZnF target evaporated on silver was bombarded with monatomic ions while a thick evaporated lithium target was bombarded by diatomic as well as monatomic ions. Both the maximum intensity and width of the two $F^{19}(p\alpha',\gamma)$ resonances (natural width, 5.2 kev and 8.0 kev) indicated a target thickness of 4.2 kev and one-half this value has been subtracted from the point of maximum intensity to obtain the resonance position.

The Li curve has been corrected for non-resonant radiation[1] and also for surface layers of carbon and oxygen of energy equivalent thickness ~1 kev. The thickness of these layers is measured by the number of elastically scattered protons observed in a magnetic spectrometer[3] simultaneously with the gamma-ray yield measurement. These layers appear on lithium targets deposited in vacuum (5×10^{-6} mm Hg) even with an auxiliary diffusion pump and liquid air trap directly connected to the target chamber. The layers increase during bombardment to energy equivalent thicknesses of several kilovolts and the apparent resonance position shifts to higher energies. We have changed to fresh targets repeatedly throughout the measurements and have corrected for the layers observed on the average for short bombardments. The resonance energy is found to be 441.4±0.5 kev which is slightly lower than the value 442.4±1.5 reported by Hudspeth and Swann.[4]

Carbon and oxygen layers have also been observed on Be foil targets and corrections have been made in the resonance energies. We have not investigated the deposition of layers on ZnF targets by the scattering method but the shift in resonance position under the amount of bombardment necessary to obtain the strong $F^{19}(p\alpha',\gamma)$ radiation is observed to be small. No correction has been made in this case or in the case of graphite targets used in the determination of the carbon cross sections. Small relativistic corrections have been included in all cases. The $Be^9(p\gamma)$ cross sections have been corrected for the stopping power measurements on beryllium recently reported.[5]

Additional information on radiation energies as well as on resonance positions has also become available.[6,7] Using a pair spectrograph Walker and McDaniel[6] at Cornell have resolved the $Li^7(p\gamma)$ spectrum into a sharp line at 17.6 Mev and a line about 2 Mev broad at 14.8 Mev. The relative intensity of the 14.8 Mev line is 0.5 at resonance. This permits a more detailed calculation of the efficiency of detection of the radiation and we have accordingly corrected the resonance cross section. Geiger-counter and electroscope results for the yield agree closely and the average has been used in the calculations.

The gamma-radiation from $F^{19}(p\alpha',\gamma)$ has been resolved into two components at 6.13±0.06 and 6.98±0.07 Mev by Walker and McDaniel[6] and the results confirmed by Rasmussen *et al.*,[7] who give 6.135±0.04 and 7.00±0.07 Mev. Recent work on the short range alpha-particle spectrum[8] indicates that there are probably two high energy gamma-rays at 6.9 and 7.1 Mev. The gamma-ray intensity measurements, although apparently not indicative of all details of the spectrum are sufficient to make reliable calculations of the total cross sections at several resonances. Separate data have been given for four resonances in this reaction and for the thick target yield at 960 kev. The resonance widths are those quoted by Bennett *et al.*[9] The cross sections are somewhat higher than those given by Bonner and Evans[10] who determine the gamma-ray yield by comparison with the alpha particle yield at the 340 kev resonance. Further work on the alpha-particle spectra and yields is now under way in this laboratory.

Two recent precision measurements[11,12] on the energy of the radiation from the first excited state in Li^7 yield a weighted mean

TABLE I. Summary of Yield and Energy Measurements.
(Revision of Table I, Rev. Mod. Phys. **20**, 248 (1948).)

Source	Resonance energy (kev)	Energy of radiation (Mev)	Thick target yield* disintegrations/proton	Partial width $\omega\gamma$(ev)	Width Γ(kev)	σ_R (cm²)
$F^{19}(p\alpha',\gamma)$	340.0±2	6.1 (96%) 7.0‡ (4%)	1.74×10^{-8}	31	3.2	8.4×10^{-26}
$Li^7(p\gamma)$	441.4±0.5	14.8 (33%) 17.6 (67%)	1.90×10^{-8}**	9.4	12	6.0×10^{-27}
$C^{12}(p\gamma)$	456.0±2‡‡	2.3	7.3×10^{-10}	0.63	35	1.2×10^{-28}
$C^{13}(p\gamma)$	554.0±2‡‡	2.3, 5.8, 8.1	1.8×10^{-10}	15	40	2.0×10^{-27}
$F^{19}(p\alpha',\gamma)$	873.5±1	6.1 (72%) 7.0‡ (28%)	3.6×10^{-7}	825	5.2	5.3×10^{-25}
	935.3±1	6.1 (77%) 7.0‡ (23%)	2.0×10^{-7}	470	8.0	1.8×10^{-25}
	All ≤960	6.1 (72%) 7.0‡ (28%)	6.9×10^{-7}	——	——	——
$Be^{9'}(p\gamma)$	998.0±4	7.4	1.78×10^{-8}	11	94	4.0×10^{-28}
	1087.0±2	6.7, 0.72	1.01×10^{-9}	0.7	4	5.3×10^{-28}
$Li^7(p\rho',\gamma)$	1030.0±5	0.478	1.2×10^{-4}††	2400	168	4.7×10^{-26}††
$F^{19}(p\alpha',\gamma)$	1092.0±2		2.4×10^{-9}	7	<1.2	$>2\times10^{-26}$

* Target materials: crystalline CaF_2, evaporated Li(92.6% Li^7), Be metal, Acheson graphite (98.9% C^{12}).
** At 850 kev the yield is 2.6×10^{-8} disintegrations/proton. The tabulated yield is that part of the yield due to the resonance at 441.4 kev.
† Plus two annihilation quanta from N^{13} which emits positrons at maximum energy 1.206±0.004 Mev.
†† Thick target yield at 1350 kev. The cross section has been corrected for non-resonant background.
‡ See discussion in text.
‡‡ The carbon resonances were compared directly with the lithium resonance at 441.4 and not with the fluorine resonance at 873.5 as in all other cases.

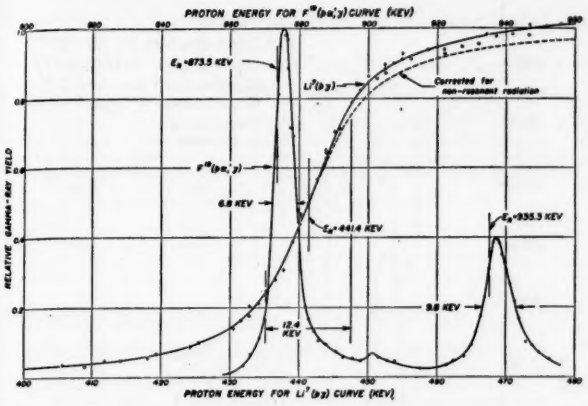

FIG. 1. Excitation curves for the reactions $F^{19}(p\alpha',\gamma)$ and $Li^7(p\gamma)$. In the fluorine reaction a target of 4.2 kev equivalent thickness for protons was used while in the lithium reaction a thick target was used.

value of 477.4±1.0 kev. From measurements on the energy of the protons inelastically scattered by Li^7 to be discussed in more detail in a forthcoming publication we find a value of 479.0±1.0 kev.[13] We have also measured the yield of the radiation following the inelastic scattering. The excitation curve from this reaction has been corrected for penetration factors for the incident and scattered protons and indicates a broad level in Be^8 at 1030±5 kev, superimposed on a continuous non-resonant background. The number of inelastically scattered protons has been measured at 1240 kev and the cross sections per 4π-steradians are 6.5×10^{-26} cm² at 81.1° and 3.6×10^{-26} cm² at 137.8°. The gamma-ray measurements which average over all angles give 5.7×10^{-26} cm² at this energy.

This work was assisted by the joint program of the ONR and the AEC.

[1] Fowler, Lauritsen, and Lauritsen, Rev. Mod. Phys. **20**, 248 (1948).
[2] Herb, Snowdon, and Sala, Phys. Rev. **75**, 246 (1949).
[3] Snyder, Lauritsen, Fowler, and Rubin, Phys. Rev. **74**, 1564 (1948).
[4] E. L. Hudspeth and C. P. Swann, Phys. Rev. **75**, 1272 (1949).
[5] C. B. Madsen and P. Venkateswarlu, Phys. Rev. **74**, 648 (1948).
[6] R. L. Walker and B. D. McDaniel, Phys. Rev. **74**, 315 (1948).
[7] Rasmussen, Hornyak, and Lauritsen, Phys. Rev. **75**, 1462 (1949).
[8] W. E. Burcham, private communication.
[9] Bennett, Bonner, Mandeville, and Watt, Phys. Rev. **70**, 882 (1946).
[10] T. W. Bonner and J. E. Evans, Phys. Rev. **73**, 666 (1948).
[11] L. G. Elliott and R. E. Bell, Phys. Rev. **74**, 1869 (1948).
[12] Hornyak, Lauritsen, and Rasmussen, in publication.
[13] Fowler, Lauritsen, and Rubin, Phys. Rev. **75**, 1471 (1949).

Thermal Conductivity of Glasses at Low Temperatures

R. BERMAN
Clarendon Laboratory, Oxford, England
April 29, 1949

IT was first shown by Debye[1] that for solid non-metals the heat conductivity, K, can be expressed in terms of a mean free path of the heat waves, Λ, by the equation $K=\text{const.}\times c_v q\Lambda$, where c_v is the heat capacity per unit volume and q is the average velocity of the waves. By applying this equation to the results of previous experiments on glasses, using the value of $\frac{1}{4}$ for the constant, the values of Λ in the neighborhood of room temperature were found to be of the order of the interatomic distances. Since q varies little with temperature, the thermal conductivity should vary as the specific heat. The few previous experiments in the hydrogen and helium regions,[2] however, had shown that at lower temperatures the heat conductivity did not fall as rapidly as the specific heat. From this it was deduced that the mean free path of the heat waves increased as the wave-length of the dominant waves became larger than the interatomic distance.

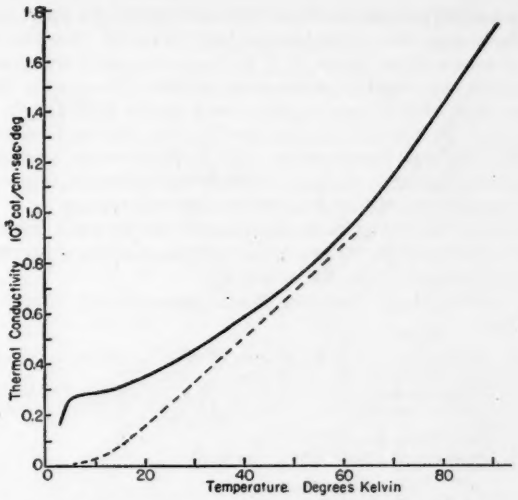

FIG. 1. Thermal conductivity of quartz glass as a function of absolute temperature. Dotted curve shows the specific heat in arbitrary units.

The present experiments were made in order to obtain continuous curves, for each specimen, of the variation of heat conductivity with temperature in the region between 2° and 90°K, from which the variation of mean free path with temperature could be calculated. Since the interpretation of the thermal conductivity of glasses has recently been discussed by Kittel,[3] it seems worth while to give a preliminary report on the results obtained for glass in the present experiments. Two kinds of glass were measured—quartz glass and Phoenix glass (a Pyrex type glass). The values for the two glasses differed by only a few percent over the whole range, and since the specific heat of Phoenix glass has not yet been measured, only the results for quartz glass are shown in Fig. 1. The deviation from proportionality to the specific heat can be seen from the dotted curve, which shows the specific heat[4] plotted in arbitrary units.

The temperature variation of the mean free path is shown in Fig. 2. At the lowest temperature at which measurements were made, 2.5°K, the mean free path is about 6×10^{-5} cm and is roughly proportional to the inverse square of the absolute temperature. If this temperature dependence continued down to lower temperatures, the mean free path would only be comparable with the dimensions of the specimen at about 0.025°K.

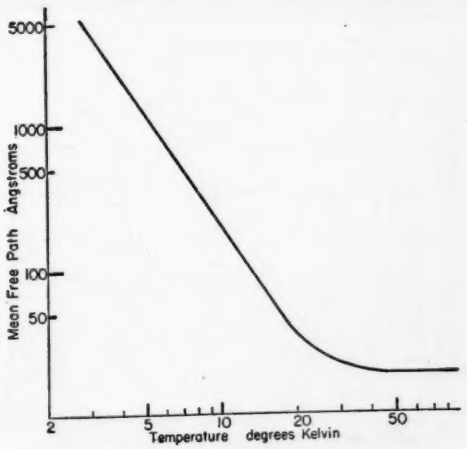

FIG. 2. Mean free path of heat waves in quartz glass as a function of absolute temperature.

In marked contrast to this is the conductivity of a rod of microcrystalline graphite which has also been measured. Over the whole temperature region below 90°K the mean free path is limited by the grain size, which is of the order of 100A. The specific heat is lower than that of quartz glass owing to the high Debye temperature. As a result of these two factors, the conductivity at 90°K is about 80 times greater, while at 1°K it would be about 50 times less than that of glass. This may be of practical interest for the temperature region obtained by magnetic cooling.

A fuller account of these experiments will be given elsewhere. Theoretical work on the conductivity of glasses at low temperatures is being carried out in this laboratory.

I wish to thank Professor F. E. Simon for his interest and advice.

[1] M. Planck *et al.*, *P. Debye in Vorträge über die Kinetische Theorie der Materie und Elektrizität* (B. G. Teubner, Leipzig, 1914).
[2] A. Eucken, Zeits. f. tech. Physik **12**, 88 (1925). K. R. Wilkinson and J. Wilks, J. Sci. Inst. and Phys. in Ind. **26**, 19 (1949). D. Bijl, to be published in Physica.
[3] C. Kittel, Phys. Rev. **75**, 972 (1949).
[4] F. Simon and F. Lange, Zeit f. Physik **38**, 227 (1926).

Energy Levels in N^{15} and N^{16}

L. D. Wyly
*Sloane Physics Laboratory, Yale University, New Haven, Connecticut**
May 31, 1949

THE experimentally determined mass values of N^{16} have shown large discrepancies. The latest values[1,2] as determined from the ground state Q-value of the $F^{19}(n,\alpha)N^{16}$ reaction and from the maximum β-decay energy of N^{16} still show differences of 0.7 mMU. An independent determination of this mass has been made from a study of the $N^{15}(d,p)N^{16}$ reaction. In connection with their photographic work on the scattering of 6.5-Mev deuterons by nitrogen, Guggenheimer, Heitler and Powell[3] found proton groups corresponding to new higher excitation levels in the N^{15} nucleus. A check of these excitation levels has been made using the counters described by Martin[4] for proton detection.

Ammonium nitrate containing 61.5 atom percent of N^{15} in the ammonium radical was obtained from the Eastman Kodak Company. The ammonia was released by reaction in an evacuated system with an aqueous solution of sodium hydroxide. The resulting ammonia gas so obtained was dried with potassium hydroxide to remove the water vapor. The first runs were taken at an observation angle of 90° using a target gas pressure of 20 cm of Hg. The results obtained for both a normal ammonia target and the enriched target at ranges beyond the alpha-particle

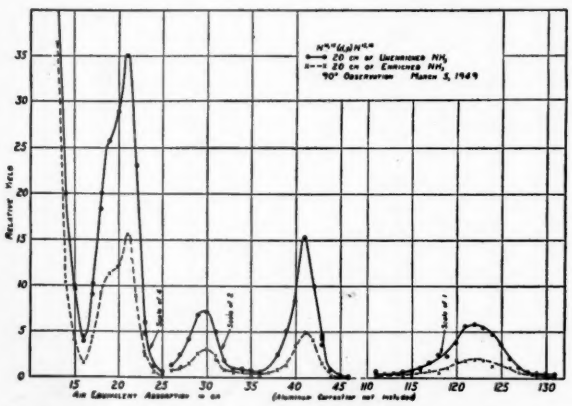

FIG. 1. The atom percent of N^{15} in the enriched target was 61.5 percent. Deuteron bombarding energy was 3.32 Mev.

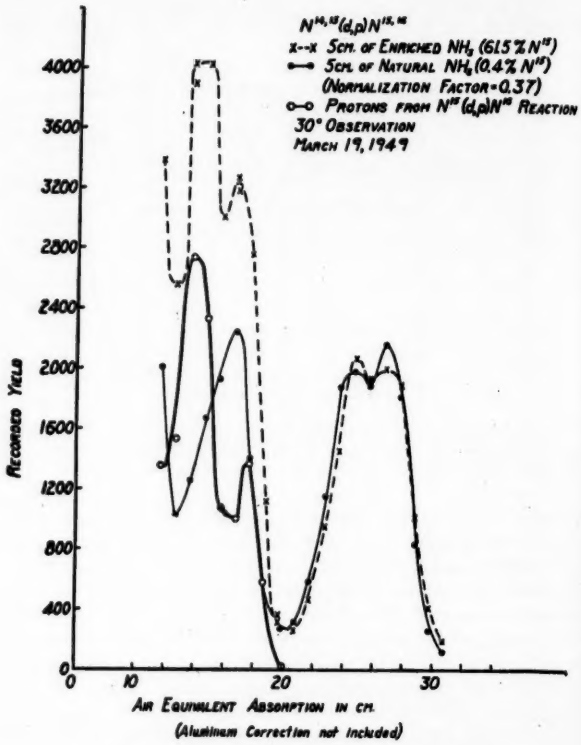

FIG. 2. Deuteron bombarding energy was 3.38 Mev.

groups arising from the associated $N^{14}(d,\alpha)C^{12}$ reaction are shown in Fig. 1. It is evident that no proton groups attributable to the $N^{15}(d,p)N^{16}$ reaction are present in this absorption interval. However, a proton group from this reaction has been found at shorter ranges as shown in Fig. 2. The proton group was deduced by normalizing the unenriched target data to the enriched target data and subtracting the former from the latter. The normalization factor was the ratio of the N^{14} present in the enriched target to that in the unenriched target; the numerical value was obtained from the relative heights of 7.2-Mev excitation proton groups and the long range alpha-particle groups. It will be noticed that there is good evidence that the group is double with the higher state at approximately 0.3-Mev excitation. Other data taken at 30° and 90° did not show the two groups as well resolved as shown in Fig. 2; however, all data did show evidence that the group is double. Using the longest range component an average ground state Q-value of 0.23 ± 0.15 Mev is obtained for the $N^{15}(d,p)N^{16}$ reaction. If the mass values of Flugge and Mattauch[5] are used for proton, deuteron, and N^{15} a mass value of 16.01121 ± 0.00023 MU is obtained for N^{16}.

The average Q-values for the $N^{14}(d,p)N^{15}$ reaction are given in Table I together with those reported by Guggenheimer, Heitler, and Powell. It is to be noted that the 6-Mev level is confirmed as well as the fact that the 7.2-Mev level is double (see Fig. 2).

TABLE I. Q-values for the $N^{14}(d,p)N^{15}$ reaction.

Present work	Guggenheimer, Heitler, and Powell
8.61 ± 0.1 Mev	8.55 Mev
3.29 ± 0.1 Mev	3.5 Mev
2.30 ± 0.1 Mev	2.5 Mev?
1.40 ± 0.1 Mev	1.3 Mev (double?)
	0.3 Mev (double?)

Furthermore there is good evidence for the proton group at an excitation of 8.2 Mev (see Fig. 2).

I am indebted to Professor E. C. Pollard, who suggested the investigation, for many helpful discussions.

* Assisted by the joint program of the ONR and the AEC.

[1] Bleuler and Rossel, Helv. Phys. Acta **20**, 445 (1947).
[2] Bleuler, Scherrer, Walter, and Zunti, Helv. Phys. Acta **20**, 96 (1947).
[3] Guggenheimer, Heitler, and Powell, Proc. Roy. Soc. **190**, 196 (1947).
[4] A. B. Martin, Phys. Rev. **72**, 378 (1947).
[5] Flugge and Mattauch, Physik. Zeits. **44**, 181 (1943).

Ionization Measurement of $He^3(np)$ and $N^{14}(np)$ and the Neutron-Hydrogen Mass Difference

W. FRANZEN,[1] J. HALPERN, AND W. E. STEPHENS
University of Pennsylvania,[2] Philadelphia, Pennsylvania
May 25, 1949

A CYLINDRICAL ionization chamber with a fine axial wire collector was filled with a highly purified mixture of two atmospheres of argon, one-tenth atmosphere of nitrogen and one-half atmosphere of helium enriched in He^3. The pulse size distribution arising from electron collection of the ionization produced by the reactions $He^3(np)H^3$ and $N^{14}(np)C^{14}$ induced by slow neutrons was observed. With a model 100-linear amplifier, modified to have a "rise time" of 16 microseconds, a "clipping time" of 5 microseconds and using an input capacity of 16 micro-microfarads, it was possible to achieve a noise equivalent to 8 kev of ionization in argon (corresponding to an r.m.s. input voltage of 2.3 microvolt). Pulses were recorded by photographing an oscillograph tube. The linearity of the system was checked by means of a precision pulser and an electronic discriminator. The system was calibrated with alpha-particles from a thin polonium source mounted on a platinum foil which could be positioned at the chamber wall or retracted.

The absence of electron capture in the gas was checked by observing the dependence of pulse height on collecting voltage. Saturation was complete at 100 volts with less than one percent variation in pulse height as the applied potential was increased from 100 to 1000 volts.

Figure 1 displays the pulse size distribution obtained from $He^3(np)$ and $N^{14}(np)$ observed simultaneously and from polonium alpha-particles observed in the same gas mixture. The observed distributions agree closely with the distributions expected for a ratio of 400 between outer and inner radii of the ionization chamber and disintegration tracks short compared to the diameter of the chamber.[3] The alpha-particle distribution is narrower due to the localization of the source. On the high energy side, all the distributions fall off sharply, the rate of fall being limited mainly by amplifier noise. This sharp cut-off and the similarity of the curves allow a precise comparison of the ionizations.

If a linear relation between energy and ionization is assumed in argon, in accordance with the results of Jesse,[4] then the energy equivalents of the total ionization produced in $He^3(np)$ and $N^{14}(np)$ are 764 ± 10 kev and 628 ± 4 kev, respectively, when a direct comparison is made with polonium alpha-particles (assumed to have an energy of 5298.4 kev).[5] A correction of -0.3 percent has been applied to these values to account for the effect of the presence of one-tenth atmosphere nitrogen. This correction is derived from the results of a separate experiment in which the total ionization due to $N^{14}(np)$ was studied as a function of nitrogen concentration in purified nitrogen-argon mixtures.

The difference in the energy values for $N^{14}(np)$ and $He^3(np)$ checks closely with the difference between the end-points of the beta-spectra of C^{14}, 156 ± 1 kev,[6] and H^3, 18 ± 1 kev,[7] and their ratio agrees with the ratio of the total ionizations of the two reactions considered independently. This agreement supports the assumption of a constant average energy per ion pair in argon. The errors quoted on the energy values are based on internal consistency and the uncertainty due to statistics alone and do not take into account any systematic errors arising from the method of calibration.

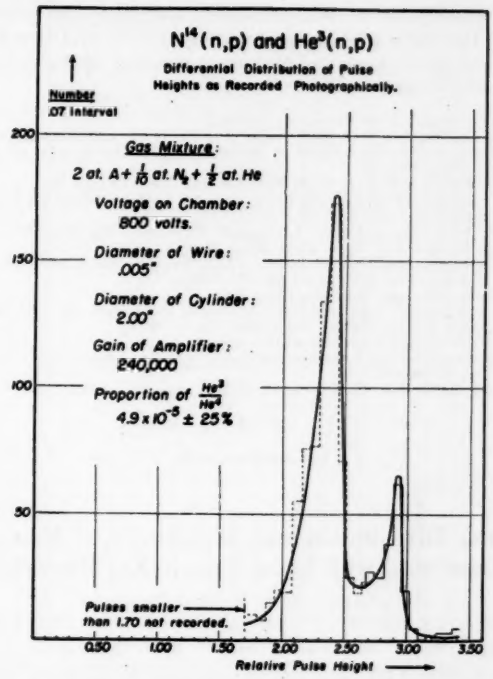

FIG. 1A. Distribution of pulse heights due to $N^{14}(np)$ and $He^3(np)$.

The energies obtained agree well with the thresholds for the inverse (pn) reactions, 620 ± 9 kev[8] and 764 ± 1 kev,[9] respectively, and an ionization determination of $N^{14}(np)$ using total ion collection, 630 ± 10 kev.[10] Assuming zero neutrino mass, our results lead to a neutron-hydrogen mass-difference of 783 ± 4 kev. This value is higher than previously supposed,[11] but agrees well with a value of 789 ± 6 kev deduced from the $D[(dn)(dp)\beta^-]$ cycle.[12] However, it is smaller than the value of 804 ± 5 kev obtained by Bell and Elliott[13] from measurement of $H(n\gamma)$ and the HH−D mass doublet.

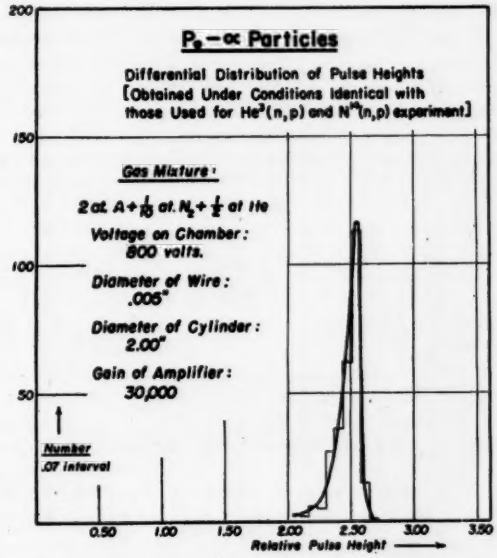

FIG. 1B. Distribution of pulse heights due to polonium alpha-particles emitted by wall source.

The helium used in this experiment had been enriched to a ratio of $He^3/He^4=4.9\times10^{-5}$ and was supplied by Professor A. O. C. Nier of the University of Minnesota to whom we are indebted for his kind cooperation.

[1] Mary Amanda Wood Research Associate.
[2] Supported in part by a joint program of the ONR and AEC and aided by a grant from the Committee on Advancement of Research of the University of Pennsylvania.
[3] P. G. Koontz and T. A. Hall, Rev. Sci. Inst. **18**, 643 (1947).
[4] W. P. Jesse and H. Forstat, Phys. Rev. **74**, 1259A (1948). W. P. Jesse and J. Sadauskis, Phys. Rev. **75**, 1110 (1949).
[5] M. G. Holloway and M. S. Livingston, Phys. Rev. **54**, 18 (1938).
[6] Cook, Langer, and Price, Phys. Rev. **74**, 548 (1948).
[7] G. C. Hanna and B. Pontecorvo, Phys. Rev. **75**, 983 (1949); Curran, Angus, and Cockroft, Phil. Mag. **40**, 53 (1949).
[8] Shoupp, Jennings, and Sun, Phys. Rev. **75**, 1 (1948).
[9] Taschek, Jarvis, Argo, and Hemmendinger, Phys. Rev. **75**, 1268 (1949).
[10] P. Huber and A. Stebler, Phys. Rev. **73**, 85 (1948).
[11] W. E. Stephens, Rev. Mod. Phys. **19**, 19 (1947).
[12] Tollestrup, Jenkins, Fowler and Lauritsen, Bull. Am. Phys. Soc. **24**, no. 4, abst. T2 (1949).
[13] R. E. Bell and L. G. Elliott, Phys. Rev. **74**, 1552 (1948).

Angular Distribution and Multiplicity of Neutrons Associated with Local Cosmic-Ray Showers

G. COCCONI AND V. COCCONI TONGIORGI
Laboratory of Nuclear Studies, Cornell University, Ithaca, New York
May 27, 1949

PRELIMINARY experiments have been performed at Ithaca (260-m elevation) to study some aspects of the local production of neutrons associated with local showers of ionizing particles. The following topics have been investigated: (a) angular distribution of neutrons, (b) multiplicity of the neutron production in lead.

The thirty Geiger-Müller counters in tray A (see Fig. 1) were connected to a discriminator that selected the events in which one and no more than one counter was struck (event 1A). The twelve counters under lead, each separated from its neighbors by 1 cm of lead, were connected in three groups, B, C and D of four counters each. Fourfold coincidences $S=1A+B+C+D$ were assumed to represent mostly showers of three or more ionizing particles produced in the lead Σ. All Geiger-Müller counters were $\frac{1}{2}$ inch$\times$10 inches.

Twenty neutron counters (1 inch$\times$19 inches proportional counters filled with enriched BF_3) were embedded in the paraffin block (38 inches$\times$26 inches$\times$26 inches) surrounding the Geiger-Müller assembly, and connected in two groups of ten counters each, N_1 and N_2, as indicated in Fig. 1. The neutrons that our detector was able to record have energies from $\sim$1 to $\sim$15 Mev. The over-all efficiency ϵ of the two neutron recording systems (paraffin plus 10 neutron counters) was estimated as close to 0.09.

Coincidences S, delayed 7 microseconds and shaped in a 200 microsecond square pulse, were put in coincidences with pulses N_1 and N_2. Coincidences S, $S+N_1$, $S+N_2$ and $S+N_1+N_2$ were registered.

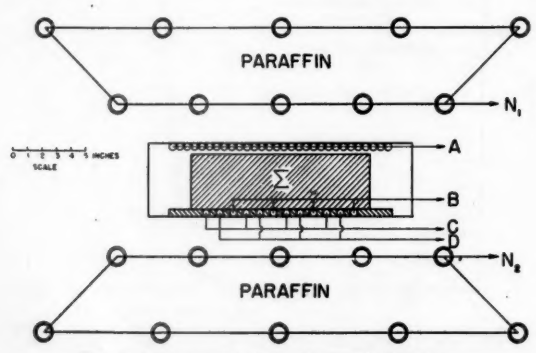

FIG. 1. Arrangement of counters and absorbers.

Measurements have been taken with thicknesses of the lead Σ ranging from $\frac{1}{4}$ inch to 3.5 inches. When the thickness of the lead Σ was smaller than 3.5 inches, the absorber was built with several lead plates evenly placed in 3.5 inches.

TABLE I. Results of the measurements.

1 Thickness of the lead Σ (inches)	2 S (h^{-1})	3 $S+N_1$ (h^{-1})	4 $S+N_2$ (h^{-1})	5 $S+N_1+N_2$ (h^{-1})	6 $\frac{S+N_1}{S+N_2}$	7 ν
3.05	4.83	0.73±0.06	0.76±0.07	0.40±0.05	0.96±0.12	22±4
2.25	8.02	0.76±0.07	0.86±0.07	0.40±0.05	0.88±0.11	20±4
1.00	17.03	0.49±0.06	0.62±0.06	0.24±0.04	0.80±0.14	16±4
0.75	23.04	0.53±0.06	0.51±0.06	0.14±0.03	1.05±0.17	10±3
0.50	27.00	0.37±0.04	0.42±0.04	0.11±0.02	0.87±0.12	10±2
0.25	31.05	0.20±0.03	0.27±0.03	0.06±0.02	0.73±0.13	10±3
0	18.00	0.06±0.04	0.06±0.04	0	1.0 ±0.80	——

The results are given in Table I. In column 6 the ratio $(S+N_1)/(S+N_2)$ is given, which represents the ratio of the showers containing neutrons traveling in forward directions to showers containing neutrons traveling in backward directions. The fact that this ratio is found close to unity indicates that the neutrons are produced fairly isotropically. This directly confirms what has been previously suggested,[1] namely that the observed neutrons are produced in evaporations of excited nuclei.

On the basis of the observed isotropy of the neutron production, the comparison of the rates $S+N_1+N_2$ (column 5) with the average $S+N$ of the rates $S+N_1$ and $S+N_2$ (columns 3 and 4) enables us to compute the average multiplicity ν with which the neutrons are produced, i.e., the average number of neutrons simultaneously produced in the energy range to which our detector was sensitive. The multiplicity ν can be deduced from the expression:

$$\frac{S+N_1+N_2}{S+N}=1-\exp\frac{[(\nu-1)\cdot(\omega/4\pi)\cdot\epsilon]}{l}$$

where ϵ is the over-all efficiency and $\omega=0.4\times4\pi$ is the solid angle at the lead Σ subtended by the paraffin in which each group of neutron counters was embedded. The results are given in column 7 of Table I. Though the statistical errors are very large, the results indicate that the multiplicity depends upon the thickness of the lead in which the events originate, decreasing as the thickness is decreased.

It is clear that different kinds of events are selected by the coincidences S when the thickness of the lead Σ is varied. With $\Sigma=3.5$ inches most of the coincidences S are due to penetrating showers, while the great majority of the showers recorded with smaller thicknesses are due to the soft component. However, the fact that the rates of coincidences $S+N_1$ and $S+N_2$ steadily decrease when the thickness Σ decreases and are extremely small for $\Sigma=0$, while electron showers generated in the lead between the counters, in the paraffin, etc. are still very frequent, indicates that the association of neutrons with electron showers, if it exists, is very small. We are therefore led to interpret the coincidences $S+N_1$ and $S+N_2$ as revealing mostly events induced by the nucleonic component. If this is the case, the average energy of the ionizing particles created in the showers, hence the average energy involved in the events, decreases with decreasing the thickness of the lead. The fact that the multiplicity also decreases shows that the number of the neutrons produced in nuclear events decreases with decreasing the energy involved in the process.

While the coincidences $S+N_1$ and $S+N_2$ registered with high thicknesses of lead are mostly due to penetrating showers, stars are likely the predominant processes recorded with small thicknesses. However the distinction between the two kinds of phenomena is merely formal, as a continuous transition from one phenomenon to the other probably occurs, when the energy involved in the nuclear processes varies.

The present data do not give answer to the question of whether or not all the ν-neutrons are produced in a *single* nuclear evaporation. However, the fact that the multiplicity of neutrons is still very high with lead thickness as small as 1 inch, leads us to think that if the primary act induces further evaporations, the radiations that cause them have very short mean free paths.

[1] Cocconi, Cocconi Tongiorgi, and Greisen, Phys. Rev. **74**, 1867 (1948).

Relation between Half-Life and Disintegration Energy in Orbital Electron Capture by Heavy Nuclei

STANLEY G. THOMPSON
Radiation Laboratory and Department of Chemistry, University of California, Berkeley, California

June 6, 1949

THE large amount of energy data now available for the alpha-emitters and negative beta-emitters in the heavy region makes it possible, through the medium of closed decay cycles, to calculate the total energies corresponding to a number of electron capture decay processes. Using this method, it is possible for the first time to study rather extensively the relationship between disintegration energy and half-life in the electron capture process. The present note summarizes the results of a number of such calculations of decay energies and shows how these are connected with the corresponding half-lives. The data used here are taken chiefly from the recent compilation by Seaborg and Perlman.[1] The electron capture decay isotope Np^{233} of 35 minutes half-life, not included in the above compilation, is also used in this correlation.[2]

In order to illustrate the method of calculation of electron capture decay energy from a closed cycle we may consider the following:

$$\begin{array}{ccc} & \overset{K}{\longleftarrow} & \\ {}_{90}Th^{229} & & {}_{91}Pa^{229} \\ \alpha\downarrow & \beta^- & \downarrow\alpha \\ {}_{88}Ra^{225} & \longrightarrow & {}_{89}Ac^{225}. \end{array}$$

It can be seen that the electron capture energy of Pa^{229} is equal to

$$E_\alpha(Pa^{229})+E_r(Pa^{229})-E_\alpha(Th^{229})-E_r(Th^{229})-E_\beta(Ra^{225})$$

where E_α corresponds to the energy of the longest range alpha-particle, E_r corresponds to the energy of recoil following alpha-emission, and E_β represents the *total disintegration energy* corresponding to the beta-decay process. Using the best values available we have $5.69+0.10-5.02-0.09-0.2=0.5$ Mev for the electron capture disintegration energy of Pa^{229}. Since this isotope decays 99 percent by electron capture and 1 percent by alpha-emission with a measured half-life of 1.5 days, this 0.5 Mev disintegration energy corresponds to a half-life of 1.5/0.99, or approximately 1.5 days.

Calculations using an extension of this method have been carried out for 15 species for which there are reliable half-life and branching data. Where the alpha-energies have not been measured they were obtained from a recent correlation between alpha-energy, mass number, and atomic number.[3] A more serious difficulty arises in estimating total beta-disintegration energies from the published values of the beta-particle upper energy limits and the gamma-ray energies, in that a knowledge of the disintegration scheme is necessary. The values chosen on which the calculations are based are summarized in Table I.

TABLE I. Total beta-disintegration energies of some heavy isotopes.

Isotope	Energy (Mev)
Bi^{213}	1.3
Ra^{225}	0.2
Pa^{233}	0.5
Pb^{211}(AcB)	1.4
Fr^{223}(AcK)	1.3
Th^{231}(UY)	0.24
Pb^{214}(RaB)	1.0
Pb^{212}(ThB)	0.6
Ra^{228}($MsTh_1$)	0.05

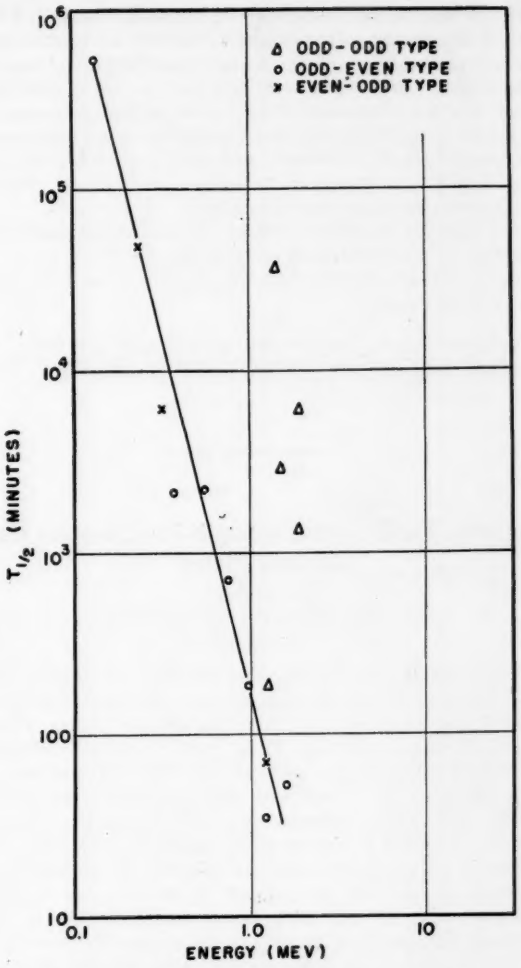

FIG. 1. Relationship between energy and half-life in electron capture decay.

Figure 1 shows a plot of the logarithm of the (partial) half-life *versus* the logarithm of the energy for the 15 species. The energy plotted here is obtained by subtracting the binding energy of the K-electron (about 100 kev in this region) from the total disintegration energy as calculated above. Thus the assumption is made that K-electron capture (rather than L-electron capture) is the predominant mode of decay. Of course the partial half-life for electron capture should be related to the energy of the particular primary transition rather than to the total energy between ground states, as is plotted here, but at present only the latter values are known. It may be noticed that it is possible to draw a line to very roughly include essentially all species other than a few of the odd-odd mass type and that the slope of this line corresponds to a half-life dependence of inverse fourth power of the energy. The number of points above this rough line is probably too small to define another line since some of these probably represent different degrees of forbiddenness and since these odd-odd nuclei seem to include more gamma-rays in their decay which should be taken into account in even a rough correlation; if a line were drawn through these points it would show a slope corresponding to a half-life dependence of greater than inverse fourth power of the energy.

It is felt that further refinements of the method presented here, in which the energy corresponding to electron capture decay to identified excited states of the product nuclei are correlated with corresponding partial half-lives, will lead to more meaningful information as to the nature of the electron capture decay process. Until more complete information is available on the gamma-rays associated with each transition, and until more is known about the ratio of K to L capture in the decay of each isotope, this relationship must be regarded as provisional.

I am indebted to Professor Glenn T. Seaborg for many interesting and helpful discussions on this subject.

This work was performed under the auspices of the U. S. Atomic Energy Commission.

[1] G. T. Seaborg and I. Perlman, Rev. Mod. Phys. **20**, 585 (1948).
[2] L. B. Magnusson and G. T. Seaborg, unpublished work (Jan., 1949).
[3] Perlman, Ghiorso, and Seaborg, Phys. Rev. **74**, 1730 (1948).

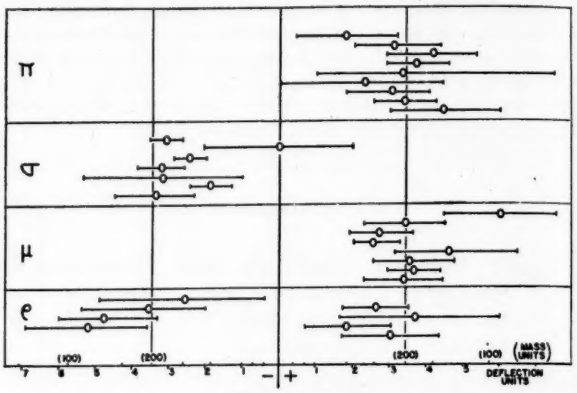

FIG. 2. Preliminary deflection measurements of cosmic-ray mesons, using nuclear plates.

Magnetic Deflection of Cosmic-Ray Mesons Using Nuclear Plates*

IAN BARBOUR
University of Chicago, Chicago, Illinois
June 1, 1949

A METHOD has been described[1] in which two nuclear plates are exposed with an air gap separating their parallel emulsion surfaces, in a perpendicular magnetic field (see Fig. 1). Using a permanent magnet weighing 65 lbs., field strength 13,300 gauss, two balloon flights were carried out with Ilford C2 emulsions, one above 90,000 ft. for 1 hour with 100-μ emulsions, the other for 3 hours with 200-μ emulsions. After development, positions of particles, stopping in the emulsion, relative to the x-ray registration dots, is plotted by means of a pantograph attached to the microscope stage,[2] and the azimuth of the track on emergence measured with an eye-piece protractor. Matching of track segments due to a single particle in the two plates is ascertained by the equality of the following quantities: (a) the dip angles, q_T and q_B in Fig. 1, between emerging track and emulsion surface, accurately measured with a tilting stage;[2] (b) grain counts, (c) estimates of scattering, and most important, (d) the two deflections, Δ_T (obtained by projecting the bottom track) and Δ_B (from projecting the top track). Where a $\pi-\mu$-decay occurs in one plate and the μ-meson crosses the air gap to stop in the other plate, the total μ-meson range gives additional certainty in matching. The magnetic radius is computed from the two independent deflection measurements, Δ_T and Δ_B. Assuming singly-charged particles, and that the energy-loss is a function of velocity only, it can be shown that $R/m=f(R/H\rho)$, where R (range), H (field), and ρ (curvature) can be experimentally determined, but m (mass) is unknown. From range-energy curves[3] for protons in an Ilford emulsion, the function f was graphed, allowing determination of the mass of other particles. The probable error in each angular deflection is the sum of: (a) theoretical average scattering angle,[4] for a particle of the range and mass determined, (b) emulsion distortion (measured "deflections" of a control series of 60 protons with *no* field approximated a Gaussian curve with standard deviation $\frac{1}{2}°$, excluding emulsion areas less than 8 mm from plate edges), (c) instrumental errors (these will be negligible when positions are re-measured with micrometer-thread stage motions readable to 1μ). As scattering introduces the greatest uncertainty, measurements on particles with range 500μ or greater are desirable. Since for a given curvature, the deflection angle will increase with the path length in the air gap, particles with small dip angles will have smaller percent errors. Events have occurred with measured deflection angles 10 times the total probable error in angle, but cases of at least twice this accuracy can be anticipated.

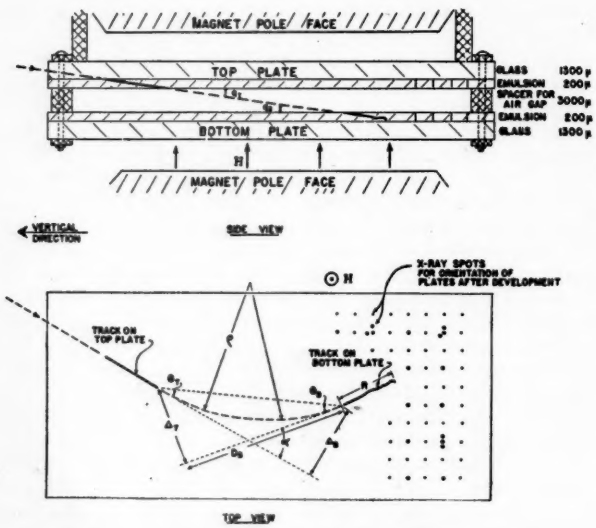

FIG. 1. Side and top view of plate assembly for magnetic deflection experiment.

After analyzing plates from the short flight, plus $\frac{1}{4}$ the emulsion area of the second flight, preliminary measurements have been obtained on 33 mesons, shown in Fig. 2. There is confirmation of the positive charge of π and μ-mesons, and the negative charge of σ (star-producing) mesons, concerning which there is no possibility of direct evidence on cosmic-ray mesons from other emulsion techniques like scattering, grain counting, etc. ρ-mesons (stopping with no visible interaction) appear about equally divided between + and −. Mass and probable error values are plotted on a "deflection unit" scale[5] and give, combining μ and ρ, 219 ± 26; for π and σ, 270 ± 23. There is no evidence in these experiments so far for the presence in appreciable abundance of "heavy" mesons, which could usually be differentiated from protons if they were negative or interacted visibly. The possible presence of "light" mesons cannot yet be excluded, as there are several tracks still "unmatched" (since a meson of mass less than $40m_e$ would experience a very large deflection, a much larger area of the opposite plate must be scanned for a possible matching segment from such a particle). After completion of analysis of the remaining $\frac{3}{4}$ of these plates, another flight is planned in which longer exposure and use of larger plates should give better statistics and accuracy.

The cooperation of Dr. Marcell Schein in this experiment is gratefully acknowledged.

* Assisted by a fellowship from the DuPont Company, and by the joint program of the ONR and the AEC.

[1] C. F. Powell, Nature **161**, 473 (1948); I. Barbour, Phys. Rev. **74**, 507 (1948).
[2] I. Barbour, Rev. Sci. Inst. **20**, 530 (1949).
[3] Lattes, Fowler, and Cuer, Proc. Phys. Soc. **59**, 883 (1947).
[4] E. J. Williams, Phys. Rev. **58**, 292 (1940); Goldschmidt-Clermont, King, Muirhead, and Ritson, Proc. Phys. Soc. **61**, 183 (1948).
[5] For any range or path length, a given increment in deflection angle is essentially represented by the same number of deflection units in all parts of the scale. Mass values are averaged, weighted as the inverse squares of probable errors, on this scale.

A Large Nuclear Disintegration Produced by a Very High Energy Alpha-Particle of the Cosmic Radiation*

J. J. Lord, Marcel Schein, and M. Vidale
Department of Physics, University of Chicago, Chicago, Illinois
May 31, 1949

INFORMATION regarding the manner in which extremely high energy nuclei interact with other nuclei is so limited that the following event of this nature is described as has been observed on an Eastman NTB-3 photographic plate, 150 microns in thickness, exposed in the stratosphere through the use of free balloons. The nuclear collision, as indicated by the tracks of the onizing particles involved, is shown in Fig. 1.

The method of grain counting has been employed in order to obtain information as to the possible nature of each track. Since the grain density is a function of the energy loss per micron, this quantitative relationship was obtained by measuring the grain densities of several long proton and meson tracks ending in the emulsion, and tracks due to single charged particles at minimum ionization. The relationship between grain density and energy loss will not be given, since it was within statistical error the same as that published by Powell and his collaborators[1] for the Kodak NT-4 emulsion.

Track A, Fig. 1, extends from the nuclear disintegration throughout the emulsion for 38,000 microns to a point in the glass backing of the plate. The measured grain densities at points 0.0, 1.5, and 3.6 cm from the disintegration are respectively 0.99, 0.98, and 0.98 grains per micron, as given by counting at each point about 500 grains.

This track, A, cannot be due to a meson, proton, or deuteron, since with this grain density, their corresponding ranges would all be less than 38,000 microns. In addition, for the above mentioned particles, including the triton, the grain density should show a considerable change along the track. The remarkable constancy of the grain density along the 38,000 microns is, however, in perfect agreement with that due to an alpha-particle close to its maximum ionization.

An alpha-particle with this grain density, which is very close to the minimum for double charged particles, would have to have an energy in excess of 3 Bev. In the plane of the plate, which was located vertically, the track A makes an angle of about 15° with the vertical. These facts strongly indicate that the alpha-particle was most likely a part of the primary cosmic radiation.

Track A' is of interest, since the measured grain density along its 3550 micron range within the emulsion is constant, and is within statistical error, the same as that of track A. This grain density corresponds either to that of a 70 Mev proton (and other singly charged particles of correspondingly low energies), or an alpha-particle of at least 3 Bev. A consideration of the sum of the energies of the particles causing the tracks other than A and A' and an assumption of an equal energy for neutrons emitted leads to a total energy release in the star of roughly 1 Bev. Thus, since A carries a momentum corresponding to at least an alpha-particle of 3 Bev energy, and since the other tracks, excluding A and A', do not show any preferential direction, momentum can be conserved only if track A' is also assumed to be due to a very high energy alpha-particle. This is in perfect agreement with the measured grain density of A'.

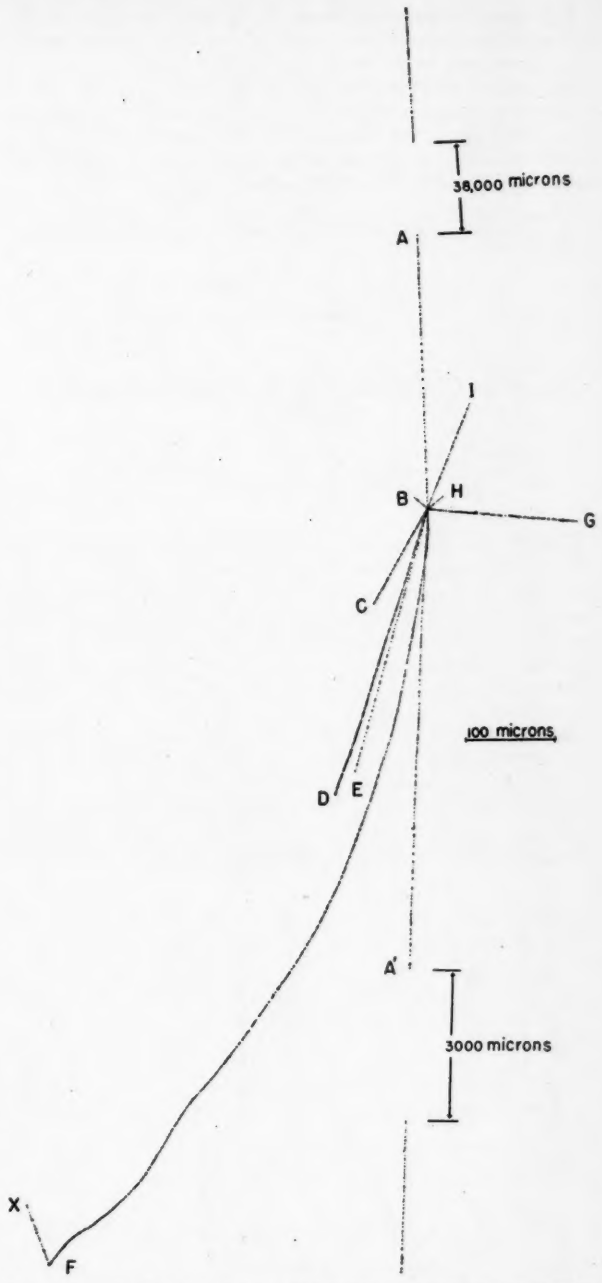

FIG. 1. Reproduction of a photograph showing a π-energy nuclear collision.

Tracks F and D end in the emulsion and were identified, respectively, as due to a π-meson and a proton. At the end of track F, a single track, X, of low grain density originates and passes into the glass backing after traversing 76 microns of emulsion. From its measured grain density track X could either be due to a μ-meson of energy, 4 Mev, or a proton of 31 Mev. The former view, which is more probable, would mean that tracks F was due to a positive π-meson undergoing the familiar decay to a μ-meson. The less likely alternative is that F could be due to a negative meson which, after stopping, is captured and produces a disintegration with the emission of a single ionizing particle with ionization which corresponds to that of a 31 Mev proton. However, it would be somewhat unusual if, as in this case, no other fragments of heavier nuclei occurred in the star.

This event is then interpreted as the collision of a primary alpha-particle of several Bev energy with a nucleus in the emulsion, which leads to the emission of several charged nucleons of energies estimated to be from 4 to 200 Mev and the production of a low energy π-meson. Since the alpha-particle lost an energy or more than 1 Bev in this encounter and then continued on with an angular deviation of 2.5°, its energy was greater than the cut-off energy for alpha-particles at 50° magnetic latitude.

* Assisted by the joint program of the ONR and the AEC.

[1] Brown, Camerini, Fowler, Murihead, Powell, and Ritson, Nature **163**, 47 (1949).

Angular Distribution of Neutrons from (d,n) Reactions*

C. E. Falk,** E. Creutz, and F. Seitz
Physics Department, Carnegie Institute of Technology, Pittsburgh, Pennsylvania

May 25, 1949

THIS letter gives further results of preliminary experiments on the angular distributions of neutrons from (d,n) reactions.[1] The theory explaining the phenomena of (d,n) reactions at high deuteron energies (approximately 200 Mev) is well known[2–4] and has been satisfactorily verified by experiments.[5] However, from the work of Roberts and Abelson[6] there is evidence that (d,n) reactions at comparatively low energies (about 13 Mev) cannot be explained by the present day theories.

Deuterons of approximately 16 Mev, produced by the University of Pittsburgh cyclotron which was made available to us through the courtesy of Dr. A. Allen, were used to bombard thick targets of various elements. The relative resulting neutron fluxes were then measured at different angles by means of threshold detectors. Different elements were used as targets in order to study distributions as functions of the atomic weight of the target and the Q value of the reactions as shown in Table I.

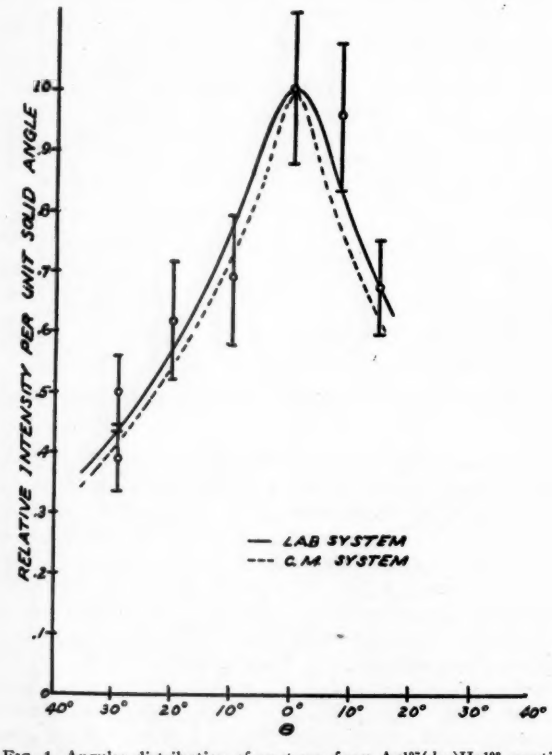

FIG. 1. Angular distribution of neutrons from $Au^{197}(d,n)Hg^{198}$ reaction. θ is angle between direction of maximum neutron intensity and other measured intensities.

TABLE I. Targets used.

Target	A	Q	
$LiBO_2$	Li-6, 7	+15 Mev	for Li
	B-10, 11	+13.8 Mev	for B
		−1.6 Mev	for O
Be	9	+4.3 Mev	
Cu	63.64	~+8 Mev	
Au	197	~+8 Mev	

Table II gives a list of the elements used for detection and the respective thresholds of the reaction.

Figures 1 and 2 show the resulting angular distributions for two typical cases, and Table III shows a summary of the experiments. It is immediately apparent that the distribution in all cases is sharply peaked in the forward direction. As there was a considerable amount of scattering of neutrons from the coils, poles, and the yoke of the cyclotron, small corrections had to be made for this effect. This was accomplished by a graphical integration of the effect over the complete area of the magnet pole pieces. Columns 4 and 5 in Table III show the corrected experimental half-widths (full width at half-maximum) of the angular distributions. The estimated experimental error in the listed half-width is ±10°. The magnitude of this experiment, however, makes it impossible as yet to determine the variation of the half-width of the distributions with A and Q.

TABLE II. Elements used for detection and threshold values.

Detector	Reaction	Half-life of product nucleus	Threshold energy	Reference
C^{12}	$C^{12}(n,2n)C^{11}$	20.5 min.	20.4 Mev	R. Sherr, Phys. Rev. **68**, 240 (1945).
Cu^{63}	$Cu^{63}(n,2n)Cu^{62}$	10.5 min.	12–13 Mev	R. Sagane, Phys. Rev. **53**, 492 (1938); E. O. Salant and N. F. Ramsay, Phys. Rev. **57**, 1075A (1940).
Ag^{107}	$Ag^{107}(n,2n)Ag^{106}$	24.5 min.	5–7 Mev	R. Sagane, Phys. Rev. **53**, 492 (1938); D. C. Graham and G. T. Seaborg, Phys. Rev. **53**, 795 (1938).
Al^{27}	$Al^{27}(n,p)Mg^{27}$	10.2 min.	~4.5	D. C. Graham and G. T. Seaborg, Phys. Rev. **53**, 795 (1938); Feld, Scalettar, and Szilard, Phys. Rev. **71**, 464 (1947).

Nevertheless, the results are of interest. In particular, the data for the gold is hard to reconcile with Serber's stripping theory.[3] Furthermore, the distinct directionality of the distribution is difficult to explain by a simple isotropic evaporation theory of a liquid drop compound nucleus.

TABLE III. Summary of experimental results.

Target	Detector	Reaction	Half-width of neutron distribution (lab. system)	(c.m. system)
$LiBO_2$	C	$Li^{6,7}(d,n)Be^{7,8}$	26°	23°
$LiBO_2$	Cu	$B^{10,11}(d,n)C^{11,12}$	30°	22°
$LiBO_2$	Ag		34°	27°
Be	Ag	$Be^{9}(d,n)B^{10}$	26°	18°
B_4C	C	$B^{10,11}(d,n)C^{11,12}$	34°	26°
Co	Cu	$Co^{59}(d,n)Ni^{60}$	26°	25°
Cu	Cu	$Cu^{63,65}(d,n)Zn^{64,66}$	26°	24°
Cu	Ag	$Cu^{63,65}(d,n)Zn^{64,66}$	48°	42°
Au	Ag	$Au^{197}(d,n)Hg^{198}$	49°	44°

In particular, the data for the gold is hard to reconcile with Serber's stripping theory.[3] Furthermore, the distinct directionality of the distribution is difficult to explain by a simple isotropic evaporation theory of a liquid drop compound nucleus.

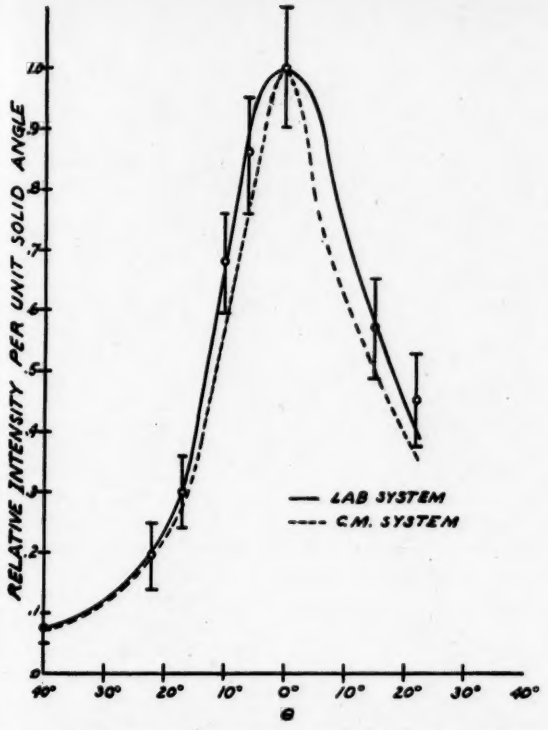

FIG. 2. Angular distribution of neutrons from a $LiBO_2$ target bombarded by 15-Mev deuterons. θ is angle between the direction of maximum neutron intensity and other measured intensities.

To obtain a better understanding of the above described phenomena, experiments are now in progress to improve this data. A four-proportional counter telescope has been built. Better experimental accuracy is expected since the error due to room scattered neutrons is eliminated. Furthermore, it will be possible to measure the neutron spectrum at different angles.

* Assisted by the ONR under Contract N7onr-30304.
** AEC Fellow.
[1] Falk, Creutz, and Seitz, Phys. Rev. **74**, 1226 (1948).
[2] J. R. Oppenheimer, Phys. Rev. **47**, 845 (1935).
[3] R. Serber, Phys. Rev. **72**, 1008 (1947).
[4] S. Dancoff, Phys. Rev. **72**, 1017 (1947).
[5] Helmholz, McMillan, and Sewell, Phys. Rev. **72**, 1003 (1947).
[6] R. B. Roberts and P. H. Abelson, Phys. Rev. **72**, 76 (1947).

Proton Stopping Power of Gold

TORBEN HUUS AND C. B. MADSEN
Institute for Theoretical Physics, University of Copenhagen, Denmark
June 2, 1949

THE previously reported measurements of the proton stopping power of beryllium[1] have been extended to gold, using the proton resonances F-339 and Al-986 as energy indicators.

A foil thickness of about ½ mg/cm² was chosen for the experiment in order to obtain a shift of the resonance peaks of approximately three times the half-width calculated from the theory of straggling.

The results found are given in Table I for three different foils, each consisting of three layers of commercial gold-leaf (content of copper less than 1 percent). An example of the measurements on the line F-339 is reproduced in Fig. 1. The broadening of the peak is only slightly greater than should be expected because of the straggling, indicating that the foils are only slightly inhomogeneous.

TABLE I. Proton stopping power for three different foils.

Resonance	Total thickness mg/cm²	Shift kev	Mean energy kev	Stopping power kev per mg/cm²
F-339	0.46	39	364	85
F-339	0.52	42	366	81
Al-986	0.46	27	1001	59
Al-986	0.51	30	1002	59
Al-986	0.52	31	1003	60

Wilcox[2] reports a value of 67 kev per mg/cm² for the stopping power of gold at a proton energy of 365 kev. This value is about 20 percent smaller than ours, but in the experiment of Wilcox, the energy shift is only of the same order of magnitude as the

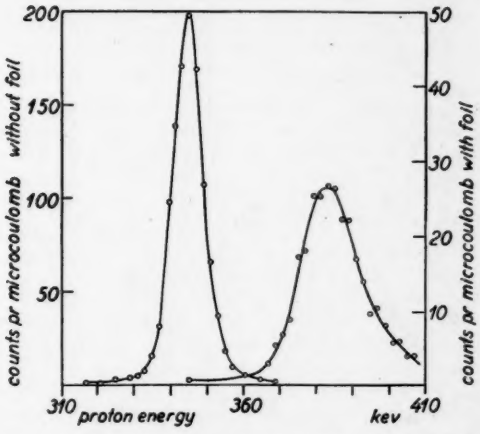

FIG. 1. The F-339 resonance measured without foil and with a 0.46 mg/cm² gold-foil inserted in the proton beam.

half-width, and the results are, for this reason, probably less accurate. The reported difference of 10 percent between the values for protons and deuterons of the same velocity may, therefore, also be expected to be within the experimental uncertainty. This explanation is in agreement with later experiments by Hall and Warshaw.[3]

[1] C. B. Madsen and P. Venkateswarlu, Phys. Rev. **74**, 648 (1948).
[2] H. Wilcox, Phys. Rev. **74**, 1743 (1948).
[3] T. A. Hall and S. D. Warshaw, Phys. Rev. **75**, 891 (1949).

The Density Field in Mach Reflection of Shock Waves

W. BLEAKNEY, C. H. FLETCHER, AND D. K. WEIMER
Palmer Physical Laboratory, Princeton University, Princeton, New Jersey
June 6, 1949

WHEN two shock waves interact with one another the result is not always a simple crossing of the two waves as would be expected from a linear theory. The nature of the more complicated phenomenon was observed by Mach.[1] Von Neumann[2] has pointed out that the interaction is equivalent to the oblique reflection of a single shock from a rigid wall and he proposed a theory by which the strengths and angles of the other discontinuities could be predicted at the point of intersection from the direction of the incoming flow and the strength of the incident shock. His theory of Mach reflection assumed that the three shocks and a slip stream were the only discontinuities present and that the pressure was constant in each of the three angular domains bounded by the three shocks at least in the neighborhood of the intersection. The experimental results of Smith[3] who determined

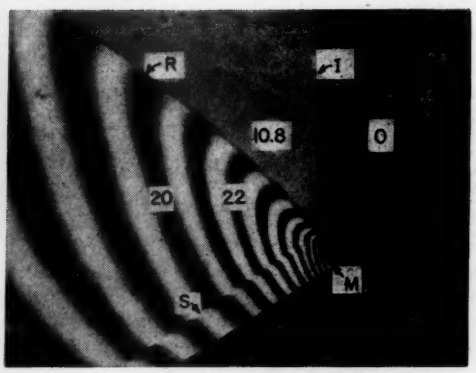

FIG. 1. Interferogram of Mach reflection. The adjustment of the instrument is such that fringes represent density contours a few of which have been numbered in the order of increasing density.

the angles involved do not agree with this "three shock" theory of von Neumann. The correct interpretation of the reflection phenomenon is very fundamental to the theory of fluid dynamics and an experiment is underway to determine the density field in air when a shock wave is reflected from a wall. Results for a particular set of initial conditions are given in this letter.

A shock tube is used[4] to generate plane shock waves which are reflected on a plane rigid wall. The phenomenon is viewed through an interferometer of the Mach-Zehnder type[5] in a direction parallel to the intersection of the plane of the shock front and the wall. A flash (~1 microsecond) interferogram with the instrument adjusted for constant difference in light paths over the entire field of view in the absence of any disturbance is shown in Fig. 1. With this "single fringe" adjustment the fringes appearing in the photograph represent contours of equal fringe shifts and hence contours of constant density or isopycnals in the gas. The incident shock I in the figure is vertical and moving at supersonic speed toward the right. The ratio of the pressure in front to that behind it is 0.80 and the angle between the shock and the wall is 60 degrees. It is followed by the reflected shock R and their point of intersection is joined to the wall by the "Mach" shock M. Trailing behind the triple intersection of the shocks is the slip stream S running nearly parallel to the wall. This discontinuity represents a stream line for the flow relative to the intersection.

Only in the region behind the reflected and Mach shocks is there a detectable variation in the density. Behind the Mach wave and near the wall the gradient of the density points forward (toward the right) indicating that in this region the shock is being followed by a rarefaction. As the point of observation recedes from the reflected shock along a stream line somewhat above the slip stream the density rises to a maximum and then falls again. At higher angles of incidence and weaker shocks this effect is much more pronounced. No certain evidence for an angular variation of density near the intersection has been found.

The theoretical explanation of these results is at present unknown, but the contours resemble somewhat those indicated by Bargmann[6] for glancing incidence, a case which he found amenable to theoretical treatment. The investigations are being continued and in particular the case of nearly glancing incidence is being explored.

The major financial support for this work was provided by the ONR, Contract N6ori-105 Task II.

[1] E. Mach, Sitzungsberichte der (Weiner) Akademie der Wissenschaften **77**, 819 (1878).
[2] J. von Neumann, "Oblique Reflection of Shocks", Explosives Research Report No. 12, Buord. U. S. Navy Department, October, 1943.
[3] L. G. Smith, Photographic Investigation of the Reflection of Plane Shocks in Air, OSRD No. 6271 (1945).
[4] Fletcher, Weimer, and Bleakney, Phys. Rev. **75**, 1294 (1949), Abstracts FA 12 and FA 13.
[5] See, for example, J. Winckler, Rev. Sci. Inst. **19**, 307 (1948).
[6] V. Bargmann, "On Nearly Glancing Reflection of Shocks," AMP Report 108.2 R, National Defense Research Committee, March, 1945.